Ecology and genomics of *Archaea* involved in anaerobic oxidation of ethane

Dissertation
zur Erlangung des Doktorgrades
der Naturwissenschaften
- Dr. rer. nat. -

Dem Fachbereich 2 Biologie/Chemie
der Universität Bremen
vorgelegt von

Cedric Hahn

Bremen, September 2021

Die vorliegende Doktorarbeit wurde in der Zeit von Juli 2017 bis September 2021 im Rahmen des Programms „International Max Planck Research School of Marine Microbiology, MarMic“ in den Abteilungen Molekulare Ökologie und HGF MPG Brückengruppe für Tiefsee-Ökologie und -Technologie am Max-Planck-Institut für Marine Mikrobiologe in Bremen angefertigt.

Diese zur Veröffentlichung erstellte Version der Dissertation enthält Korrekturen.

Gutachter: Dr. Katrin Knittel
Gutachter: Dr. Tristan Wagner

Prüfer: Prof. Dr. Rudolf Amann
Prüfer: Prof. Dr. Michael Friedrich

Datum des Promotionskolloquiums: 04.11.2021

“But nature is always more subtle, more intricate, more elegant than what we are able to imagine.”

- Carl Sagan

2021

Cedric Hahn

ORCID: 0000-0002-2581-7215

Summary

In deep sediment layers, geothermal heat degrades organic matter into a complex mix of hydrocarbons. These compounds migrate towards the sediment surface, where a rich microbial community of anaerobic and aerobic microorganisms oxidizes them. Microorganisms involved in anaerobic alkane oxidation have been identified for most compounds. However, the anaerobic oxidation of the second most abundant alkane, ethane, was unexplored. This thesis aimed to cultivate an anaerobic ethane oxidizer and extend our understanding of the anaerobic oxidation of ethane.

In this work, an ethane-degrading thermophilic archaeon was cultured and named "*Candidatus* Ethanoperedens thermophilum" (**Chapter 2**). Using metagenomic, transcriptomic, and metabolomic data, *Ca.* E. thermophilum was shown to activate ethane using a methyl-coenzyme M reductase (MCR) homolog. Ethane is completely oxidized to CO_2, and electrons are passed to the sulfate-reducing partner bacterium. In a fluorescence in-situ hybridization (CARD-FISH) study, ethanotrophs were detected at various hydrocarbon seepage sites.

In **chapter 3**, a modified mRNA-FISH protocol was developed to analyze activity dynamics in spatially segregated consortia. Tetra-labeled oligonucleotide probes were used to target the mRNA of the metabolic key enzyme of the ethanotroph, ethyl-coenzyme M reductase (ECR). With this method, activity differences were shown and appear to be dependent on the position in the archaeal monospecies cluster and distance from the nearest partner cell.

Chapter 4 describes the structural characterization of the ethane-specific MCR homolog from *Ca.* E. thermophilum. The first structure of a non-canonical MCR showed many sophisticated differences from canonical MCR structures, and the enzyme was named ethyl-coenzyme M reductase after its presumed function. The ECR contains a novel dimethylated F_{430}-cofactor and has many amino acid substitutions at the active site building a widened catalytic chamber. Additionally, large insert regions form loops at the enzyme surface, marking the entry to a hydrophobic tunnel that leads ethane to the catalytic chamber.

This study forms the base for understanding enzymes involved in the anaerobic oxidation of ethane and a potential future biotechnological application.

Zusammenfassung

In tiefen Sedimentschichten werden durch geothermische Wärme organische Stoffe zu einem komplexen Mix von Kohlenwasserstoffen abgebaut. Diese Verbindungen wandern zur Sedimentoberfläche, wo sie von einer diversen mikrobiellen Gemeinschaft oxidiert werden können. Mikroorganismen die in anaerobe Alkanoxidation involviert sind wurden für die meisten Verbindungen identifiziert. Die anaerobe Oxidation des zweithäufigsten Alkans, Ethan, war jedoch bisher unerforscht. Ziel dieser Arbeit war es, einen anaeroben Ethanoxidierer zu kultivieren und unser Verständnis der anaeroben Oxidation von Ethan zu erweitern.

In dieser Arbeit konnte ein ethanabbauendes thermophiles Archaeon kultiviert werden und erhielt den Namen „*Candidatus* Ethanoperedens thermophilum“ **(Kapitel 2)**. Mit Hilfe von Metagenomik-, Transkriptomik- und Metabolitdaten wurde gezeigt, dass *Ca.* E. thermophilum Ethan mit Hilfe eines Methyl-Coenzym M Reduktase- (MCR) Homologs aktiviert. Ethan wird vollständig zu CO_2 oxidiert und die Elektronen an das sulfatreduzierende Partnerbakterium weitergegeben. In einer Fluoreszenz in-situ Hybridisierung (CARD-FISH) basierten Untersuchung wurden die ethanotrophe Archaeen an verschiedenen Kohlenwasserstoffsickerstellen nachgewiesen.

In **Kapitel 3** wurde ein modifiziertes mRNA-FISH Protokoll entwickelt um die Aktivitätsdynamik in räumlich getrennten Konsortien zu analysieren. Es wurden vierfach-markierte Oligonukleotidsonden wurde verwendet, die spezifisch an die mRNA des metabolischen Schlüsselenzyms Ethyl-Coenzym M Reduktase (ECR) der ethanotrophen Archaeen binden. Mit dieser Methode wurden Aktivitätsunterschiede abhängig von der Position der Archaeen in den Konsortien und der Entfernung zur nächsten Partnerzellen gezeigt.

Kapitel 4 beschreibt die strukturelle Charakterisierung des ethanspezifischen MCR-Homologs aus *Ca.* E. thermophilum. Die erste Struktur einer nicht-kanonischen MCR zeigte viele ausgefeilte Unterschiede zu kanonischen MCR-Strukturen. Das Enzym wurde nach seiner vermuteten Funktion Ethyl-Coenzym M Reduktase (ECR) benannt. Die ECR enthält einen neuartigen dimethylierten F_{430}-Kofaktor. Sie weist zahlreiche Aminosäuresubstitutionen am aktiven Zentrum auf, die für eine vergrößerte katalytische Kammer, im Vergleich zur kanonischen MCR, verantwortlich sind. Zusätzlich bilden große Insertionsbereiche Schleifen an der Außenseite des Enzyms, die den Eingang zu einem hydrophoben Tunnel markieren, der Ethan in die katalytische Kammer führt.

Diese Studie bildet die Grundlage für das Verständnis von Enzymen, die an der anaeroben Oxidation von Ethan beteiligt sind, sowie für eine mögliche zukünftige biotechnologische Anwendung.

Abbreviations

AAA	AOM-associated archaea
AAI	average amino acid identity
ACDS	acetyl-CoA decarbonylase:synthase
ADH	alcohol dehydrogenase
AGC	automatic gain control
ANI	average nucleotide identity
ANME	anaerobic methanotrophic archaea
AOE	anaerobic oxidation of ethane
AOM	anaerobic oxidation of methane
AOR	tungstate-containing aldehyde ferredoxin oxidoreductase
ASS	alkylsuccinate synthase
ATP	adenosine triphosphate
BES	2-bromoethanesulfonic acid
BONCAT	bioorthogonal noncanonical amino acid tagging
CARD	catalyzed reporter deposition
cfb	coenzyme F_{430} biosynthesis
Clamp-FISH	click-amplifying fluorescence in-situ hybridization
CLSM	confocal laser scanning microscope
CoA	coenzyme A
CobM	precorrin-4 C(11)-methyltransferase
CoM	coenzyme M
CV	column volume
DAPI	4',6-diamidin-2-phenylindol
DIC	dissolved inorganic carbon
DIET	direct interspecies electron transfer
DNA	desoxyribonucleic acid
DSR	dissimilatory sulfate reductase
DTT	dithiothreitol
ECH	energy conserving hydrogenase complex
ECR	ethyl-coenzyme M reductase
EDTA	ethylenediaminetetraacetic acid
EPR	electron paramagnetic resonance
FA	formamide
FISH	fluorescence in-situ hybridization
FPO	$F_{420}H_2$ dehydrogenase
FRH	F_{420}-dependent reductase
FSR	F_{420}-dependent sulfite reductase
FTR	$F_{420}H_2$:quinone oxidoreductase
FWD/FMD	formylmethanofuran dehydrogenase
GB	Guaymas Basin
GC content	guanine-cytosine content
gDNA	genomic DNA
GoM	Gulf of Mexico
GWP	global warming potential
HCR-FISH	hybridization chain reaction fluorescence in-situ hybridization

HDR	coenzyme B-coenzyme M heterodisulfide reductase
HEPES	4-(2-hydroxyethyl)-1-piperazineethanesulfonic acid
HESI	heated electrospray ionization
HR	Hydrate Ridge
hrCN PAGE	clear native polyacrylamide gel electrophoresis
HRP	horseradish peroxidase
LC	Loki's Castle
LC-MS/MS	liquid chromatography with tandem mass spectrometry
MAG	metagenome assembled genomes
MALDI-TOF	matrix-assisted laser desorption/ionization time of flight
MAS	methylalkylsuccinate synthase
MCR	methyl-coenzyme M reductase
MDA	multiple displacement amplification
MER	F_{420}-dependent methylene-H_4MPT reductase
metF	N5,N10-methylenetetrahydrofolate reductase
MF/MFR	methanofuran
MHC	multiheme c-type cytochrome
Mp	methanophenazine
MPT	methanopterin
mRNA	messenger ribonucleic acid
MS	mass spectrometry
MTR	Na^+-translocating methyl-H_4MPT coenzyme M methyltransferase
NAD	nicotinamide adenine dinucleotide
PBS	phosphate-buffered saline
PCR	polymerase chain reaction
PFA	paraformaldehyde
pMMO	particulate methane monooxygenase
rcf	relative centrifugal force
RNF	Na^+-translocating ferredoxin–NAD oxidoreductase
ROI	region of interest
RPKM	reads per kilobase per million
rpm	rounds per minute
rRNA	ribosomal ribonucleic acid
RT	room temperature
RT-qPCR	real-time reverse transcription polymerase chain reaction
RV	research vessel
SCG	single-cell amplified genome
SD	standard deviation
SDS	sodium dodecyl sulfate
SDS PAGE	sodium dodecyl sulfate polyacrylamide gel electrophoresis
SIP	stable-isotope probing
SMTZ	sulfate-methane transition zone
SR	sulfate reduction
SRB	sulfate-reducing bacteria
TCA cycle	tricarboxylic acid cycle
UHPLC	ultra-high-performance liquid chromatography
UV	ultraviolet

Contents

Chapter 1

Introduction

1.1 Natural hydrocarbons and their impact on climate

Natural hydrocarbon seeps can be found throughout the oceans, mostly along continental margins, forming crucial deep-sea habitats (German et al. 2011). The main processes leading to the formation of hydrocarbons in the subsurface sediments are microbial transformations and the thermocatalytic decay of organic matter. Microbial transformation happens in anoxic subsurface sediments, where microorganisms degrade and ferment recalcitrant organic material. These processes leave behind simple molecules like organic acids, H_2, and CO_2 that methanogenic archaea can use to form methane (Zinder 1993, Thauer et al. 2008). In anoxic sediments with low concentrations of sulfate, nitrate, Mn(IV), or Fe(III), methane is a significant end product that migrates towards the upper sediment layers (Thauer et al. 2008). Geothermal activity drives thermocatalytic decay. At temperatures greater than 100°C, complex organic matter is transformed and broken down, resulting in the release of various alkanes and other hydrocarbons that can migrate to the surface (Mahlstedt, 2018).

Dissolved methane can form methane hydrates, a type of water ice with trapped gaseous hydrocarbons, and its stability is controlled by temperature, pressure, and methane concentration (Kvenvolden 1993, Kvenvolden 1995). The formation of these gas hydrates can only occur when the bottom water temperature is below ~2°C, and water depth exceeds ~300 m (Kvenvolden 1995). In deep subsurface sediments, the temperature rises, and therefore gas hydrates are only stable from the seabed to the melting depth. This area is called the "hydrate stability zone." The carbon isotopic composition of gas hydrates determines the origin of methane. The methane of biogenic origin has $\delta^{13}C$ values < -60‰, whereas thermogenic methane has $\delta^{13}C$ values > -60‰ (Bernard et al. 1976). While gas hydrates of biogenic origin contain almost exclusively methane (> 99%), gas of thermogenic origin forms hydrates with more significant portions of C_{2+}-alkanes like ethane, propane, butane, and pentane (Sassen et al. 2004, Lu et al. 2007, Norville and Dawe 2007). These more complex hydrates are more stable than pure methane hydrates and can contain > 24% C_{2+}- alkanes, dominated by ethane, but also contain substantial amounts of propane and butane (Lu et al. 2007).

The majority of the gaseous hydrocarbons migrating to the surface either end up as gas hydrates or get degraded by the microbial community within the sediment (Judd 2004). Hydrocarbons that escape from the seabed in large bubbles mostly disperse in the water column and oxidize there (Grant and Whiticar 2002). Therefore, natural hydrocarbon emission to the atmosphere from these natural sources is relatively low (Etiope and Klusman 2002, Etiope and Ciccioli 2009). With deep ocean temperatures increasing due to climate change, the temperature-sensitive gas hydrates destabilize (Archer et al. 2009). As a result, fewer hydrocarbons will be trapped in gas hydrates in the future. Additionally, the outburst from the destabilized gas hydrates will have a strong short-term effect. Models suggest an additional temperature increase of 0.5 – 0.6°C connected to gas hydrate release if the earth's climate increases by 3°C (Archer et al. 2009).

The main climate-active gas released from natural seeps is methane. Methane, after carbon dioxide, is the second most important anthropogenic greenhouse gas and has a global warming potential (GWP) of 25 (Boucher et al. 2009). It has a short lifetime in the atmosphere of only 10 years, but the oxidation to CO_2 causes a long-term effect. Also, the C_{2+} alkanes are relevant for the climate if they reach the atmosphere, foremost ethane is essential in this context (Forster et al. 2007). Ethane is the non-methane hydrocarbon with the most extended lifetime in the atmosphere. It has a moderate direct climate effect but more substantial indirect effects, leading to a GWP of 5.5 – 10 (Thompson et al. 2003, Forster et al. 2007, Hodnebrog et al. 2018). Understanding seep dynamics is of great importance regarding the potential climate effects and the native microbial community is a crucial part of regulating the natural hydrocarbon emission.

1.2 Cold seep and hydrothermal vent systems

The areas where natural hydrocarbons emerge to the seabed are called seeps or vents, and they form oasis-like ecosystems at the seafloor. In general, we differentiate between cold seeps and hydrothermal vents. Marine cold seeps are located in the hydrate stability zone and, as the name indicates, release cold fluids enriched in hydrocarbons. At active plate margins, deep geothermal activity fuels cold seeps with thermogenic compounds that migrate to the surface (Suess 2020). At passive continental margins, overpressure and changes in sediment permeability can lead to the release of hydrocarbon-rich fluids (Suess 2014). In addition, destabilization of gas hydrates and buried organic-rich sediments can fuel cold seep environments (Römer et al. 2014, Skarke et al. 2014, Wallmann et al. 2018). A well-studied

cold seep site at an active plate margin with large gas hydrate deposits along the hydrate stability limit is the Cascadia margin off Oregon (Bohrmann et al. 1998, Sahling et al. 2002). The complex gas hydrates in the Cascadia margin are of thermogenic origin, and the two main components are methane and ethane with 75.36% and 11.41%, respectively (Lu et al. 2007). Other important constituents are propane with 5.66% and butane and iso-butane with 2.11 and 1.22, respectively (Lu et al. 2007).

The Gulf of Mexico is a well-studied site for passive margin seeps and is generated from underlying salt strata (Suess 2020). Salt domes push through the deep sediments and facilitate the migration of fluids and liquid hydrocarbons to the surface. Deep reservoirs build up immense pressure, causing the rise of hydrocarbons to the seafloor surface, where they are emitted as gas flares and natural oil spills. As most deep deposit-fueled seep sites, the Gulf of Mexico is a cold seep with temperatures of 2 – 4°C. At locations where oil reaches the surface, it has a lava-like flow and solidifies quickly, covering the surrounding area with a brittle asphalt layer (Brüning et al. 2010). Complex gaseous hydrocarbons of thermogenic origin accompany the oil seeps and form gas hydrates (Sahling et al. 2016). The Gulf of Mexico cold seeps offer a great variety of short and long hydrocarbons that emerge to the surface.

If geothermal activity leads to the emission of fluids with elevated temperatures, the resulting structures are called hot seep or hydrothermal vents. Hydrothermal vents occur at seafloor spreading zones with magma chambers 1 – 3 kilometers beneath the surface (Kelley et al. 2002, German et al. 2004). The Mid-Atlantic Ridge and the Arctic Mid-Ocean Ridge are slow or ultra-slow spreading zones, respectively, and harbor extensive and long-lived hydrothermal vent systems (Rona et al. 1986, Pedersen et al. 2010). These hydrothermal vents release hot fluids of up to 320°C, enriched in reduced compounds attracting rich deep-sea fauna (Pedersen et al. 2010, Baumberger et al. 2016). The sea floor surrounding the vents is covered by basalt and basically sediment-free, limiting the microbial communities to the basalt surface and cracks (Rona et al. 1986, Steen et al. 2016).

The Guaymas Basin's hydrothermal vents in the Gulf of California are a well-studied example of a heated hydrocarbon seep with diverse and rich microbial sediment communities (Figure 1-1). The Guaymas Basin is a young marginal rift basin showing active seafloor spreading. High riverine sediment fluxes and productive surface waters cause a substantial deposition of organic matter (Lonsdale and Becker 1985). This deposition leads to a thick layer of organic-rich sediment atop the spreading center. High pressure and temperatures of 200 – 300°C quickly transform buried organic matter into diverse hydrocarbons (Teske and Carvalho 2020). The temperature gradient is steep in the surface sediments, reaching temperatures above

>80°C within 50 cm below the surface (Teske et al. 2021). The sharp temperature gradient limits the habitable zone for microorganisms, and rising hot fluids require regular recolonization of sediments exposed to the hot fluids. The microorganisms in these zones are thermophilic or thermotolerant, and some of them specialize in the use of methane and other alkanes (Teske and Carvalho 2020).

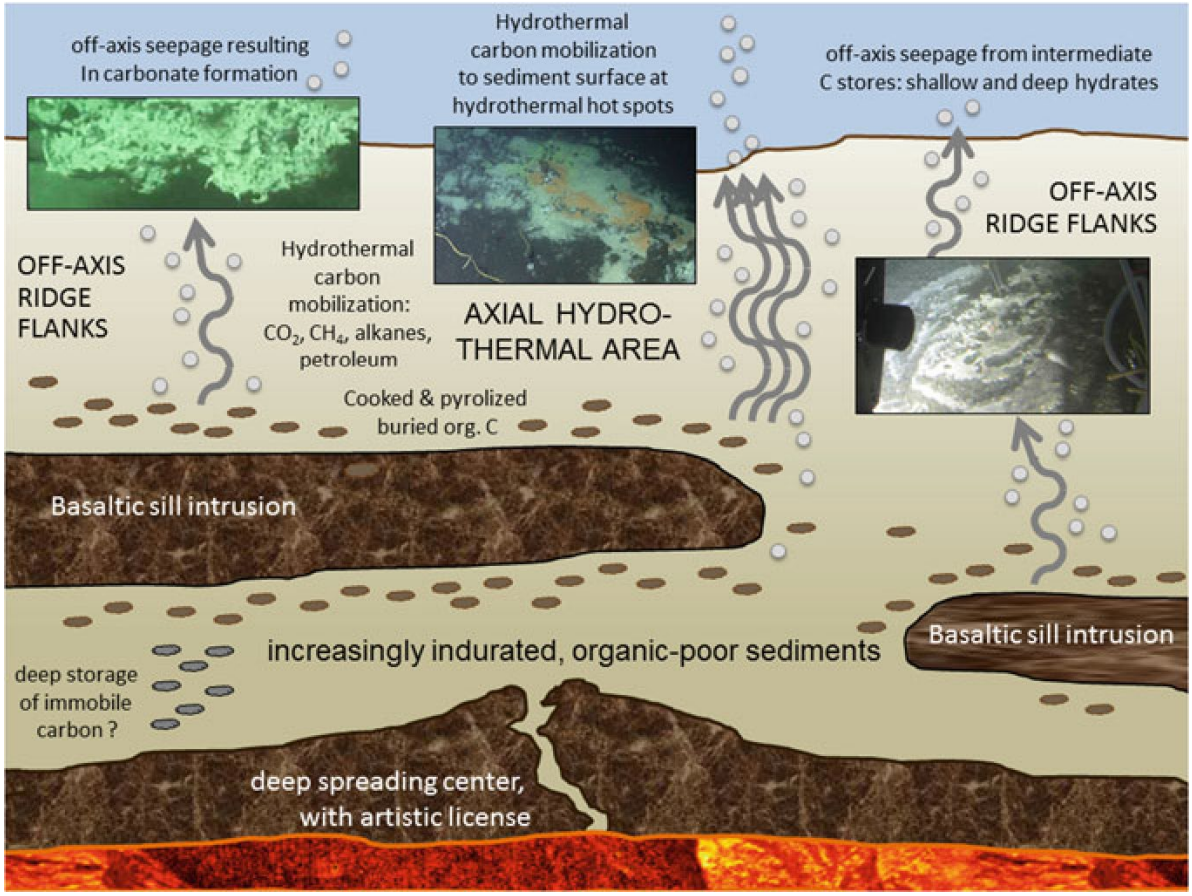

Figure 1-1 Concept sketch of Guaymas Basin hydrothermal vent system. Deep spreading center fuels thermocatalytic decay of hydrocarbons that migrate towards the surface. The axial hydrothermal area is subjected to hot fluids combined with concentrations of complex thermogenic hydrocarbons. Organic rich sediment layer harbors diverse microbial communities. Transferred from Teske and Carvalho (2020).

1.3 Discovery and metabolism of anaerobic oxidation of methane

Methane migrating from deeper layers of the sediment is oxidized with sulfate migrating from the water column. Geochemical analysis of methane-rich sediments had predicted the presence of this process already in the 1970s (Barnes and Goldberg 1976, Reeburgh 1976). These zones of mutual depletion of sulfate and methane are called sulfate-methane transition zone (SMTZ). The underlying reactions were measured using radiolabeled methane and sulfate tracers, and the process was called anaerobic oxidation of methane (AOM) (Hinrichs et al. 1999, Boetius et al. 2000).

In 1980 a study showed that 2-bromoethanesulfonic acid (BES), an inhibitor of methanogenesis, inhibits anaerobic methane oxidation. This finding raised the idea that organisms related to methanogens could perform AOM (Zehnder and Brock 1980). Later it was suggested that symbiotic consortia of methanogen-like organisms and sulfate-reducing bacteria that exchange molecular intermediates such as hydrogen perform AOM (Hoehler et al. 1994). It took a few more years until 16S rRNA gene sequences identified a distinct branch within the methanogens, the ANME-1 archaea, as a likely candidate for the methane oxidation in sediments (Hinrichs et al. 1999). Additionally, the same study found a single sequence of a second methanogen-related organism, later identified as ANME-2 (Hinrichs et al. 1999). Using fluorescence in-situ hybridization (FISH) with specific probes for ANME-2 and sulfate-reducing bacteria (SRB) of the branch *Desulfosarcina/Desulfococcus*, consortia of these organisms were visualized in hydrocarbon-rich sediments, indicating that those are responsible for the sulfate dependent AOM (Boetius et al. 2000). These consortia can represent >90% of the microbial community in layers of SMTZ of active seep sites (Boetius et al. 2000, Orphan et al. 2001, Michaelis et al. 2002). This finding makes AOM consortia a crucial part of seep communities and a significant methane sink in anoxic environments (Knittel et al. 2005, Niemann et al. 2006).

Phylogenetically, anaerobic methanotrophic archaea (ANME) are divided into the polyphyletic groups ANME-1, ANME-2 and ANME-3 within the class of Methanomicrobia (Knittel and Boetius 2009). The ANME-1 linage belongs to the recently defined order *Ca.* Methanophagales, whereas the ANME-2 and ANME-3 belong to the order of Methanosarcinales (Adam et al. 2017). All ANME archaea use a reversed version of the methanogenesis pathway, with the key enzyme methyl-Coenzyme M reductase (MCR), mediating the initial binding of methane to the Coenzyme M (Figure 1-2). The methyl group is transferred to tetrahydromethanopterin (H_4MPT) by the Na+-translocating methyl-H4MPT coenzyme M methyltransferase (MTR). In the next step, the methyl-tetrahydromethanopterin is oxidized to methylene-tetrahydromethanopterin. In all methanogens and ANME-2, the enzyme F_{420}-dependent methylene-H4MPT reductase (MER) catalyzes this step. ANME-1 genomes lack the *mer* gene. Instead, the N5,N10-methylene-tetrahydrofolate (metF), acquired by horizontal gene transfer from bacteria, mediates this step (Meyerdierks et al. 2010, Krukenberg et al. 2018). From there on, the substrate is further oxidized in the reverse methanogenesis pathway, and finally, CO_2 is released (Figure 1-2).

AOM has a meager energy yield close to the bare minimum that allows microbial life (Thauer 2011). The low energy yield results in doubling times of 7 months for these organisms

(Nauhaus et al. 2002, Nauhaus et al. 2007). The energy yield of sulfate-dependent AOM under standard conditions is -21 kJ/mol of methane, which equals less than 2 generated ATPs per oxidized methane (Scheller et al. 2010, Thauer 2011). Energy conservation in ANME archaea is driven by electron flow-dependent H^+ and Na^+ pumps, creating gradients that fuel ATPases (Figure 1-3C). The Na^+ gradient is also required for methyl group transfer from the Coenzyme M to tetrahydromethanopterin by the MTR (Evans et al. 2019). The $F_{420}H_2$ dehydrogenase (FPO) drives the H^+ gradient. The Na^+-translocating ferredoxin–NAD oxidoreductase (RNF) maintains the sodium gradient in ANME-2. Gene sequences for this enzyme have also been found in the strain ANME-1-THS but are missing in other ANME-1 genomes (Krukenberg et al. 2018, Borrel et al. 2019). Energy conserving hydrogenases are crucial for hydrogenotrophic methanogens, but for AOM they are not required and consequently not found in ANME genomes (Thauer 2011, Krukenberg et al. 2018). Some [FeFe]-hydrogenases were described in ANME-1 genomes but lack the active site features essential for hydrogenase activity (Meyerdierks et al. 2010, Thauer 2011, Wang et al. 2019). All genomic studies of ANME-1 and ANME-2 rely on incomplete metagenome-assembled genomes (MAGs), and no closed genome of an MCR-dependent alkanotrophic archaeon has been published yet.

AOM is not limited to sulfate reduction as electron-sink but can also use alternative electron acceptors (Figure 1-2). In a bioreactor incubation with sediments from a Dutch channel, a new clade distantly related to ANME-2 coupled AOM to nitrate reduction (Raghoebarsing et al. 2006). This new clade was named AOM-associated archaea (AAA) and later renamed ANME-2d, despite its polyphyletic relationship to the other ANME-2 clades (Knittel and Boetius 2009, Haroon et al. 2013). However, the name ANME-2d was initially used for environmental sequences from the hydrocarbon seeps in the Gulf of Mexico (Mills et al. 2003, Mills et al. 2004, Mills et al. 2005, Martinez et al. 2006). The phylogenetic clade formed by these sequences was later renamed GoM-Arc1 (Lloyd et al. 2006). I will use ANME-2d for the mostly limnic methanotrophs that perform nitrate- or metal-dependent AOM and GoM-Arc1 for marine archaea found at various seep sites. These two groups are phylogenetically distinct and represent sister lineages within the order of Methanosarcinales (Knittel and Boetius 2009). The first described ANME type species was *Ca.* Methanoperedens nitroreducens from the ANME-2d linage. It harbors a complete reverse methanogenesis pathway and genes for reducing nitrate to nitrite acquired by horizontal gene transfer (Haroon et al. 2013). Consequently, the ANME-2d lineage was renamed to *Ca.* Methanoperedenaceae. The *Ca.* Methanoperedenaceae family is metabolically diverse and contains the first described

organisms to perform AOM coupled to iron and manganese reduction (Ettwig et al. 2016, Cai et al. 2018, Leu et al. 2020).

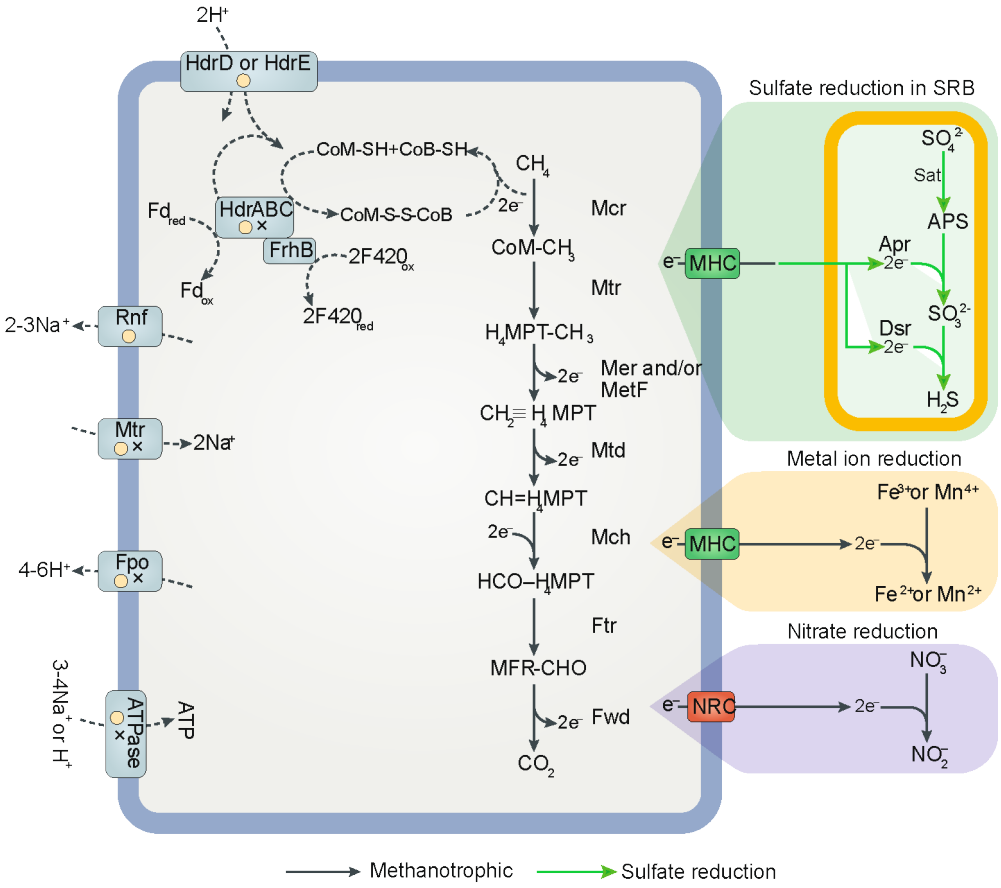

Figure 1-2 Current understanding of metabolic pathway of methanotrophic archaea. ANME cells (blue rectangle) use the reverse methanogenesis pathway to oxidize methane to CO_2 fully. Reverse methanogenesis has been shown for the clades ANME-1, ANME-2abc, *Ca.* Methanoperedens (ANME-2d) and ANME-3. There is still limited genomic and physiological knowledge of ANME-3, so it will not be further mentioned. Circles within enzyme complexes mark genes present in ANME-2 genomes; crosses mark genes present in ANME-1. Enzymes with a cross and circle are present in all methanotrophs. ANME-1 uses metF instead of Mer. ANME-2d couples AOM to the reduction of nitrate, iron, and manganese. Sulfate-reducing bacteria (yellow rectangle) use reducing equivalents from AOM for the reduction of sulfate. Modified from Evans et al. (2019).

1.4 Syntrophy in sulfate-dependent AOM

ANME archaea lack genes for dissimilatory sulfate reduction, and for sulfate-dependent AOM, they require sulfate-reducing partner bacteria (SRB). Different SRB, mainly from the Deltaproteobacteria, have been identified, but factors determining the phylogenetic composition of consortia are not fully understood yet. The phylogenetic affiliation of SRB in consortia seems to depend on two main factors, temperature and nutrient exchange, i.e., diazotrophic capability (Holler et al. 2011, Green-Saxena et al. 2014, Krukenberg et al. 2018, Metcalfe et al. 2021). The deep branching deltaproteobacterial species *Ca.* Desulfofervidus auxilii is the dominant SRB partner strain in geothermally heated seep environments and high-

temperature incubations (>50°C) (Krukenberg et al. 2016, Wegener et al. 2016). In cold and moderate seep environments, the diversity of partner bacteria is much broader. Most SRB at these hydrocarbon seeps are affiliated to *Desulfosarcina/Desulfococcus* (DSS, SEEP-SRB1) or the deep branching SEEP-SRB2 (Kleindienst et al. 2012). Patterns in the co-occurrence of ANME-2b and SEEP-SRB1g were linked to the diazotrophic activity of the bacterial partner (Metcalfe et al. 2021). This finding proposes nutrient exchange as an essential factor for pairing (Metcalfe et al. 2021). ANME-3 has so far mostly been detected with partner cells from *Desulfobulbus/Desulforhopalus* (Niemann et al. 2006, Lösekann et al. 2007). ANME-1 and ANME-2a/c predominantly pair with SEEP-SRB1a and SEEP-SRB2 (Schreiber et al. 2010, Kleindienst et al. 2012). Despite indications for specific nutrient exchange in this syntrophy, factors determining the pairing of alkanotrophic bacteria and SRB remain unknown.

AOM consortia organize in different ways. Often ANME and SRB appear segregated in different zones within the consortia (Figure 1-3A). However, mixed consortia or individual ANME cells without apparent partner bacteria have also been found (Knittel et al. 2005, Knittel and Boetius 2009). To allow energy-yielding methanotrophy, reducing equivalents liberated by the methanotrophs need to be neutralized. In sulfate-dependent AOM, the SRB consume the reducing equivalents in the reduction of sulfate to sulfide. The molecular mechanisms underlying the reducing equivalent exchange within AOM consortia are not resolved yet. It has been speculated that the partner organisms exchange intermediate substrates via diffusive flux, but for most compounds maintaining the gradient would reduce the energy gain too much to make it a feasible process (Sørensen et al. 2001). Additionally, none of these possible intermediates was measured in AOM enrichment cultures (Nauhaus et al. 2002). The addition of different potential intermediates like colloidal sulfur, carbon monoxide, methyl sulfide, methanol, acetate, or formate to AOM cultures did not yield a response by the partner organism, indicating that these intermediates are not relevant for the transfer in the consortium (Wegener et al. 2015). Considering these studies, an exchange of reducing equivalents via intermediates is unlikely. The most widely accepted theory suggests direct interspecies electron transfer (DIET) between the methanotrophs and their partner bacteria. Both partner organisms highly express extracellular cytochromes (Krukenberg et al. 2018). In addition, pili-based nanowire-like structures may facilitate the electron transfer (Figure 1-3B) (Wegener et al. 2015). Models for electric conductivity between the syntrophic partners considering intermixing and distance between cells are most fitting to observed activities (McGlynn et al. 2015, He et al. 2019, He et al. 2021). Alternatively, the ANME archaea might be incomplete sulfate reducers themselves. In this hypothesis, the partner disproportionate zero-valent sulfur

(Milucka et al. 2012). The only SRB partner bacterium isolated so far, the thermophilic Deltaproteobacterium *Ca.* Desulfofervidus auxilii, is an obligate sulfate reducer. *Ca.* Desulfofervidus auxilii is incapable of elemental sulfur metabolism, indicating that, at least for thermophilic environments, the second theory is unlikely (Krukenberg et al. 2016). So far, no proliferating culture performing sulfate-dependent AOM has been established in which ANME cells thrive without partners, suggesting an obligate syntrophy.

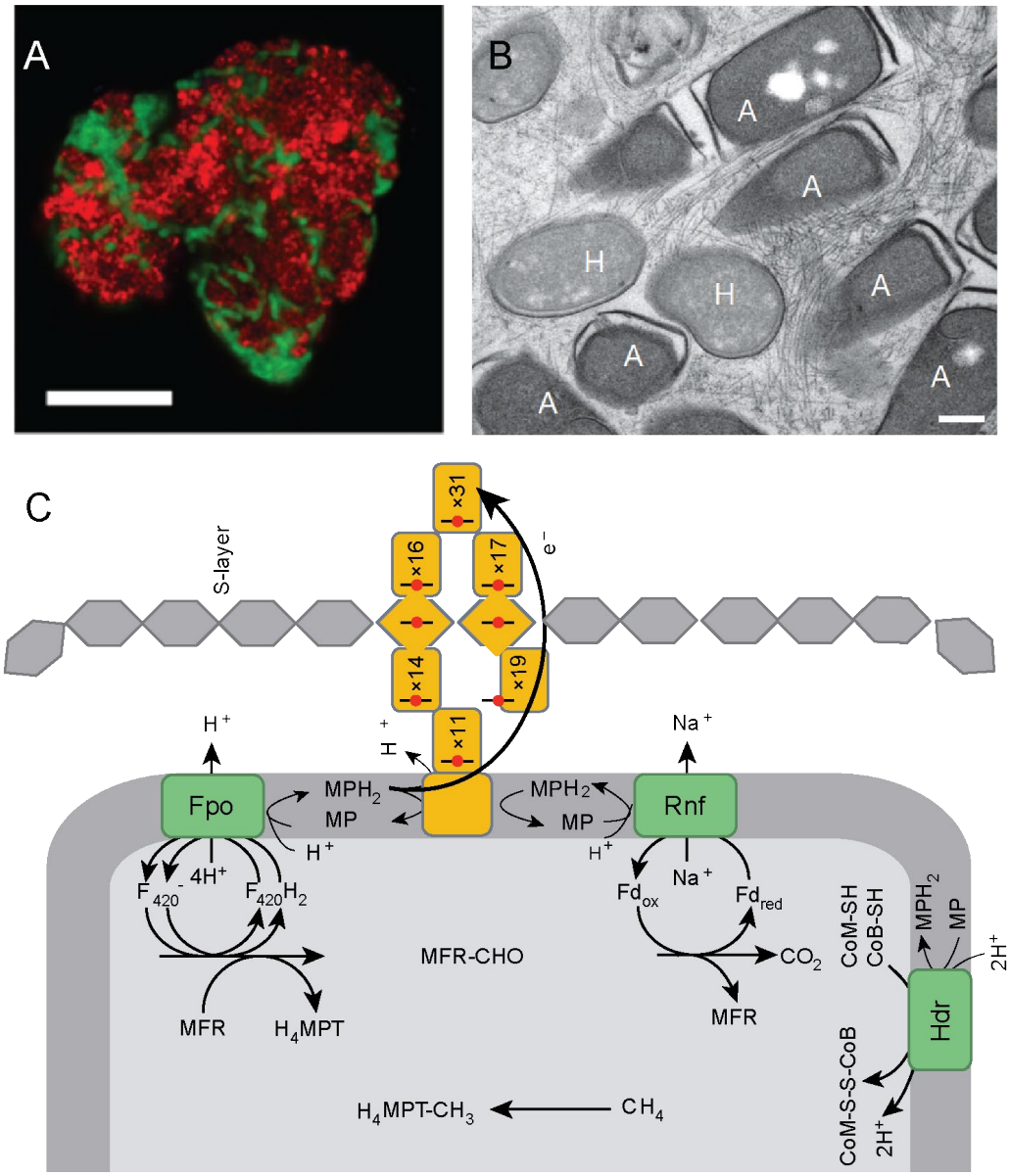

Figure 1-3 Direct electron transfer in AOM consortia and model for energy conservation in ANME-2. **A** Fluorescence micrograph of ANME-2 (red, ANME-2-538) and the sulfate-reducing partner (green, DSS658) in a segregated consortium. Scale bar 10 µm. Transferred from Wegener et al. (2016). **B** Micrograph of a thin section of ANME-1 cells (A) and Hot-Seep-1 cells (H) surrounded by nanowire structures. Scale bar 300 nm. Transferred from (Wegener et al. 2015). **C** Simplified scheme for energy conservation and electron transfer from ANME-2a-c to the sulfate-reducing partner bacterium. Reducing equivalents from methane oxidation are generated through the methyl branch of the Wood–Ljungdahl pathway. They are deposited in the membrane-bound methanophenazine pool (Mp/MpH_2) by the enzymes Hdr, Fpo, and Rnf that oxidize CoM-SH/CoB-SH, $F_{420}H_2$, and Fd_{red}, respectively. CoB-SH and CoM-SH are reduced by MCR and MTR, respectively (reaction not shown). The electrons are transported by multiheme c-type cytochromes (orange) from MpH_2 to the syntrophic partner. Modified from (McGlynn et al. 2015). Image idea adapted from Scheller et al. (2020).

1.5 Chemistry of bacterial anaerobic alkane activation

Alkanes are saturated hydrocarbons. Linear alkanes are called *n*-alkane and have the general formula C_nH_{2n+2}. The similar electronegativity of hydrogen (2.20) and carbon (2.55) causes the formation of non-polar σ-bonds, making the compounds very stable and unreactive at low temperatures (Wilkes et al. 2020). Organisms have to perform a homolytic cleavage of a C-H or a C-C bond to create an alkyl radical that is accessible. For the homolytic cleavage, cells have to invest substantial amounts of energy, known as the homolytic bond dissociation energy (McMillen and Golden 1982). The cleavage of terminal C-H bonds requires more significant energy than the cleavage of subterminal C-H bonds since the required energy is linked to the stability of the formed radical (Wilkes et al. 2020). Therefore, the smallest *n*-alkanes, methane and ethane, which do not contain subterminal C-H bonds, are especially hard to metabolize.

Aerobic alkanotrophs perform an oxygen-dependent radical reaction to hydroxylate the alkanes, forming alcohols as primary intermediates. Such reactions are not possible in the absence of molecular oxygen. Hence, for long time alkanes were believed to be inert in anoxic sediments. The first anaerobic hydrocarbon-degrading bacteria were isolated in the 1990s (Aeckersberg et al. 1991). In the following years, various cultures on various alkanes were established. The so-far best-known pathway for the anaerobic alkane activation is the addition to fumarate. This process has been demonstrated for *n*-alkanes ranging from C_3 to C_{20}. The reaction is mediated by enzymes from the pyruvate formate lyase family called (1-methylalkyl)succinate synthase (MAS) or alternatively alkylsuccinate synthase (ASS) (Grundmann et al. 2008, Callaghan et al. 2010). In this reaction, the alkane is activated at the secondary carbon atom by a glycyl radical reaction in the catalytic subunit masD/assA and then added to fumarate, yielding a (1-methylalkyl) succinate (Rabus et al. 2001). Subsequently, the (1-methylalkyl)succinate is transferred to a coenzyme A (CoA), yielding (1-methylalkyl)succinyl-CoA. (1-methylalkyl)succinyl-CoA is rearranged to (2-methylalkyl)malonyl-CoA and finally decarboxylated to (R)-4-methyloctanoyl-CoA, which is then subjected to ß-oxidation, yielding acetyl-CoA and (R)- 2-methylhexanoyl-CoA (Wilkes and Rabus 2020). In the well-studied hexane oxidation, the 2-methylhexanoyl-CoA would be epimerized and degraded in two more rounds of ß-oxidation to two acetyl-CoA and one propionyl-CoA. This case yields a total of three acetyl-CoA that can be introduced to the TCA cycle and a propionyl-CoA that can be used to regenerate fumarate (Wilkes et al. 2002).

The activation does not happen in all instances at the subterminal carbon. In the case of propane, activation of the terminal carbon was demonstrated with an estimated activation rate of 30% at the terminal and 70% at the subterminal carbon (Kniemeyer et al. 2007, Jaekel et al. 2014). Activation of methane or ethane by addition to fumarate has been suggested, but microorganisms performing such reactions are not known (Thauer and Shima 2008). Alkane activation by addition to fumarate only occurs in the realm of *Bacteria* except for the archaeon *Archaeoglobus fulgidus* strain VC-16 (Khelifi et al. 2014). *Archaeoglobus fulgidus* is a hyperthermophilic sulfate reducer that most likely acquired its alkane oxidation genes via horizontal gene transfer from bacteria. Organisms can perform this process with diverse electron acceptors, including sulfate, nitrate, manganese, and ferric iron, but can also grow under methanogenic conditions (Zengler et al. 1999, Weelink et al. 2009, Widdel et al. 2010, Berdugo-Clavijo and Gieg 2014, Embree et al. 2014). In marine seep environments, sulfate-reducing bacteria of the class Deltaproteobacteria are the key players in alkane activation by addition to fumarate (Acosta-González et al. 2013, Kleindienst et al. 2014, Stagars et al. 2016).

An alternative mechanism for bacterial alkane activation is the anaerobic hydroxylation described for the Deltaproteobacterium *Desulfococcus oleovorans* strain Hxd3 (Aeckersberg et al. 1998). Instead of adding two carbon atoms, like in the addition to fumarate, the n-alkane activation in *D. oleovorans* indicated the carboxylation of one carbon atom (Aeckersberg et al. 1998, Wilkes and Rabus 2020). When growing *D. oleovorans* on alkanes with odd carbon numbers, it produces even-numbered fatty acids (Aeckersberg et al. 1998). In the proposed pathway, a putative alkane hydroxylase (AHY) introduces a hydroxyl group to the subterminal carbon, yielding alkane-2-ols (Heider et al. 2016). Subsequently, the substrate is dehydrogenated and carboxylated at the tertiary carbon and then transferred to coenzyme A, resulting in a 2-acetylalkanoate-CoA that is subjected to ß-oxidation. This pathway needs further research, and little is known about its environmental importance for n-alkane oxidation (Shou et al. 2021).

1.6 Chemistry of archaeal anaerobic alkane activation

Archaea developed a completely different strategy to attack *n*-alkanes. As described before, they use a reverse version of the well-described methanogenesis pathways that can run bi-directional due to the relatively flat energy profile of all of its intermediates (Thauer 2011, Scheller et al. 2020). The overall mechanism is well-studied in methane formation by methanogens, but our experimental data of methanotrophic MCR is still limited. In contrast to

the glycyl radical reaction described for bacterial alkane activation, methanotrophic archaea use organometallic chemistry to cleave methane's particularly strong C-H bond. The crucial enzyme carrying out this initial challenging step is the MCR (Figure 1-4A). The MCR of methanogens and methanotrophs is highly conserved (Knittel and Boetius 2009, Shima et al. 2012, Wagner et al. 2017). Therefore, it was expected that MCR should have the capability to work bi-directional. Indeed, it was shown that MCR from a methanogen is capable of methane oxidation at rates observed for AOM (Scheller et al. 2010).

Investigations of pink Black Sea mats containing relatively homogenous populations of ANME-1 cells led to the first structural description of a methanotrophic MCR (Shima et al. 2012). The acquired ANME-1 MCR crystal structure showed a resolution of 2.1Å, giving detailed insights into the biochemical properties of archaeal methane oxidation (Shima et al. 2012). The ANME-1 MCR complex has a size of 300 kDa, consisting of a compact heterohexameric structure $(\alpha\beta\gamma)_2$ that is virtually identical to methanogenic MCR (Ermler et al. 1997, Grabarse et al. 2001, Scheller et al. 2020). ANME-1 archaea contain a methylthio-F_{430}-cofactor instead of the classical F_{430}-cofactor, but this alteration does not seem crucial for methane activation since ANME-2 cells have a classical F_{430}-cofactor (Figure 1-4B) (Mayr et al. 2008). Also, the active site in ANME-1 MCR is highly similar to the active site of methanogens. The only difference are five additional cysteine residues that might be used as a redox-relay system for the re-activation to the Ni(I) state (Prakash et al. 2014). These observations led to the conclusion that methanogenic and methanotrophic MCR uses the same catalytic mechanism.

MCR with its nickel F_{430}-cofactor can catalyze the challenging methane oxidation by converting methane and the CoM-S-S-CoB disulfide to a methyl-thioether (methyl-S-CoM) and a thiol (HS-CoB) (Figure 1-4C). However, the exact catalytic mechanism of this reaction is still disputed (Scheller et al. 2020). So far, the reaction could not be reproduced in laboratory experiments, but two main theories explain the chemistry behind methane activation by MCR. The first theory suggests a radical mechanism involving a highly endergonic hydrogen atom abstraction by a thiyl radical from methane. A methyl radical would be formed that would immediately combine with a Ni(II)-thiolate to form methyl-CoM and F_{430} in the Ni(I) oxidation state (Pelmenschikov and Siegbahn 2003, Chen et al. 2012). The described reaction is supported by spectroscopic evidence and matches measured kinetic isotope effects (Scheller et al. 2013, Wongnate et al. 2016). The second theory describes an organometallic mechanism in which a non-radical C-H bond activation is initiated by coordinating methane to the nickel center of F_{430} to form an organometallic complex (Scheller et al. 2020). Electron paramagnetic

resonance (EPR) spectroscopic data showed that the cofactor F_{430} is able to form Ni-C, Ni-H, and Ni-S bonds (Harmer et al. 2005, Hinderberger et al. 2006, Yang et al. 2007, Harmer et al. 2008, Sarangi et al. 2009).

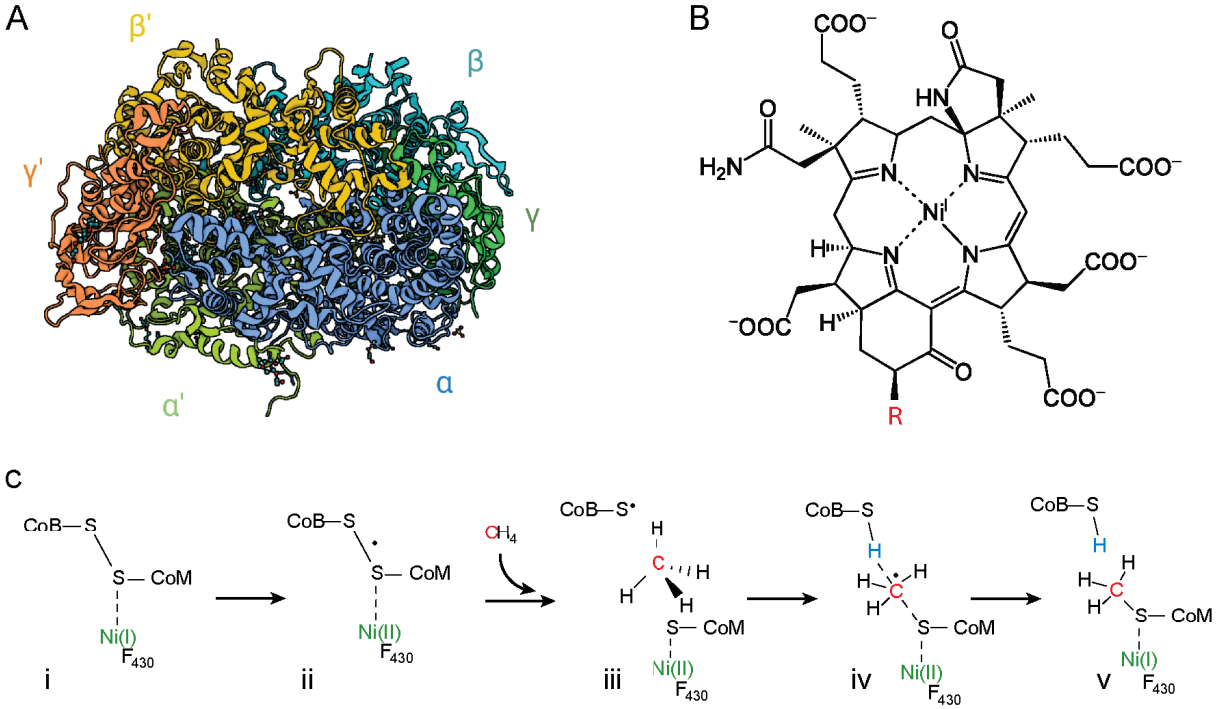

Figure 1-4 Chemistry of MCR-based methane activation. **A** Heterohexameric structure $(\alpha\beta\gamma)_2$ of ANME-1 MCR homolog from Black Sea mats (3SQG)(Shima et al. 2012). **B** Structure of cofactor F_{430}. R =S-CH3 for 17''-methylthio-F_{430} in ANME-1 and R =H for ANME-2 + 3 as found in methanogens (Mayr et al. 2008, Scheller et al. 2020). **C** Potential reaction of the methyl radical mechanism adapted in reverse from Shima et al. (2020). The precise process is still disputed.

1.7 Microbes involved in anaerobic oxidation of non-methane alkanes

AOM appears to be the primary metabolic process in anoxic seep sediments, but in seeps that transport complex hydrocarbons, sulfate reduction rates can exceed methane oxidation rates by more than two magnitudes (Joye et al. 2004, Omoregie et al. 2009, Orcutt et al. 2010, Bowles et al. 2011). Porewater profiles from complex, hydrocarbon-rich sediments indicate that next to methane, short-chain alkanes, such as ethane, propane, and butane, are depleted in the SMTZ (Quistad and Valentine 2011, Bose et al. 2013, Laso-Pérez et al. 2019). The mitigation of non-methane fluxes in seep sediments has been observed earlier, but knowledge about microbial processes of anaerobic short-chain alkane oxidation was limited. Some sulfate-reducing bacteria (SRB) from the Deltaproteobacteria can anaerobically oxidize short-chain alkanes (C_2 – C_5) or longer hydrocarbons (Kniemeyer et al. 2007, Widdel and Grundmann 2010, Bose et al. 2013). These bacteria use the addition to fumarate by the (1-methylalkyl)succinate synthase (MAS) for alkane activation. A phylogenetic analysis of the

catabolic subunit masD from different seep sites revealed many bacterial alkanotrophs (Stagars et al. 2016). Enrichment-based experiments with sediments from the Amon mud volcano and the Guaymas Basin showed a fast bacterial response to butane and dodecane (Kleindienst et al. 2014). The study concluded that these alkane oxidizers are the key alkane degraders at marine seeps (Kleindienst et al. 2014). However, most studies did not consider the potential role of *Archaea* in anaerobic non-methane alkane degradation at marine seeps. Until recently, the belief was that MCR-based alkane activation is limited to C_1-compounds.

The MCR is a highly conserved enzyme and structural analyses revealed only minor differences between methanogenic and methanotrophic MCR, including a methylthio-F_{430} cofactor variant in ANME-1 (Shima et al. 2012, Wagner et al. 2017). However, all known MCR structures' folding and active site architecture is almost identical (Wagner et al. 2017). This high degree of conservation reflects in the catabolic subunit alpha (McrA) protein sequence, a commonly used phylogenetic marker for these organisms (Knittel and Boetius 2009). Recently, a new type of highly divergent MCR was detected in MAGs of the phylum Bathyarchaeota (Figure 1-5) (Evans et al. 2015). These MAGs were the first archaea outside the Euryarchaeota phylum harboring *mcr* genes. The original study suggested that this new MCR type catalyzes methane oxidation (Evans et al. 2015). Soon after, Laso-Pérez et al. (2016) discovered similar divergent MCR types in MAGs of *Ca.* Syntrophoarchaeum, in samples retrieved from a butane-oxidizing culture. *Ca.* Syntrophoarchaeum branches deeply in the Euryarchaeota, adjacent to the order of *Ca.* Methanophagales, forming the order of *Ca.* Syntrophoarchaeales (Adam et al. 2017). Metabolite analysis revealed the formation of butyl-CoM in this culture, indicating that the novel MCR type is responsible for butane activation (Laso-Pérez et al. 2016). Both described *Ca.* Syntrophoarchaeum genomes contain four copies of divergent MCR, all branching far off the canonical MCRs and are closest related to Bathyarchaeota MCR sequences (Laso-Pérez et al. 2016). A third unclassified member of the *Ca.* Syntrophoarchaeales order was discovered recently, branching far off the two described species, *Ca.* S. caldarius and *Ca.* S. butanivorans (Dong et al. 2020). This *Ca.* Syntrophoarchaeales member only contains two non-canonical MCR sequences with unknown substrate range (Dong et al. 2020).

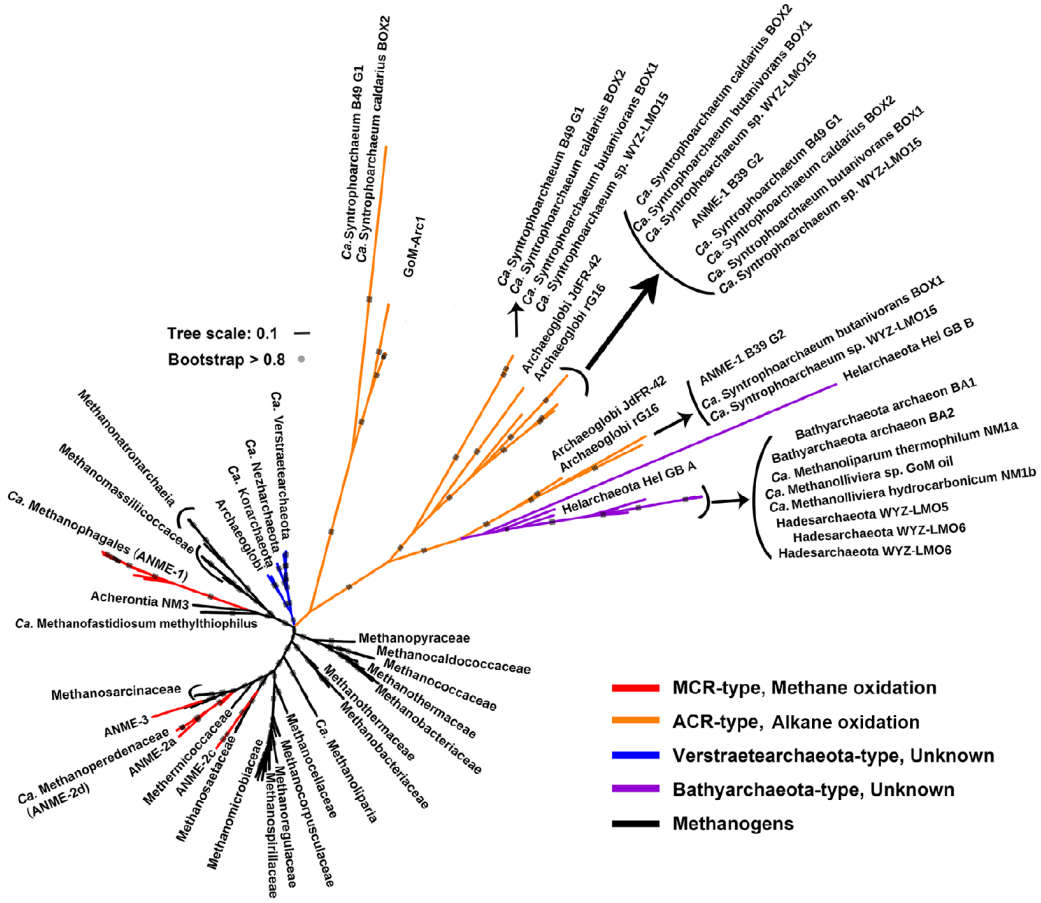

Figure 1-5 Current phylogenetic tree with McrA amino acid sequences from canonical and non-canonical MCR-homologs. Colored branches indicate predicted or experimentally shown substrate as following: Methane oxidation (red), non-methane alkane oxidation (orange), unknown function Verstraetearchaeota-type (blue), unknown Bathyarchaeota-type (purple), and methanogenesis (black). Figure modified from Wang et al. (2021).

1.8 MCR diversity and the fate of ethane

In recent years, the non-canonical MCR type was discovered in many additional MAGs, suggesting a high diversity and importance of *Archaea* for the anaerobic oxidation of non-methane hydrocarbons (Figure 1-5). New non-canonical MCR sequences were discovered in *Ca.* Polytropus marinifundus (Archaeoglobi) from deep subseafloor sediment samples, retrieved from the Juan de Fuca Ridge, Pacific, and in a Hadesarchaeon from the Jinze Hot Spring, Yunnan, China (Boyd et al. 2019, Wang et al. 2019). Additionally, Helarchaeota from the Asgard superphylum contain non-canonical MCR sequences and possibly play a role in anaerobic hydrocarbon oxidation in deep sediments (Zhang et al. 2021). Hydrocarbon oxidizing archaea are not limited to short-chain alkanes but can likely also activate longer hydrocarbon chains. The class *Ca.* Methanoliparia (former DC06 cluster) contains two MCR copies, a canonical MCR and a non-canonical MCR closest related to MCR sequences of Bathyarchaeota and Hadesarchaeota (Borrel et al. 2019, Laso-Pérez et al. 2019). A

disproportionation of alkanes has been proposed for *Ca.* Methanoliparia, where the non-canonical MCR is responsible for activating a long-chain alkane, and the canonical MCR would act as classical methanogenic MCR, releasing methane (Laso-Pérez et al. 2019). *Ca.* Methanoliparia cells have been found in diverse oil-contaminated anoxic environments and were localized with in-situ hybridization in or on oil droplets without apparent partner cells. So far, no active culture a *Ca.* Methanoliparia could be established, and their proposed pathway remains to be confirmed.

Despite the progress made in understanding microbial oxidation of non-methane alkanes, the fate of the second most abundant alkane ethane remained elusive. Ethane has been described as "a hydrocarbon with essentially unexplored microbiology and biochemistry under anoxic conditions" (Widdel and Grundmann 2010). The only bacterial culture capable of anaerobic ethane oxidation was a slurry incubation with 16S rRNA sequences linked to the deltaproteobacterial strain Bus5 (Kniemeyer et al. 2007, Bose et al. 2013). Ethane can be measured at most seep sites in substantial amounts, and its origin is assumed to be thermogenic. Recently, MAGs of the GoM-Arc1 clade that contain a single non-canonical MCR homolog were described in metagenomic studies (Dombrowski et al. 2017, Borrel et al. 2019). This MCR homolog branches far off other non-canonical MCRs, indicating the specialization on an alkane substrate other than methane or butane (Figure 1-5) (Laso-Pérez et al. 2019). In contrast to *Ca.* Syntrophoarchaeum, GoM-Arc1 genomes contain no beta-oxidation pathway, which leads to the prediction that these organisms might thrive on ethane (Borrel et al. 2019). GoM-Arc1 16S rRNA gene sequences appear at high frequencies at various seep sites and often co-occur with ANME archaea, suggesting that they have an essential role in seep sediment communities (Lloyd et al. 2006, Orcutt et al. 2010, Dowell et al. 2016). As an anaerobic ethane oxidizer, archaea from the GoM-Arc1 clade would fill a significant gap in our understanding of seep environments and the mechanistic of MCR-based alkane activation.

1.9 Aims and hypotheses

Geochemical data strongly suggest that microbial ethane oxidation occurs within sediments, but no organisms performing such a process have been discovered at the start of my thesis. The overall aim of my thesis was to culture such organisms from gas-rich sediments and analyse their ecophysiology. Based on this aim, my thesis followed these hypotheses:

H1: Thermophilic variants of ethane oxidizing archaea can be cultured from hydrothermally heated sediments of the Guaymas Basin.

The Guaymas Basin hydrothermal vent site is ideal for the cultivation of anaerobic alkane oxidizers. Diverse hydrocarbons, including short-chain alkanes, migrate to the heated sediment surface, and the first centimeters of the sediment harbor a dense thermophilic alkanotrophic community (Teske and Carvalho 2020). These conditions make the presence of an ethane oxidizing strain at this site likely. Additionally, MAGs of the suspected ethane oxidizing clade GoM-Arc1 have been recovered from this site (Dombrowski et al. 2017). Thermophilic ANME archaea have higher activities and shorter doubling times than mesophilic, cold water adapted ANME (Holler et al. 2011, Wegener et al. 2016). Assuming an MCR homolog-based pathway for the anaerobic oxidation of ethane, a thermophilic strain would allow faster cultivation and consequently higher biomass production allowing follow-up experiments.

H2: Ethane oxidizing archaea thrive in partnerships with sulfate-reducing bacteria. The activity of individual cells might be a function of the proximity of these partners and could be visualized by the expression of key genes in the organisms.

In consortia of ethane oxidizing archaea and their SRB partner, similar to many AOM consortia, the partner organisms are spatially segregated. This organization is not well understood and counterintuitive, considering their obligate syntrophy. We will use a direct FISH method to target the mRNA of the key gene for anaerobic oxidation of ethane. The direct labeling will allow dynamic visualization of expression-based activity patterns in the archaeal monospecies aggregates within the consortia and correlate the signal intensity to the expression level in the archaeal cells. Furthermore, we could investigate the influence of the distance to the bacterial-archaeal interface on archaeal activity.

H3: Archaea activate ethane with a specific MCR homolog. The MCR homolog will have unique features that will help understand which structural changes allow for the use of ethane instead of methane.

Once we establish a thermophilic culture performing anaerobic oxidation of ethane, we would have the opportunity to harvest enough biomass to explore this new process on enzymatic levels. We aim for the crystallization of the key gene for anaerobic oxidation of

ethane, the MCR homolog. A crystal structure of the enzyme with high diffraction would allow a detailed study of changes in the enzyme. The first successful visualization of a non-canonical MCR homolog would revolutionize our understanding of MCR specificity towards alkanes.

1.10 Contribution to manuscripts

Chapter 2: "Candidatus Ethanoperedens," a Thermophilic Genus of Archaea Mediating the Anaerobic Oxidation of Ethane

Cedric Jasper Hahn, Rafael Laso-Pérez, Francesca Vulcano, Konstantinos-Marios Vaziourakis, Runar Stokke, Ida Helene Steen, Andreas Teske, Antje Boetius, Manuel Liebeke, Rudolf Amann, Katrin Knittel, Gunter Wegener

Published in: mBio Volume 11 • Number 2 • 28 April 2020. DOI: 10.1128/mBio.00600-20

Author contributions: C.J.H., K.K., and G.W. designed the research. A.T. and G.W. retrieved the original Guaymas Basin sediment sample. F.V., K.-M.V., R.S., I.H.S., and A.B. retrieved additional samples. C.J.H. and G.W. performed the cultivation, physiology, and isotope experiments. C.J.H., F.V., K.-M.V., and K.K. performed fluorescence microscopy. C.J.H., M.L., and G.W. performed metabolite analysis. C.J.H., R.L.-P., R.A., K.K., and G.W. performed metagenomic and phylogenetic analyses and developed the metabolic model, C.J.H. and G.W. wrote the manuscript with contributions from all coauthors.

Chapter 3: Spatial resolution of ethyl-coenzyme M reductase gene expression in ethane-oxidizing microbial consortia

Cedric J. Hahn, Andreas Ellrott, Gunter Wegener, Rudolf Amann, and Katrin Knittel

Manuscript in preparation.

Author contributions: C.J.H., R.A. and K.K. designed the research. C.J.H. and G.W. performed the cultivation. C.J.H. and K.K. designed the mRNA-FISH probes and performed fluorescence microscopy. C.J.H. conducted mRNA-FISH experiments. C.J.H., A.E. and K.K. prepared the semi-automated signal counting and signal analysis. C.J.H., G.W. and K.K. wrote the manuscript with contributions from all coauthors.

Chapter 4: Crystal structure of a key enzyme for anaerobic ethane activation

Cedric J. Hahn*, Olivier N. Lemaire*, Jörg Kahnt, Sylvain Engilberge, Gunter Wegener, Tristan Wagner

* Authors contributed equally to the work.

Published in: Science 373 (6550), 118-121, July 2021. DOI: 10.1126/science.abg1765

Author contributions: C.J.H., O.N.L., G.W., and T.W. designed the research. C.J.H., O.N.L., and G.W. performed cultivation and culture experiments. C.J.H., O.N.L., and T.W. purified and crystallized the proteins. S.E., O.N.L., and T.W. collected x-ray data and built the models. O.N.L. and T.W. analyzed the structures. S.E. and T.W. performed and analyzed the xenon-pressurization experiments. J.K., O.N.L., and T.W. analyzed the F_{430} cofactor and posttranslational modifications. C.J.H., O.N.L., G.W., and T.W. interpreted the data and wrote the paper, with contributions and final approval of all co-authors.

Additional contribution

Anaerobic Degradation of Non-Methane Alkanes by "*Candidatus* Methanoliparia" in Hydrocarbon Seeps of the Gulf of Mexico

Rafael Laso-Pérez, Cedric Hahn, Daan M. van Vliet, Halina E. Tegetmeyer, Florence Schubotz, Nadine T. Smit, Heiko Sahling, Gerhard Bohrmann, Antje Boetius, Katrin Knittel, Gunter Wegener

Published in: mBio Volume 10 • Number 4 • 27 August 2019. DOI: 10.1128/mBio.01814-19

G.W., G.B., H.S., and F.S. retrieved the original samples. R.L.-P. and G.W. designed the research experiments. G.W., F.S., N.T.S., and T.P. carried out the geochemical analysis. K.K. and C.H. designed the CARD-FISH probes and performed microscopy. H.E.T. prepared and sequenced the DNA libraries. R.L.-P. and D.M.V.V. performed 16S rRNA gene tag sequencing analysis. R.L-P. performed metagenomic analyses. R.L.-P., G.W., and A.B. developed the metabolic model and wrote the manuscript, with contributions from all coauthors

Chapter 2

"*Candidatus* Ethanoperedens," a Thermophilic Genus of Archaea Mediating the Anaerobic Oxidation of Ethane

Cedric Jasper Hahn[a], Rafael Laso-Pérez[a,b,c], Francesca Vulcano[d], Konstantinos-Marios Vaziourakis[a,e], Runar Stokke[d], Ida Helene Steen[d], Andreas Teske[f], Antje Boetius[a,b,c], Manuel Liebeke[a], Rudolf Amann[a], Katrin Knittel[a], Gunter Wegener[a,b,c]

[a]Max-Planck Institute for Marine Microbiology, 28359 Bremen, Germany
[b]MARUM, Center for Marine Environmental Sciences, University of Bremen, Bremen, Germany
[c]Alfred Wegener Institute Helmholtz Center for Polar and Marine Research, 27570 Bremerhaven, Germany
[d]K.G Jebsen Centre for Deep Sea Research and Department of Biological Sciences
[e]University of Patras, Patras, Greece
[f]The University of North Carolina at Chapel Hill, Chapel Hill, NC, USA

Published in:
mBio Volume 11 • Number 2 • 28 April 2020
DOI: 10.1128/mBio.00600-20

Received: 13 March 2020
Accepted: 23 March 2020
Published online: 21 April 202

2.1 Abstract

Cold seeps and hydrothermal vents deliver large amounts of methane and other gaseous alkanes into marine surface sediments. Consortia of archaea and partner bacteria thrive on the oxidation of these alkanes and its coupling to sulfate reduction. The inherently slow growth of the involved organisms and the lack of pure cultures have impeded the understanding of the molecular mechanisms of archaeal alkane degradation. Here, using hydrothermal sediments of the Guaymas Basin (Gulf of California) and ethane as the substrate, we cultured microbial consortia of a novel anaerobic ethane oxidizer, "*Candidatus* Ethanoperedens thermophilum" (GoM-Arc1 clade), and its partner bacterium "*Candidatus* Desulfofervidus auxilii," previously known from methane-oxidizing consortia. The sulfate reduction activity of the culture doubled within one week, indicating a much faster growth than in any other alkane-oxidizing archaea described before. The dominance of a single archaeal phylotype in this culture allowed retrieval of a closed genome of "*Ca.* Ethanoperedens," a sister genus of the recently reported ethane oxidizer "*Candidatus* Argoarchaeum." The metagenome-assembled genome of "*Ca.* Ethanoperedens" encoded a complete methanogenesis pathway including a methyl-coenzyme M reductase (MCR) that is highly divergent from those of methanogens and methanotrophs. Combined substrate and metabolite analysis showed ethane as the sole growth substrate and production of ethyl-coenzyme M as the activation product. Stable isotope probing demonstrated that the enzymatic mechanism of ethane oxidation in "*Ca.* Ethanoperedens" is fully reversible; thus, its enzymatic machinery has potential for the biotechnological development of microbial ethane production from carbon dioxide.

2.2 Importance

In the seabed, gaseous alkanes are oxidized by syntrophic microbial consortia that thereby reduce fluxes of these compounds into the water column. Because of the immense quantities of seabed alkane fluxes, these consortia are key catalysts of the global carbon cycle. Due to their obligate syntrophic lifestyle, the physiology of alkane-degrading archaea remains poorly understood. We have now cultivated a thermophilic, relatively fast-growing ethane oxidizer in partnership with a sulfate-reducing bacterium known to aid in methane oxidation and have retrieved the first complete genome of a short-chain alkane-degrading archaeon. This will greatly enhance the understanding of nonmethane alkane activation by noncanonical methyl-coenzyme M reductase enzymes and provide insights into additional metabolic steps and the mechanisms underlying syntrophic partnerships. Ultimately, this knowledge could lead

to the biotechnological development of alkanogenic microorganisms to support the carbon neutrality of industrial processes.

Keywords

alkane degradation, archaea, syntrophy, methyl-coenzyme M reductase, model organism, hydrothermal vents

2.3 Introduction

In deep marine sediments, organic matter undergoes thermocatalytic decay, resulting in the formation of natural gas (methane to butane) and crude oil. If not capped, the gas fraction will rise toward the sediment surface due to buoyancy, porewater discharge, and diffusion. Most of the gas is oxidized within the sediments coupled to the reduction of the abundant electron acceptor sulfate (Hinrichs and Boetius 2002, Reeburgh 2007). Responsible for the anaerobic oxidation of alkanes are either free-living bacteria or microbial consortia of archaea and bacteria. Most free-living bacteria use alkyl succinate synthases to activate the alkane, forming succinate-bound alkyl units as primary intermediates (Rabus et al. 2001). Usually, these alkanes are completely oxidized, and this process is coupled to sulfate reduction in the same cells, as has been shown, for example, in the deltaproteobacterial butane-degrading strain BuS5 (Kniemeyer et al. 2007). However, alkane oxidation in seafloor sediments is to a large extent performed by dual species consortia of archaea and bacteria (Boetius et al. 2000, Chen et al. 2019). As close relatives of methanogens, the archaea in these consortia activate alkanes as thioethers and completely oxidize the substrates to CO_2. The electrons released during alkane oxidation are consumed by the sulfate-reducing partner bacteria.

The anaerobic methane-oxidizing archaea (ANME) activate methane using methyl-coenzyme M (CoM) reductases (MCRs) that are highly similar to those of methanogens, forming methyl-coenzyme M as the primary intermediate (Shima et al. 2012). The methyl group is oxidized via a reversal of the methanogenesis pathway (Hallam et al. 2004). Thermophilic archaea of the genus "*Candidatus* Syntrophoarchaeum" thrive on the oxidation of butane and propane. In contrast to ANME, they contain four highly divergent MCR variants, which generate butyl and propyl-coenzyme M (CoM) as primary intermediates (Laso-Pérez et al. 2016). Based on genomic and transcriptomic evidence, the CoM-bound alkyl units are transformed to fatty acids and oxidized further via beta-oxidation. The reactions transforming the CoM-bound alkyl units to CoA-bound fatty acids and the enzymes performing

such reactions are so far unknown. The CoA-bound acetyl units are completely oxidized in the Wood-Ljungdahl pathway including the upstream part of the methanogenesis pathway. In hydrogenotrophic methanogens, the enzymes of this pathway are used to reduce CO_2-forming methyl-tetrahydromethanopterin for methanogenesis and for biomass production. In "*Ca.* Syntrophoarchaeum," this pathway is used in reverse direction for the complete oxidation of acetyl-CoA. Both the thermophilic ANME-1 and "*Ca.* Syntrophoarchaeum" form dense consortia with their sulfate-reducing partner bacterium "*Candidatus* Desulfofervidus" (HotSeep-1 clade) (Holler et al. 2011, Krukenberg et al. 2016). The transfer of reducing equivalents between the alkane-oxidizing archaea and their partners is likely mediated by pilus-based nanowires and cytochromes produced by the two consortial partners (Walker et al. 2018). For a critical view on electron transfer in anaerobic oxidation of methane (AOM) consortia, see reference (Walker et al. 2018).

Sulfate-dependent ethane oxidation has been described multiple times in slurries of marine sediments (Kniemeyer et al. 2007, Adams et al. 2013, Bose et al. 2013). The first functional description of this process was based on a cold-adapted culture derived from Gulf of Mexico sediments (Chen et al. 2019). In this culture, "*Candidatus* Argoarchaeum" (formerly known as GoM-Arc1 clade) activates ethane with the help of divergent MCRs that are phylogenetically placed on a distinct branch next to those of "*Ca.* Syntrophoarchaeum." Based on the presence of all enzymes of the Wood-Ljungdahl pathway that can be used for acetyl-CoA oxidation, it has been suggested that the CoM-bound ethyl groups are transferred to CoA-bound acetyl units. The required intermediates for this reaction mechanism are so far unknown (Chen et al. 2019). "*Ca.* Argoarchaeum" forms unstructured consortia with yet-unidentified bacterial partners and grows slowly with substrate turnover rates comparable to AOM (Chen et al. 2019). Additional metagenome-assembled genomes (MAGs) of the GoM-Arc1 clade derived from the Guaymas Basin and the Gulf of Mexico have similar gene contents, suggesting that these GoM-Arc1 archaea are ethane oxidizers (Dombrowski et al. 2017, Borrel et al. 2019).

To date, the understanding of short-chain alkane-metabolizing archaea mainly relies on comparison of their genomic information with those of methanogens that are well characterized with regard to their enzymes. Due to the slow growth of the alkane-oxidizing archaea and the resulting lack of sufficient biomass, specific biochemical traits remain unknown. For instance, the structural modifications of noncanonical MCRs or the proposed transformation of the CoM-bound alkyl to CoA-bound acetyl units in the short-chain alkane degraders has not been proven. Here, we describe a faster-growing, thermophilic ethane-oxidizing culture from

sediments of the Guaymas Basin. Metagenomic analyses of Guaymas Basin sediments revealed a great diversity of potential alkane degraders with divergent MCR enzymes (Laso-Pérez et al. 2016, Dombrowski et al. 2018). With ethane as sole energy source and sulfate as electron acceptor, we obtained well-growing meso- and thermophilic ethane-degrading enrichment cultures from these sediments. Their low strain diversity makes them particularly suitable for assessing the pathways of the anaerobic oxidation of ethane.

Taxonomy of "*Candidatus* Ethanoperedens thermophilum." Etymology: *ethano* (new Latin), pertaining to ethane; *peredens* (Latin), consuming, devouring; *thermophilum* (Greek), heat-loving. The name implies an organism capable of ethane oxidation at elevated temperatures. Locality: enriched from hydrothermally heated, hydrocarbon-rich marine sediment of the Guaymas Basin at 2,000 m water depth, Gulf of California, Mexico. Description: anaerobic, ethane-oxidizing archaeon, mostly coccoid, about 0.7 μm in diameter, forms large irregular cluster in large dual-species consortia with the sulfate-reducing partner bacterium "*Candidatus* Desulfofervidus auxilii."

2.4 Results and discussion

2.4.1 Establishment of meso- and thermophilic ethane-oxidizing enrichment cultures.

Sediments were sampled from the gas- and oil-rich sediments covered by sulfur-oxidizing mats of the Guaymas Basin. From these sediments and artificial seawater medium, a slurry was produced under anoxic conditions and distributed into replicate bottles. These bottles were supplied with an ethane headspace (2 atm) and incubated at 37°C and 50°C. Additional growth experiments were performed with methane, and controls were set up with a nitrogen atmosphere. As a measure of metabolic activity, sulfide concentrations were tracked over time (for further details, see Materials and Methods). Both methane and ethane additions resulted in the formation of 15 mM sulfide within 4 months. Nitrogen controls produced only little sulfide (<2 mM) that likely corresponds to the degradation of alkanes and organic matter from the original sediment. Subsequent dilution (1:3) of the ethane and methane cultures and further incubation with the corresponding substrates showed faster, exponentially increasing sulfide production in the ethane culture, suggesting robust growth of the ethane-degrading community (Figure 2-1A). After three consecutive dilution steps, virtually sediment-free cultures were obtained. These cultures produced approximately 10 mM sulfide in 8 weeks. All further experiments were conducted with the faster-growing 50°C culture (Ethane50).

Sequencing of metagenomes, however, was done on both, the 50°C and 37°C (Ethane37) culture.

A stoichiometric growth experiment with the Ethane50 culture (Figure 2-1B) showed that ethane was completely oxidized while sulfate was reduced to sulfide according to the formula $4\ C_2H_6 + 7\ SO_4^{2-} \rightarrow 8\ HCO_3^- + 7\ HS^- + 4\ H_2O + H^+$.

An experiment tracking the exponential development of sulfide over time suggested doubling times of only 6 days at low sulfide concentrations of <5 mM (Figure 2-1B), which is substantially faster than estimated for thermophilic AOM consortia, with about 60 days (Holler et al. 2011), and also faster than the cold-adapted anaerobic ethane-oxidizing cultures (Chen et al. 2019). Sulfide concentrations over 5 mM seemed to suppress activity and growth of the ethane-oxidizing microorganisms (Figure 2-1C). Hence, flowthrough bioreactors could be beneficial to increase biomass yields of anaerobic ethane degraders.

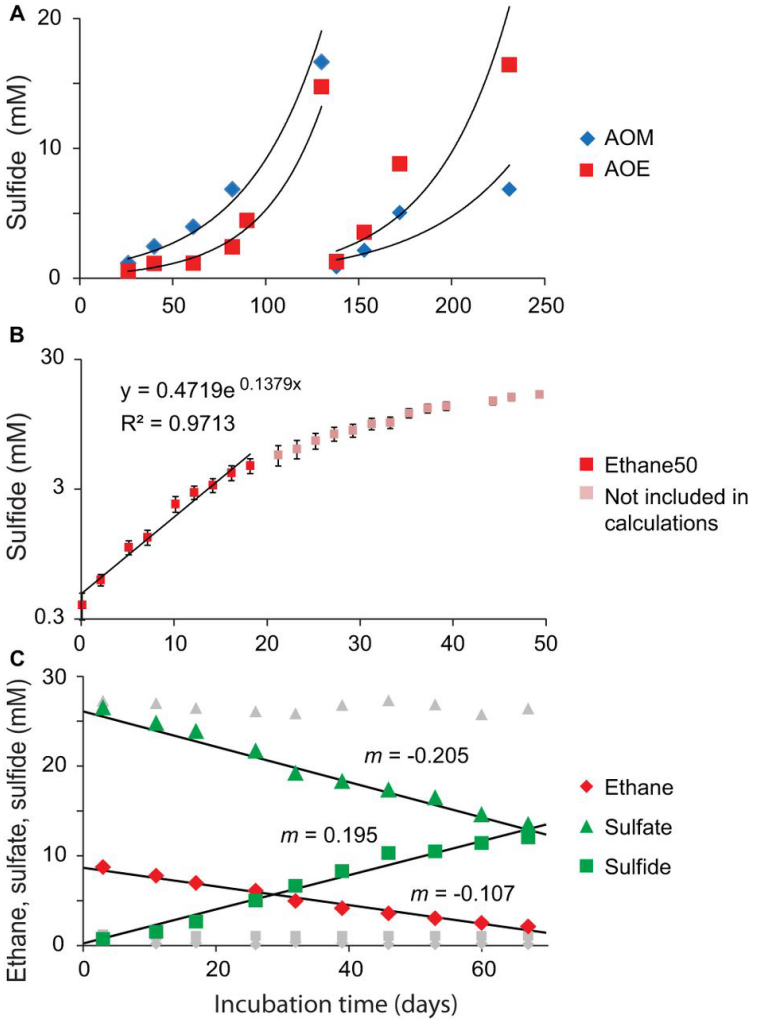

Figure 2-1 Cultivation and stoichiometry test of the Ethane50 culture. (A) Rates of methane-dependent (blue) and ethane-dependent (red) sulfide production in sediments of the Guaymas Basin incubated at 50°C. (B) Determination of activity doubling times in anaerobic ethane-oxidizing culture. Logarithmic y axis with sulfide production shows a decrease in activity at 3 mM sulfide and estimated activity doubling times in low sulfide concentrations of 6 to 7 days. (C) Development of ethane (diamonds), sulfate (triangles), and sulfide (squares) concentrations in the Ethane50 culture. Gray symbols show corresponding concentrations measured in control incubations without ethane addition (data from 1 of 3 replicate incubations; for complete data, see Table S2-8). The ratios of the slopes of sulfate and sulfide to ethane (1.92 and 1.82, respectively) are close to the stoichiometric ratios of sulfate reduction and ethane oxidation. The small offset may relate to biomass production and sampling artifacts.

2.4.2 Microbial composition of the Ethane50 culture.

Amplified archaeal and bacterial 16S rRNA genes of the original sediment and early, still sediment-containing cultures (150 days of incubation) were sequenced to track the development of microbial compositions over time (for primers, see Table S2-1 in the supplemental material). The original sediment contained large numbers of ANME-1 and the putative partner bacterium "*Ca.* Desulfofervidus." The AOM culture became further enriched in ANME-1 archaea and "*Ca.* Desulfofervidus," whereas in the Ethane50 culture the GoM-Arc1 clade increased from <0.1% in the original sediment to roughly 35% of all archaea (Figure 2-2A). Notably, the relative abundance of "*Ca.* Desulfofervidus" increased also in the

Ethane50 culture. This indicates that "*Ca.* Desulfofervidus" was also involved as a partner bacterium in the thermophilic ethane culture.

To visualize the cells involved in the anaerobic oxidation of ethane (AOE), oligonucleotide probes specific for the GoM-Arc1 clade and "*Ca.* Desulfofervidus" were applied on the Ethane50 culture using catalyzed reporter deposition fluorescence in-situ hybridization (CARD-FISH; for probes, see Table S2-1). The Ethane50 culture contained large and tightly packed consortia with sizes of up to 40 µm in diameter formed by GoM-Arc1 and "*Ca.* Desulfofervidus" cells (Figure 2-2D and E). In the consortia, archaea and bacteria grew spatially separated. These large consortia apparently develop from small but already dense consortia found in the inoculate, similar to what was found for cold-adapted AOM consortia (Nauhaus et al. 2007). Such a separation of the partner organisms is also characteristic for consortia in the butane-degrading culture (Laso-Pérez et al. 2016) and for most AOM consortia (Knittel and Boetius 2009). In contrast, in thermophilic AOM consortia of ANME-1 and "*Ca.* Desulfofervidus," the partner cells appear well mixed (Wegener et al. 2016). The Ethane50 culture differs from the cold-adapted ethane-oxidizing culture, in which "*Ca.* Argoarchaeum" forms rather loose assemblages with yet-uncharacterized bacteria (Chen et al. 2019).

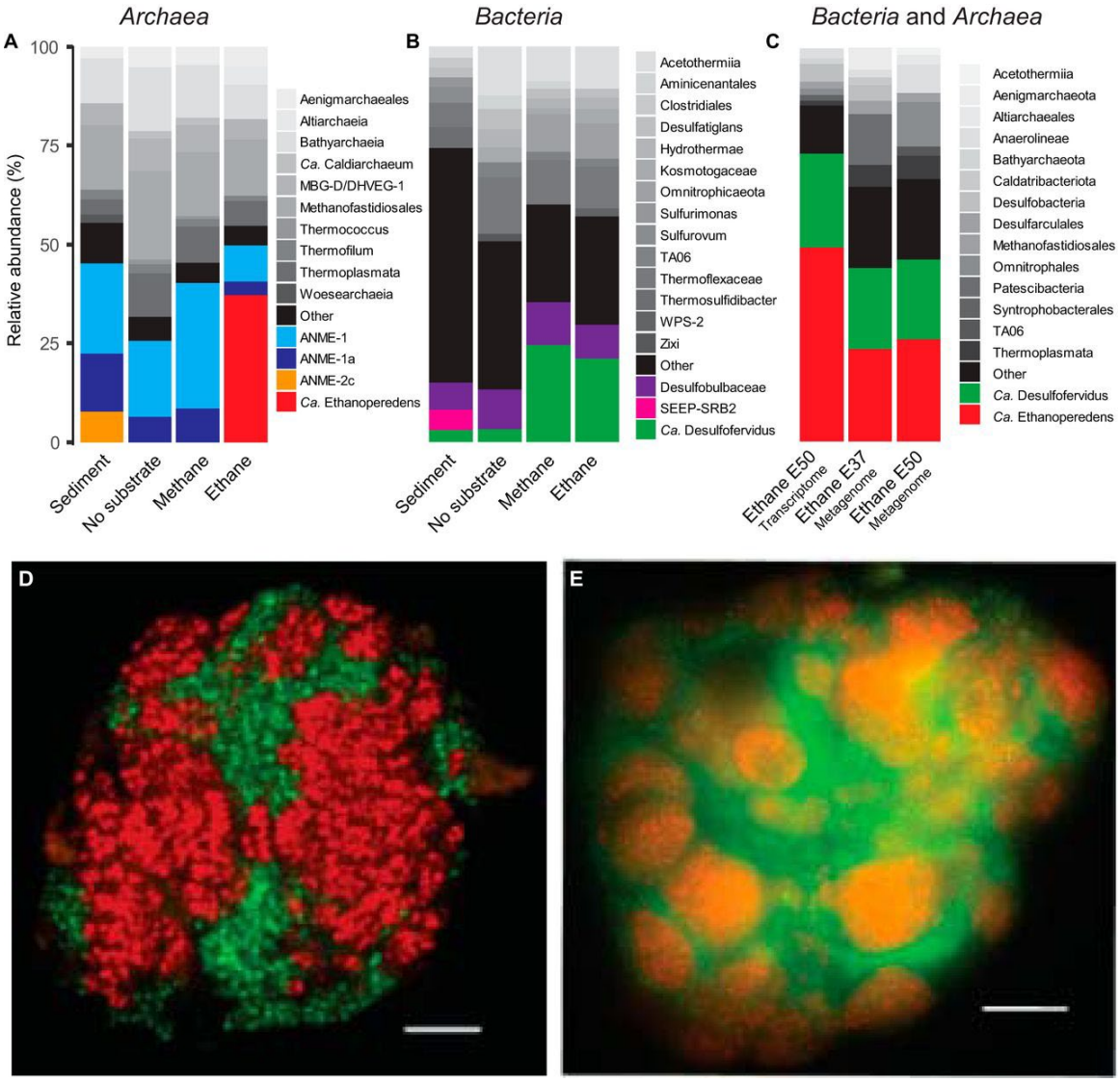

Figure 2-2 Microbial composition of the Ethane50 culture. (A and B) Relative abundance of phylogenetic clades of archaea (A) and bacteria (B) based on 16S rRNA gene amplicon sequencing present in the inoculated sediment, and in cultures with no substrate, with methane and ethane after 150 days of incubation. (C) Relative abundance of active microbial groups based on 16 rRNA fragments recruited from the genome of Ethane37 and Ethane50 after 2.5 years of incubation and the transcriptome of the Ethane50 culture after 1 year of incubation with ethane. (D and E) Laser-scanning micrograph (D) and epifluorescence micrograph (E) of microbial consortia stained with probes specific for the GoM-Arc1 clade (red, Alexa 594) and "*Ca.* Desulfofervidus" (green, Alexa 488) in the Ethane50 culture. Bar, 10 µm.

To analyze the metabolic potential of the microorganisms involved in ethane degradation, Ethane37 and Ethane50 cultures were subjected to transcriptomic and genomic analysis. The 16S rRNA sequences extracted from the shotgun RNA reads of the Ethane50 culture were strongly dominated by GoM-Arc1 (50%) and "*Ca.* Desulfofervidus" (20%; Figure 2-2C), supporting a crucial role of these two organisms in thermophilic ethane degradation. Long-read DNA sequencing for the Ethane50 culture resulted in a partial genome of GoM-Arc1 with 76.2% completeness (GoM-Arc1_E50_DN), whereas by applying this approach to the Ethane37 culture, we obtained a closed genome of the GoM-Arc1 archaeon (GoM-Arc1_E37). The two GoM-Arc1 genomes share an average nucleotide identity (ANI) of 98%; hence, a

complete consensus genome for Ethane50 (GoM-Arc1_E50) was obtained by mapping long reads of the Ethane50 culture on the closed GoM-Arc1_E37 genome (see Materials and Methods and Table S2-2). GoM-Arc1_E50 had a size of 1.92 Mb and a GC content of 46.5%. To assess the genomic diversity of archaea of the GoM-Arc1 clade, additionally a MAG of GoM-Arc1 from the Loki's Castle hydrothermal vent field (GoM-Arc1-LC), with a completeness of 68% and eight single-cell amplified genomes (SAGs) from different cold seeps and different completenesses (10% to 59%) were retrieved (Table S2-4). The MAG GoM-Arc1-LC and the eight single cells have an average nucleotide identity (ANI) of over 90%, suggesting that they belong to the same or closely related species. The 16S rRNA gene identity is in the range of 99.5%, supporting a definition as same species, and shows that the same species of GoM-Arc1 can be found in diverse seep sites (Table S2-2 and Figure S2-1). Together with several MAGs of the GoM-Arc1 clade archaea from public databases (Dombrowski et al. 2018, Borrel et al. 2019, Chen et al. 2019) these MAGs now provide an extensive database for the genomic description of the GoM-Arc1 clade. All GoM-Arc1 clade genomes have an estimated size smaller than 2 Mb, which is in the range of the other thermophilic alkane degraders, such as "*Ca.* Syntrophoarchaeum" (1.5 to 1.7 Mb) and ANME-1 (1.4 to 1.8 Mb) (Laso-Pérez et al. 2016, Krukenberg et al. 2018). The genome is, however, much smaller than the 3.5-Mb genome of the mesophilic sister lineage "*Candidatus* Methanoperedens." This organism thrives on methane and is able to reduce nitrate or metals without partner bacteria (Haroon et al. 2013, Cai et al. 2018).

All GoM-Arc1 genomes contain the genes encoding the enzymes of the methanogenesis pathway, including a highly similar divergent-type MCR and the Wood-Ljungdahl pathway, but no pathway for beta-oxidation of longer fatty acids. Hence, it is likely that all members of this clade are ethane oxidizers. Based on 16S rRNA gene phylogeny and a genome tree based on 32 marker genes, the GoM-Arc1 clade divides into two subclusters. According to a 16S rRNA gene identity of ~95% (Figure S2-1) and an average amino acid identity (AAI) of ~63% (Figure 2-3A; Table S2-3), these clusters should represent two different genera. One cluster contains the recently described ethane oxidizer "*Candidatus* Argoarchaeum ethanivorans" and genomes derived from cold environments including the Gulf of Mexico and the moderately heated Loki's Castle seeps (Steen et al. 2016). The second cluster includes the thermophilic GoM-Arc1 strains found in the Ethane50 and Ethane37 cultures and sequences of other MAGs from the Guaymas Basin (Dombrowski et al. 2017, Dombrowski et al. 2018). Based on the substrate specificity (see results below) and its optimal growth at elevated temperatures, we propose to name the Ethane50 strain of GoM-Arc1 "*Candidatus* Ethanoperedens

thermophilum" *(Ethanoperedens*, Latin for nourishing on ethane; *thermophilum*, Latin for heat loving).

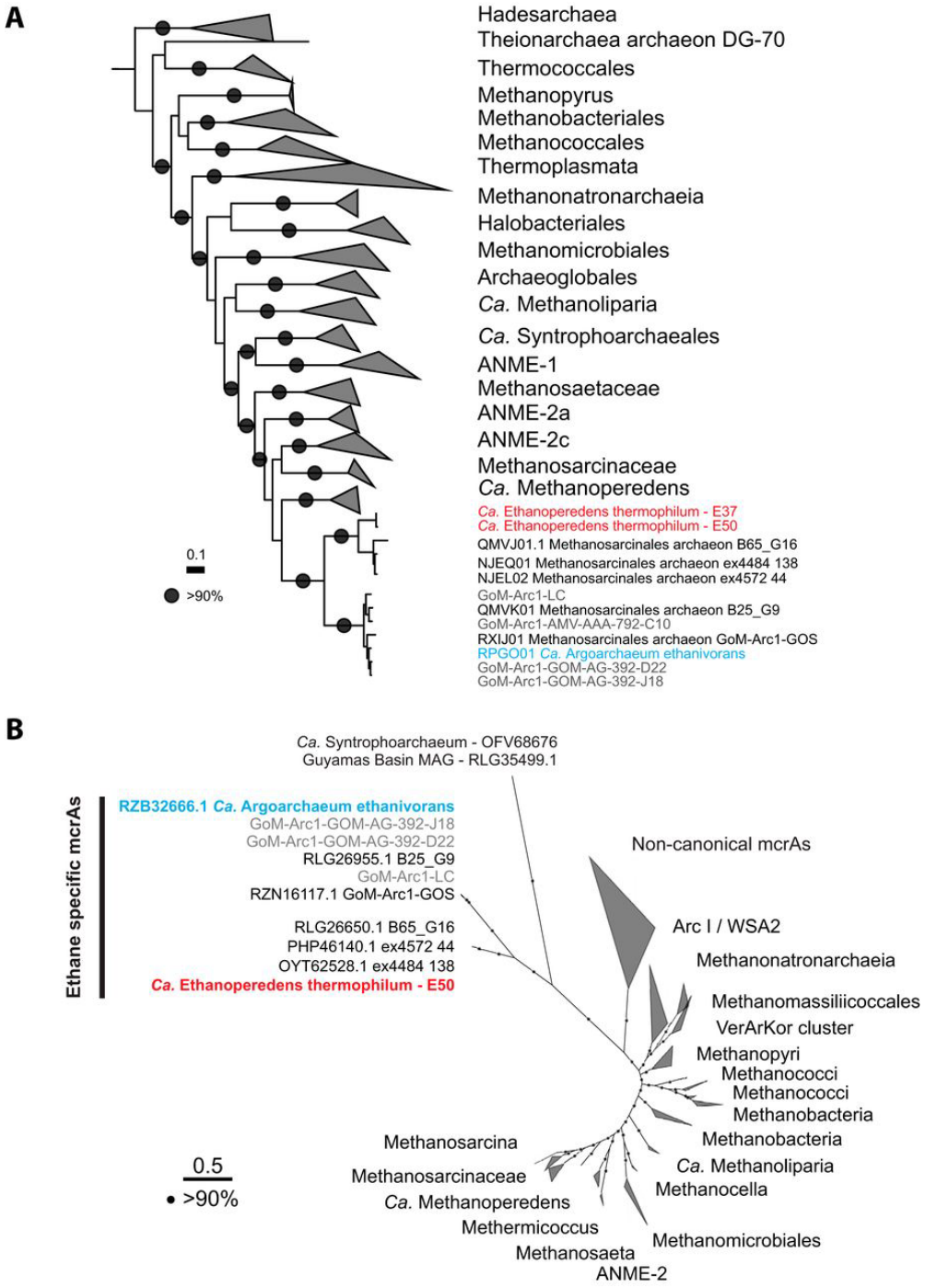

Figure 2-3 Phylogenetic affiliation based on 32 marker genes and mcrA amino acid sequences of "*Ca.* Ethanoperedens." (A) Phylogenetic affiliation of "*Ca.* Ethanoperedens" within the Euryarchaeota based on 32 aligned marker gene amino acid sequences; outgroup is Thaumarchaeota. The scale bar indicates 10% sequence divergence. (B) Phylogenetic affiliation of mcrA amino acid sequences. The mcrA sequences of GoM-Arc1 form a distinct branch within the noncanonical, potentially multicarbon alkane-activating MCRs. The *mcrA* genes of the GoM-Arc1 cluster can be further divided into those from cold-adapted organisms, including "*Ca.* Argoarchaeum ethanivorans," and the cluster including the thermophiles of the genus "*Ca.* Ethanoperedens." Sequences from the Ethane50 enrichment are depicted in red, environmental sequences from metagenomes and single-cell genomes from this study are in gray, and "*Ca.* Argoarchaeum ethanivorans" sequences are in blue. The VerArKor cluster contains mcrA sequences belonging to the Verstraetearchaeota, Archaeoglobus, and Korarchaeota.

2.4.3 Genomic and catabolic features of "*Ca.* Ethanoperedens."

The main catabolic pathways of "*Ca.* Ethanoperedens" are a complete methanogenesis and a Wood-Ljungdahl pathway (Figure 2-4). Its genome encodes only one MCR. The three MCR subunits αβγ are on a single operon. The amino acid sequence of the alpha subunit (mcrA) of "*Ca.* Ethanoperedens" is phylogenetically most closely related to the recently described divergent-type MCR of "*Ca.* Argoarchaeum" with an amino acid identity of 69% but also with all other mcrA sequences of GoM-Arc1 archaea (Dombrowski et al. 2017, Dombrowski et al. 2018, Chen et al. 2019, Laso-Pérez et al. 2019). These MCRs form a distinct cluster in comparison to other divergent MCRs and to the canonical MCRs of methanogens and methanotrophs (Figure 2-3B). The similarity of GoM-Arc1 mcrA sequences to the described canonical and noncanonical sequences is below 43%, and changes in the amino acid sequences are also found in the highly conserved active site of the enzyme (Figure S2-2). The relative expression of the *mcr* subunits compared to all reads mapping to "*Ca.* Ethanoperedens" (reads per kilobase per million mapped reads [RPKM], i.e., *mcrA* = 9,790) is at least two times higher than the expression of all other genes of the main catabolic pathway (Figure 2-4; Table S2-5). The relative *mcr* expression of "*Ca.* Ethanoperedens" is higher than the expression of the multiple *mcr* genes in "*Ca.* Syntrophoarchaeum" but lower than the expression of *mcr* in thermophilic ANME-1 archaea (Laso-Pérez et al. 2016, Krukenberg et al. 2018). The relatively low expression of *mcr* in short-chain alkane-oxidizing archaea can be explained by the properties of their substrates. Short-chain alkane oxidation releases larger amounts of energy than methane oxidation. Furthermore, the cleavage of C-H bonds in multicarbon compounds requires less energy than the cleavage of C-H bonds of methane (Ruscic 2015); hence, less MCR might be required to supply the organism with sufficient energy.

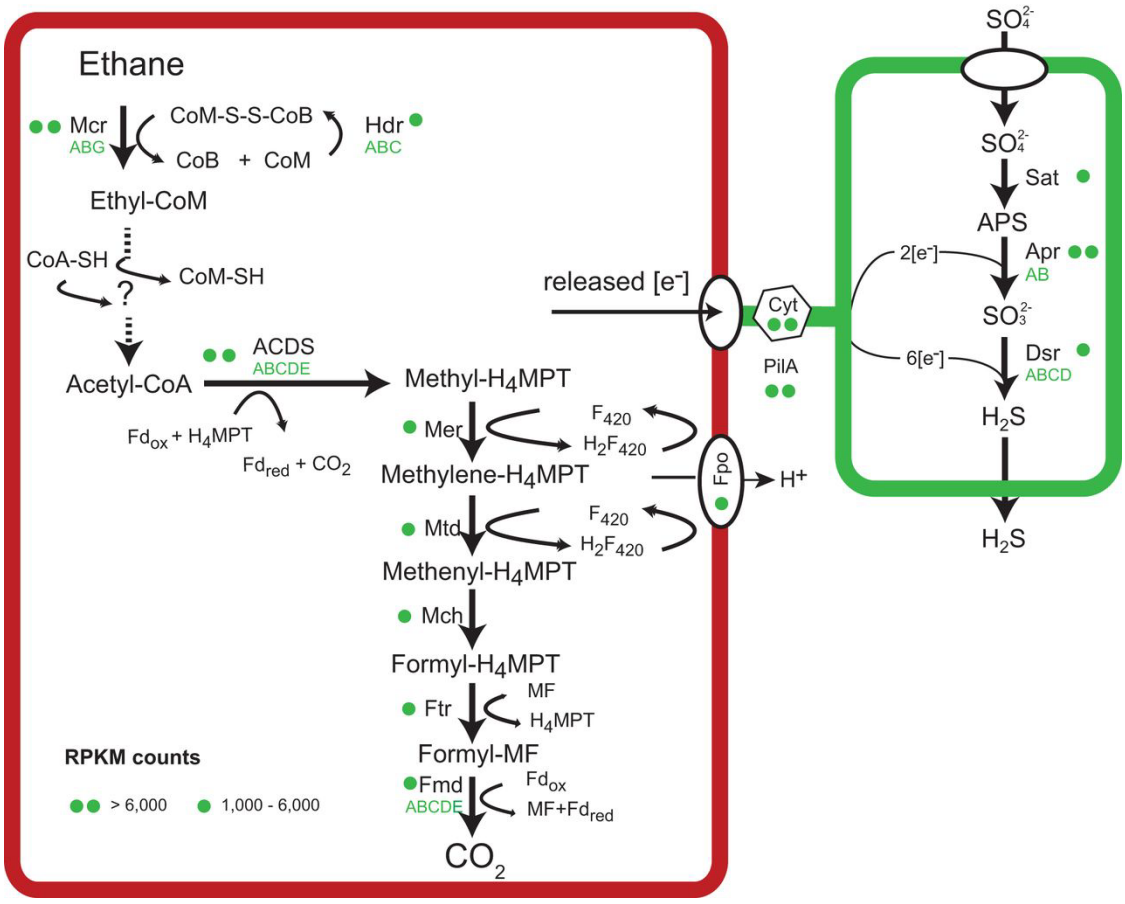

Figure 2-4 Metabolic model of anaerobic ethane oxidation in "*Ca.* Ethanoperedens thermophilum." Ethane is activated in the ethane-specific MCR. The produced CoM-bound ethyl groups are consecutively oxidized and transformed to CoA-bound acetyl units. Acetyl-CoA is cleaved using the ACDS of the Wood-Ljungdahl pathway. The remaining methyl groups are fully oxidized on the reversed methanogenesis pathway. Similarly to ANME archaea and "*Ca.* Syntrophoarchaeum," "*Ca.* Ethanoperedens" does not contain a reductive pathway; hence, electrons released during ethane oxidation are transferred to the partner bacterium "*Ca.* Desulfofervidus auxilii." Therefore, in both partners, cytochromes and pili are present and expressed, similarly to what is described in thermophilic consortia performing AOM (Krukenberg et al. 2018) (for detailed expression patterns, see Table S2-5).

To test the substrates activated by the MCR of "*Ca.* Ethanoperedens," we supplied different alkanes to the active Ethane50 culture replicates and analyzed the extracted metabolites. Cultures supplied with ethane show the m/z 168.9988 of the authentic ethyl-CoM standard (Figure 2-5A and B), which was not observed in the control incubation without substrate. Moreover, addition of 30% [1-^{13}C]ethane resulted in the increase of masses expected for [1-^{13}C]ethyl-CoM and [2-^{13}C]ethyl-CoM (Figure 2-5C). This confirms that "*Ca.* Ethanoperedens" produces ethyl-CoM from ethane. To test substrate specificity of "*Ca.* Ethanoperedens," we provided culture replicates with four different gaseous alkanes (methane, ethane, propane, and n-butane and a mix of all four substrates). Besides the ethane-amended culture, sulfide was produced only in the Ethane50 culture supplied with the substrate mix (Figure S2-3). In agreement with this, no other alkyl-CoM variant apart from ethyl-CoM was detected (Figure 2-5A). This shows that the MCR of "*Ca.* Ethanoperedens" and most likely all

MCR enzymes of GoM-Arc1 archaea (Figure 2-3B) activate ethane but no or only trace amounts of methane and other alkanes. The high substrate specificity of the MCR is crucial for GoM-Arc1 archaea, since they lack the fatty acid degradation pathway that is required to degrade butane and propane (Laso-Pérez et al. 2016). "*Ca.* Ethanoperedens" contains and expresses a complete methyltransferase (*mtr*). The corresponding enzyme might cleave small amounts of methyl-CoM that might be formed as a side reaction of the MCR. The methyl unit would be directly transferred to the methylene-tetrahydromethanopterin (H_4-MPT) reductase (*mer*) and oxidized in the upstream part of the methanogenesis pathway to CO_2 (Figure 2-4).

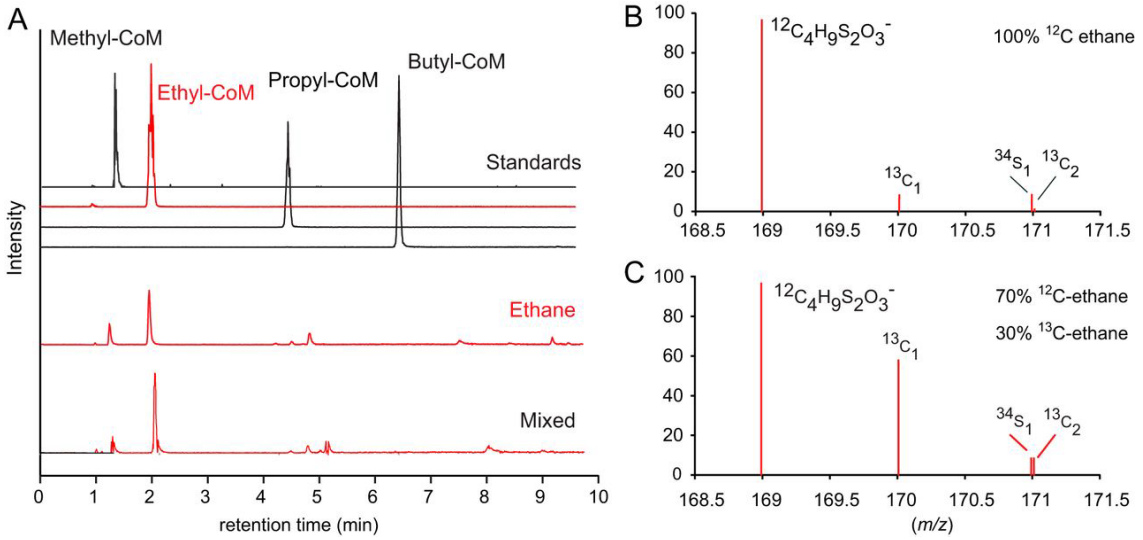

Figure 2-5 Detection of coenzyme M-bound intermediates in the Ethane50 culture. (A) Top four lines show total ion counts for UHPLC peaks for authentic standards of methyl-, ethyl-, propyl-, and butyl-CoM, respectively, and chromatograms for ethane and mixed alkane gases (methane to butane). (B and C) Mass spectra (m/z 168.5 to 171.5) for culture extracts after providing the Ethane50 culture with nonlabeled ethane (B) and 30% ^{13}C-labeled ethane (C). Diagrams show the relative intensities (y axes) for ethyl-CoM-H ($12C_4H_9S_2O^-$) (calculated m/z 168.9988) and its isotopologues with [1-^{13}C]ethyl-CoM or [2-^{13}C]ethyl-CoM or one ^{34}S isotope.

Based on the observed net reaction and the genomic information, "*Ca.* Ethanoperedens" completely oxidizes ethane to CO_2. In this pathway, coenzyme A-bound acetyl units are oxidized in the Wood-Ljungdahl pathway including the upstream part of the methanogenesis pathway (Figure 2-4). Our model, however, does not explain how CoM-bound ethyl groups are oxidized to acetyl units and ligated to CoA. Similar transformations are required in the other multicarbon alkane-oxidizing archaea, such as "*Ca.* Syntrophoarchaeum" and "*Ca.* Argoarchaeum" (Laso-Pérez et al. 2016, Chen et al. 2019). Those oxidation reactions lack biochemical analogues; hence, genomic information alone allows only indirect hints on their function. In "*Ca.* Ethanoperedens," a release of ethyl units and transformation as free molecules (ethanol to acetate) is unlikely, because a formation of acetyl-CoA from acetate would require CoA ligases, which are not present in the genome. Instead, the transformation of ethyl into acetyl units could be performed by a tungstate-containing aldehyde ferredoxin oxidoreductase

(AOR) that could catalyze the oxidation with cofactors such as CoM or CoA. In the archaeon Pyrococcus furiosus, AORs transform aldehydes to the corresponding carboxylic acid (Heider et al. 1995). Both "*Ca.* Ethanoperedens" and "*Ca.* Argoarchaeum" genomes contain three *aor* copies, and in all cases these genes are located either in close proximity to or on operons with genes of the methanogenesis pathway. We detected a high expression of two of the three *aor* genes (RPKM *aor* = 3,805 and 7,928), indicating a viable function of the enzymes. Likewise, very high protein concentrations of these enzymes were shown for "*Ca.* Argoarchaeum" (Chen et al. 2019), supporting the hypothesis of a critical function. An *aor* gene is also present in the butane oxidizer "*Ca.* Syntrophoarchaeum," yet its expression is rather moderate (Laso-Pérez et al. 2016), which puts in question its role in the catabolic pathway of this organism. In contrast, ANME archaea do not contain or overexpress *aor* genes, likely because the encoded enzymes have no central role in their metabolism. We searched the cell extracts for potential intermediates in the pathway, but based on retention time and mass, we were not able to detect potential intermediates such as ethyl-CoA. Similarly, acetyl-CoA, the substrate of the Wood-Ljungdahl pathway, was not detected. A lack of detection, however, does not exclude those compounds as intermediates. Instead, the compound turnover might be very fast, which could be required for an efficient net reaction. Additionally, a mass spectrometric detection of unknown intermediates could be hindered by compound instability or loss during the extraction. Further metabolite studies and enzyme characterizations are required to understand the role of AOR in alkane oxidation

Acetyl-CoA, the product formed by the above-proposed reactions, can be introduced into the Wood-Ljungdahl pathway. The acetyl group is decarboxylated by the highly expressed acetyl-CoA decarbonylase/synthase (ACDS), and the remaining methyl group is transferred to tetrahydromethanopterin (H_4-MPT). The formed methyl-H_4-MPT can then be further oxidized to CO_2 following the reverse methanogenesis pathway (Figure 2-4). "*Ca.* Ethanoperedens" lacks genes for sulfate or nitrate reduction, similarly to other genomes of the GoM-Arc1 clade. The electrons produced in the oxidation of ethane thus need to be transferred to the sulfate-reducing partner bacterium "*Ca.* Desulfofervidus auxilii," as previously shown for the anaerobic oxidation of methane and butane. In co-cultures of "*Ca.* Argoarchaeum" and their partner bacteria, Chen and coworkers (2019) suggest the transfer of reducing equivalents via zero-valent sulfur between the loosely aggregated "*Ca.* Argoarchaeum" and its partner bacterium, analogous to the hypothesis of Milucka et al. (2012). In the Ethane50 culture, such a mode of interaction is highly unlikely, as the partner "*Ca.* Desulfofervidus auxilii" is an

obligate sulfate reducer, incapable of sulfur disproportionation (Krukenberg et al. 2016). Based on genomic information, direct electron transfer appears to be more likely. Alkane-oxidizing archaea and their partner bacterium "*Ca.* Desulfofervidus auxilii," produce cytochromes and pilus-based nanowires when supplied with their substrate (McGlynn et al. 2015, Wegener et al. 2015, Laso-Pérez et al. 2016). Also, "*Ca.* Ethanoperedens" contains 11 different genes for cytochromes with expression values of up to 14,800 RPKM representing some of the highest-expressed genes in the culture (Table S2-5). Interestingly, "*Ca.* Ethanoperedens" also contains and expresses a type IV pilin protein with a high RPKM value of 11,246. The partner bacterium "*Ca.* Desulfofervidus" also shows a high expression of pili and cytochromes under ethane supply, showing their potential importance for the interaction of these two organisms in the syntrophic coupling of ethane oxidation to sulfate reduction.

2.4.4 Environmental distribution of GoM-Arc1 archaea.

16S rRNA gene sequences clustering with "*Ca.* Ethanoperedens" and "*Ca.* Argoarchaeum" have been found in hydrocarbon-rich marine environments like cold-seep and hot-vent environments, including asphalt seeps in the Gulf of Mexico and the Guaymas Basin hydrothermal vents in the Gulf of California (Lloyd et al. 2006, Orcutt et al. 2010, Dowell et al. 2016). In some environments like oil seeps of the Gulf of Mexico and gas-rich barite chimneys of Loki's Castle, 16S rRNA gene surveys have shown that up to 30% of archaeal gene sequences belonged to the GoM-Arc1 clade (Laso-Pérez et al. 2019). To estimate absolute abundances and potential partnerships of GoM-Arc1 in the environment, we performed CARD-FISH on samples from different seep and vent sites across the globe (Figure 2-6). With up to 108 cells per ml, archaea of the GoM-Arc1 clade were particularly abundant in cold-seep sediments in the northern Gulf of Mexico (station 156). This cold seep transports thermogenic hydrocarbon gases that are particularly enriched in short-chain alkanes (Bohrmann et al. 2008, Brüning et al. 2010). Other cold-seep and hot-vent sediments from the Guaymas Basin, Hydrate Ridge, and Amon Mud Volcano contain between 105 and 106 GoM-Arc1 cells per ml of sediment, which represents 1 to 5% of the archaeal community (Figure 2-6A). At all sites, we found that GoM-Arc1 associates with partner bacteria. At the hydrothermally heated site in the Guaymas Basin, GoM-Arc1 aggregated with "*Ca.* Desulfofervidus," the partner bacterium of the Ethane37 and Ethane50 cultures. At Loki's Castle, GoM-Arc1 and "*Ca.* Desulfofervidus" were co-occurring in barite chimneys based on sequence information, yet they were not found to form the same tight consortia as at other sites. At the temperate site Katakolo Bay in Greece, GoM-Arc1 archaea formed consortia with very large, yet unidentified vibrioform bacteria

(Figure 2-6B to F). These cells hybridized with a probe for Deltaproteobacteria but not with probes for known partner bacteria (for probes, see Table S2-1). At the cold-seep sites, the associated cells could not be stained with probes for the known partner bacteria of cold-adapted ANME, including SEEP-SRB1 and SEEP-SRB2, and also not with that for "*Ca.* Desulfofervidus." It remains an important question as to how the archaea can select only a few specific types of bacteria as partners in the anaerobic alkane oxidation and for which specific traits they are selected. Based on their global presence in hydrocarbon-rich environments, GoM-Arc1 archaea could be considered key players in the anaerobic oxidation of ethane in marine sediments. Their role would be similar to the role of ANME archaea in AOM.

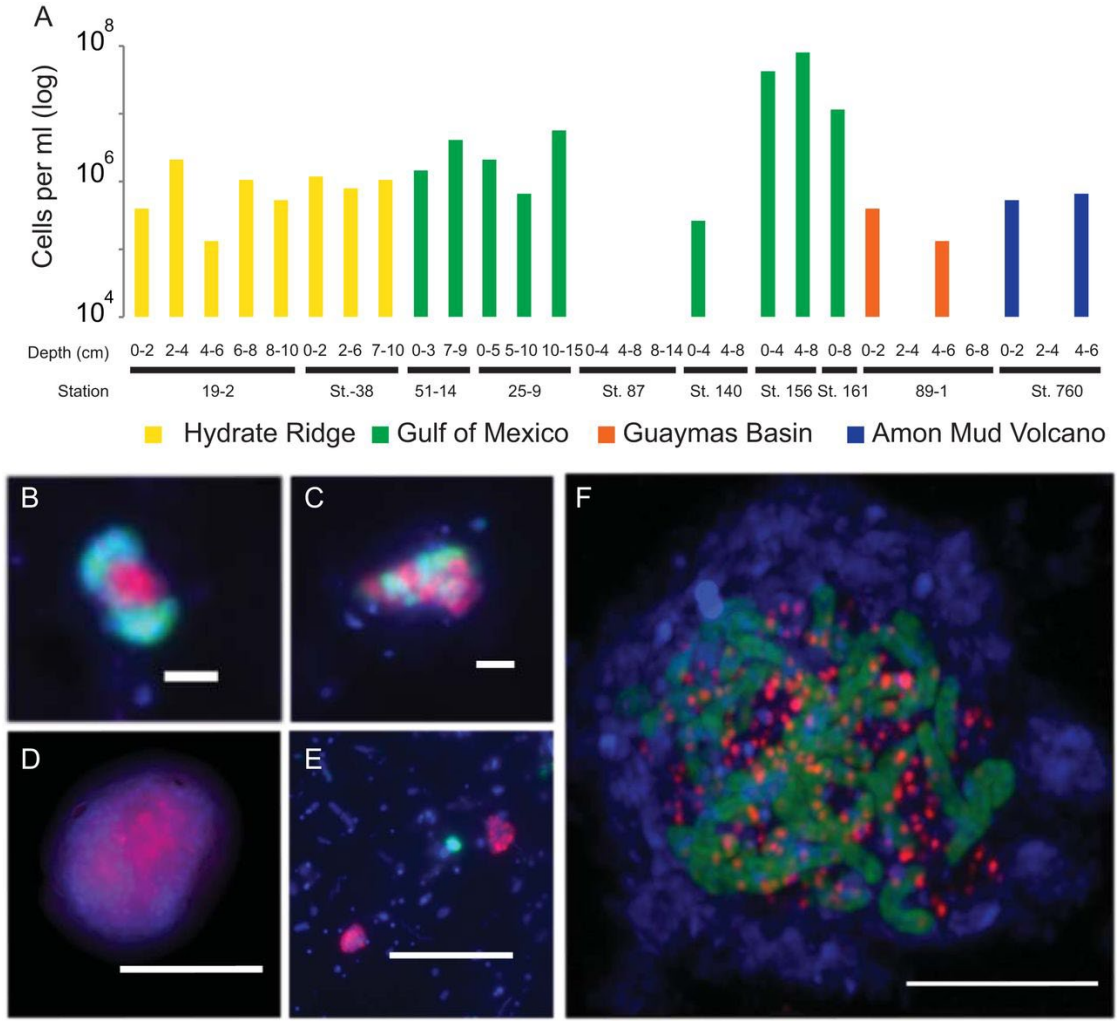

Figure 2-6 Abundance and exemplary micrographs of GoM-Arc1 archaea in sediments from cold seeps and Guaymas Basin. (A) Abundance estimations of archaeal cells detected by the GoM-Arc1-specific probe GOM-ARCI-660 in a CARD-FISH survey. Detection limit, approximately 5 X 10^4 cells per ml sediment. (B to F) Epifluorescence (B to E) and laser scanning (F) micrographs of environmental samples using CARD-FISH with combination of the GoM-Arc1-specific probe (red) and the general bacterial probe EUB-338 (green). Environmental samples originated from the seep sites Hydrate Ridge, Oregon (B); Gulf of Mexico (C); Guaymas Basin (D); Loki's Castle (E); and Katakolo Bay, Greece (F). Bars, 5 µm (D to F) and 2 µm (B and C).

2.4.5 Future possible applications of "*Ca.* Ethanoperedens."

Archaea of the GoM-Arc1 cluster are likely the dominant, if not the only, organisms capable of anaerobic oxidation of ethane on the global seafloor. An important further task is to assess deep oil and gas reservoirs for their diversity of ethane oxidizers. The rapid growth of "*Ca.* Ethanoperedens" and the streamlined genome make it a model organism for the study of anaerobic ethanotrophy in archaea. The biochemistry of short-chain alkane-oxidizing archaea will be of high interest for future biotechnological applications. An organism using the metabolism of "*Ca.* Ethanoperedens" in the reverse direction should be able to produce ethane, similarly to methane production by methanogens. Yet, there is scarce isotopic evidence for the existence of ethanogenic organisms in nature (Hinrichs et al. 2006). Furthermore, under common environmental conditions thermodynamics favor the production of methane from inorganic carbon over the production of ethane. To test the general reversibility of the ethane oxidation pathway, we incubated the active Ethane50 culture with ^{13}C-labeled inorganic carbon and traced the label transfer into ethane. Within 18 days ^{13}C ethane values increased from -3‰ to +120‰, whereas isotopic compositions in the nonlabeled culture remained stable (Figure S2-4). Considering the forward rate and ethane stock, the back reaction amounts to 1.5‰ to 3% of the forward reaction, which is in the range for back fluxes of carbon measured in AOM (Holler et al. 2011, Wegener et al. 2016). This experiment shows that the ethane oxidation pathway is fully reversible. To test the net ethane formation in the Ethane50 culture, we removed sulfate from culture aliquots and added hydrogen as electron donor. These cultures formed between 1 and 17 µmol liter^{-1} ethane within 27 days (Table S2-10). The ethane production was, however, a very small fraction (0.08%) of the ethane oxidation rate in replicate incubations with ethane and sulfate. No ethane was formed in the presence of hydrogen and sulfate. We interpret the ethane formation in the culture as enzymatic effect in the ethane-oxidizing consortia. Bacterial hydrogenases will fuel reducing equivalents into the pathway, which may ultimately lead to the reduction of carbon dioxide to ethane. A growing culture could not be established under these conditions, however, the experiments suggest that related or genetically modified methanogenic archaea could thrive as ethanogens. A complete understanding of the pathway and enzymes of GoM-Arc1 archaea, however, is required to develop the biotechnological potential of an ethanogenic organism. To allow energy-conserving electron flows in this organism, a genetically modified methanogen should be used as host organism. For a targeted modification of such archaea, the pathway of ethane

oxidation must be completely understood, and research should focus especially on the transformation of coenzyme M-bound ethyl units to coenzyme A-bound acetyl units.

2.5 Material and methods

2.5.1 Inoculum and establishment of alkane-oxidizing cultures

This study is based on samples collected during R/V Atlantis cruise AT37-06 with submersible Alvin to the Guaymas Basin vent area in December 2016 (for locations, see Table S2-6 in the supplemental material). A sediment sample was collected by push coring within a hydrothermal area marked by conspicuous orange-type Beggiatoa mats (dive 4869, core 26, 27 0.4505 N 111°24.5389 W, 2,001-m water depth, 20 December 2016). The sampling site was located in the hydrothermal area where, during a previous Alvin visit, sediment cores containing locally ^{13}C-enriched ethane had indicated ethane-oxidizing microbial activity (Dowell et al. 2016). In-situ temperature measurements using the Alvin heat flow probe revealed a steep temperature gradient reaching 80°C at 30- to 40-cm sediment depth. The retrieved samples contained large amounts of natural gas as observed by bubble formation. Soon after recovery, the overlying Beggiatoa mat was removed, and the top 10 cm of the sediment was filled into 250-ml Duran bottles, which were gastight sealed with butyl rubber stoppers. In the home laboratory, sediments were transferred into an anoxic chamber. There, a sediment slurry (20% sediment and 80% medium) was produced with synthetic sulfate reducer (SR) medium (pH 7.0) (Widdel and Bak 1992, Laso-Pérez et al. 2018) and distributed into replicate bottles (sediment dry weight per bottle, 1.45 g). These bottles were amended with methane or ethane (0.2 MPa) or kept with an N2 atmosphere without alkane substrate. These samples were incubated at 37°C, 50°C, and 70°C. To determine substrate-dependent sulfide production rates, sulfide concentrations were measured every 2 to 4 weeks using a copper sulfate assay (Cord-Ruwisch 1985). Ethane-dependent sulfide production was observed at 37°C and 50°C but not at 70°C. When the sulfide concentration exceeded 15 mM, the cultures were diluted (1:3) in SR medium and resupplied with ethane. Repeated dilutions led to virtually sediment-free, highly active cultures within 18 months. A slight decrease of the initial pH value to 6.5 led to increased ethane oxidation activity and faster growth in the culture.

2.5.2 Quantitative substrate turnover experiment

The Ethane50 culture was equally distributed in six 150-ml serum flasks using 20 ml inoculum and 80 ml medium. Three replicate cultures were amended with 0.05-MPa ethane in

0.1-MPa N_2-CO_2, while 3 negative controls were amended with 0.15-MPa N_2-CO_2. Both treatments were incubated at 50°C. Weekly, 0.5-ml headspace gas samples were analyzed for ethane content using an Agilent 6890 gas chromatograph in splitless mode equipped with a packed column (Supelco Porapak Q, 6 ft by 1/8 ft by 2.1-mm stainless steel column, oven temperature 80°C). The carrier gas was helium (20 ml per minute), and hydrocarbons were detected by flame ionization detection. Each sample was analyzed in triplicates and quantified against ethane standards of 5, 10, and 100%. Derived concentrations were converted into molar amounts by taking the headspace size, pressure, and temperature into account. Results were corrected for sampled volumes. Sulfide concentrations were measured as described above. To determine sulfate concentrations, 1 ml of sample was fixed in 0.5 ml zinc acetate. Samples were diluted 1:50 with deionized water (MilliQ grade; >18.5 MD), and samples were measured using nonsuppressed ion chromatography (Metrohm 930 Compact IC Metrosep A PCC HC/4.0 preconcentration and Metrosep A Supp 5-150/4.0 chromatography column).

2.5.3 DNA extraction, 16S rRNA gene amplification, and tag sequencing

DNA was extracted from the different cultures and the original sediment with the Mo Bio Power soil DNA extraction kit (Mo Bio Laboratories Inc., Carlsbad, CA, USA) using a modified protocol. Twenty milliliters of the culture was pelleted via centrifugation (5,000 X g; 10 min). The pellet was resuspended in phosphate-buffered saline (PBS) and transferred to the PowerBeat tube (Mo Bio Power soil DNA extraction kit; Mo Bio Laboratories Inc., Carlsbad, CA, USA). The cells were lysed by three cycles of freezing in liquid nitrogen (20 s) and thawing (5 min at 60°C). After cooling down to room temperature, 10 µl of proteinase K (20 mg ml^{-1}) was added and incubated for 30 min at 55°C. Subsequently, 60 µl of solution C1 (contains SDS) was added, and the tubes were briefly centrifuged. The samples were homogenized 2 times for 30 s at 6.0 m/s using a FastPrep-24 instrument (MP Biomedicals, Eschwege, Germany). In between the runs, the samples were kept on ice for 5 min. After these steps, the protocol was followed further according to the manufacturer's recommendations. DNA concentrations were measured using a Qubit 2.0 instrument (Invitrogen, Carlsbad, CA, USA). Two nanograms of DNA was used for amplicon PCR, and the product was used for 16S rRNA gene amplicon library preparation according to the 16S metagenomic sequencing library preparation guide provided by Illumina. The Arch349F-Arch915R primer pair was used to amplify the archaeal V3-V5 region, and the Bact341F-Bact785R primer pair was used for the bacterial V3-V4 region (see Table S2-1 in the supplemental material). Amplicon libraries for both Archaea and Bacteria were sequenced on an Illumina MiSeq instrument (2- by 300-bp

paired-end run, v3 chemistry) at CeBiTec (Bielefeld, Germany). After analysis, adapters and primer sequences were clipped from the retrieved sequences using cutadapt (Martin 2011) (v1.16) with 0.16 (-e) as maximum allowed error rate and no indels allowed. Resulting reads were analyzed using the SILVAngs pipeline using the default parameters (https://ngs.arb-silva.de/silvangs/) (Quast et al. 2012, Yilmaz et al. 2014, Glockner et al. 2017).

2.5.4 Extraction of high-quality DNA, library preparation, and sequencing of gDNA

Biomass from 200 ml of the Ethane50 and Ethane37 cultures was pelleted by centrifugation and resuspended in 450 µl of extraction buffer. Genomic DNA was retrieved based on a modified version of the protocol described in reference Zhou et al. (1996), including three extraction steps. Resuspended pellet was frozen in liquid N_2 and thawed in a water bath at 65°C. Another 1,350 µl of extraction buffer was added. Cells were digested enzymatically by proteinase K (addition of 60 µl of 20 mg/ml, incubation at 37°C for 1.5 h under constant shaking at 225 rpm) and chemically lysed (addition of 300 µl 20% SDS for 2h at 65°C). Samples were centrifuged (20 min, 13,000 X g), and the clear supernatant was transferred to a new tube. Two milliliters of chloroform-isoamyl alcohol (16:1, vol/vol) was added to the extract, mixed by inverting, and centrifuged for 20 min at 13,000 X g. The aqueous phase was transferred to a new tube, mixed with 0.6 volumes of isopropanol, and stored overnight at -20°C for DNA precipitation. If precipitate formed, sample was heated to 65°C for 5 min and then centrifuged for 40 min at 13,000 X g. The supernatant was removed, and the pellet was washed with ice-cold ethanol (80%) and subjected to centrifugation for 10 min at 13,000 X g. The ethanol was removed, and the dried pellet was resuspended in PCR-grade water. This procedure yielded 114 µg and 145 µg high-quality genomic DNA (gDNA) from the Ethane37 and the Ethane50 cultures, respectively. Samples were sequenced with Pacific Biosciences Sequel as a long amplicon (4 to 10 kb) and long-read gDNA library at the Max Planck-Genome-Centre (Cologne, Germany). To evaluate the microbial community, we extracted 16S rRNA gene reads using Metaxa2 (Bengtsson-Palme et al. 2015) and taxonomically classified them using the SILVA ACT online service (Pruesse et al. 2012). For assembly, either HGAP4 (implemented in the SMRTlink software by PacBio) or Canu (https://github.com/marbl/canu) was used. The closed GoM-Arc1 genome from the Ethane37 culture was prepared manually by the combination of assemblies from the two above-mentioned tools. The final genome was polished using the resequencing tool included in the SMRTLink software by PacBio. For noncircularized de novo genomes, the resulting contigs were mapped via minimap2

(https://github.com/lh3/minimap2; parameter: '-x asm10') to a reference genome. The reference consensus genomes were prepared using the resequencing tool implemented in the SMRTLink software of PacBio using either the circular GoM-Arc1 de novo genome from this study or the publicly available "*Ca.* Desulfofervidus" genome (accession no. NZ_CP013015.1) as reference. Final genomes were automatically annotated using Prokka (Seemann 2014), and the annotation was refined manually using the NCBI BLAST interface (Johnson et al. 2008). Average nucleotide and amino acid identities were calculated using Enveomics tools (Rodriguez-R and Konstantinidis 2016).

2.5.5 Single-cell genomics

Anoxic sediment aliquots were shipped to the Bigelow Laboratory Single Cell Genomics Center (SCGC; https://scgc.bigelow.org). Cells were separated, sorted, and lysed, and total DNA was amplified by multiple displacement amplification. Single-cell DNA was characterized by 16S rRNA gene tag sequences (Stepanauskas et al. 2017, Laso-Pérez et al. 2019). The single-cell amplified DNA from Gulf of Mexico samples was analyzed and sequenced as described before in Laso-Pérez et al. (2019). Single-cell amplified DNA from Amon Mud Volcano AAA-792_C10 was sequenced with HiSeq 3000 and MiSeq technology, and reads were assembled using SPAdes (Nurk et al. 2013) with the single-cell mode. Assembled reads were binned based on tetranucleotides, coverage, and taxonomy using MetaWatt (Strous et al. 2012). The final SAG was evaluated for completeness and contamination using CheckM (Parks et al. 2015). Genome annotation was performed as described above.

2.5.6 Extraction of RNA, reverse transcription, sequencing, and read processing

Extraction and sequencing of total RNA was performed in triplicates. RNA was extracted from 150 ml active Ethane50 culture grown in separate bottles at 50°C. Total RNA was extracted and purified as described in reference (Laso-Pérez et al. 2016) using the Quick-RNA miniprep kit (Zymo Research, Irvine, CA, USA) and RNeasy MinElute cleanup kit (Qiagen, Hilden, Germany). Per sample, at least 150 ng of high-quality RNA was obtained. The RNA library was prepared with the TruSeq stranded total RNA kit (Illumina). An rRNA depletion step was omitted. The samples were sequenced on an Illumina NextSeq with v2 chemistry and 1- by 150-bp read length. The sequencing produced ~50-Gb reads per sample. Adapters and contaminant sequences were removed, and reads were quality trimmed to Q10 using bbduk v36.49 from the BBMAP package. For phylogenetic analysis of the active

community, 16S rRNA reads were recruited and classified based on SSU SILVA release 132 (Pruesse et al. 2012) using phyloFlash (Gruber-Vodicka et al. 2020). Trimmed reads were mapped to the closed genomes of "*Candidatus* Ethanoperedens thermophilum" and "*Ca.* Desulfofervidus" using Geneious Prime 2019.2.1 (Biomatters, Ltd., Auckland, New Zealand) with a minimum mapping quality of 30%. The expression level of each gene was quantified by counting the number of unambiguously mapped reads per gene using Geneious. To consider gene length, read counts were converted to reads per kilobase per million mapped reads (RPKM).

2.5.7 Phylogenetic analysis of 16S rRNA genes, marker genes, and mcrA amino acid sequences.

A 16S rRNA gene-based phylogenetic tree was calculated using publicly available 16S rRNA sequences from the SSU Ref NR 128 SILVA database (Quast et al. 2012). The tree was constructed using ARB (Ludwig et al. 2004) and the FastTree 2 package (Price et al. 2010) using a 50% similarity filter. Sequence length for all 16S rRNA genes was at least 1,100 bp. After tree calculation, partial sequences retrieved from single cells were included into the tree. ARB (Ludwig et al. 2004) was used for visualization of the final tree. The marker gene tree was calculated using 126 publicly available genomes and genomes presented in this study. The tree was calculated based on aligned amino acid sequences of 32 marker genes picked from known archaeal marker genes (Table S2-7) (Rinke et al. 2013). For the preparation of the aligned marker gene amino acid sequences, we used the phylogenomic workflow of Anvi'o 5.5 (Eren et al. 2015). The marker gene phylogeny was calculated using RAxML version 8.2.10 (Stamatakis 2014) with the PROTGAMMAAUTO model and LG likelihood amino acid substitution. One thousand fast bootstraps were calculated to find the optimal tree according to RAxML convergence criteria. The software iTOL v3 was used for tree visualization (Letunic and Bork 2016). The mcrA amino acid phylogenetic tree was calculated using 358 sequences that are publicly available or presented in this study. The sequences were manually aligned using the Geneious Prime 2019.2.1 (Biomatters, Ltd., Auckland, New Zealand) interface, and 1,060 amino acid positions were considered. The aligned sequences were masked using Zorro (https://sourceforge.net/projects/probmask/), and a phylogenetic tree was calculated using RAxML version 8.2.10 (Stamatakis 2014) using the PROTGAMMAAUTO model and LG likelihood amino acid substitution. One thousand fast bootstraps were calculated. The tree was visualized with iTOL v3 (Letunic and Bork 2016).

2.5.8 Catalyzed reported deposition fluorescence in-situ hybridization (CARD-FISH)

Aliquots of the Ethane50 culture and environmental samples were fixed for1h in 2% formaldehyde, washed three times in PBS (pH 7.4)-ethanol (1:1), and stored in this solution. Aliquots were sonicated (30 s; 20% power; 20% cycle; Sonoplus HD70; Bandelin) and filtered on GTTP polycarbonate filters (0.2-µm pore size; Millipore, Darmstadt, Germany). CARD-FISH was performed according to reference (Pernthaler et al. 2002) including the following modifications. Cells were permeabilized with a lysozyme solution (PBS [pH 7.4], 0.005 M EDTA [pH 8.0], 0.02 M Tris-HCl [pH 8.0], 10 mg ml^{-1} lysozyme; Sigma-Aldrich) at 37°C for 60 min followed by proteinase K solution treatment (7.5 µg ml^{-1} proteinase K [Merck, Darmstadt, Germany] in PBS [pH 7.4], 0.005 M EDTA [pH 8.0], 0.02 M Tris-HCl [pH 8.0]) at room temperature for 5 min. Endogenous peroxidases were inactivated by incubation in a solution of 0.15% H_2O_2 in methanol for 30 min at room temperature. Horseradish peroxidase (HRP)-labeled probes were purchased from Biomers.net (Ulm, Germany). Tyramides were labeled with Alexa Fluor 594 or Alexa Fluor 488. All probes were applied as listed in Table S2-1. For double hybridization, the peroxidases from the first hybridization were inactivated in 0.15% H_2O_2 in methanol for 30 min at room temperature. Finally, the filters were counterstained with DAPI (4=,6=diamino-2-phenylindole) and analyzed by epifluorescence microscopy (Axiophot II imaging; Zeiss, Germany). Selected filters were analyzed by confocal laser scanning microscopy (LSM 780; Zeiss, Germany) including the Airyscan technology.

2.5.9 Synthesis of authentic standards for metabolites

To produce alkyl-CoM standards, 1 g of coenzyme M was dissolved in 40 ml 30% (vol/vol) ammonium hydroxide solution, and to this solution 1.8 to 2 g of bromoethane, bromopropane, or bromobutane was added. The mixture was incubated for 5 h at room temperature under vigorous shaking and then acidified to pH 1 with HCl. The produced standard had a concentration of approximately 25 mg ml^{-1}, which for mass spectrometry measurements was diluted to 10 µg ml^{-1}.

2.5.10 Extraction of metabolites from the Ethane50 culture

In the anoxic chamber, 20 ml of Ethane50 culture was harvested into 50-ml centrifuge tubes. Tubes were centrifuged at 3,000 relative centrifugal force (rcf) for 10 min, and the supernatant was removed. The pellet was resuspended in 1 ml acetonitrile-methanol-water (4:4:2, vol/vol/vol) mixture in lysing matrix tubes (MP Biomedicals, Eschwege, Germany)

with glass beads. Afterward, the tubes were removed from the anoxic chamber and the samples were mechanically lysed in a FastPrep homogenizer (MP Bio) with 5 cycles with 6 M/s for 50 s and cooling on ice for 5 min between the homogenization steps. Finally, the samples were centrifuged for 5 min at 13,000 X g, and the supernatant was transferred to a new tube and stored at -20°C.

2.5.11 Solvents for LC-MS/MS

All organic solvents were liquid chromatography-mass spectrometry (LC-MS) grade, using acetonitrile (ACN; BioSolve, Valkenswaard, The Netherlands), isopropanol (IPA; BioSolve, Valkenswaard, The Netherlands), and formic acid (FA; BioSolve, Valkenswaard, The Netherlands). Water was deionized by using the Astacus MembraPure system (MembraPure GmbH, Berlin, Germany).

2.5.12 High-resolution LC-MS/MS.

The analysis was performed using a QExactive Plus Orbitrap (Thermo Fisher Scientific) equipped with a heated electrospray ionization (HESI) probe and a Vanquish Horizon ultra-high-performance liquid chromatography (UHPLC) system (Thermo Fisher Scientific). The metabolites from cell extracts were separated on an Accucore C30 column (150 by 2.1 mm, 2.6 µm; Thermo Fisher Scientific), at 40°C, using a solvent gradient created from the mixture of buffer A (5% acetonitrile in water, 0.1% formic acid) and buffer B (90/10 IPA-ACN, 0.1% formic acid). The solvent gradient was the following: fraction B of 0, 0, 16, 45, 52, 58, 66, 70, 75, 97, 97.15, and 0%, at -2 min (prerun equilibration) and 0, 2, 5.5, 9, 12, 14, 16, 18, 22, 25, 32.5, 33, 34.4, and 36 min of each run, and a constant flow rate of 350 µl min^{-1}. The sample injection volume was 10 µl. The MS measurements were acquired in negative mode for a mass detection range of 70 to 1,000 Da. In alternation, a full MS and MS/MS scans of the eight most abundant precursor ions were acquired in negative mode. Dynamic exclusion was enabled for 30 s. The settings for full-range MS1 were mass resolution of 70,000 at 200 m/z, automatic gain control (AGC) target of 5 X 105, and injection time of 65 ms. Each MS1 was followed by MS2 scans with the following settings: mass resolution of 35,000 at 200 m/z, AGC target of 1 X 106, injection time of 75 ms, loop count of 8, isolation window of 1 Da, and collision energy set to 30 eV.

2.5.13 Determination of carbon back flux into the ethane pool

Aliquots of active AOM culture (50 ml) were transferred into 70-ml serum bottles with N_2:CO_2 headspace. In the stable-isotope probing (SIP) experiment, addition of 99% ^{13}C-labeled

dissolved inorganic carbon (DIC) (1 ml, 350 mM) led to 3-^{13}C-DIC values of +25,000‰ as measured by cavity ringdown spectrometry. Ethane (2 atm = 1.8 mM) was added to both experiments, and cultures were stored at 50°C. To determine the overall ethane oxidation activity, sulfide concentrations were measured every few days as described above and converted to ethane oxidation rates using ratios in the chemical formula in Results and Discussion. To measure the development of ethane 3-^{13}C values, 1 ml of the gas phase was sampled every few days and stored in 10-ml Exetainer vials with 2 ml NaOH, and ethane isotopic composition was measured using gas chromatography coupled via a combustion interface to isotope ratio mass spectrometry (Trace GC Ultra with Carboxene-1006 Plot column, 40°C oven temp., carrier gas He with flow rate 3 ml min^{-1}; coupled via GC IsoLink to Delta V isotope ratio MS).

2.5.14 Net ethane production test

To test for net ethane production, in 156-ml serum flasks replicate incubations with about 0.5 g (wet weight) active Ethane50 culture in 100 ml of sulfate-free medium was prepared. Four different conditions were tested in three biological replicates with the addition of (i) 1.5 atm H_2; (ii) conditions replicating the first but with only 0.05 g biomass; (iii) 1.5 atm H_2 plus 28 mM sulfate; and (iv) an activity control with addition of sulfate and 1.5 atm ethane. Cultures were incubated over 27 days at 50°C, and sulfate and ethane concentrations were monitored as described above.

2.5.15 Data availability

All sequence data are archived in the ENA database under the INSDC accession numbers PRJEB36446 and PRJEB36096. Sequence data from Loki's Castle are archived under NCBI BioSample number SAMN13220465. The 16S rRNA gene amplicon reads have been submitted to the NCBI Sequence Read Archive (SRA) database under the accession number SRR8089822. All sequence information has been submitted using the data brokerage service of the German Federation for Biological Data (GFBio) (Diepenbroek et al. 2014), in compliance with the Minimal Information about any (X) Sequence (MIxS) standard (Yilmaz et al. 2011), but some data are still under ENA embargo.

2.6 Acknowledgements

We thank Susanne Menger for her contribution in culturing the target organisms, Janine Beckmann for metabolite analysis, and Heidi Taubner, Jenny Wendt, and Xavier Prieto Mollar

(Hinrichs Lab, MARUM, University of Bremen) for performing isotope analyses. We are indebted to Andreas Ellrott for assisting in confocal microscopy and Gabriele Klockgether for her kind help with gas chromatography. We thank Matthew Schechter for analyzing the community compositions in a lab rotation. We also thank Tristan Wagner for vivid discussions on the metabolism of Ethanoperedens. We thank Bigelow SCGC for their work in sequencing single-cell genomes used in this study. We are enormously grateful to I. Kostadinov and the GFBIO for support and help during data submission. We are indebted to the crew and science party of R/V Atlantis and HOV Alvin expedition AT37-06. This study was funded by the Max Planck Society and the DFG Clusters of Excellence 'The Ocean in the Earth System' and 'The Ocean Floor—Earth's Uncharted Interface' at MARUM, University of Bremen. Additional funds came from the ERC ABYSS (grant agreement no. 294757) to A.B. R/V Atlantis and HOV Alvin expedition AT37-6 was funded by NSF grant 1357238 to A. Teske.

2.7 Supplemental material

2.7.1 Supplemental figures

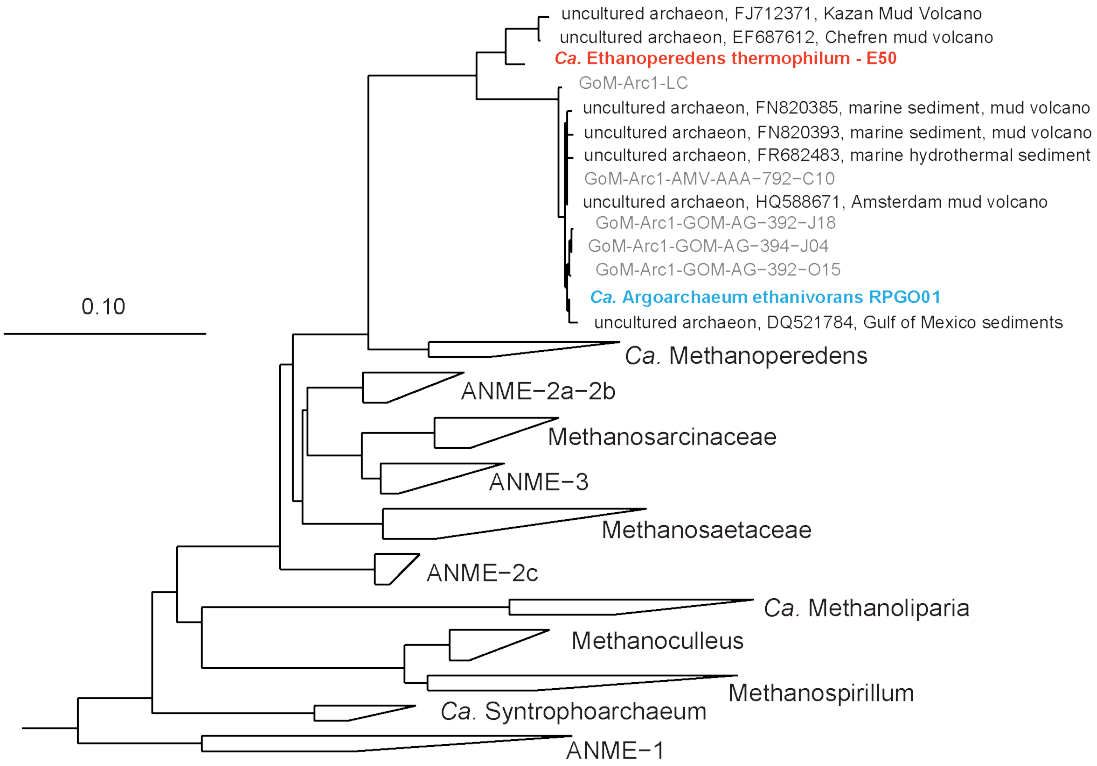

Figure S2-1 Phylogenetic affiliation of the GoM-Arc1 clade archaea with other archaea based on 16S rRNA gene comparison. The tree was constructed using ARB (Ludwig et al. 2004) and the FastTree 2 package (Price et al. 2010) using a 50% similarity filter. 410 sequences with a length of at least 1100 bp, excluding partial sequences retrieved from single cells, were used. Bar shows 10% sequence divergence.

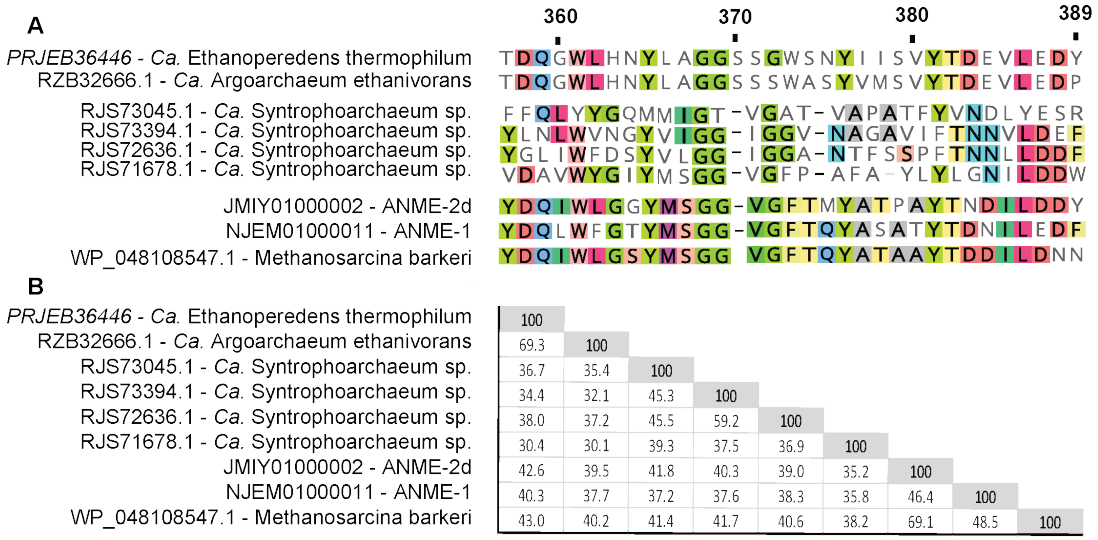

Figure S2-2 Comparison of mcrA sequences from the GoM-Arc1 clade to described canonical and non-canonical mcrA sequences. A, alignment of the active site of the mcrA from different representative genomes. The four different *Ca.* Syntrophoarchaeum sequences belong to the same genome bin. Amino acid positions refer to *Ca.* E. thermophilum E50 mcrA sequence. B, identity matrix of mcrA sequences based on NCBI blastp alignment.

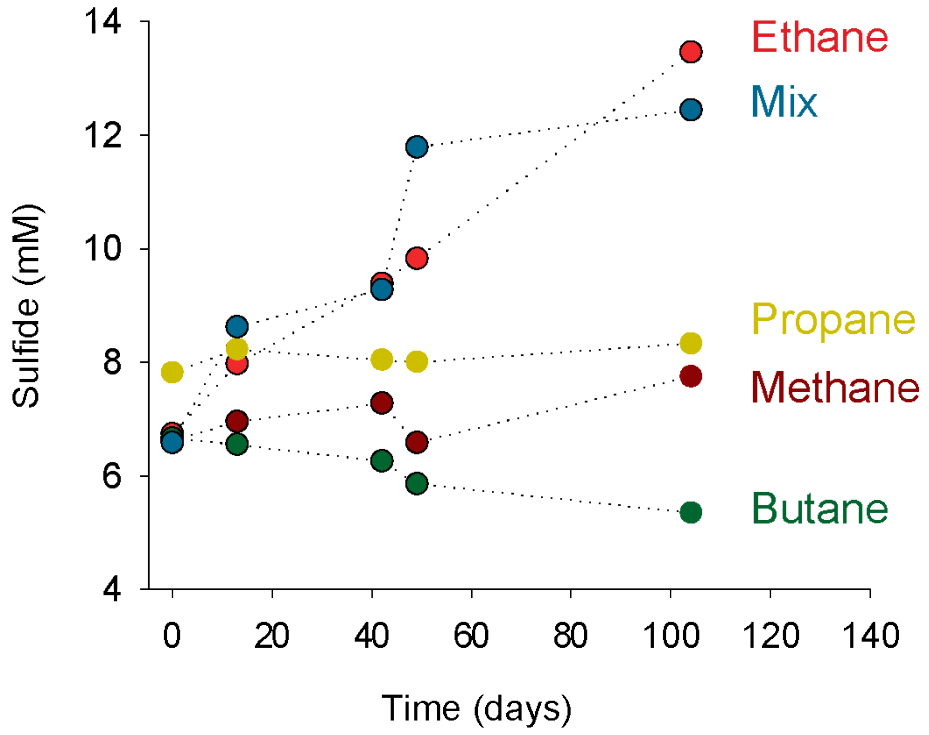

Figure S2-3 Development of sulfide concentrations in substrate experiments in replicate incubations of the Ethane50 culture supplied with (**A**) ethane, alternative alkanes or a mix of these substrates; and (**B**) ethane and sulfate compared to ethane with elemental sulfur or only elemental sulfur. Results show that that ethane is the only alkane used as electron donor in *Ca.* E. thermophilum, and sulfate is the only used electron acceptor. Further, elemental sulfur is not disproportionated.

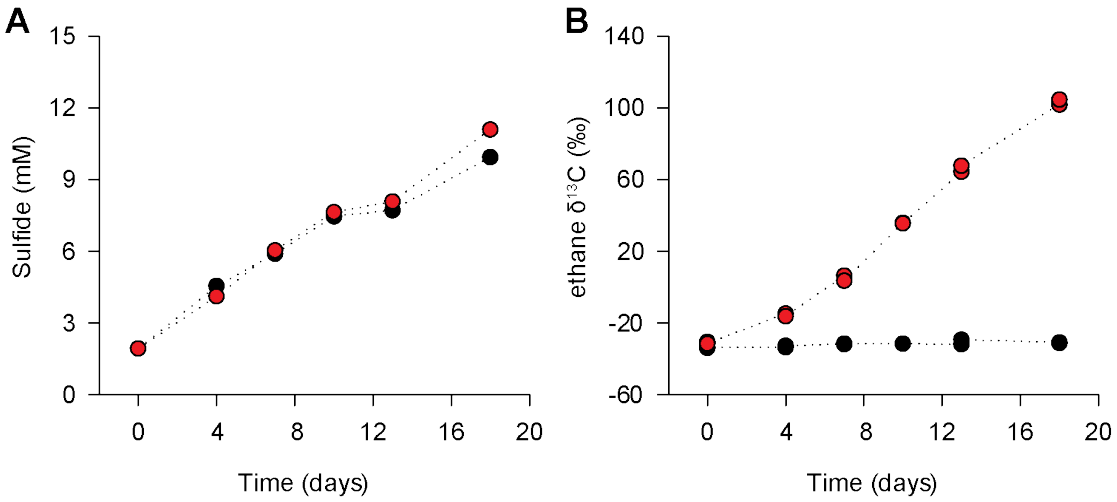

Figure S2-4 Test for the transfer of inorganic carbon into ethane in the ethane 50 culture. A, development of sulfide concentrations in the culture with ethane as energy source and sulfate as electron acceptor B, development of $\delta^{13}C$ values in ethane in the two cultures (controls $\delta^{13}C$ DIC -35‰) ^{13}C-DIC amended culture with $\delta^{13}CDIC$ =+25994 ‰. Based on simple mass balance calculations on the development of fractions we infer that sulfate-dependent anaerobic AOM in these enrichments is accompanied by a back flow of inorganic carbon amounting to 1-3% of the forward rate. This back reaction indicates a general reversibility of ethane oxidation.

2.7.2 Supplemental tables

Table S2-1 PCR primers used the amplification of archaeal and bacteria 16S rRNA genes and oligonucleotide probes used for CARD-FISH.

Primer name	**Ref. in probeBase database**	**Sequence 5'→3'**		**Reference**
Arch349F	S-D-Arch-0349-a-S-17	GYG CAS CAG KCG MGA AW		Takai and Horikoshi (2000)
Arch915R	S-D-Arch-0915-a-A-20	GTG CTC CCC CGC CAA TTC CT		(Amann et al. 1990)
Bact341F	S-D-Bact-0341-b-S-17	CCT ACG GGN GGC WGC AG		(Herlemann et al. 2011)
Bact785R	S-D-Bact-0785-a-A-21	GAC TAC HVG GGT ATC TAA TCC		(Herlemann et al. 2011)
Probe name	**Specificity**	**Sequence 5'→3'**	**FA %**	**Reference**
EUB338 I	Bacteria	GCTGCCTCCCGTAGGAGT	35	(Amann et al. 1990)
EUB338 II	supplement to EUB338	GCAGCCACCCGTAGGTGT	35	(Daims et al. 1999)
EUB338 III	supplement to EUB338	GCTGCCACCCGTAGGTGT	35	(Daims et al. 1999)
GOM-ARCI-660	most GoM Arc 1, *Methanocellaceae*	AGTACCTCCTACCTCTCCC	35	(Laso-Pérez et al. 2019)
c1GOM-ARCI-660	most ANME-2d (competitor)	AGTACCTCCCACCTCTCCC		(Laso-Pérez et al. 2019)
c2GOM-ARCI-660	*Methanosaetaceae* / *Methanobacteriales* (most ANME-2d (competitor)	AGTACCTCCAACCTCTCCC		(Laso-Pérez et al. 2019)
c3GOM-ARCI-660	Diverse archaeal groups (competitor)	AGTACCTCCGACCTCTCCC		(Laso-Pérez et al. 2019)
HotSeep1-1465	*Ca.* Desulfofervidus	CGCCGACCACACCTTGGG	20	(Krukenberg et al. 2016)
DSS658	*Desulfosarcina/ Desulfococcus*	TCCACTTCCCTCTCCCAT	50	(Manz et al. 1998)
DELTA495	*Most Deltaproteobacteria*	AGTTAGCCGGTGCTTCCT	35	(Loy et al. 2002)

Table S2-2 ANI similarity matrix for GoM-Arc1 and ANME-2d related genomes. Enveomics tools were used for the calculation (Rodriguez-R and Konstantinidis 2016).

	GoM-Arc1_E37	GoM-Arc1_E50	GoM-Arc1_E50_DN	GoM-Arc1-AAA-792-C< 75	GoM-Arc1-AG-392-D22	GoM-Arc1-AG-392-E03	GoM-Arc1-AG-392-J18	GoM-Arc1-AG-392-M11	GoM-Arc1-AG-392-O15	GoM-Arc1-AG-393-N10	GoM-Arc1-AG-394-J04	RPGO01 Ca. Argoarchaeum ethanivora	Methanosarcinales archaeon B25-G9	GoM-Arc1-LC	JMIY01 Ca Methanoperdens nitroreducens	LKCM01 Ca Methanoperdens BLZ1	Ca Methanoperdens Mnv1	NJEL02 Methanosarcinales archaeon ex4572-44	NJEQ01 Methanosarcinales archaeon ex4484-	QMVJ01 Methanosarcinales archaeon B65-G16	RXIJ01 GoM-Arc1-GOS
GoM-Arc1_E37	100.0	98.4	98.3	< 75.0	78.5	< 75.0	80.4	81.6	< 75.0	< 75.0	< 75.0	78.4	83.4	< 75.0	< 75.0	< 75.0	< 75.0	83.4	83.1	84.4	78.7
GoM-Arc1_E50	98.4	100.0	99.9	< 75.0	78.0	< 75.0	79.5	80.6	< 75.0	< 75.0	< 75.0	78.4	83.3	< 75.0	< 75.0	< 75.0	< 75.0	83.3	83.3	84.3	78.8
GoM-Arc1_E50_DN	98.3	99.9	100.0	< 75.0	78.2	< 75.0	81.9	82.2	< 75.0	< 75.0	< 75.0	80.8	83.2	< 75.0	< 75.0	< 75.0	< 75.0	83.2	82.8	84.3	79.7
GoM-Arc1-AAA-792-C10	< 75.0	< 75.0	10.0	100.0	90.3	90.7	90.2	90.2	90.7	90.0	90.2	90.3	< 75.0	92.6	< 75.0	< 75.0	< 75.0	< 75.0	< 75.0	< 75.0	89.5
GoM-Arc1-AG-392-D22	78.5	78.0	78.2	90.3	100.0	98.4	95.8	95.4	94.3	96.8	98.5	95.4	77.8	90.3	< 75.0	< 75.0	< 75.0	77.8	81.4	80.2	93.3
GoM-Arc1-AG-392-E03	< 75.0	< 75.0	< 75.0	90.7	98.4	100.0	96.0	96.3	94.3	97.4	99.8	95.4	< 75.0	91.2	< 75.0	< 75.0	< 75.0	< 75.0	< 75.0	< 75.0	93.3
GoM-Arc1-AG-392-J18	80.4	79.5	81.9	90.2	95.8	96.0	100.0	95.2	94.5	96.5	96.0	95.3	77.7	90.1	< 75.0	< 75.0	< 75.0	77.7	76.7	78.7	93.4
GoM-Arc1-AG-392-M11	81.6	80.6	82.2	90.2	95.4	96.3	95.2	100.0	95.1	94.9	95.0	95.4	< 75.0	90.3	< 75.0	< 75.0	< 75.0	< 75.0	< 75.0	79.2	93.6
GoM-Arc1-AG-392-O15	< 75.0	< 75.0	< 75.0	90.7	94.3	94.3	94.5	95.1	100.0	94.3	94.3	94.4	< 75.0	90.5	< 75.0	< 75.0	< 75.0	< 75.0	< 75.0	< 75.0	92.5
GoM-Arc1-AG-393-N10	< 75.0	< 75.0	< 75.0	90.0	96.8	97.4	96.5	94.9	94.3	100.0	97.1	95.2	< 75.0	90.8	< 75.0	< 75.0	< 75.0	< 75.0	< 75.0	< 75.0	93.1
GoM-Arc1-AG-394-J04	< 75.0	< 75.0	< 75.0	90.2	98.5	99.8	96.0	95.0	94.3	97.1	100.0	95.3	< 75.0	90.5	< 75.0	< 75.0	< 75.0	< 75.0	< 75.0	< 75.0	93.4
RPGO01 Ca. Argoarchaeum ethanivorans	78.4	78.4	80.8	90.3	95.4	95.4	95.3	95.4	94.4	95.2	95.3	100.0	79.0	91.1	< 75.0	< 75.0	< 75.0	79.0	82.7	81.0	93.7
Methanosarcinales archaeon B25-G9	83.4	83.3	83.2	10.0	77.8	10.0	77.7	< 75.0	< 75.0	< 75.0	< 75.0	79.0	100.0	< 75.0	< 75.0	< 75.0	< 75.0	100.0	99.8	99.7	78.5
GoM-Arc1-LC	< 75.0	< 75.0	< 75.0	92.6	90.3	91.2	90.1	90.3	90.5	90.8	90.5	91.1	< 75.0	100.0	< 75.0	< 75.0	< 75.0	< 75.0	< 75.0	< 75.0	89.8
JMIY01 Ca Methanoperdens nitroreducens	< 75.0	< 75.0	< 75.0	< 75.0	< 75.0	< 75.0	< 75.0	< 75.0	< 75.0	< 75.0	< 75.0	< 75.0	< 75.0	< 75.0	100.0	76.6	100.0	< 75.0	< 75.0	< 75.0	< 75.0
LKCM01 Ca Methanoperdens BLZ1	< 75.0	< 75.0	< 75.0	< 75.0	< 75.0	< 75.0	< 75.0	< 75.0	< 75.0	< 75.0	< 75.0	< 75.0	< 75.0	< 75.0	76.6	100.0	76.6	< 75.0	< 75.0	< 75.0	< 75.0
Ca Methanoperdens Mnv1	< 75.0	< 75.0	< 75.0	< 75.0	< 75.0	< 75.0	< 75.0	< 75.0	< 75.0	< 75.0	< 75.0	< 75.0	< 75.0	< 75.0	100.0	76.6	100.0	< 75.0	< 75.0	< 75.0	< 75.0
NJEL02 Methanosarcinales archaeon ex4572-44	83.4	83.3	83.2	< 75.0	77.8	< 75.0	77.7	< 75.0	< 75.0	< 75.0	< 75.0	79.0	100.0	< 75.0	< 75.0	< 75.0	< 75.0	100.0	99.8	99.7	78.5
NJEQ01 Methanosarcinales archaeon ex4484-138	83.1	83.3	82.8	< 75.0	81.4	< 75.0	76.7	< 75.0	< 75.0	< 75.0	< 75.0	82.7	99.8	< 75.0	< 75.0	< 75.0	< 75.0	99.8	100.0	99.7	78.2
QMVJ01 Methanosarcinales archaeon B65-G16	84.4	84.3	84.3	< 75.0	80.2	< 75.0	78.7	79.2	< 75.0	< 75.0	< 75.0	81.0	99.7	< 75.0	< 75.0	< 75.0	< 75.0	99.7	99.7	100.0	78.5
RXIJ01 GoM-Arc1-GOS	78.7	78.8	79.7	89.5	93.3	93.3	93.4	93.6	92.5	93.1	93.4	93.7	78.5	89.8	< 75.0	< 75.0	< 75.0	78.5	78.2	78.5	100.0

Table S2-3 AAI similarity matrix for GoM-Arc1 and ANME-2d related genomes. Enveomics tools were used for the calculation (Rodriguez-R and Konstantinidis 2016)

	GoM-Arc1-AAA-792-C10	GoM-Arc1-AG-392-D22	GoM-Arc1-AG-392-E03	GoM-Arc1-AG-392-J18	GoM-Arc1-AG-392-M11	GoM-Arc1-AG-392-O15	GoM-Arc1-AG-393-N10	GoM-Arc1-AG-394-J04	RPGO01 Ca. Argoarchaeum ethanivorans	GoM-Arc1_E37	GoM-Arc1_E50	RXIJ01 GoM-Arc1-GOS	Methanosarcinales archaeon B25-G9	Methanosarcinales archaeon ex4484-138	Methanosarcinales archaeon ex4572-44	GoM-Arc1-LC	Methanosarcinales archaeon B65-G16	LKCM01 Ca Methanoperdens BLZ1	JMIY01 Ca Methanoperdens nitroreducens
GoM-Arc1-AAA-792-C10	100.0	72.3	57.1	75.0	60.9	61.0	55.8	66.8	80.7	58.4	58.4	79.0	75.5	55.7	58.4	78.4	59.2	48.6	49.5
GoM-Arc1-AG-392-D22	72.3	100.0	80.0	85.0	74.1	66.0	81.1	88.0	88.8	60.4	60.4	88.2	80.4	61.0	61.2	81.4	61.2	50.3	51.3
GoM-Arc1-AG-392-E03	57.1	80.0	100.0	75.4	60.2	58.1	69.1	77.7	76.2	54.8	54.1	74.8	64.5	51.1	52.5	64.7	53.7	46.8	46.7
GoM-Arc1-AG-392-J18	75.0	85.0	75.4	100.0	78.2	72.2	70.7	82.9	90.1	59.7	59.7	86.3	78.6	58.7	59.4	80.2	60.2	49.8	49.9
GoM-Arc1-AG-392-M11	60.9	74.1	60.2	78.2	100.0	62.0	48.5	61.3	83.5	56.9	57.0	80.6	71.0	54.5	56.6	73.0	55.7	47.5	48.2
GoM-Arc1-AG-392-O15	61.0	66.0	58.1	72.2	62.0	100.0	54.4	62.8	75.6	53.2	53.0	73.3	67.2	52.3	53.1	67.7	53.9	45.9	46.9
GoM-Arc1-AG-393-N10	55.8	81.1	69.1	70.7	48.5	54.4	100.0	74.5	74.1	54.3	54.7	76.7	65.3	50.6	49.6	68.3	52.1	46.3	45.9
GoM-Arc1-AG-394-J04	66.8	88.0	77.7	82.9	61.3	62.8	74.5	100.0	83.2	58.1	57.2	81.0	72.8	56.4	56.5	74.7	57.5	49.0	49.8
RPGO01 Ca. Argoarchaeum ethanivorans	80.7	88.8	76.2	90.1	83.5	75.6	74.1	83.2	100.0	62.7	62.5	90.7	84.4	63.1	63.5	87.2	62.7	51.2	52.1
GoM-Arc1_E37	58.4	60.4	54.8	59.7	56.9	53.2	54.3	58.1	62.7	100.0	98.6	63.4	62.6	80.0	80.8	63.1	80.9	51.1	52.6
GoM-Arc1_E50	58.4	60.4	54.1	59.7	57.0	53.0	54.7	57.2	62.5	98.6	100.0	63.4	62.6	79.7	81.0	63.1	80.6	50.9	52.6
RXIJ01 GoM-Arc1-GOS	79.0	88.2	74.8	86.3	80.6	73.3	76.7	81.0	90.7	63.4	63.4	100.0	84.7	63.7	63.5	86.1	63.2	52.1	52.4
Methanosarcinales archaeon B25-G9	75.5	80.4	64.5	78.6	71.0	67.2	65.3	72.8	84.4	62.6	62.6	84.7	100.0	62.9	62.9	84.7	61.0	50.5	52.0
NJEQ01 Methanosarcinales archaeon ex4484-138	55.7	61.0	51.1	58.7	54.5	52.3	50.6	56.4	63.1	80.0	79.7	63.7	62.9	100.0	94.8	62.1	95.5	51.1	52.0
NJEL02 Methanosarcinales archaeon ex4572-44	58.4	61.2	52.5	59.4	56.6	53.1	49.6	56.5	63.5	80.8	81.0	63.5	62.9	94.8	100.0	62.5	97.3	51.6	52.8
GoM-Arc1-LC	78.4	81.4	64.7	80.2	73.0	67.7	68.3	74.7	87.2	63.1	63.1	86.1	84.7	62.1	62.5	100.0	62.2	51.5	52.3
QMVJ01 Methanosarcinales archaeon B65-G16	59.2	61.2	53.7	60.2	55.7	53.9	52.1	57.5	62.7	80.9	80.6	63.2	61.0	95.5	97.3	62.2	100.0	50.0	51.2
LKCM01 Ca Methanoperdens BLZ1	48.6	50.3	46.8	49.8	47.5	45.9	46.3	49.0	51.2	51.1	50.9	52.1	50.5	51.1	51.6	51.5	50.0	100.0	67.9
JMIY01 Ca Methanoperdens nitroreducens	49.5	51.3	46.7	49.9	48.2	46.9	45.9	49.8	52.1	52.6	52.6	52.4	52.0	52.0	52.8	52.3	51.2	67.9	100.0

Table S2-2 - Summary of SAGs and MAGs presented in this study.

Internal name	Organism	Sample source	Genome type	Completeness (%)	Size (MB)	Contamination (%)
GoM-Arc1_E50_DN	*Ca.* E. thermophilum	GBE50	MAG	78	1.48	1.3
GoM-Arc1_E50	*Ca.* E. thermophilum	GBE50	Ref. genome	98	1.92	2.1
GoM-Arc1_E37	*Ca.* E. thermophilum	GBE37	Closed genome	99	1.92	2.3
GoM-Arc1-LC	*Ca.* A. ethanivorans	LC	MAG	68	1.25	0
GoM-Arc1-AMV-AAA_792_C10	*Ca.* A. ethanivorans	AMW	SAG	31	0.68	0.7
GoM-Arc1-GOM-AG-392-D22	*Ca.* A. ethanivorans	GoM	SAG	59	1.22	0.7
GoM-Arc1-GOM-AG-392-E03	*Ca.* A. ethanivorans	GoM	SAG	10	0.25	0
GoM-Arc1-GOM-AG-392-J18	*Ca.* A. ethanivorans	GoM	SAG	56	0.95	1.3
GoM-Arc1-GOM-AG-392-M11	*Ca.* A. ethanivorans	GoM	SAG	28	0.55	0
GoM-Arc1-GOM-AG-392-O15	*Ca.* A. ethanivorans	GoM	SAG	25	0.64	0
GoM-Arc1-GOM-AG-393-N10	*Ca.* A. ethanivorans	GoM	SAG	10	0.27	0
GoM-Arc1-GOM-AG-394-J04	*Ca.* A. ethanivorans	GoM	SAG	32	0.62	0
HotSEEP1_E50_DN	*Ca.* D. auxilii	GBE50	MAG	71	1.77	5
HotSEEP1_E50	*Ca.* D. auxilii	GBE50	Ref. genome	95	2.54	3.7
HotSEEP1_E37	*Ca.* D. auxilii	GBE37	MAG	87	1.8	3.5
HotSEEP1_E37_DN	*Ca.* D. auxilii	GBE37	Ref. genome	95	2.54	4.1

GBE=Guaymas Basin 50°C enrichment, LC=Loki's Castle, GoM=Gulf of Mexico; AMV=Amon Mud Volcano; MAG=metagenome assembled genome; SAG=Single amplified genome; Ref. genome=consensus reference genome

Table S2-3 Genomes and gene expression data of the Ethane50 culture and overview of genes potentially involved in the ethane metabolism and electron cycling in the Ethane50 culture. Expression values shown in triplicates for *Ca.* E. thermophilum and *Ca.* D. auxilii.

Large excel table can be downloaded under following link:

https://journals.asm.org/doi/suppl/10.1128/mBio.00600-20/suppl_file/mbio.00600-20-st003.xlsx

Table S2-4 Overview of environmental sampling sites used for this study.

Location	Cruise	Station	Location (latitude, longitude)	Site description	Methods applied	Site reference
Hydrate Ridge	SO148/1	19-2	44.34104, -125.08807	Beggiatoa mat and gas hydrates	CARD-FISH; Cell abundance estimation	(Linke and Suess 2001)
Hydrate Ridge	SO148/1	38-1	44.34186, -125.08847	Calyptogena field and gas hydrates	CARD-FISH; Cell abundance estimation	(Linke and Suess 2001)
Guaymas Basin	AT15-40	4489-1	27.0468, -111.24537	Yellow mat and hydrocarbon rich	CARD-FISH; Cell abundance estimation	(Meyer et al. 2013)
Guaymas Basin	AT37-06	4869-26	27.00, -111.24	Orange microbial mat and hydrocarbon rich	Cultivation; CARD-FISH; DNA and RNA sequencing	(Meyer et al. 2013)
Gulf of Mexico	M114/2	19351-14	21.8999, -93.43518	Microbial mat and crude oil	Single cell genomes	(Sahling et al. 2016)
Gulf of Mexico	M67/2	10625-9	21.53907, -93.262049	Oily sediment	CARD-FISH; Cell abundance estimation	(Bohrmann et al. 2008)
Gulf of Mexico	SO174	140	21.90002, -93.43727	Gas hydrates, oil and carbonates	CARD-FISH; Cell abundance estimation	(Bohrmann and Schenck 2003)
Gulf of Mexico	SO174	156	27.78247, -91.50777	Tubeworms and gas hydrates	CARD-FISH; Cell abundance estimation	(Bohrmann and Schenck 2003)
Gulf of Mexico	SO174	161	27.55807, -90.98098	Gas hydrates, oily sediment, melted gas hydrates	CARD-FISH; Cell abundance estimation	(Bohrmann and Schenck 2003)
Amon Mud Volcano	M70-2	760-113	32.221299, 31.426623	Bacterial mat and gassy seep	Single cell genome; CARD-FISH; Cell abundance estimation	(Dupré et al. 2008)
Locis Castle	R/V G.O. Sars cruise to the LCVF in 2009 and 2010	BaCh2	73.3399, 8.097	Small barite chimney and hydrothermal sediment densely populated with S. contortum	CARD-FISH; Metagenomics	(Steen et al. 2016)
Katakolo Bay	/	/	37.64477, 21.32019	Gassy seep	CARD-FISH	(Etiope et al. 2013)

Table S2-5 Marker genes used for calculation of genome tree based on archaeal marker genes presented in Rinke et al. (2013).

Excel table can be downloaded under following link:

https://journals.asm.org/doi/suppl/10.1128/mBio.00600-20/suppl_file/mbio.00600-20-st005.xlsx

Table 2-6 Development of ethane, sulfide and sulfate concentrations in E50 culture in triplicates.

Ethane (mmol)										
Days of incubation	**3**	**11**	**17**	**26**	**32**	**39**	**46**	**53**	**60**	**67**
Ethane_1	8.73	7.76	6.97	6.11	4.96	4.14	3.58	3.03	2.49	2.11
Ethane_2	8.67	7.54	6.95	6.02	4.81	3.88	3.22	2.73	2.28	1.95
Ethane_3	8.83	7.74	6.89	6.33	5.23	4.48	3.81	3.22	2.74	2.32
Negative_1	1.24	1.08	1.08	1.08	1.08	1.08	1.08	1.08	1.08	1.08
Negative_2	1.24	1.08	1.08	1.08	1.08	1.08	1.08	1.08	1.08	1.08
Negative_3	1.24	1.08	1.08	1.08	1.08	1.08	1.08	1.08	1.08	1.08
Sulfide (mmol)										
Days of incubation	**3**	**11**	**17**	**26**	**32**	**39**	**46**	**53**	**60**	**67**
Ethane_1	0.73	1.53	2.65	5.02	6.65	8.29	10.29	10.47	11.42	12.04
Ethane_2	0.87	1.45	2.51	4.44	5.02	6.15	7.60	7.20	8.76	8.44
Ethane_3	0.84	1.35	2.65	4.51	5.85	6.84	8.00	7.96	10.76	10.98
Negative_1	0.73	0.18	0.29	0.11	0.36	0.29	0.15	0.15	0.22	0.15
Negative_2	0.73	0.07	0.15	0.04	0.29	0.36	0.22	0.15	0.33	0.18
Negative_3	0.80	0.15	0.11	0.04	0.29	0.25	0.18	0.22	0.29	0.04
Sulfate (mmol)										
Days of incubation	**3**	**11**	**17**	**26**	**32**	**39**	**46**	**53**	**60**	**67**
Ethane_1	17.69	16.55	15.93	14.48	12.83	12.21	11.58	11.00	9.75	9.02
Ethane_2	17.26	17.04	16.11	14.63	14.36	13.56	13.50	12.85	12.16	11.80
Ethane_3	17.03	17.11	0.20	14.72	14.07	13.37	12.69	12.02	10.52	10.12
Negative_1	18.17	18.00	17.64	17.39	17.23	17.86	18.21	17.90	17.17	17.60
Negative_2	17.87	18.07	17.41	16.94	17.99	17.88	18.14	18.04	17.48	16.75
Negative_3	17.58	17.93	17.85	17.67	17.15	18.22	18.01	18.33	17.08	17.77

Table 2-7 Development of sulfide concentration in E50 culture in 10 replicates.

	Sulfide (mmol)																				
Days of incubation	**0**	**2**	**5**	**7**	**10**	**12**	**14**	**16**	**18**	**21**	**23**	**25**	**27**	**29**	**31**	**33**	**35**	**37**	**39**	**44**	**46**	**49**
E501to10C1	0.33	0.58	1.09	1.31	2.62	2.95	3.42	4.40	4.87	6.22	6.69	7.20	8.51	9.31	9.67	9.71	11.75	14.11	14.62	15.60	16.40	16.91
E501to10C2	0.18	0.58	1.09	1.38	2.44	2.95	3.13	4.40	4.91	5.64	6.44	7.89	8.47	8.76	10.15	10.55	12.04	13.82	14.51	15.89	16.11	17.24
E501to10C3	0.33	0.62	1.27	1.53	2.69	3.35	3.82	4.84	5.45	6.29	7.45	7.96	9.16	9.45	10.65	10.98	13.20	13.78	14.00	15.93	17.35	17.42
E501to10C4	0.47	0.58	1.16	1.31	2.58	2.87	3.78	4.36	5.02	6.36	6.98	7.85	9.67	9.85	10.62	11.05	13.27	14.07	14.25	16.29	17.05	18.29
E501to10C5	0.36	0.51	0.95	1.20	2.00	2.73	2.95	4.00	4.33	5.53	5.89	7.05	8.00	8.73	9.53	9.56	10.76	12.07	12.69	14.51	16.36	16.33
E501to10C6	0.44	0.73	1.16	1.35	2.40	2.98	2.95	4.29	4.51	5.64	5.75	7.02	7.93	8.51	10.00	10.18	11.05	12.55	13.20	13.53	15.02	16.36
E501to10C7	0.36	0.65	1.09	1.31	2.40	2.95	3.42	3.85	4.36	5.16	6.00	6.84	7.24	8.15	8.76	9.38	10.73	11.35	11.93	13.24	14.15	14.18
E501to10C8	0.47	0.58	1.13	1.42	2.44	3.16	3.45	3.96	5.20	5.89	6.69	7.85	8.51	8.84	10.40	10.58	13.05	13.64	13.78	14.76	16.55	16.65
E501to10C9	0.44	0.55	0.87	0.98	1.67	2.18	2.58	3.13	3.75	4.47	4.98	5.89	6.65	7.13	8.04	8.36	10.40	10.95	11.35	13.20	13.96	14.44
E501to10C10	0.44	0.58	0.87	1.02	2.00	2.40	2.91	3.27	3.60	4.55	5.02	6.22	6.98	7.67	9.16	8.91	11.38	11.89	12.98	13.20	13.45	15.85

Table S2-8 Development of ethane and sulfide concentrations in triplicates of the Ethane50 culture with hydrogen gas (1.5 atm) with and without sulfate.

Ethane (µmol per liter culture)				
Days of incubation	**0**	**5**	**19**	**27**
Positive_S1	1.5 atm	1.5 atm	1.5 atm	1.5 atm
Positive_S2	1.5 atm	1.5 atm	1.5 atm	1.5 atm
Positive_S3	1.5 atm	1.5 atm	1.5 atm	1.5 atm
No_SO42-_S4	1.00	0.11	0.26	0.22
No_SO42-_S5	0.77	0.34	3.24	5.65
No_SO42-_S6	0.50	1.04	11.22	17.05
With_SO42_S7	0.31	0.17	0.20	0.20
With_SO42_S8	0.21	0.20	0.22	0.27
With_SO42_S9	0.31	0.14	0.14	0.15
Sulfide (mmol per liter culture)				
Days of incubation	**0**	**5**	**19**	**27**
Positive_S1	0.11	2.04	9.89	13.78
Positive_S2	0.07	6.40	22.69	27.38
Positive_S3	0.07	1.96	9.31	11.42
No_SO42-_S4	0.11	0.00	0.15	0.25
No_SO42-_S5	0.11	0.29	0.11	0.29
No_SO42-_S6	0.18	0.25	0.22	0.15
With_SO42_S7	0.11	0.00	0.62	1.09
With_SO42_S8	0.07	0.40	1.71	2.51
With_SO42_S9	0.07	0.40	1.64	2.40

Chapter 3

Spatial resolution of ethyl-coenzyme M reductase gene expression in ethane-oxidizing microbial consortia

Cedric J. Hahn[1], Andreas Ellrott[1], Gunter Wegener[1,2,3], Rudolf Amann[1], and Katrin Knittel[1]

[1] Max-Planck Institute for Marine Microbiology, 28359 Bremen, Germany

[2] MARUM, Center for Marine Environmental Sciences, University of Bremen, Bremen, Germany

[3] Alfred Wegener Institute Helmholtz Center for Polar and Marine Research, Bremerhaven, Germany

Manuscript in preparation.

3.1 Abstract

At gas-rich vents and seeps, microbial consortia of ethane-oxidizing archaea and sulfate-reducing bacteria mitigate the flux of ethane from deep marine sediments into the oceanic water column. The ethanotrophic archaea lack a reductive pathway. Instead, they transfer the liberated electrons to their partner bacteria. A well-mixed arrangement of both partners would favor the syntrophic interactions via the transfer of molecular intermediates in the consortia. However, fluorescence in-situ hybridization (FISH) images of consortia show that the cells are spatially segregated. The anaerobic oxidation of ethane (AOE) by the archaea is driven by ethane activation by the key enzyme ethyl-coenzyme M reductase (ECR). Here, we visualized gene transcripts for the catabolic alpha subunit of ethyl-coenzyme M reductase (*ecrA*) and investigated its expression within the consortia. We designed a set of six probes targeting different regions of the *ecrA* transcript sequence, and each probe was labeled with four fluorophores. These probes were hybridized to fixed samples of an AOE culture enriched from heated sediment from the Guaymas Basin, Gulf of California. Signal intensity corresponds to the *ecrA* expression level within archaeal-bacterial consortia. Using this direct mRNA-FISH technique, we analyzed 67 monospecies clusters of *Ca.* Ethanoperedens for the expression of *ecrA*. This analysis revealed differences in *ecrA* expression in the archaeal monospecies cluster. Central regions of the clusters showed lower *ecrA* expression, independent of the size of the cluster. A 3D image of a *Ca.* Ethanoperedens monospecies cluster at the outside of a consortium showed the highest transcription activity at the archaeal-bacterial interface, while the activity in cells with greater distance to the partner bacteria was lower. The direct mRNA-FISH staining approach allowed the visualization of fine-scaled activity differences in microbial consortia.

3.2 Introduction

The symbiotic partnership between alkanotrophic archaea and sulfate-reducing bacteria (SRB) is of great importance for the understanding of the cycling of short-chain alkanes in deep marine sediments (Knittel and Boetius 2009, Evans et al. 2019). Multicellular consortia of alkanotrophic archaea and SRB are responsible for the degradation of large parts of the short-chain alkanes within the anoxic sediment layers and thus prevent gas emissions to the water

column and, finally, the atmosphere (Boetius et al. 2000, Joye et al. 2004, Etiope and Ciccioli 2009, Mastalerz et al. 2009, Laso-Pérez et al. 2016, Laso-Pérez et al. 2019, Hahn et al. 2020). Despite the importance of these consortia, we still lack an understanding of their internal organization. Since the partner cells depend on the transfer of reducing equivalents for growth, a mixing of the cells would be expected to minimize the distance between the archaea and bacteria. Instead, most alkanotrophic archaea form segregated consortia that result in large distances between these partners (Knittel et al. 2005, Laso-Pérez et al. 2016, Wegener et al. 2016, Hahn et al. 2020).

Consortia describe functional assemblages of cells living in a syntrophic relation. In segregated alkanotrophic consortia, the archaeal cells form monospecies clusters that are surrounded by several layers of bacterial cells. Alkanotrophic consortia can consist of a single archaeal monospecies cluster surrounded by bacterial cells or several archaeal clusters with bacterial cells in between (Knittel et al. 2005, Wegener et al. 2016, He et al. 2021). Based on bioorthogonal noncanonical amino acid tagging (BONCAT) and active $^{15}NH_4$ assimilation, it has been shown that in segregated alkanotrophic consortia, all cells are active, and only in monospecies clusters with large distances to the archaeal-bacterial interface a decrease in metabolic activity can be measured (McGlynn et al. 2015, Hatzenpichler et al. 2016, He et al. 2021). The cell activity drops by >70% when the distance to the bacterial-archaeal interface reaches 15 µm for bacteria and 30 µm for archaea (He et al. 2021). An alternative way to measure the activity of cells is to target the transcribed mRNA of key genes for their metabolism. The mRNA is an instable product and has a high turnover rate in cells, which is estimated to be in the range of minutes in most cases (Selinger et al. 2003, Andersson et al. 2006, Chan et al. 2018, Vargas-Blanco and Shell 2020). This high turnover rate allows for the detection of dynamic changes of functions and activities in microbial communities. The gene expression in microbial communities can be assessed by real-time reverse transcription polymerase chain reaction (RT-qPCR) or metatranscriptomic studies (Nolan et al. 2006, Frias-Lopez et al. 2008). The dynamic characteristics of mRNA can also be used as a functional activity indicator on a single-cell level by fluorescence in-situ hybridization (FISH). This approach was used to visualize expressed particulate methane monooxygenase (pMMO) and link it to 16S rRNA-based identity in environmental sediment samples (Pernthaler and Amann 2004). The mRNA was hybridized with polynucleotide probes (450 nucleotides) labeled with horseradish peroxidase (HRP), and an amplified fluorescent signal was achieved in a secondary catalyzed reporter deposition (CARD) reaction (Pernthaler et al. 2002, Pernthaler and Amann 2004). Also, oligonucleotide-based approaches to assess activity on mRNA level have been

presented, using different amplification based methods like RNase H-assisted rolling circle amplification (Roll)-, click-amplifying (Clamp)- and hybridization chain reaction (HCR)-FISH (Wu et al. 2018, Rouhanifard et al. 2019, Takahashi et al. 2020, Metcalfe et al. 2021). Amplification based FISH methods are good to target low abundance target molecules, but are in general time intensive, and a direct correlation to target gene abundance is not possible. In a study using directly labeled oligonucleotide probes, Skinner et al. (2013) were able to correlate mRNA expression rates to mRNA-FISH signal intensity directly. However, they used an extensive probe set of 48 – 76 oligonucleotides per target for *Escherichia coli* pure cultures. In a recent study, *mcrA* transcripts were stained in a *Methanosarcina barkeri* culture and an ANME-2 enrichment with a novel technique called fluorescent in-situ hybridization of transcript-annealing molecular beacons (FISH-TAMB). This technique uses directly labeled molecular beacons that contain oligonucleotide sequences and can hybridize to target sequences without prior fixation (Harris et al. 2021). In general, mRNA-FISH holds more challenges than 16S rRNA-FISH since specific mRNAs are present in far lower copy numbers compared to 16S rRNA sequences. While only about 50 mRNA sequence copies can be expected at a time for a highly expressed gene, the number of ribosomal bound 16S rRNA can exceed 1000 copies (Skinner et al. 2013). In addition to the low copy numbers, mRNA sequences are less stable than 16S rRNA and can easily be degraded by RNases. Therefore, mRNA-FISH requires more careful handling of samples.

In this study, we work with the enrichment culture Ethane50 containing consortia of the anaerobic ethane oxidizer *Ca.* Ethanoperedens thermophilum and its sulfate-reducing partner bacterium (SRB) *Ca.* Desulfofervidus auxilii (Hahn et al. 2020). This culture grows at 50°C with ethane as the sole substrate and has an exceptionally high activity for alkanotrophic cultures, with doubling times of approximately 7 days (Hahn et al. 2020). Consortia in the Ethane50 culture can reach up to 100 µm in diameter and are tightly packed with spatially segregated bacterial and archaeal cells. The spatially segregated consortia form multiple archaeal monospecies clusters surrounded by bacterial partner cells. *Ca.* Ethanoperedens cells highly express the key gene for anaerobic oxidation of ethane (AOE), the ethyl-coenzyme M reductase (ECR) (Hahn et al. 2021). Here, we adapted the before mentioned method of mRNA-targeted FISH to assess the transcription-based activity of *Ca.* Ethanoperedens within consortia of the Ethane50 culture. We used tetra labeled oligonucleotides to hybridize to transcripts of the catalytic subunit alpha of the ECR (*ecrA*). This amplification independent approach allows for dynamic mRNA detection with a probe set of only six probes. We used this technique to assess the *ecrA* expression-based activity of *Ca.* Ethanoperedens

thermophilum cells and investigated how increasing distance to the bacterial-archaeal interface affects expression of this key gene for ethane consumption.

3.3 Material and methods

3.3.1 Origin and maintenance of Ethane50 culture

Sediment samples for the establishment of the Ethane50 culture derived from the Guaymas Basin hydrothermal vent and were collected during the RV Atlantis mission AT 37-06 with the submarine Alvin in December 2016. Sediment aliquots were mixed with SR medium for sulfate-reducing bacteria (Widdel and Bak 1992), and ethane was added as substrate. Samples were incubated at 50°C in 100 ml injection vials, and activity was tracked by measurement of ethane-dependent sulfide production using a copper sulfate assay (Cord-Ruwisch 1985). The active cultures were diluted several times over the period of one year until a sediment-free culture was established (for details, see Laso-Pérez et al. (2018) and Hahn et al. (2020)). Cultures were further kept at 50°C in 1 l Duran flasks with 800 ml medium and 1.5 bar ethane in the headspace. The medium was exchanged once 15 mM sulfide was formed, and when 10 mM sulfide was formed within ~7 days, cultures were diluted 1:10.

3.3.2 Phylogeny of MCR and ECR alpha subunits

400 complete or nearly complete amino acid sequences of the alpha subunits of MCR and ECR were automatically aligned with ClustalΩ (Sievers et al. 2011) with default parameters. Sequences were obtained from public databases. Complete sequences were used, and 957 amino acid positions were considered for the analysis. Aligned sequences were masked using Zorro (https://sourceforge.net/projects/probmask/). The phylogenetic tree was calculated with RAxML version 8.2.12 (Stamatakis 2014) with PROTGAMMAAUTO model, LG likelihood amino acid substitution settings, and 100 fast bootstraps. The final tree was visualized with iTol v6 (Letunic and Bork 2016).

3.3.3 *EcrA* mRNA probe design

Four *Ca.* Ethanoperedens, four *Ca.* Argoarchaeum and four canonical MCR *ecr*A gene sequences were translated to amino acid sequences using translatorX (Abascal et al. 2010). An automated alignment was created using ClustalW (Larkin et al. 2007) with default parameters. The amino acid alignment was then used as a backbone for the nucleic acid alignment. Aligned *ecrA* gene sequences were manually checked for highly conserved regions to design the probes. Six probes with a length of 39 – 40 bases with zero mismatches to the cultures *Ca.*

Ethanoperedens E37 and E50 were designed (Figure 3-1A). The probes showed no more than two mismatches to environmental *ecrA* gene sequences of the genus *Ca.* Ethanoperedens. Sequence similarity between *Ca.* Ethanoperedens and *Ca.* Argoarchaeum was too low to find a probe that covers the *ecrA* of both genera. The dissimilarity to canonical MCR is considerable so that a false binding can be excluded with at least 11 mismatches (Figure 3-1). Only about 4 mismatches would still allow binding of the probe to oligonucleotide sequences of a length of 40 bases. Probes were ordered from biomers.net (Ulm, Germany) with 4xAlexa488 fluorophores attached.

Table 3-1 Probes targeting *ecrA* mRNA sequences. Four Alexa488 fluorophores per probe were directly attached to either guanine or cytosine. Modifications on the probe sequences are indicated by a "6" for modified guanine or a "7" for modified cytosine.

Probe name	Probe sequence	G+C-content [%]
ecrA-245	T6CCCACTCGCG6TCAAGACCT6TTATCCTGTAGGTCT6C	57.5
ecrA-367	G7ATATCGTCGTAG7ACTGCTGCATTG7AGGGTTGTT7TC	52.5
ecrA-529	7TGGGTTTGTCT7TGCTGTGTGCTC7ATCATGATCGCA7C	55
ecrA-584	CT6CCAGTTCATC6TTTCCTGTGAA6CACTTGGCATA6C	51.3
ecrA-996	6ACCTTTACT6GGTCAATTCCGCC6TCAAGCCCTTCGA6T	55
ecrA-1148	TA6ATTGCGCC6TGGTATCC6TAGTCTTCGA6CACCTCAT	52.5

3.3.4 mRNA fluorescence in-situ hybridization (mRNA-FISH)

Aliquots from the Ethane50 culture were fixed in 4% formaldehyde for 1.5 h at room temperature. Fixed samples were washed two times in PBS (pH 7.4) and afterward stored at -20°C in PBS-ethanol (1:1). An aliquot was filtered on GTTP polycarbonate filters (0.2 µm pore size; Millipore, Darmstadt, Germany) at -200 mbar pressure. Filters were stored at -20°C. The FISH experiment was performed on a filter section. The reaction was started in a screw cap polyethylene hybridization chamber with a tissue soaked in deionized water mixed with formamide concentration according to hybridization buffer and 2.25 M NaCl. 45 µl of the hybridization buffer (0.9 M NaCl, 20 mM Tris-HCl pH 8.0, 35% (vol/vol) formamide, 1% (wt/vol) Blocking Reagent (Roche Diagnostics, Germany), 10% (wt/vol) dextran sulfate and 0.02 % (wt/vol) sodium dodecyl sulfate (SDS); modified from Pernthaler et al., 2002) were mixed with 5 µl probe mix containing 8.4 pmol/µl of each probe. The probes were labeled with four Alexa-488 tyramides. The hybridization buffer probe mixture was placed in 50 µl droplets on a petri dish, and filter pieces were placed face down into the droplet. Petri dish with filter pieces was placed in the reaction chamber and incubated for 3 h at 46°C. After the

hybridization, the filter pieces were removed from the hybridization mixture and incubated in pre-warmed stringent washing buffer (0.08 M NaCl, 20 mM Tris-HCl pH 8.0, 5 mM EDTA pH 8.0, 0.01 (wt/vol) SDS) for 15 minutes at 48°C. Filter sections were washed 30 seconds in deionized water and briefly dipped in 80% ethanol. Filter sections were air-dried and then placed face down in a 70 µl droplet of DAPI solution (4,'6'-diamino-2-phenylindole; 1 µg/ml in deionized water). Filter pieces were incubated for 7 minutes at room temperature and then washed for 30 seconds in deionized water and briefly dipped in absolute ethanol. After air-drying, the filter pieces were placed on microscopy slides with mounting solution (Citifluor AF1, Electron Microscopy Sciences, Hatfield, USA and Vectashield, Vector Laboratories, California, USA; 3:1 (vol/vol)) and were stored at -20°C. For double hybridization of *Ca*. Ethanoperedens and *ecrA* mRNA, 2.5 µl probe working solution of the probe GOM-Arc-I-660 tetra-labeled with Alexa-594 targeting 16S rRNA of *Ca*. Ethanoperedens (Laso-Pérez et al. 2019) and 2.5 µl of the *ecrA* mRNA probe mix were added to the hybridization buffer. Stained filter pieces were analyzed by confocal laser scanning epifluorescence microscopy (CLSM; model LSM 780; Zeiss, Germany), including the Airyscan technology.

3.3.5 Determination of *ecrA* mRNA signal distribution

Fluorescent micrographs were taken with the CLSM showing double hybridized cells with probes specific for the 16S rRNA gene of *Ca.* Ethanoperedens and the *ecrA* mRNA sequence were used for image analysis. For image preparation, individual stack layers were imported into ZEN software (black edition, Zeiss, Germany). Images were "min/max" scaled in the *ecrA* mRNA probe signal containing channel. Afterward, the channel background was reduced by limiting the signal to the peak region. Image sections containing consortia were exported from Zen using the "cut region" function. Images were then transformed to greyscale in Irfanview (https://www.irfanview.com/). *EcrA* mRNA probe signals were automatically counted using ACMEtool3 (Bennke et al. 2016) (M. Zeder; https://www.mpi-bremen.de/automated-microscopy.html). Following parameters were used for the automated counting of mRNA-FISH signals: Preprocessing: lowpass filter, kernel size = 3, iterations = 3; Cell detection: dynamic threshold, min. intensity = 128, kernel size = 6, offset = 8. The exact area of the archaeal monospecies clusters was manually defined based on DAPI signals, corresponding to 16S rRNA probe GoM-Arc-I-660 FISH signals targeting *Ca.* Ethanoperedens. A region of interest (ROI) was manually drawn around the monospecies clusters. Automatically detected mRNA signals were manually verified, and signals missed by the software were added manually. Finally, numbers of mRNA signals and their exact position

within a region of interest (x-, y-coordinates) were exported to Excel. The signal position was calculated from the bounding boxes vertices x- and y-coordinates by using the following equation to determine its central point (calculation according to Probandt et al. (2018)):

Eq. I $$center_x = left + \frac{right - left}{2}$$

Eq. 2 $$center_y = top + \frac{bottom - top}{2}$$

Coordinates of the boundary points of the ROI were used to define the monospecies cluster area. From the ROI boundary, several distance classes towards the monospecies cluster center were defined by steps of 0.54 µm corresponding to the average cell diameter of *Ca.* Ethanoperedens cells. These distance classes will further be called rings for simplicity. Coordinates of the *ecrA* mRNA FISH signals were then assigned to the monospecies cluster area, i.e., ring number and signals per ring were counted. The signals per ring were normalized against the ring area, yielding signals per µm^2 for each distance ring (see Figure S3-1 for visual example).

3.3.6 Average cell size of *Ca.* Ethanoperedens

To define the ring width for the calculation of the *ecrA* mRNA-FISH signal distribution, an average cell diameter for *Ca.* Ethanoperedens had to be calculated. We prepared images for ACMEtool3 as described before and used ROI to define the area of individual *Ca.* Ethanoperedens cells based on DAPI signals corresponding to 16S rRNA probe FISH signals. *Ca.* Ethanoperedens have a coccoid shape, and therefore a spherical shape was assumed for the diameter calculation.

Eq. 3 $$cell\ diameter = \left(\sqrt{\frac{cell\ area}{\pi}}\right) * 2$$

The calculated diameter was scaled for the conversion from pixel to µm depending on the scaling factor (see Tab. S3-1 for details). 30 cells were measured, and a mean diameter of 0.54 µm with a standard deviation of 0.13 µm was calculated.

3.4 Results

3.4.1 In-situ detection of ethyl-coenzyme M reductase transcripts

To study changes in the transcription-based activity of ethanotrophic cells in densely packed consortia, we designed a set of six tetra-labeled oligonucleotide probes. The probes are 39 – 40 nucleotides in length and have a GC content in the range of 51.3 – 57.5%. These probes were used for FISH to target mRNA transcripts of the catalytic alpha subunit of the *ecr* gene (Figure 3-1A). The probe set is specific for *ecrA* transcripts of the thermophilic ethanotrophic genus *Ca.* Ethanoperedens, including sequences from enrichment cultures and Guaymas Basin sediment samples (Figure 3-1B) (Dombrowski et al. 2017, Dombrowski et al. 2018, Hahn et al. 2020). The probes have no mismatches to the two sequences of *Ca.* E. thermophilum growing in the Ethane37 and Ethane50 cultures. They have up to two mismatches to *ecrA* from metagenome-assembled genomes of uncultured *Ca.* Ethanoperedens strains. Nevertheless, with two mismatches on 40 bases, the probes would still bind to the target (Moraru et al. 2011). Although the ECR is a homolog of the methyl-coenzyme M reductase (MCR), false-positive signals from other MCR homologs can be excluded. The sequence similarity to canonical and non-canonical *mcrA* sequences is low, with an identity of ~50% and at least nine mismatches for each probe-target region (Figure 3-1AB). The ethane-oxidizing archaeon *Ca.* Argoarchaeum contains an *ecrA* homolog with a nucleotide sequence similarity of ~68% to *Ca*. Ethanoperedens *ecrA* (Chen et al. 2019, Hahn et al. 2020) and at least five mismatches to all designed probes (Fig 3-1A). Thus, members of the genus *Ca.* Argoarchaeum could not be targeted. Developing a universal ecrA probe set for detecting all known ethanotrophs was impossible due to the high sequence dissimilarity of *ecrA* between the two genera. Hence, the designed *ecr*A primers are specific to *Ca.* Ethanoperedens.

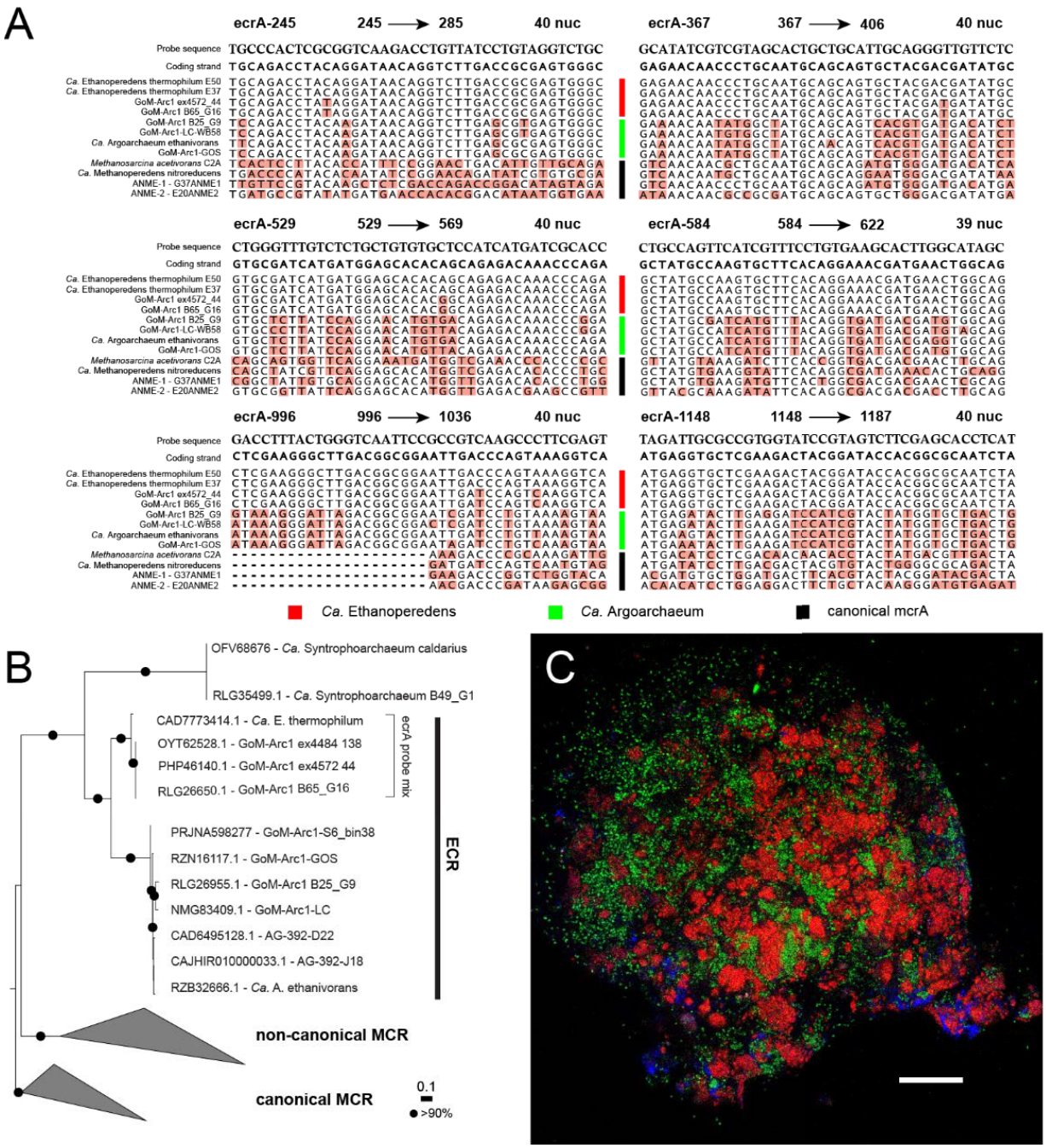

Figure 3-1 Alignment of *ecrA* genes, the phylogeny of alpha subunits of MCR/ECR and micrograph of a *Ca.* Ethanoperedens/*Ca.* Desulfofervidus consortium. A Alignment of publically available sequences of *ecrA* and *mcrA* for the target sites of the six *ecrA* mRNA probes (*Ca.* Ethanoperedens (red bar), *Ca.* Argoarchaeum (green bar) and canonical *mcr*A (black bar); additional sequence information Table S3**)**. Light red background indicates mismatches to the probe sequence. Given positions refer to *Ca.* Ethanoperedens thermophilum E50 *ecrA* sequence. **B** Phylogenetic tree based on 400 amino acid sequences of the alpha subunit of ECR and MCR. ECR sequences form a distinct branch divided into sequences affiliated to *Ca.* Argoarchaeum and *Ca.* Ethanoperedens. The ecrA probe mix only targets *ecr*A sequences affiliated with *Ca.* Ethanoperedens. Scale bar indicates 10% sequence divergence and ● indicates bootstrap values of > 90%. **C** Epifluorescence micrograph of microbial consortia stained with probes for *Ca.* Ethanoperedens (GOM-Arc1-660, red) and *Ca.* Desulfofervidus (HotSeep1-1465, green, Krukenberg et al. (2016)) in the Ethane50 culture. Cells were counterstained with DAPI (blue). Scale bar 20 µm.

For the tetra-labelled *ecrA* mRNA probe mix, we used a simple FISH protocol that can be executed within 4 – 5 hours (see material and methods). The staining is based on the direct

labeling of target cells since the fluorophores are directly attached to the probes. A great advantage of direct labeling is that the signal strength correlates with the amount of probe bound to mRNA transcripts and, consequently, with the gene's expression in individual cells. The binding of 24 fluorophores (6 probes x 4 fluorophores) per mRNA molecule can be achieved when all six probes bind to the target sequence. For a highly expressed gene, we expect ~50 mRNA copies per cell (Skinner et al. 2013). Therefore, each cell may hybridize with around 1200 fluorophores, which exceeds the minimum amount of ~400 fluorophores per cell for detection (Hoshino et al. 2008, Schimak et al. 2016, Barrero-Canosa et al. 2017).

At the time of the harvest of the Ethane50 culture, the activity was confirmed by high rates of ethane-dependent sulfide production (~10 mM sulfide within 10 days). Confocal laser-scanning microscopy (CLSM) with Airyscan technology allowed the detection of *ecrA* mRNA probe signals. A double hybridization of the samples with the tetra labeled 16S rRNA probe GOM-Arc1-660 locates the *ecrA* probe fluorochrome in the cells of *Ca.* E. thermophilum (Fig 3-2A-D). *EcrA* mRNA signals were detected at several spots within the archaeal cells, indicating areas of *ecrA* mRNA accumulation. In comparison, the 16S rRNA targeting probe caused a bright signal equally distributed over the whole cell area (Figure 3-2B). The probe signal was clearly distinguishable from the background signal that was emitted from the consortia matrix and the SRB partner cells (Figure 3-2C). This background signal appeared blurry without identifiable spots. As a negative control, we used cultures that were incubated without ethane. Starved *Ca.* Ethanoperedens cells did not show *ecrA* signals (Figure 3-2G).

3.4.2 Induction of *ecrA* transcription

To test how substrate availability affects *ecrA* gene transcription in *Ca.* E. thermophilum, we studied *ecrA* transcript-based activity in three different growth conditions (for details, see materials and methods). Condition A) Active Ethane50 culture grown for seven days on ethane; condition B) Ethane50 culture starved for five days without ethane in the medium and condition C) induction of ethane oxidation by adding 1 bar ethane to the starved culture and incubation for three days before subsampling. The active Ethane50 culture showed specific *ecrA* mRNA signals as described before. Hybridization of the starved cells resulted in no specific signals, and only an unspecific background signal was detectable (Figure 3-2E-H). In contrast, starvation did not affect the signal intensity of the 16S rRNA probe. The re-induced *Ca*. Ethanoperedens cells showed clear signals that appeared to be even stronger than the signals of cells that have been constantly exposed to ethane (Figure 3-2I-L).

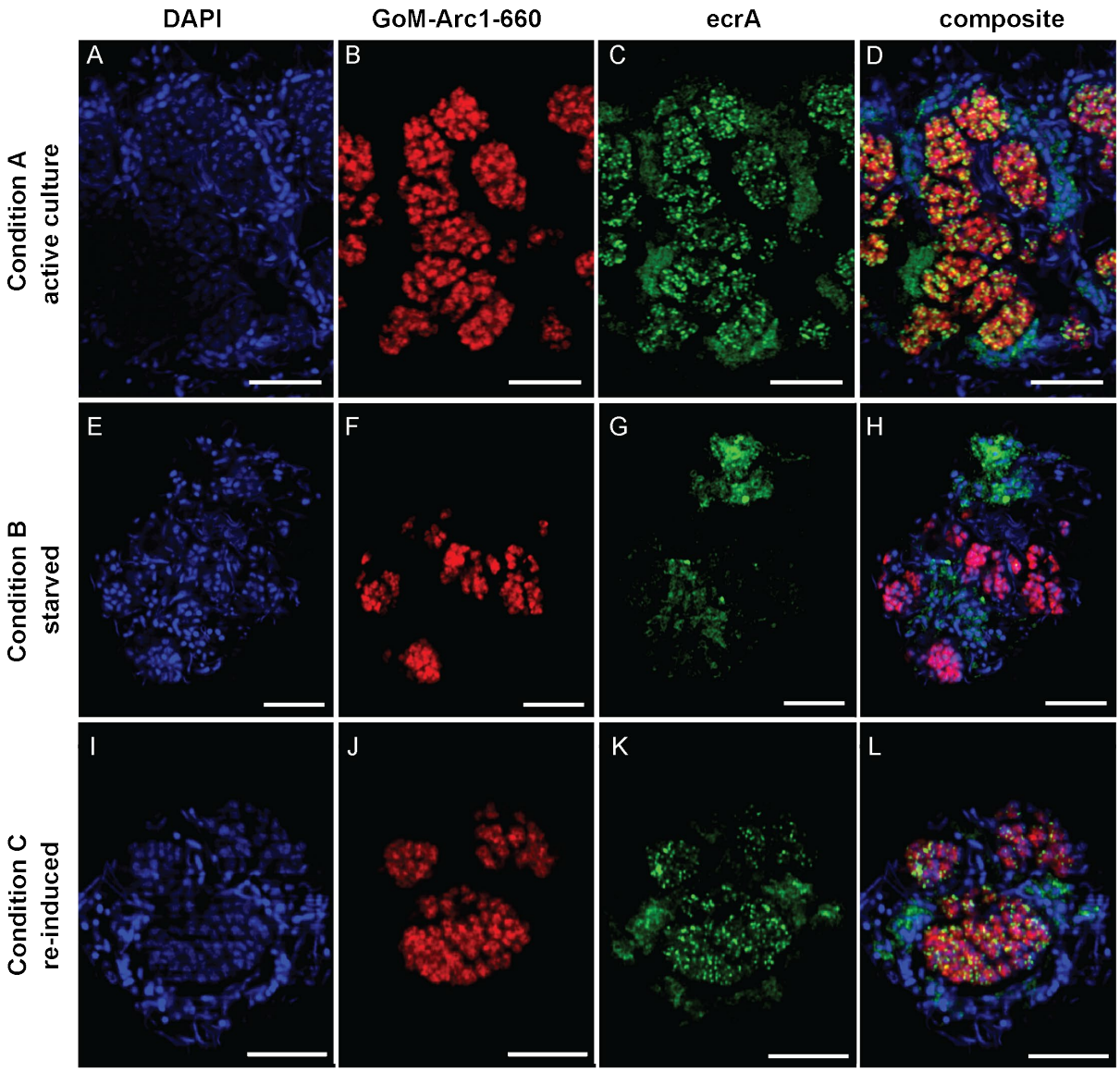

Figure-3-2 Laser scanning micrographs of Ethane50 culture stained with ecrA probe. Panels **A-D** show an active Ethane50 culture; panels **E-H** show an Ethane50 culture incubated five days without ethane, and panels **I-L** show a re-induced Ethane50 culture three days after ethane addition. *Ca.* Ethanoperedens cells were hybridized with the 16S rRNA probe GOM-Arc1-660 (red) and the mRNA targeting *ecrA* probe mix (green). Samples were counterstained with DAPI (blue). Scale bar indicates 2 µm.

3.4.3 Spatial distribution of *ecrA* gene expression

Ca. Ethanoperedens and its sulfate-reducing partner bacterium are organized in segregated consortia of a size of 4 to over 100 µm in diameter. These consortia consist of a single or of multiple archaeal monospecies clusters surrounded by the bacterial partner cells (Figure 3-1C). We investigated a total of 67 *Ca.* E. thermophilum monospecies clusters with diameters between 3 µm and 13 µm. Such monospecies clusters consist of ~20 to ~1750 cells, assuming spherical shapes. Monospecies clusters were divided into rings for data analysis, ranging from the bacteria-archaeal interface to the center, with a ring width of the average cell size of *Ca.* Ethanoperedens of 0.54 µm. The average number of signals ranged between 1 and

3 signal per µm^2 with a standard deviation (SD) of +/- ~1 throughout the monospecies cluster. Even cells in the center of larger monospecies clusters, with a distance of up to 6.48 µm to the bacterial-archaeal interface, show *ecrA* expression (Figure 3-3). However, most signals per µm^2 were counted within 1.62 µm to the bacterial-archaeal interface with ~2.5 signals per µm^2 (+/- 1.04 – 1.40 SD), indicating that cells close to the bacterial-archaeal interface might be slightly more active. In the distance range from 1.63 to 3.78 µm, the counted signals dropped to ~1.5 signals per µm^2 (+/- 0.86 – 1.63 SD). We observed a trend of generally fewer signals in the central region of the monospecies clusters, independent of their total size (Figure 3-3). For the distance classes above 3.78 µm, the average signal count increased to up to 3 signals per µm^2. However, for these distances, no more than three monospecies clusters were analyzed. Therefore, the data for these size classes has to be interpreted with care. More monospecies clusters would need to be analyzed for a stronger statement about activity in distances larger than 3.78 µm from partner cells.

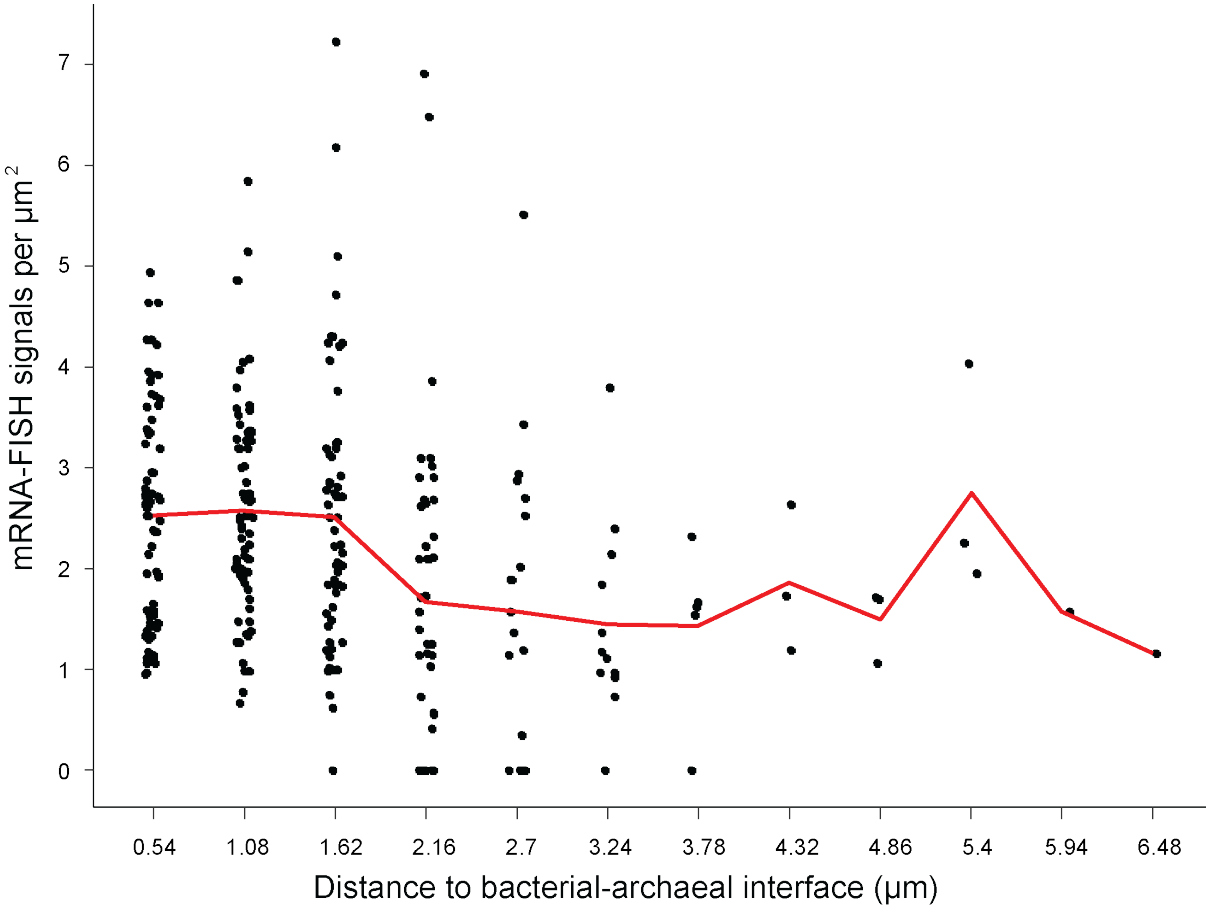

Figure 3-3 Density of *ecrA* mRNA- FISH signals as a function of distance to the bacterial-archaeal interface. *Ca.* Ethanoperedens monospecies clusters were segmented into rings for analysis with a width of 0.54 µm from the edge to the center. Detected *ecr*A specific FISH signals were automatically counted and normalized against the ring area. Red line indicates the mean signals per µm^2 for each distance class ring.

3.4.4 Distribution of *ecrA* mRNA signals within a stacked image of a *Ca.* Ethanoperedens monospecies cluster

The activity seemed to be reduced towards the center on the level of individual monospecies clusters independent of size. To test this hypothesis, we prepared a stacked image of a complete *Ca.* Ethanoperedens monospecies cluster (Figure 3-4A-C). We counted *ecrA* mRNA signals in 19 layers of 0.232 µm thickness and calculated the signals per μm^2 for each ring in each layer (Figure 3-4D). The thickness per layer is less than the diameter of a *Ca.* Ethanoperedens cell (0.54 µm) and therefore, three layers could show signals for the same cell. We decided to consider each layer as an independent sample and accept that some cells may contribute *ecrA* transcript signals to more than one layer. In 15 out of the 19 layers, the *ecrA* expression increased towards the outside of the monospecies cluster, indicating higher cell activity closer to the bacterial-archaeal interface. On average, the signals per μm^2 increased from the center at 3.24 µm distance with 0.86 (+/- 0.91 SD) towards the outside at 0.54 µm distance with 1.36 (+/- 0.51 SD). However, the five topmost layers of the monospecies cluster showed low activity at the 0.54 µm distance with only 0.69 signals per μm^2 (+/- 0.20 SD) compared to 1.60 signals per μm^2 (+/- 0.33 SD) for the 14 lower layers. A closer investigation of the whole consortium suggests that the top area of the monospecies cluster was located at the edge of the consortium and not surrounded by partner bacteria or consortium matrix (Figure S3-2). The cells in the top area would therefore have a large distance to the bacterial-archaeal interface. The background glow of the cell-matrix only surrounds the bottom part of the *Ca.* Ethanoperedens monospecies cluster. However, the shape of the consortium might also have been altered during sample preparation.

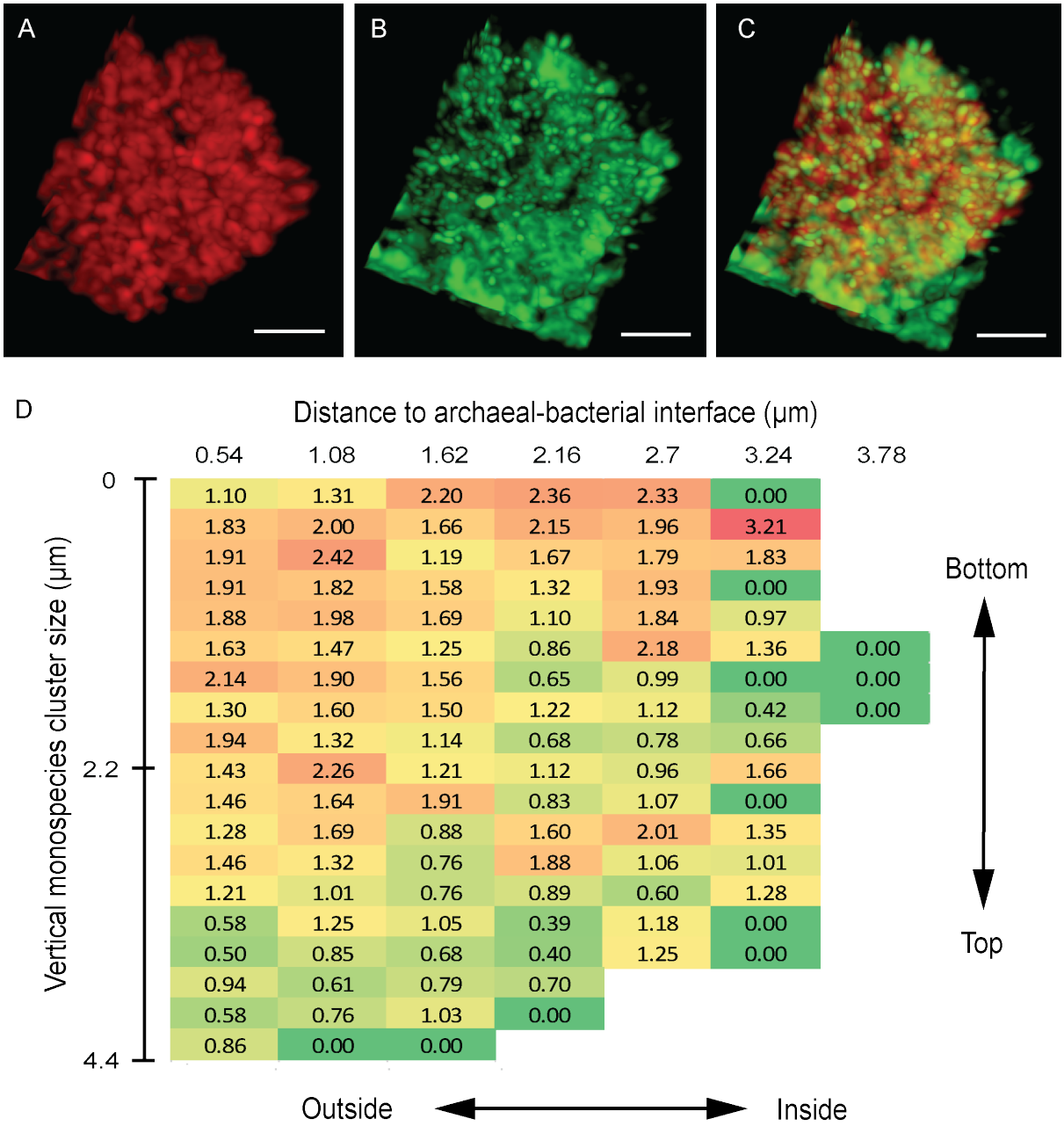

Figure 3-4 Distribution of ecrA mRNA-FISH signals in a single *Ca.* Ethanoperedens monospecies cluster. A-C 3D image of *Ca.* Ethanoperedens monospecies cluster calculated from 30 layers. 16S rRNA probe GoM-Arc1-660 (red) shows *Ca.* Ethanoperedens and mRNA targeting probe shows ecrA transcripts (green). Scale bar indicates 2 µm. **D** EcrA mRNA signal distribution through depicted monospecies cluster in 19 vertical layers. Layers were counted independently, and the monospecies cluster was segmented into rings of 0.54 µm width from the edge to the center. The values shown are signals per µm^2 for each ring. Heatmap color code lowest value green to highest value red.

3.5 Discussion

3.5.1 Dynamic detection of *ecrA* transcripts

EcrA probes showed signals corresponding to *ecrA* expression in the *Ca.* Ethanoperedens monospecies clusters. Additionally, we demonstrated that our mRNA-FISH protocol could detect dynamic changes in mRNA transcription activity. After just five days without ethane, the number of *ecrA* transcripts in *Ca.* Ethanoperedens cells were too low for

signal detection (Figure 3-2). The appearance of the observed probe signals was in line with earlier studies using either amplified (Pernthaler and Amann 2004, Rouhanifard et al. 2019, Tsuneoka and Funato 2020) or directly labeled (Skinner et al. 2013, Harris et al. 2021) mRNA-FISH probes. However, the signal intensity of the *ecrA* mRNA probe was low, and signals could only be visualized with the Zeiss Airyscan technology. The Airyscan module uses a 32 channel detector where each channel functions as a single, small pinhole (Huff 2015). This technology allows for very light-efficient imaging, with improved resolution and signal-to-noise ratio (Huff 2015). With a common epifluorescence microscope, the probe signal could not be distinguished from the background noise emitted by the consortium matrix.

The rapid decrease of *ecrA* expression observed after the removal of ethane was remarkable. *Ca.* Ethanoperedens depends on sufficient ECR enzyme concentration to activate its sole substrate, ethane (Hahn et al. 2020). An unregulated *ecr* expression would provide for a constantly high amount of ECR enzymes in case the substrate becomes available again. However, *Ca.* Ethanoperedens cells appear to downregulate the *ecr* expression when no substrate is available. This behavior would only be feasible if *Ca.* Ethanoperedens has a mechanism of substrate-induced upregulation of the metabolic key gene. So far, little is known about transcriptional regulation in methanogenic and alkanotrophic archaea, and the research in this field is still in its early stage (Shalvarjian and Nayak 2021). However, the methanogen *Methanococcus maripaludis* shows gene regulation as a response to the availability of H_2 and formate (Hendrickson et al. 2007, Hendrickson et al. 2008, Costa et al. 2013). Substrate-dependent gene regulation was also found in the acetoclastic methanogens from the order Methanosarcinales (Reichlen et al. 2012). Therefore, *Ca.* Ethanoperedens might also be able to actively downregulate its metabolic key gene's expression to reduce its energy consumption. The fast response to ethane induction measured by sulfide production and *ecrA* mRNA-FISH would indicate that *Ca.* Ethanoperedens has a mechanism to dynamically react to substrate availability.

3.5.2 *ecrA* expression patterns in *Ca.* Ethanoperedens monospecies cluster

The *ecrA* mRNA signal distribution we observed suggests high activity in most regions of the *Ca.* Ethanoperedens monospecies cluster, with active *ecrA* transcription in cells up to 6.48 µm from the bacterial-archaeal interface. In the studied enrichments, *Ca.* Ethanoperedens cells appear in monospecies clusters of 3 – 13 µm in diameter. These monospecies clusters are surrounded by their partner bacteria (Figure 3-1C) that use the reducing equivalents from AOE to perform sulfate reduction (Hahn et al. 2020). Thus, the archaea need to transfer their

electrons to the sulfate-reducing partner bacteria efficiently. The molecular basis of the interspecies electron transfer in these alkanotrophic consortia is still under discussion but is most likely mediated by direct electron transfer via pili-based nanowires (Wegener et al. 2015). Electrons can be transferred efficiently over longer distances through such conductive pili (Reguera et al. 2005, Summers et al. 2010). A direct interspecies electron transfer (DIET) via conductive pili may allow a rather uniform distribution of activity through the monospecies clusters since electrons can be transferred rather independently of the distance to the partner cell. For an intermediate exchange system based on diffusion (mediated interspecies electron transfer, or MIET), we would expect higher activity towards the bacterial-archaeal interface due to the build-up of reaction products (Orcutt and Meile 2008, He et al. 2019). The decrease of activity towards the center in such a system would be rather sharp.

The distance independent expression activity in medium-sized monospecies clusters (<30 µm in diameter) is in line with observations made using BONCAT and nanoSIMS-resolved stable isotope probing (McGlynn et al. 2015, Hatzenpichler et al. 2016). Our study confirmed that increasing distance to the bacterial-archaeal interface does not inhibit cell activity within small to medium-sized archaeal monospecies clusters and that cells at the interface are not necessarily the most active cells (Figure 3-3) (McGlynn et al. 2015). However, we find that cells with a distance greater than 2.16 µm to the bacterial-archaeal interface have a lower activity based on the counted signals per μm^2. Often the small central area did not cover any *ecrA* mRNA signals, leading to a value of zero signals per μm^2 for these distance classes. Indeed, when looking at individual monospecies cluster micrographs, the central regions had fewer or no *ecrA* mRNA signals. While results shown in Figure 3-3 suggested a lower cell activity with increasing distance to the bacterial-archaeal interface, it appears to be rather an effect of lower cell activity in the central region, independent of the total monospecies cluster size. It also has to be considered that some *Ca.* Ethanoperedens monospecies clusters are located at the outside edge of a consortium and are not fully surrounded by partner bacteria. For cells in these clusters the distances to the partner bacteria might vary compared to those monospecies clusters fully surrounded by partner bacteria. However, a simultaneous staining of *Ca.* Ethanoperedens, *Ca.* Desulfofervidus and the *ecrA* mRNA would be required to better correlate the distance of active *Ca.* Ethanoperedens cells to the bacterial-archaeal interface.

The reason for the decreased activity in the central region of the monospecies cluster cannot be explained by our data. Nutrient limitation appears unlikely since also small clusters showed decreased activity in the central region. So far, the availability and distribution of nutrients within the monospecies clusters have not been investigated. However, the even uptake

of ^{15}N labeled ammonium throughout segregated AOM consortia would suggest an even nutrient distribution in the Ethane50 consortia (McGlynn et al. 2015). A recent study showed that an increased distance between partner cells increases the ohmic resistance for the electron transfer, and archaeal cells lost 70% of activity in distances >30 µm (He et al. 2021). A decreased activity might also be linked to cell division patterns in consortia. Assuming that the transfer of electrons to the partner bacteria depends on a direct connection via conductive pili, cells dividing in the central region of a monospecies cluster might have to establish a connection first. It is unknown if cells share the network of nanowires within consortia or if every cell has to establish its own connection to the partner cell (Wegener et al. 2015). Cell division might also directly impact *ecrA* expression by inhibition.

3.5.3 Case study for a monospecies cluster at the consortia edge

We observed spatial differences in *ecrA* expression in our stacked image study of a single monospecies cluster at the edge of a consortium (Figure 3-4). As in other monospecies clusters, the central region has fewer signals per μm^2 compared to cells closer to the archaeal-bacterial interface. However, we also observed a decrease in activity towards the top part of the monospecies cluster. The top part does not show the unspecific signal of the consortia matrix, indicating the absence of bacterial partners in this region (Figure S3-2). Assuming the lack of a bacterial-archaeal interface in this region, the distance for cells located in the top part to their partner cells would greatly increase. The monospecies cluster had a vertical diameter of 4.42 µm. However, the cluster appeared squeezed towards the bottom, and the actual vertical distance might have been larger. The squeezing might be an artifact from the underpressure needed for filtration. Since a possible decrease in activity caused by ohmic resistance in the nanowires would be gradual rather than total, we might see a distance-related partial reduction of activity. He et al. (2021) modeled that archaeal cells lose 70% of their activity within 30 µm from the bacterial-archaeal interface. Our observation would indicate that the reduced activity by ohmic resistance might be visible at less than 30 µm with a sensitive method like mRNA-FISH. One must also consider that the signal's absence does not equal complete inactivity but only indicates that the mRNA copy number is insufficient for signal detection. Additionally, the signal intensity should be used as a cell activity indicator in future studies since the direct mRNA staining allows a correlation of signal intensity to mRNA copy number.

3.5.4 Outlook: Environmental *ecrA* mRNA detection and partner localization

We presented a set of six probes targeting the *ecrA* mRNA sequence of the genus *Ca.* Ethanoperedens from environmental and cultured strains. In this study, the probes were only applied to *Ca.* Ethanoperedens cells from the Ethane50 culture. However, the probe coverage for the environmental *Ca.* Ethanoperedens sequences is good, with no more than two mismatches on 40 bases. Therefore, an environmental application of the probe set should be possible. Our understanding of the *ecrA* diversity in the environment is still limited. For the *ecrA* of the genus *Ca.* Ethanoperedens, only five sequences have been published, three sequences were published from two metagenomics studies with Guaymas Basin sediment samples (Dombrowski et al. 2017, Dombrowski et al. 2018), and two sequences come from enrichments from the Guaymas Basin (Hahn et al. 2020). The in-situ abundance of *Ca.* Ethanoperedens in the Guaymas Basin is very low with ~0.1% relative abundance (Hahn et al. 2020). However, *ecrA* sequences of the genus *Ca.* Argoarchaeum have been found at multiple locations, including the Scotian Basin (Dong et al. 2020), Guaymas Basin (Dombrowski et al. 2018), Gulf of Mexico (Borrel et al. 2019, Chen et al. 2019, Laso-Pérez et al. 2019, Hahn et al. 2020) and Loki's Castle (Hahn et al. 2020). In some locations, the anaerobic ethane oxidizers reach relative abundances of up to 30%, and FISH studies showed their existence at many seep sites (Laso-Pérez et al. 2019, Hahn et al. 2020). An extension of the probe set to target the *ecrA* mRNA of *Ca.* Argoarchaeum would allow for a study of the *ecrA* expression in environmental samples. A spiking experiment could be conducted to test if *ecrA* mRNA-FISH with environmental samples is feasible. By mixing fixed Ethane50 culture with environmental samples, we could exclude the presence of inhibiting substances in the environmental samples that might prevent a successful hybridization. The environmental *ecrA* expression detection by mRNA-FISH could be used to show active ethane oxidation and thereby extend our understanding of AOE in marine sediments.

A triple hybridization could be conducted using specific probes for *Ca.* Ethanoperedens, the sulfate-reducing partner bacterium *Ca.* Desulfofervidus auxilii and the ecrA specific probes presented in this study to better understand archaeal-bacterial dynamics. The *Ca.* Desulfofervidus auxilii 16S rRNA specific probe Hot-SEEP1-1465 (Krukenberg et al. 2016) could be labeled with an Alexa-647 fluorophore, which would complement the fluorophores Alexa-488 and Alexa-594 used in this study. The triple hybridization would help to locate the bacterial-archaeal interface. The information could be used to better differentiate between monospecies clusters located in the middle of a consortium or at the edge and allow

for a more accurate correlation of *ecrA* expression-based activity and distance to the bacterial-archaeal interface.

Additionally, the signal brightness of the *ecrA* probe should be taken into account for activity prediction. Since we used directly labeled oligonucleotides for mRNA hybridization, an increase in signal brightness correlates with an increase in mRNA copy numbers. This increase in brightness can be quantified by calculating mean gray values from gray scale transformed micrographs. The additional information from the location of the partner bacteria and probe brightness will help to understand activity dynamics in spatially segregated consortia further.

3.6 Supplementary data

Table S3-1 Cells measured to determine the average cell diameter of *Ca.* Ethanoperedens. The scaling parameter was used to convert pixel to µm.

	Sample	Area	Diameter	Scaling	Size (µm)
Cell1	147_2_R1E_t2_1	195.33	15.8	0.035	0.55
Cell2	147_2_R1E_t2_1	244.88	17.7	0.035	0.62
Cell3	147_2_R1E_t2_1	247.97	17.8	0.035	0.62
Cell4	147_2_R1E_t2_1	198.11	15.9	0.035	0.56
Cell5	147_2_R1E_t2_1	273.03	18.6	0.035	0.65
Cell6	147_2_R1E_t2_1	193.43	15.7	0.035	0.55
Cell7	147_2_R1E_t2_1	247.6	17.8	0.035	0.62
Cell8	147_2_R1E_t2_1	251.57	17.9	0.035	0.63
Cell9	147_2_R1E_t2_1	234.7	17.3	0.035	0.61
Cell10	147_2_R1E_t2_1	263.43	18.3	0.035	0.64
Cell11	147_2_R1E_t2_1	264.86	18.4	0.035	0.64
Cell12	147_2_R1E_t2_1	346.73	21.0	0.035	0.74
Cell13	147_2_R1E_t2_1	304.02	19.7	0.035	0.69
Cell14	147_2_R1E_t2_1	381.72	22.0	0.035	0.77
Cell15	147_2_R1E_t2_1	251.26	17.9	0.035	0.63
Cell16	147_2_R1E_t2_2	206.91	16.2	0.035	0.57
Cell17	147_2_R1E_t2_2	239.99	17.5	0.035	0.61
Cell18	147_2_R1E_t2_2	296.5	19.4	0.035	0.68
Cell19	147_2_R1E_t2_1	146.52	13.7	0.035	0.48
Cell20	147_2_R1E_t2_1	90.1	10.7	0.035	0.38
Cell21	147_2_R1_t2_3	91.19	10.8	0.035	0.38
Cell22	147_2_R1_t2_3	107.88	11.7	0.035	0.41
Cell23	147_2_R1E_t2_2_l13	44.79	7.6	0.049	0.37
Cell24	147_2_R1E_t2_2_l13	37	6.9	0.049	0.34
Cell25	147_2_R1E_t2_2_l13	42.9	7.4	0.049	0.36
Cell26	147_2_R1E_t2_2_l13	54.73	8.3	0.049	0.41

Cell27	147_2_R1E_t2_2_l13	58.1	8.6	0.049	0.42
Cell28	147_2_R1E_t2_2_l13	57.87	8.6	0.049	0.42
Cell29	147_2_R1E_t2_2_l13	47.94	7.8	0.049	0.38
Cell30	147_2_R1E_t2_2_l13	51.69	8.1	0.049	0.40

Table S3-2 Raw counting data of mRNA-FISH signals counted with ACMEtool3. "Distance" shows the distance class ring from the bacterial-archaeal interface, with the maximum distance shown in µm. Values for monospecies cluster shown in signals per μm^2 for each distance class.

Distance µm	0.54	1.08	1.62	2.16	2.70	3.24	3.78	4.32	4.86	5.40	5.94	6.48
Cluster_1	0.95	0.67	1.02	0.73								
Cluster_2	0.96	1.35	1.27	0.00	0.00							
Cluster_3	1.31	2.23	1.21	0.00								
Cluster_4	1.08	1.69	1.82	2.65								
Cluster_5	2.74	1.91	2.63	2.62								
Cluster_6	2.63	3.00	1.43									
Cluster_7	1.39	0.98	0.99	0.57	0.00							
Cluster_8	2.22	3.30	7.22									
Cluster_9	2.48	1.79	1.27	0.00								
Cluster_10	1.46	1.34	2.06	0.41								
Cluster_11	2.37	3.19	3.25	6.48								
Cluster_12	1.46	2.40	2.38	1.57	2.88	1.11						
Cluster_13	1.14	1.48	1.49	1.71	1.15	1.36	1.62	1.73	1.70	1.96	1.57	1.17
Cluster_14	1.94	1.91	1.76	2.11	2.02	2.14	1.55	2.63	1.72	2.26		
Cluster_15	2.14	2.36	2.85	2.90	2.69	3.80						
Cluster_16	2.87	3.19	3.11	2.68	1.57	1.17						
Cluster_17	1.53	1.27	1.83	3.02	2.93	1.84						
Cluster_18	2.75	3.35	1.62	2.31	3.43	2.39	0.00					
Cluster_19	1.18	2.68	2.77	2.10	2.52	0.00						
Cluster_20	1.92	1.48										
Cluster_21	1.95	3.37										
Cluster_22	1.10	1.07	0.62	0.56	0.00							
Cluster_23	1.43	2.10	0.75	3.09								
Cluster_24	1.54	2.52	1.55	1.40	1.19							
Cluster_25	2.52	2.75	2.75									
Cluster_26	2.71	1.60	0.74	0.00								
Cluster_27	1.06	3.36	4.23	3.85								
Cluster_28	1.42	1.94	4.30									
Cluster_29	1.07	1.86	1.19	1.03	0.00							
Cluster_30	1.33	2.31	2.51	2.91								
Cluster_31	1.64	1.38	2.24	1.73	1.37	0.74	1.67	1.20	1.06	4.03		
Cluster_32	3.18	2.00	3.13									
Cluster_33	1.34	0.99	1.13	1.16	0.35	0.93	2.33					
Cluster_34	2.53	2.13	1.97									
Cluster_35	3.23	2.05										
Cluster_36	2.67	3.27	3.19	2.10								
Cluster_37	1.11	0.77	1.00	1.14	0.00							
Cluster_38	4.27	2.10	2.71	0.00								
Cluster_39	1.60	2.51	1.83	1.25	1.89	0.96						
Cluster_40	3.93	4.86	2.71									
Cluster_41	3.35	3.79	3.76	2.68								
Cluster_42	4.64	2.20	5.09									

Cluster_43	2.74	2.69										
Cluster_44	3.95	1.28	4.23									
Cluster_45	3.86	5.14										
Cluster_46	4.22	2.67	4.29									
Cluster_47	3.73	4.04	4.72									
Cluster_48	2.68	2.43	0.00									
Cluster_49	2.96	3.62										
Cluster_50	3.61	3.43	1.89									
Cluster_51	3.48	3.58	2.51	0.00								
Cluster_52	3.33	3.52										
Cluster_53	4.93	3.96										
Cluster_54	4.64	3.57	4.06	0.00								
Cluster_55	2.39	2.75	2.16	3.10								
Cluster_56	3.69	3.20										
Cluster_57	3.62	3.29	2.81	0.00								
Cluster_58	2.37	2.00	4.21	0.00								
Cluster_59	2.79	1.97	2.93	6.90								
Cluster_60	3.38	3.35	2.84	0.00								
Cluster_61	2.95	2.86	3.24									
Cluster_62	2.63	2.48	2.03									
Cluster_63	3.71	3.01	6.17									
Cluster_64	1.97	4.08										
Cluster_65	2.95	5.84										
Cluster_66	2.72	2.09	2.22	2.23								
Cluster_67	2.61	2.70	2.04	2.10	5.50							
Average	2.51	2.57	2.53	1.73	1.64	1.49	1.43	1.85	1.49	2.75	1.57	1.17
StDev	1.05	1.04	1.40	1.63	1.52	1.02	0.86	0.73	0.37	1.12	0.00	0.00
n=	67	67	56	40	18	11	5	3	3	3	1	1

Table S3-3-1 *mcrA*/*ecrA* sequences used to design *ecrA* mRNA probes (shown in Figure 3-1A).

Strain	Genus	Product	Acc. Number
Ca. Ethanoperedens thermophilum E50	*Ca.* Ethanoperedens	Ethyl-CoM	LR991654.1
Ca. Ethanoperedens thermophilum E37	*Ca.* Ethanoperedens	Ethyl-CoM	LR991653.1
GoM-Arc1 ex4572_44	*Ca.* Ethanoperedens	Ethyl-CoM	PHP46140.1
GoM-Arc1 B65_G16	*Ca.* Ethanoperedens	Ethyl-CoM	RLG26650.1
GoM-Arc1 B25_G9	*Ca.* Argoarchaeum	Ethyl-CoM	RLG26955.1
GoM-Arc1-LC-WB58	*Ca.* Argoarchaeum	Ethyl-CoM	NMG83409.1
Ca. Argoarchaeum ethanivorans	*Ca.* Argoarchaeum	Ethyl-CoM	RZB32666.1
GoM-Arc1-GOS	*Ca.* Argoarchaeum	Ethyl-CoM	RZN16117.1
Methanosarcina acetivorans C2A	*Methanosarcina*	Methane	NC_003552
Ca. Methanoperedens nitroreducens	*Ca.* Methanoperedens	Methyl-CoM	KCZ72673.1
ANME-1 - G37ANME1	*Ca.* Methanophagales	Methyl-CoM	PXF51295.1
ANME-2 - E20ANME2	ANME-2	Methyl-CoM	PXF60686.1

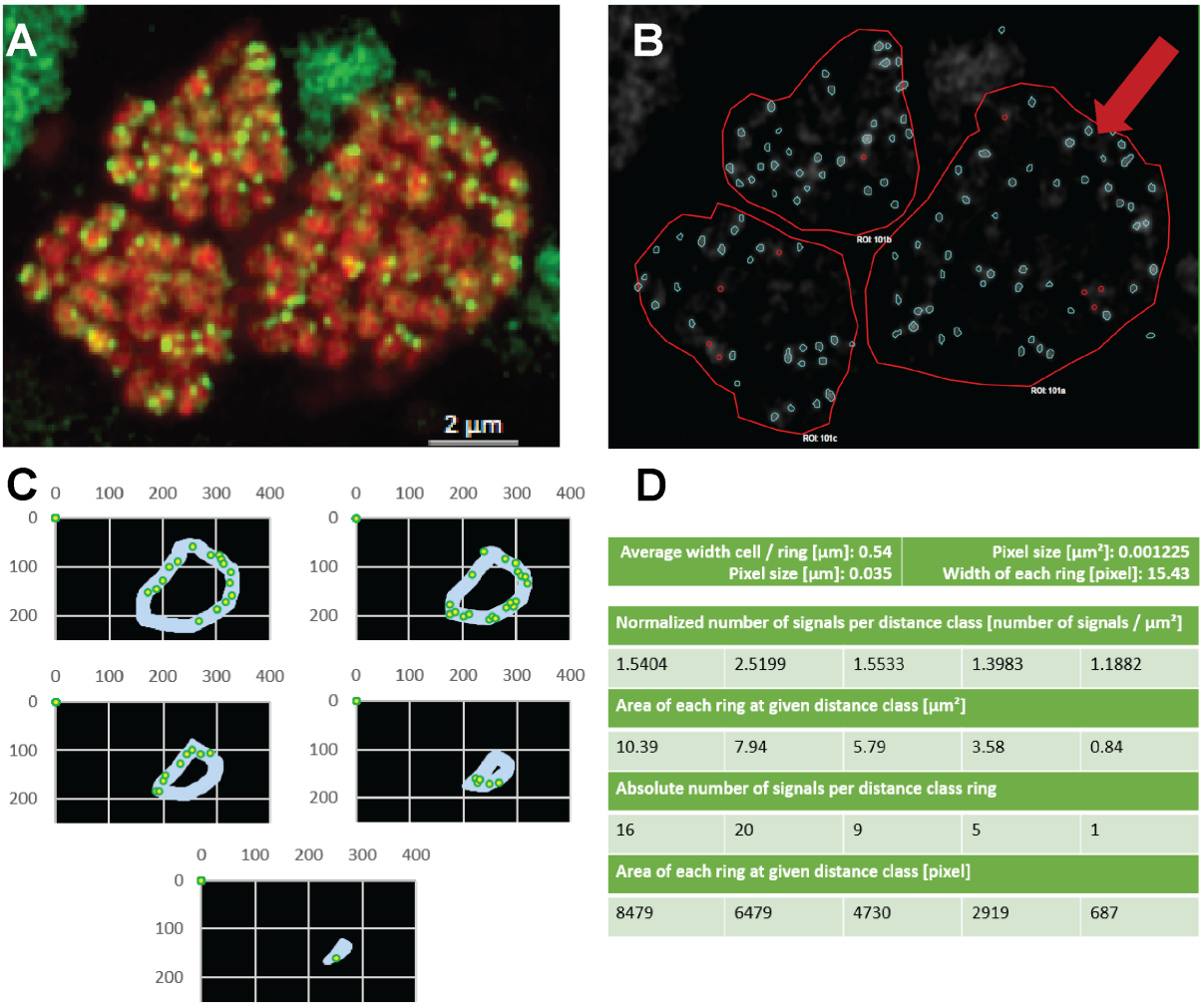

Average width cell / ring [µm]: 0.54 Pixel size [µm]: 0.035			Pixel size [µm²]: 0.001225 Width of each ring [pixel]: 15.43	
Normalized number of signals per distance class [number of signals / µm²]				
1.5404	2.5199	1.5533	1.3983	1.1882
Area of each ring at given distance class [µm²]				
10.39	7.94	5.79	3.58	0.84
Absolute number of signals per distance class ring				
16	20	9	5	1
Area of each ring at given distance class [pixel]				
8479	6479	4730	2919	687

Figure S3-1 Example for image processing and calculation of *ecrA* mRNA signal distribution. **A** Original CLSM image of *Ca.* Ethanoperedens monospecies cluster. FISH staining of *Ca.* Ethanoperedens (GOM-Arc1-660, red) and *ecrA* mRNA (*ecrA* probe mix, green). **B** Greyscale image imported to ACMEtool3 of the same archaeal monospecies cluster. Red arrow indicated monospecies cluster further highlighted in panels C and D. Red line indicates manually defined ROIs, blue spots show cell signals marked automatically by ACMEtool3, and red spots

indicate manually added signals. **C** Distance class rings from bacterial-archaeal interface to center (= average *Ca.* Ethanoperedens cell diameter). Green dots indicate signals counted for the corresponding distance class ring. **D** Final result for calculation of signals per µm^2 for this exemplary monospecies cluster.

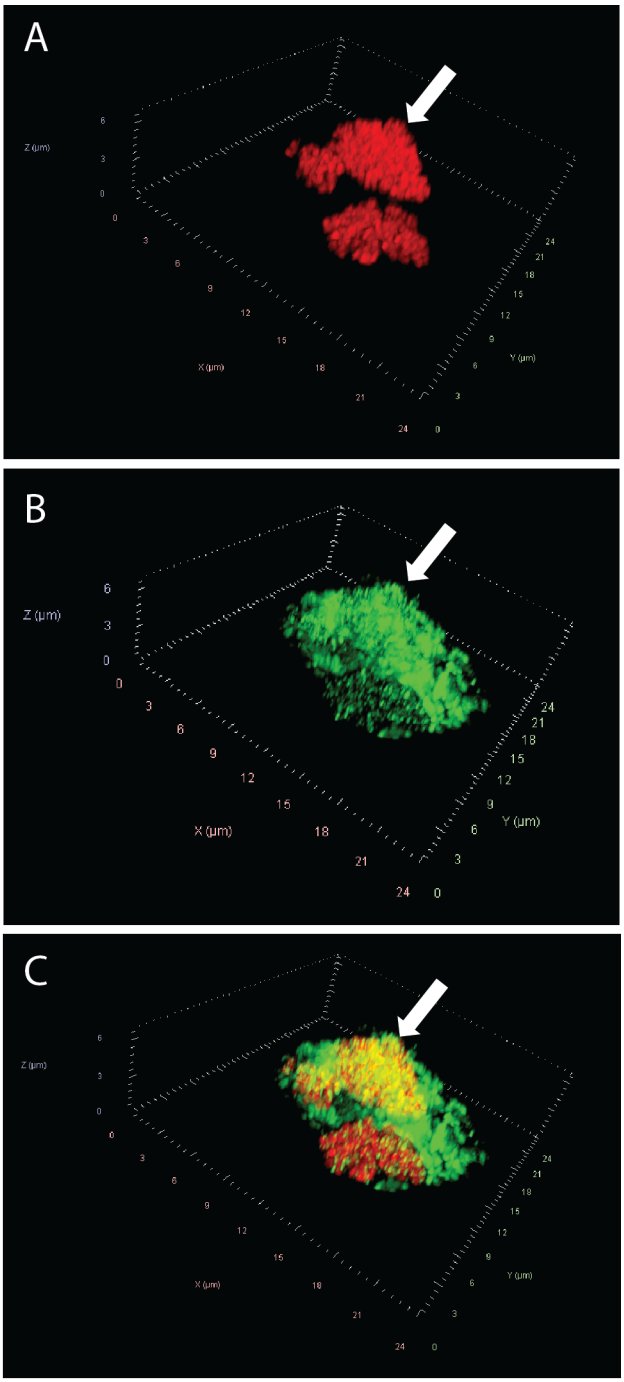

Figure S3-2 3D image of Ethane50 consortium calculated from 30 stacked layers. 16S rRNA probe GoM-Arc1-660 (red) shows *Ca.* Ethanoperedens and mRNA targeting probe mix shows *ecrA* transcripts (green). White arrows indicate the top part of the monospecies cluster analyzed in Figure 3-4.

Chapter 4

Crystal structure of a key enzyme for anaerobic ethane activation

Cedric J. Hahn[1]†, Olivier N. Lemaire[1]†, Jörg Kahnt[2], Sylvain Engilberge[3]‡, Gunter Wegener[1,4,5]*, Tristan Wagner[1]*

[1]Max Planck Institute for Marine Microbiology, Bremen 28359, Germany.
[2]Max Planck Institute for Terrestrial Microbiology, Marburg, Germany.
[3]Paul Scherrer Institute (PSI), Villigen PSI, Villigen, Switzerland.
[4]Center for Marine Environmental Sciences (MARUM), University of Bremen, Bremen, Germany.
[5]Alfred Wegener Institute Helmholtz Center for Polar and Marine Research, Bremerhaven, Germany.

*Corresponding author. Email: gwegener@mpi-bremen.de (G.W.); twagner@mpi-bremen.de (T.W.)
†These authors contributed equally to the work.
‡Present address: European Synchrotron Radiation Facility (ESRF), Grenoble, France.

Published in:
Science 373 (6550), 118-121.
DOI: 10.1126/science.abg1765

Received: December 15, 2020
Accepted: May 28, 2021
Published: July 02, 20

4.1 Abstract

Ethane, the second most abundant hydrocarbon gas in the seafloor, is efficiently oxidized by anaerobic archaea in syntrophy with sulfate-reducing bacteria. Here, we report the 0.99-angstrom-resolution structure of the proposed ethane-activating enzyme and describe the specific traits that distinguish it from methane-generating and -consuming methyl-coenzyme M reductases. The widened catalytic chamber, harboring a dimethylated nickel-containing F_{430} cofactor, would adapt the chemistry of methyl-coenzyme M reductases for a two-carbon substrate. A sulfur from methionine replaces the oxygen from a canonical glutamine as the nickel lower-axial ligand, a feature conserved in thermophilic ethanotrophs. Specific loop extensions, a four-helix bundle dilatation, and posttranslational methylations result in the formation of a 33-angstrom-long hydrophobic tunnel, which guides the ethane to the buried active site as confirmed with xenon pressurization experiments.

4.2 Main text

Natural seeps perfuse the marine seafloor with a variety of different hydrocarbons, including alkane gases (Clark et al. 2000, Etiope and Ciccioli 2009). Most of the volatile fraction is consumed within the sediment by a process coupled to the reduction of sulfate (Boetius et al. 2000, Joye et al. 2004, Etiope and Ciccioli 2009, Mastalerz et al. 2009, Laso-Pérez et al. 2019), which is mainly carried out by consortia of anaerobic alkane-oxidizing archaea and sulfate-reducing bacteria (Boetius et al. 2000, Orphan et al. 2001, Holler et al. 2011, Laso-Pérez et al. 2016, Chen et al. 2019, Laso-Pérez et al. 2019, Hahn et al. 2020). The oxidation of the generated sulfide represents the basis of light-independent ecosystems in the deep sea (Sibuet and Olu 1998, Boetius et al. 2000, Orphan et al. 2001, Holler et al. 2011, Chen et al. 2019, Hahn et al. 2020). Ethane is the second-most abundant gaseous alkane, but its natural emissions from sediments are estimated to be rather low (Etiope and Ciccioli 2009). This low emission results from efficient metabolism of microorganisms that consume the ethane within the seafloor. Recent discoveries pointed out two archaeal species that activate and completely oxidize ethane under anoxic conditions: *Candidatus* Argoarchaeum ethanivorans (Chen et al. 2019) and *Candidatus* Ethanoperedens thermophilum (Hahn et al. 2020). These two closely related species belonging to the GoM-Arc1 clade are widely present in marine subsurface sediments (Chen et al. 2019, Laso-Pérez et al. 2019, Hahn et al. 2020). Analogously to the anaerobic oxidation of methane (AOM), the ethanotrophs generate ethyl-coenzyme M from ethane and coenzyme M (HS-CoM). It has been proposed that such

activation works in the same fashion in other alkane-oxidizing archaea (Laso-Pérez et al. 2016, Borrel et al. 2019, Laso-Pérez et al. 2019). It is assumed that ethyl-CoM is further metabolized to acetyl-coenzyme A (acetyl-CoA) by a so-far-unknown process (Chen et al. 2019, Hahn et al. 2020). The acetyl-CoA decarbonylase-synthase complex turns acetyl-CoA into CO_2 and methyl-H_4MPT, and the methyl group is oxidized to CO_2. These organisms depend on ethane as substrate and are incapable of metabolizing other alkanes (Chen et al. 2019, Hahn et al. 2020). Generated electrons are transferred to the partner bacteria, supposedly through external cytochromes, nanowires, or diffusible sulfur species, as already discussed for consortia performing the AOM (McGlynn et al. 2015, Wegener et al. 2015, Chen et al. 2019, Hahn et al. 2020).

The central enzyme for alkane-activation in ethanotrophs was proposed to be the methyl-CoM reductase (MCR) (Chen et al. 2019, Miller and Booker 2019, Thauer 2019, Hahn et al. 2020, Wang et al. 2021). Extensively studied in methanogens, MCR harbors a specific Ni-porphinoid F_{430} cofactor that catalyzes the reduction of a CoM-bound methyl group with coenzyme B (HS-CoB), forming methane and the heterodisulfide CoM-S-S-CoB (Ermler et al. 1997, Wongnate et al. 2016, Thauer 2019). The anaerobic methane-oxidizing archaea (ANME) reverse the methanogenesis pathway, using MCR to activate methane, forming methyl-CoM and HS-CoB (Hallam et al. 2004, Meyerdierks et al. 2010). MCR produced by the ANME-2 clade contains the canonical F_{430} cofactor, whereas a methylthio-F_{430}-cofactor was found in MCR from the ANME-1 clade (Krüger et al. 2003, Shima et al. 2012, Kaneko et al. 2014). The MCR-homolog from ethanotrophs would capture ethane and generate ethyl-CoM and HS-CoB. This hypothesis is corroborated by three observations: (i) genes coding for the three subunits of the MCR-homolog are among the most expressed (Chen et al. 2019, Hahn et al. 2020); (ii) ethyl-CoM was formed during anaerobic oxidation of ethane (AOE) by the consortium when incubated in the presence of ethane (Chen et al. 2019, Hahn et al. 2020); and (iii) MCR from methanogenic archaea was shown to generate ethane from ethyl-CoM and HS-CoB, yet with rates much lower than for methane generation from methyl-CoM (Gunsalus et al. 1978, Scheller et al. 2013). The alkane capture machinery in *Ca*. E. thermophilum appears to be specialized for ethane; ethyl-CoM was the only detectable alkyl-CoM in cells incubated with a mixture of different alkanes (Hahn et al. 2020). Moreover, in ethanotrophs the protein sequences of the MCR subunits are substantially different from methanogenic MCRs, with large insertions and substitutions of canonical residues (Figure S4-1 and Table S4-1). Understanding the specific structural features of this enzyme may explain how MCR was adapted to accommodate ethane.

To obtain material for MCR-homolog structure determination, we used a thermophilic AOE enrichment cultured from sediments collected at the Guaymas Basin hydrothermal vents (Hahn et al. 2020). The culture has a doubling time of only 7 days (Hahn et al. 2020), which is notable compared with thermophilic AOM cultures isolated from the same site that exhibit doubling times of 50 days (Holler et al. 2011). *Ca.* E. thermophilum and its sulfate-reducing bacterial partner, *Candidatus* Desulfofervidus auxilii, constitute most of the active population of the enrichment (Hahn et al. 2020). When we amended the culture medium with the methyl-CoM analog 2-bromoethane sulfonate (BES), a known inhibitor of alkyl-CoM reductases (Thauer 2019), both ethane consumption and sulfide production decreased, dependent on the amount of BES (Figure 4-1A and Figure S4-2). A control ANME culture showed the same sensitivity at similar BES concentrations (Figure 4-1A). The results corroborate the hypothesis of an MCR-like enzyme performing ethane activation.

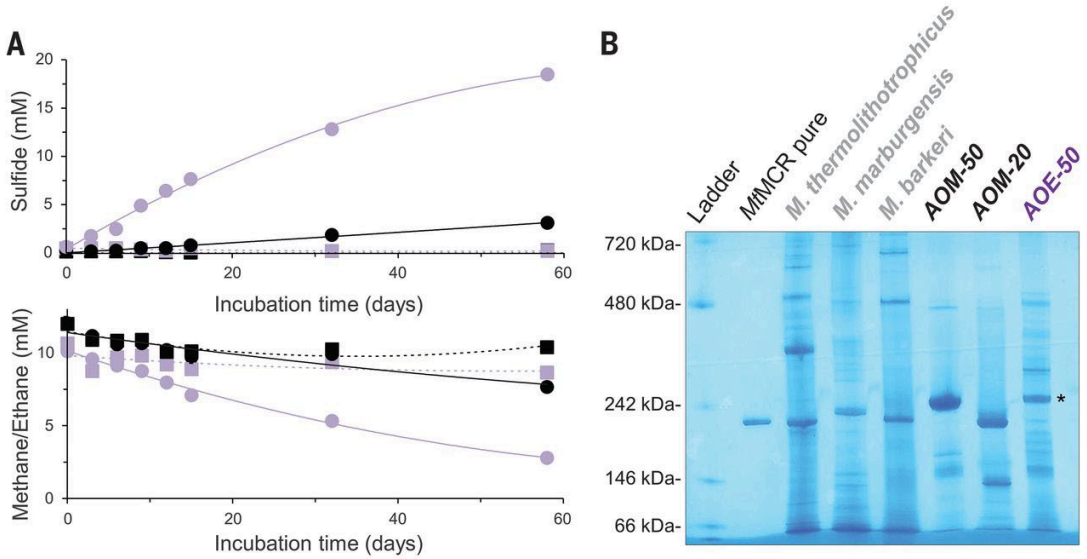

Figure 4-1 Inhibition of AOE and comparison of cell extracts from methanogen cultures and methanotrophic and ethanotrophic enrichments. (A) Sulfide generation and alkane degradation in AOM (black) and AOE (purple) cultures incubated at 50°C, in the absence (circles, full lines) or presence (squares, dashed lines) of the MCR-specific inhibitor 2-bromoethane sulfonate at 10 mM (Figure S4-2). (B) High-resolution clear native polyacrylamide gel electrophoresis of purified MCR from *M. thermolithotrophicus* (MtMCR, 1.5 mg) and soluble extracts from hydrogenotrophic (*M. thermolithotrophicus* and *M. marburgensis*) and methylotrophic (*Methanosarcina barkeri*) methanogens, AOM and AOE enrichments (10 mg each). The asterisk indicates the position of the MCR homolog from *Ca.* E. thermophilum.

MCR relative abundance in cell extracts from hydrogenotrophic and methylotrophic methanogens as well as ANME-1, ANME-2, and *Ca*. E. thermophilum were compared (Figure 4-1B). Native gel profiles of all methanogens indicate an intense band at a size corresponding to isolated MCR. As expected from previous reports (Krüger et al. 2003, Shima et al. 2012), the methanotrophic enrichments exhibit a band attributed as MCR with much stronger intensity

compared with that of methanogens, resulting from the overproduction of MCR that characterizes these consortia (Wang et al. 2014, Krukenberg et al. 2018). The profile of *Ca.* E. thermophilum contained a protein at a similar position on the native gel that we confirmed with mass spectrometry to be the MCR-homolog (supplementary materials, materials and methods). Compared with the high relative abundance of MCR in ANME enrichments, the cell extract profile of AOE enrichment appears to have a stronger background, similar to that of pure cultures of methanogens. Such lower MCR abundance could result from the lower energy required for the activation of CH bonds of ethane than of methane (Scheller et al. 2013, Thauer 2019). This, and the overall higher energy yield of sulfate-dependent ethane oxidation (Thauer 2011, Chen et al. 2019), may explain the observed faster growth as compared with those of respective methane-oxidizing cultures.

We purified (Figure S4-3) and crystallized anaerobically the native MCR from *Ca.* E. thermophilum. The x-ray crystal structure was solved and refined to 0.99-Å resolution (Table S4-2) and presents an organization similar to the eight structurally characterized homologs of MCR from methanogens and ANME-1 (Figure 4-2A and Table S4-1). The MCR of *Ca.* E. thermophilum has the canonical 2($\alpha\beta\gamma$) organization and is 20 kDa larger as compared with *Methanothermobacter marburgensis*, resulting from insertions (α10-18, α90-111, α330-340, β70-95, and γ227-240) found in all three subunits. These insertions are present in the enzymes from other ethanotrophs but absent in those of methanogens and methanotrophs (Figure S4-4). The insertions are located in the same area of the protein surface and redesign the surface charges without interfering with the HS-CoB tunnel, a hydrophilic cavity that connects the bulk solvent to the catalytic center containing HS-CoM and F_{430} (Figure 4-2B and Figure S4-5). The active site organization and coenzymes position indicate a Ni(II)-inactive state. HS-CoM and HS-CoB are present at full occupancy. Most of the residues involved in HS-CoM and HS-CoB binding are conserved with other MCRs, with the exception of the α'Ala^{259} and γTyr^{120}, which are perfectly conserved in ethanotrophs, replacing the canonical arginine and leucine to position the carboxy-group of HS-CoB and sulfonate-group of HS-CoM, respectively (Figures S4-1, S4-4, and S4-6).

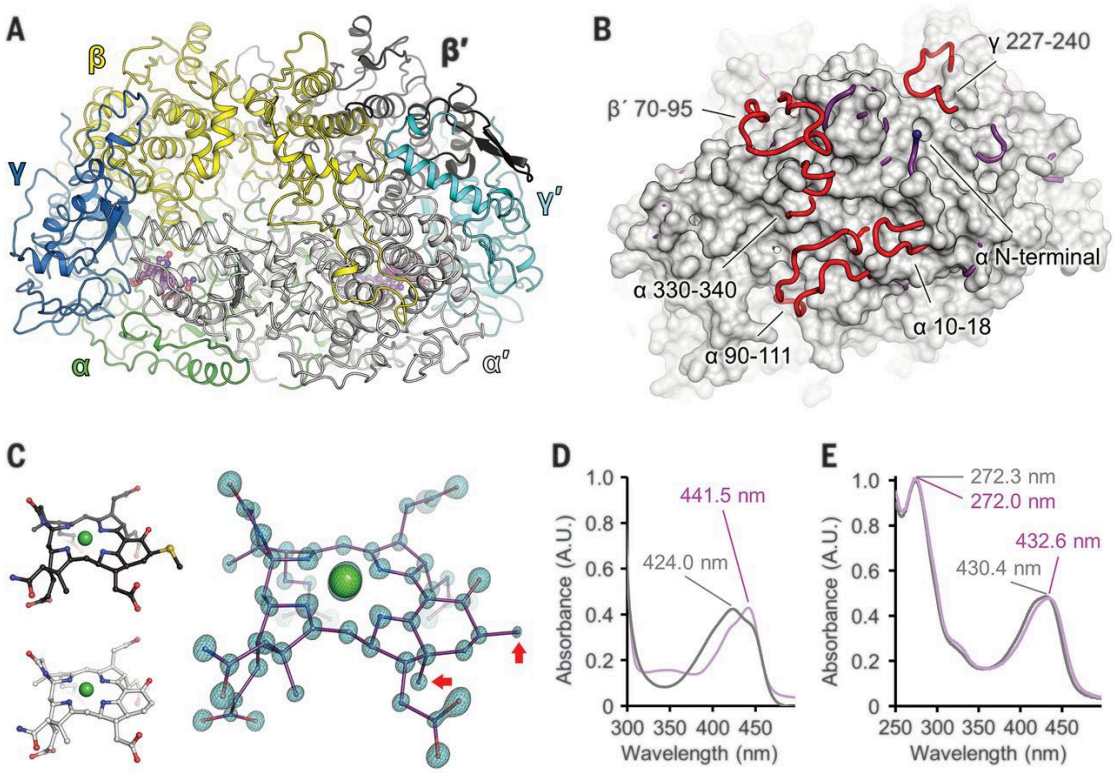

Figure 4-2 Structure of the MCR from *Ca.* E. thermophilum and its dimethylated F_{430}-cofactor. (A) Overall structural organization of the MCR-homolog from *Ca.* E. thermophilum (PDB 7B1S) represented in cartoon where each subunit harbors a different color code. Prime symbols correspond to the opposing monomers. (B) Superposition of MCR from *Ca.* E. thermophilum (purple) and MCR type I from *M. marburgensis* (PDB 5A0Y, white surface) (Wagner et al. 2016). The additional loops in *Ca.* E. thermophilum (red) are protruding from the *M. marburgensis* surface. (C) Structure of the cofactor F_{430} from *M. marburgensis* (white) (Wagner et al. 2016), the methylthio-F_{430} of ANME-1 from Black Sea mats (PDB 3SQG, black) (Shima et al. 2012), and the dimethylated-F_{430} from *Ca.* E. thermophilum (purple). The green ball represents nickel, and the methylations are indicated with red arrows. The $2F_o$-F_c map is contoured at 6s and shown as a transparent blue surface with a black mesh. (D) UV-visible spectra of MCRs (both at 78 mM concentration) and (E) the extracted F_{430} (normalized for comparison) from *Ca.* E. thermophilum (purple) and *M. thermolithotrophicus* (gray).

The core of the enzyme embeds the Ni-porphinoid F_{430}-cofactor, exhibiting two methylations of the carbon backbone according to the unambiguous electron density (Figure 4-2C). Mass spectrometry and hydrolytic profile confirmed the presence and the position of these methylations (Figures S4-7 and S4-8). A gene (locus FHEFKHOI_00788) annotated as a putative uroporphyrinogen-III C methyltransferase and accompanying the coding sequence of the co-factor F_{430} synthetase (*cfbE*) (Zheng et al. 2016, Moore et al. 2017) could be a candidate for the methylation of F_{430} (Figure S4-9). Sequence alignment and phylogenetic analysis indicate that this gene is an additional copy of the *cobM* gene, which is specific to ethanotrophs (Figure S4-9C). The protein encoded by the locus FHEFKHOI_00788 groups in a distinct branch of the CobM methyltransferase phylogenetic tree (Figure S4-9C). The second homolog branches with CobM sequences from other alkanotrophs and methanogens.

The ultraviolet (UV)-visible spectrum of the purified protein exhibits a different pattern with a maximal absorption peak at 441.5 nm, compared with 424.0 nm for a methanogenic MCR (Figure 4-2D). We extracted the dimethylated-F_{430} from the protein to evaluate whether the differences in the spectra are due to the cofactor modifications or a specific protein environment. The extracted dimethylated-F_{430} showed a maximal absorbance at 432.6 nm, thus shifted compared with the classical F_{430}, which has a maximum at 430.4 nm (Figure 4-2E). Hence, the observed shift of protein-bound F_{430} mostly results from differences in its coordination in the enzyme rather than its methylations.

Contrary to all structurally characterized MCRs, the enzyme from *Ca.* E. thermophilum coordinates the nickel by means of a methionine instead of the canonical glutamine. The sulfur from the methionine interacts with the nickel without disturbing the metal position in the porphinoid ring (Figure 4-3, A and B, and Figure S4-10). The methionine substitution cannot be considered as a prerequisite for ethane activation because the canonical glutamine is conserved in the MCR of the ethane oxidizer *Ca.* A. ethanivorans and relatives from cold seep environments (Figure S4-1 and S4-4). MCRs from methanogens and ANME archaea have virtually identical active sites, illustrating the selective pressure on the residues necessary for this complicated reaction (Figure S4-11, A and B) (Shima et al. 2012, Thauer 2019). It is therefore noteworthy to observe a different composition of the active site in the MCR-homolog from ethane oxidizers (Figure 4-3C). The most notable differences are in the loop α367-374, carrying the bulky αTrp^{373} that replaces the canonical phenylalanine. This loop displaced the porphinoid ring owing to hydrogen bond network from the αAsn^{375} and accompanied by a clamping effect from αTyr^{376} and αPhe^{441}, causing a tilting of the ring by 11.4° compared with other MCRs (Figure 4-3C and Figure S4-11B). As a result, the distance between the thiol groups of HS-CoM and HS-CoB is the longest reported so far in inactive Ni(II) structures of MCRs, with 6.6 Å compared with the 6.3 Å on average (Figure 4-3, A and B). The catalytic chamber gains in volume (Figure 4-3, D and E, and Figure S4-11, C and D), allowing ethane binding through appropriate van der Waals interactions. The chamber widening could impair the correct positioning of a classic cofactor F_{430} on the protein scaffold (Figure 4-3, C to E, and Figure S4-11). However, the additional methylations on the F_{430} would structurally overcome this issue by maintaining its correct position and the integrity of the porphinoid planarity. We propose that these methylations accommodate the cofactor in this dilated active site and assure its appropriate environment to maintain its reactivity (Figure 4-3, C to E).

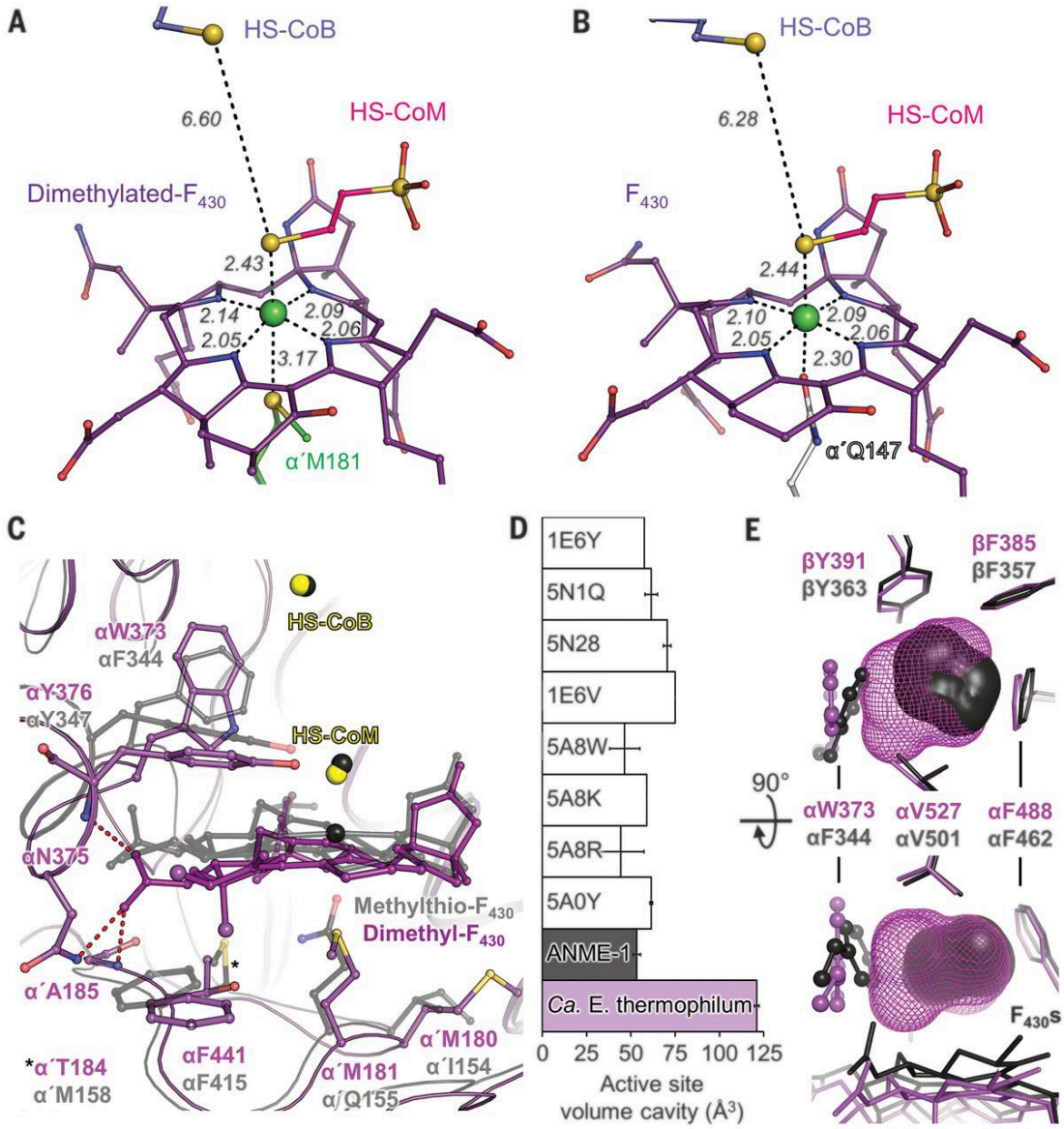

Figure 4-3 A widened active site to accommodate ethane. (A and B) Nickel coordination in atomic resolution structures of *Ca.* E. thermophilum [(A), PDB 7B1S] and MCR type I from *M. marburgensis* [(B), PDB 5A0Y]. Distances between the nickel (green ball) and its surrounding atoms are indicated with dashes and given in angstroms. (C) Cartoon representation of MCR from ANME-1 (transparent black, with nickel as ball, PDB 3SQG) superposed on the C terminus of the a-subunit of *Ca.* E. thermophilum (purple). HS-CoM, HS-CoB reactive thiols are shown as balls. F_{430}s and residues involved in the tilting of the dimethylated-F_{430} are shown as balls and sticks, and hydrogen bonds are indicated with red dashes. Most ethanoic and propanoic groups of the F_{430}s and water network were omitted for clarity. (D) Volume of each of the catalytic cavities in MCR structures from methanogens (white, indicated by PDB codes) (supplementary materials, materials and methods), methanotroph (black), and ethanotroph (purple) are reported on the histogram. (E) Comparison of the catalytic cavity volume between MCR from ANME-1 (black surface) and *Ca.* E. thermophilum (purple mesh). Surrounding residues are shown as sticks. The αTrp^{373} position is indicated with balls and sticks.

The structure of MCR from *M. marburgensis* revealed a spherical electron density between the thiols of HS-CoM and HS-CoB (Thauer 2019). Similarly, the MCR of *Ca.* E. thermophilum has a weak elongated electron density at this position. The modeling of a diatomic molecule such as ethane would be preferred to a water molecule, albeit static disorder in the cavity could also lead to the observed density (Figure S4-12). To confirm the

ethane-binding site and characterize a putative path inside the enzyme, we performed a xenon-pressurization experiment. Across the whole MCR from *Ca.* E. thermophilum, 16 Xe sites were unambiguously detected (Figure S4-13 and Table S4-3). The major Xe site was found at the ethane site, between the two coenzymes, without interfering with the thiol groups. A second site was detected in a hydrophobic cavity located between the active site and the surface. Computational analysis confirmed that this cavity is part of an extended tunnel of 33 Å length (Figure 4-4). According to the atomic-resolution structure, the tunnel is devoid of water molecules, attesting to its hydrophobic properties, which are ideal for the diffusion of hydrophobic gases such as ethane. All other Xe sites were found on the surface in hydrophobic pockets. No Xe was detected in the coenzyme tunnel because the proteins in the crystal systematically contain both HS-CoM and HS-CoB, preventing Xe diffusion into the tunnel. A similar computational analysis did not detect a similar tunnel in MCRs from *M. marburgensis* and ANME-1.

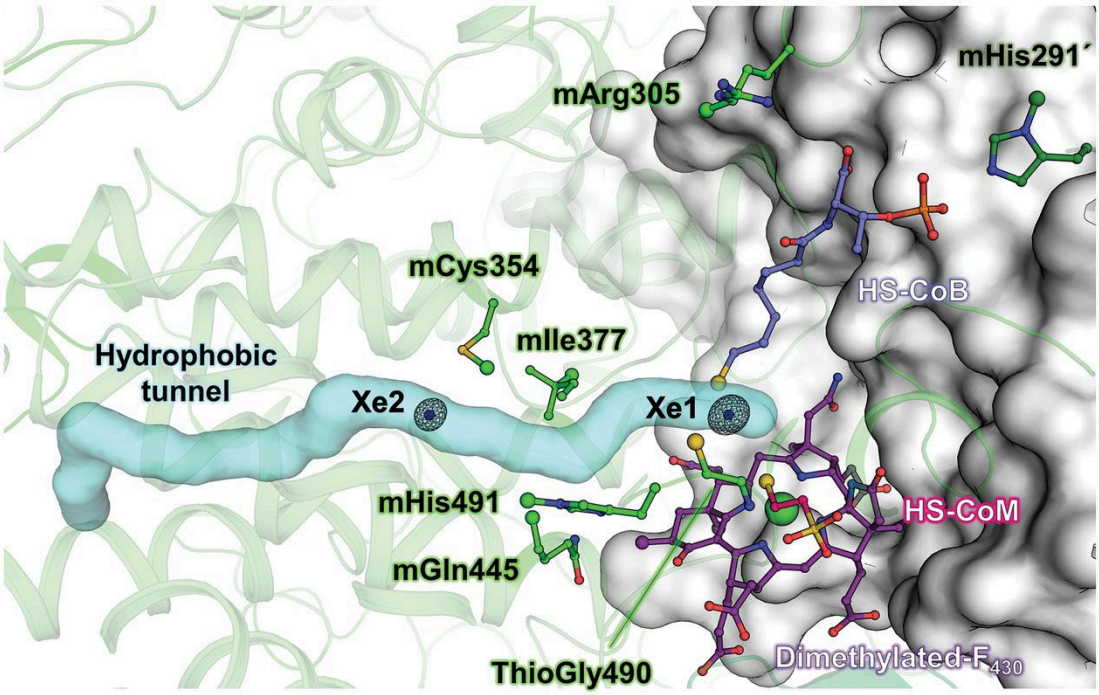

Figure 4-4 Ethane tunnel supporting gas diffusion toward the catalytic chamber. The protein is displayed in cartoon, with the a′-subunit as white surface. Posttranslational modifications, cofactor, and coenzymes are shown in sticks, with additional methyls and sulfurs as green and yellow balls, respectively. The hydrophobic tunnel calculated by the CAVER program (Chovancova et al. 2012) creating a route for the substrate to the catalytic center of the enzyme is shown as a cyan surface. The anomalous Fourier map contoured at 15s shown as black mesh indicates the position of Xe atoms obtained with xenon-pressurization experiment (PDB 7B2C), indicated with dark blue spheres.

The MCR from *M. marburgensis* can generate ethane from ethyl-CoM and HS-CoB, albeit with low affinity and activity compared with methane production (Gunsalus et al. 1978, Scheller et al. 2013). Xenon-pressurization of crystals from *M. marburgensis* MCR isoform I [named type I, in reference to Wagner et al. (2016)] revealed 12 Xe sites exclusively located at the surface of the enzyme in hydrophobic pockets (Figure S4-14 and Table S4-3), and no Xe could be detected in the catalytic chamber. These results suggest that the internal tunnel is specific to ethane oxidizers and could allow for efficient transport of ethane to the catalytic center. In *Ca.* E. thermophilum, the tunnel is formed at the interface of a four-helix bundle from the α subunit (helices 340-367, 373-382, 443-463, and 527-544). It is covered and flanked at the outer surface by the specific additional loops and the helix 385-401 (Figure S4-15). The opposite side of the tunnel, opening in the active site, is covered with posttranslationally modified residues: S-methylcysteine-354, 3-methylisoleucine-377, 2(*S*)-methylglutamine-445, and N^2-methylhistidine-491 (Figure 4-4, S4-15 and S4-16). The N^2-methylhistidine-491 is of particular interest because this residue is a tyrosine or phenylalanine in all other MCRs (Figure S4-1 and S4-4). Installation of these modifications would require a specific machinery that will need further investigation. Other modifications systematically found in methane-releasing MCRs were detected in the electron density and confirmed with mass spectrometry (Figure S4-16).

Our results reveal specific structural features harbored by the MCR-homolog of the ethane oxidizer *Ca.* E. thermophilum, which favors ethane consumption over methane or larger alkanes (Hahn et al. 2020). We propose to rename this enzyme, which is the entry point for anaerobic oxidation of ethane, to ethyl-CoM reductase (ECR). Assuming a similar organization of the active Ni(I) enzyme, the larger volume of the catalytic cavity would likely impair correct positioning of methane. The chamber volume would not be sufficient to accommodate alkanes larger than ethane, especially in the heterodisulfide-containing enzyme. Moreover, the hydrophobic tunnel inner diameter (average bottleneck radius 1.02 Å) would already prevent more voluminous alkanes such as propane from accessing the active site. Future investigations should resolve how the ECR active site constrains a particular reactive state of the ethane, allowing its exclusive and efficient capture.

Acknowledgements

We thank the Max Planck Institute for Marine Microbiology and the Max-Planck-Society for continuous support. We thank the SOLEIL and SLS synchrotrons for beam time allocation and the respective beamline staffs of Proxima-1 and X06DA for

assistance with data collection, with specific regards to P. Legrand. We also acknowledge C. Probian and R. Appel for their continuous support in the Microbial Metabolism laboratory. We are thankful to R. Amann and R. K. Thauer for their critical views on the manuscript and their stimulating discussions. We thank K. Knittel for her inputs during a regular exchange. We thank A. Teske for organizing the sampling campaign of the Guaymas Basin hydrothermal vents (NSF grant 1357238).

Funding

Additional funds came from the Deutsche Forschungsgemeinschaft funding the Cluster of Excellence "The Ocean Floor—Earth's Uncharted Interface" (EXC-2077-390741603) at MARUM, University Bremen. S.E. was granted by SNF grant 200021_182369.

Competing interests

The authors declare no competing interests

Data and materials availability

All structures were validated and deposited in the Protein Data Bank (PDB) under the following accession numbers: 7B1S, native ethyl-coenzyme M reductase from *Ca.* E. thermophilum; 7B2C, Xenon-pressurized ethyl-coenzyme M reductase from *Ca.* E. thermophilum and 7B2H, Xenon-pressurized methyl-coenzyme M reductase from *M. marburgensis*. Raw and processed data for x-ray crystallography and mass spectrometry experiments are hosted at Zenodo (Hahn et al. 2021). All other data are available in the manuscript or the supplementary materials.

4.3 Supplementary materials

4.3.1 Materials and Methods

4.3.1.1 Origin and cultivation of Ethane50, AOM50 and AOM20 enrichments

The Ethane50 culture derived from heated sediments of the Guaymas Basin hydrothermal vents sampled during RV Atlantis mission AT 37-06 with submarine Alvin in December 2016. The culture was retrieved by incubating sediment aliquots in sulfate reducer

(SR) medium (Widdel and Bak 1992) with ethane as substrate at 50°C in 100 ml injection vials. Activity in these cultures was tracked by measuring ethane-dependent sulfide production using a copper sulfate assay (Cord-Ruwisch 1985). Ethane-dependent sulfide formation was observed after three months, and the active cultures were diluted multiple times and further incubated at 50°C, yielding a sediment free, highly active ethane-degrading culture within one year [for details see Laso-Pérez et al. (2018) and Hahn et al. (2020)]. For this study, large amounts of Ethane50 culture were grown in 1 l Duran flasks with 900 ml SR medium and ethane headspace (0.2 MPa). In this assay, the medium was exchanged when sulfide concentration reached around 15 mM and cultures were diluted 1:10 when sulfide production exceeded 10 mM in 7 days. Similarly, the AOM50 culture derived from the Guaymas Basin (sampled during RV Atlantis mission AT 15-56 in December 2009) and cultivation was performed with methane as sole provided energy substrate. The cultivation conditions and microbial compositions have been described before (Holler et al. 2011, Wegener et al. 2016, Krukenberg et al. 2018, Laso-Pérez et al. 2018). The ANME-2 dominated AOM20 culture derived from sediments from Amon Mud Volcano, Eastern Mediterranean Sea, retrieved during Nautinil Expedition RV Atalante in 2003. Cultivation was performed at room temperature (20°C) with methane as sole energy substrate. The microbial composition of this culture is well-described (Wegener et al. 2016).

4.3.1.2 Cultivation of methanogenic archaea

Methanothermococcus thermolithotrophicus DSM 2095, *Methanothermobacter marburgensis* DSM 2133 and *Methanosarcina barkeri* DSM 800 were obtained from the Deutsche Sammlung von Mikroorganismen und Zellkulturen GmbH, Braunschweig, Germany. *M. barkeri* was cultivated at 37°C under strict anoxic conditions in a medium which composition was already described (Karrasch et al. 1989). Sterile and anoxic methanol (1 % v/v) was added as carbon and energy source. The initial gas phase contained N_2/CO_2 (90/10 %) at 50 kPa. The overpressure coming from the metabolic activity during growth was regularly evacuated. *M. marburgensis* was cultivated at 65°C under strict anoxic condition in minimal medium (Schönheit et al. 1980) and *M. thermolithotrophicus* at 65°C under strict anoxic condition in a medium containing, per liter, 9.76 g of 2-(N-morpholino)ethanesulfonic acid (MES) buffer, 558 mg KH_2PO_4, 1 g KCl, 25.13 g NaCl, 840 mg $NaHCO_3$, 700 mg Na_2SO_4, 367.5 mg $CaCl_2 \times 2\ H_2O$, 7.725 g $MgCl_2 \times 6\ H_2O$, 1.18 g NH_4Cl, 61.1 mg, nitrilotriacetic acid (NTA), 6.16 mg $FeCl_2 \times 4\ H_2O$, 3.3 mg $Na_2WO_4 \times 2\ H_2O$, 2.42 mg $Na_2MoO_4 \times 2\ H_2O$, 2 µM $Na_2SeO_3 \times 5\ H_2O$, 0.4 g resazurin, 10 ml of anoxic trace element solution. The pH was set at 6

by addition of 1 M KOH. Trace element solution contained, per liter, 1.36 g NTA, 91.4 mg $MnCl_2 \times 6\ H_2O$, 183.3 mg $FeCl_3 \times 6\ H_2O$, 60.26 mg $CaCl_2 \times 2\ H_2O$, 180.8 mg $CoCl_2 \times 6\ H_2O$, 90 mg $ZnSO_4 \times 7\ H_2O$, 35.21 mg $CuSO_4 \times 5\ H_2O$, 46 mg $Na_2MoO_4 \times 2\ H_2O$ and 90 mg $NiCl_2 \times 6\ H_2O$. Both organisms were cultivated in flasks with a medium:gas ratio of 1:9 with a 100 kPa gas phase containing H_2/CO_2 (80/20 %) mixture. The *M. thermolithotrophicus* biomass used for MCR purification was obtained from a 2 l fermenter. For all three methanogens, the cells were harvested in late-exponential phase by centrifugation and kept frozen at −80°C under anoxic conditions before use.

4.3.1.3 Influence of 2-bromoethane sulfonate (BES) on AOM and AOE

In an anaerobic chamber, replicates of AOM50 and Ethane50 cultures were prepared in 126 ml serum flasks with 80 ml medium and 46 ml headspace. Anoxic BES (1 M) was added to the different cultures in order to reach 0.1 mM, 1 mM, 10 mM final concentration (n=3 each). As substrates, 20 ml of methane or ethane were added to the headspace. All cultures were incubated at 50°C. Sulfide production from sulfate reduction was measured with a copper sulfate assay (Cord-Ruwisch 1985). Methane and ethane concentrations were analyzed from 0.2 ml headspace samples on an Agilent 6890 gas chromatograph in splitless mode equipped with a packed column (Supelco Porapak Q, 6 ft by 1/8 ft by 2.1 mm stainless steel column, oven temperature 80°C). Helium was used as carrier gas (20 ml min^{-1}) and hydrocarbons were detected using flame ionization detection. For figure construction, replicates are presented and polynomial regression fits are drawn. For Figure 4-1A, polynomial regression fit equations and R^2 are: Sulfide generation: AOE: $y=-0.0034x^2+0.5081x+0.3779$ ($R^2=0.995$); AOE + BES: $y=-0.0001x^2+0.0137x+0.4954$ ($R^2=0.6075$); AOM: $y=-0.00005x^2+0.051x+0.0169$ ($R^2=0.988$); AOM + BES: $y=-0.0001x^2+0.0039x+0.1471$ ($R^2=0.3757$); Alkane consumption: AOE: $y=-0.0011x^2+0.1925x+10.142$ ($R^2=0.9932$); AOE + BES: $y=-0.0004x^2+0.0399x+9.817$ ($R^2=0.3093$); AOM: $y=-0.0003x^2+0.0803x+11.395$ ($R^2=0.8673$); AOM + BES: $y=-0.0014x^2+0.0969x+11.464$ ($R^2=0.6904$). All individual replicates are presented in Figure S4-2, with the respective polynomial regression fit equations and R^2.

4.3.1.4 Protein extraction and purification

Exponentially growing Ethane50 culture was used for the protein extraction. The medium was removed with a stainless steel needle by applying N_2:CO_2 (90:10 %) overpressure. After a 3 min long flushing with N_2:CO_2 (90:10 %), the cells were pelleted by centrifugation

for 15 min at 16,250*g* in an anaerobic chamber filled with a N_2/CO_2 atmosphere (90:10 %) at room temperature and the supernatant was removed. Cells were suspended in SR medium (Widdel and Bak 1992) and stored at −80°C under an N_2:CO_2 (90:10 %) atmosphere until purification. Cell lysis and preparation of extracts were performed in an anaerobic chamber filled with an N_2/CO_2 atmosphere (90:10 %) at room temperature. A volume of 9 ml of sedimented cells, corresponding to 4 l of cultures, was suspended in two volumes of a 50 mM tricine buffer, pH 8, 2 mM dithiothreitol (DTT; Buffer A). The lysis protocol included a sonication step (BANDELIN Sonopuls HD 2200) followed by three rounds of French Press at around 1000 PSI (6.895 MPa), yielding to a homogenous deep-black extract. To minimize oxygen contamination, the French press cell was flushed with N_2 and washed twice with anoxic buffer A. Soluble extract (105.4 mg of total proteins) was obtained by ultracentrifugation at 140,000*g* for one hour at 4°C. Enzyme purification was carried out under anaerobic conditions in a Coy tent, filled with an N_2/H_2 atmosphere (95:5 %), at 20°C and under yellow light. For each step, chromatography columns were washed with at least three-column volume (CV) with the corresponding loading buffer and samples were filtrated on 0.2 µm filters prior loading. During purification, the enzyme was followed by high resolution Clear Native PolyAcrylamide Gel Electrophoresis (hrCN PAGE, see below), Sodium Dodecyl Sulfate PAGE (SDS PAGE) and absorbance monitoring at 280, 415 and 550 nm.

Extracts were diluted with Buffer A to obtain a final 13-fold dilution before being loaded on 4 × 5 ml anion exchanger HiTrap™ Q HP columns (GE Healthcare) equilibrated with the same buffer. After a 2 CV washing, proteins were eluted with a 0 to 0.75 M NaCl linear gradient for 7.5 CV at a 2 ml min^{-1} flow rate. The fractions of interest containing MCR from *Ca.* E. thermophilum eluted between 0.36 M and 0.43 M NaCl. The pooled fractions were diluted with three volumes of an anoxic 50 mM Tris-HCl Buffer, pH 7.6, 2 mM DTT (Buffer B) containing 2 M ammonium sulfate, before being loaded on a Source™ 15PHE 4.6/100 PE (GE Healthcare) equilibrated with the same buffer. After a 4 CV washing, proteins were eluted with a 1.6 to 0 M ammonium sulfate linear gradient for 53 CV at a 1 ml min^{-1} flow rate. The enzyme eluted between 0.58 M and 0.43 M ammonium sulfate. Pooled fractions were supplemented with 1 M ammonium sulfate and loaded a second time on Source™ 15PHE 4.6/100 PE, the protein being eluted with a 0.9 to 0.3 M ammonium sulfate linear gradient for 10 CV at a 1 ml min^{-1} flow rate. The enzyme eluted in one peak between 0.63 M and 0.42 M ammonium sulfate. Fractions of interest were pooled, concentrated on 30-kDa cut-off centrifugal concentrator (nitrocellulose, Vivaspin from Sartorius) and size-exclusion chromatography using a Superdex 200 Increase 10/300 GL (GE Healthcare) was used as last

purification step. The enzyme eluted in a Gaussian peak with an 11.1 ml elution volume. The purification process yielded 4.8 mg of pure enzyme. The pooled fractions were concentrated, and the protein was directly used for anaerobic crystallization or flash-frozen in liquid nitrogen and stored at −80°C under aerobic conditions. The MCR from *Ca.* E. thermophilum is considered to be in the inactive Ni(II) state based on the structure and therefore no activities were tested.

The MCR from *M. thermolithotrophicus* was purified from 20 g of wet cells. Pellet was suspended in 5 volumes of 50 mM Tris-HCl pH 8, 2 mM DTT (Buffer C) in an anoxic tent filled with N_2:CO_2 (90:10 %). Cells were lysed by osmotic shock followed by sonication (BANDELIN Sonopuls HD 2200). Unbroken cells and debris were discarded by centrifugation for 30 min at 16,250*g* at room temperature under an N_2:CO_2 (90:10 %) atmosphere. Enzyme purification was carried out under anaerobic conditions in a Coy tent, filled with an N_2/H_2 atmosphere (95:5 %), at 20°C and under yellow light. For each step, chromatography columns were washed with at least three-column volume (CV) with the corresponding loading buffer and samples were filtrated on 0.2 µm filters prior loading. During purification, the enzyme was followed by SDS PAGE and absorbance monitoring at 280 and 415 nm. The soluble fraction was diluted with two volumes of Buffer C before being loaded on 4 × 5 ml anion exchanger HiTrap™ Q HP columns equilibrated with the same buffer. After a 2 CV washing, proteins were eluted with a 0 to 0.5 M NaCl linear gradient for 6 CV at a 2 ml min^{-1} flow rate. The fractions of interest eluted between 0.31 M and 0.40 M NaCl. The pooled fractions were diluted with 5 volumes of an anoxic Buffer B containing 2 M ammonium sulfate, before being loaded on a HiTrap™ Phenyl Sepharose HP 5 ml (GE Healthcare) equilibrated with the same buffer. After a 4 CV washing, proteins were eluted with a 1.5 to 0.6 M ammonium sulfate linear gradient for 24 CV at a 1 ml min^{-1} flow rate. The enzyme eluted between 0.95 M and 0.68 M ammonium sulfate. Fractions of interest were pooled, concentrated on 30-kDa cut-off centrifugal concentrator (nitrocellulose, Vivaspin from Sartorius) and size-exclusion chromatography using a Superdex 200 Increase 10/300 GL was used as last purification step. The enzyme eluted in a Gaussian peak with an 11.04 ml elution volume. The pooled fractions were concentrated, flash-frozen in liquid nitrogen and stored at −80°C under aerobic conditions.

The MCR homologue from *M. marburgensis*, used for crystallization and xenon-pressurization experiments, was purified according to a protocol already described (Wagner et al. 2016). For all samples, protein concentration was estimated according to the Bradford methods by using the protein assay dye reagent concentrate from BioRad. A bovine

serum albumin standard was used to estimate protein concentration. Samples were recorded by spectrophotometric absorbance at 595 nm.

4.3.1.5 High resolution clear native polyacrylamide gel electrophoresis (hrCN PAGE)

The hrCN PAGE protocol was adapted from (Lemaire et al. 2018). The electrophoresis was performed in an anaerobic chamber filled with a N_2:CO_2 (90 %:10 %) atmosphere. Fresh anaerobic samples were used. Glycerol (20 % v/v final) was added to samples and 0.001 % (w/v) Ponceau S is used as a protein migration marker. The anaerobic electrophoresis cathode buffer contained a buffer mixture of 50 mM tricine; 15 mM Bis-Tris at a pH 7 supplemented with 0.05 % (w/v) sodium deoxycholate; 0.01 % (w/v) dodecyl maltoside and 2 mM DTT. The anaerobic anode buffer contained 50 mM Bis-Tris buffer, pH 7; 2 mM DTT. hrCN PAGE were carried out using an 8 to 15 % linear polyacrylamide gradient, incubated overnight in an anaerobic tent, soaking in anaerobic cathode buffer. Gels were run with a constant 20 mA current using a PowerPac™ Basic Power Supply (Bio-Rad). After electrophoresis, protein bands were stained with Instant Blue™ (Expedeon).

4.3.1.6 Protein crystallization

Crystals were obtained by initial screening at 20°C using the sitting drop method on a 96-Well MRC 2-Drop Crystallization Plates in polystyrene (SWISSCI). The crystallization reservoir contained 90 µl of mother liquor. Crystallization drop contained a mixture of 0.6 µl protein and 0.6 µl precipitant. Crystals of the MCR homologue from *Ca.* E. thermophilum were obtained by initial screening using the JBScreen Pentaerythritol screen from Jena Bioscience in a Coy tent under an N_2:H_2 atmosphere (95:5 %). The crystallization reservoir contained 45 % (w/v) Pentaerythritol Propoxylate (5/4 PO/OH), 100 mM Tris/HCl pH 8.5 and 400 mM potassium chloride. The initial protein concentration was 16.22 mg ml^{-1}. The crystal used for xenon-pressurization derived from the same crystallization condition. Both structures of MCR homologue from *Ca.* E. thermophilum were obtained from crystals prepared from the same purification. Crystal used for xenon-pressurization of *M. marburgensis* MCR homologue was obtained under aerobic condition using a crystallization reservoir containing 27.5 % (v/v) polyethylene glycol 400, 100 mM 4-(2-hydroxyethyl)-1-piperazineethanesulfonic acid (HEPES) pH 7.5, 250 mM $MgCl_2$, 200 mM NaCl and 20 mM 2-oxoglutarate. The crystallized sample was in 25 mM Tris-HCl pH 7.6, 10% glycerol and 2 mM DTT at a protein concentration of 25 mg ml^{-1}.

4.3.1.7 Xenon-pressurization experiment

Crystals were harvested using a MiTeGen MicroRT loop. In order to protect the crystal during xenon-pressurization, a part of the plastic capillary, usually used for room temperature diffraction experiments, was placed around it. The loop was then mounted in an Oxford Xcell xenon chamber. Xe pressure was gradually increased using a manual pump to reach 25 bars. After 7 min, pressure was slowly released and the crystal immediately plunged in liquid nitrogen. Data collection was performed at 100 K using a wavelength of 1.5498 Å for MCR from *Ca.* E. thermophilum and 2.0750 Å for MCR type I of *M. marburgensis* on the X06DA beamline of the Swiss Light Source synchrotron in Villigen, Switzerland. Integration of the diffraction frames yielded a complete dataset with an overall resolution of 1.80 Å for MCR from *Ca.* E. thermophilum and 2.12 Å for *M. marburgensis*. These datasets were used to compute anomalous Fourier maps.

4.3.1.8 X-ray data collection, model building and refinement

MCR crystals from *Ca.* E. thermophilum were directly frozen in liquid nitrogen under anoxic conditions prior to x-ray diffraction studies. All diffraction experiments were performed at 100 K. Initial screenings of the MCR from *Ca.* E. thermophilum was performed at Proxima-1 at the SOLEIL synchrotron, Saclay. The best diffracting crystals were collected at the X06DA beamline of the Swiss Light Source synchrotron in Villigen, Switzerland. The data were processed and scaled with autoPROC (Vonrhein et al. 2011). Structures of MCR from *Ca.* E. thermophilum were further processed with STARANISO correction integrated in the autoPROC pipeline (Tickle et al. 2018) (STARANISO. Cambridge, United Kingdom: Global Phasing Ltd.). The first structure of the MCR from *Ca.* E. thermophilum was solved by molecular replacement with Phenix (Liebschner et al. 2019) using MCR type II from *Methanothermobacter wolfeii* (PDB 5A8W) as a template.

All models were manually built via Coot (Emsley et al. 2010). Xenon-pressurized structures of MCR type I from *M. marburgensis* and MCR from *Ca.* E. thermophilum were refined with PHENIX.REFINE (Liebschner et al. 2019) and BUSTER (BUSTER version 2.10.3. (Bricogne et al. 2017)), respectively. Xe occupancies were adjusted and refined. Correlations between refined Xe atom occupancies and ANODE peak heights (Thorn and Sheldrick 2011) are given in Table S4-3. The atomic resolution structure of MCR from *Ca.* E. thermophilum was refined by Phenix (Liebschner et al. 2019) (version 1.17.1-3660) following

this process: 1) the protein was built at a resolution of 1.5-Å by using the Non-Crystallography Symmetry and Translational-Liberation Screw (TLS) options; 2) when the model was completed, the resolution was extended to 0.99-Å. The STARANISO software was used to correct for anisotropy in the diffraction data. The diffraction limits (local (I)/sig(I) > 1.2) along the h, k, and l axes were 1.07, 0.99, and 1.14A, respectively. Further refinement was performed without TLS but by refining with all atoms anisotropic. The last refinement steps were performed with hydrogens in riding position for all models. Hydrogens were omitted in the final deposited models. All models were ultimately validated by the MolProbity server (Chen et al. 2010) (http://molprobity.biochem.duke.edu). The Table S4-2 contains the statistics of data collection, refinement as well as the PDB codes for the deposited models. X-ray crystallography raw and processed data are accessible at Zenodo (Hahn et al. 2021).

4.3.1.9 Structural analyses

All figures were generated and rendered with PyMOL (Version 1.8, Schrödinger, LLC). Internal tunnel prediction was performed by CAVER (Chovancova et al. 2012) by applying a probe radius of 1.0-Å. Volumes of the catalytic chamber cavity calculations were performed by HOLLOW (Ho and Gruswitz 2008) by applying a grid factor of 0.05-Å and a sphere radius of 20-Å starting from the Tyr391 or homologous residues in other MCRs (MCR from *Ca.* E. thermophilum numbering). The water molecules generated by HOLLOW corresponding to the catalytic chamber were isolated and their respective volume was calculated through the Voss Volume Voxelator server (Voss and Gerstein 2010)with a probe radius of 0. Each site from each MCR were processed individually. Results were averaged and the standard deviations for multiple sites are shown in Figure 4-3D. Thus, the number of replicates depends on the number of MCR catalytic sites in the asymmetric unit. PDB codes in Figure 4-3D corresponds to the following structures from: *M barkeri* (Grabarse et al. 2000) (PDB 1E6Y), *M. thermolithotrophicus* (Wagner et al. 2017) (PDB 5N1Q), *Methanotorris formicicus* (Wagner et al. 2017) (PDB 5N28), *Methanopyrus kandleri* (Grabarse et al. 2000) (PDB 1E6V), *Methanothermobacter wolfeii* type I (Wagner et al. 2016) (PDB 5A8K) and II (Wagner et al. 2016) (PDB 5A8W), *M. marburgensis* type I and II (Wagner et al. 2016) (PDB 5A8R), ANME-1 from Black Sea mats (Shima et al. 2012) (PDB3SQG) and *Ca.* E. thermophilum.

4.3.1.10 Bioinformatic analyses

Gene annotation was extracted from publicly available sequences. Annotations were confirmed using the BLASTx search (Altschul et al. 1997) against the NCBI non-redundant protein sequences database. To identify the genes involved in the biosynthetic pathway of

cofactor F_{430} (*cfbA-E*), we designed BLAST+ databases for the genomes and searched for *cfb* genes using the BLASTx algorithm. Genes described in Zheng et al. (2016) from *Methanosarcina acetivorans* C2A were used as reference. Identified genes were confirmed by a BLASTx search against the NCBI non-redundant protein sequences database.

4.3.1.11 MCR amino acid sequence alignment and methyltransferase phylogeny

The complete amino acid sequences of 33 MCR (Figure S4-1 and S4-4) from methanogenic, methanotrophic and ethanotrophic archaea were aligned using Clustal Omega (Sievers et al. 2011) with default parameters. The three subunits α, β and γ were aligned separately. All sequences used for the alignment are publicly available. For elaboration of Figure S4-1, a manual refinement by scanning for patterns of the alignment in Geneious Prime (v. 2019.2.3, Biomatters, Ltd., Auckland, New Zealand) was performed and a selection of seven MCR sequences was picked for visualization, but the highlighting for consensus sequences and identity values refer to complete alignment. The Figure S4-4 was generated by Espript 3.0 (Robert and Gouet 2014) server (ESPript - http://espript.ibcp.fr).

For the phylogenetic analysis of methyltransferases, 223 publicly available amino acid sequences of methanogens and alkanotrophs were aligned using Clustal Omega (Sievers et al. 2011) with default parameters. The sequences were obtained by a BLAST research using sequence of the protein encoded by the locus FHEFKHOI_00788 as query. 904 amino acid positions were considered for the analysis and aligned sequences were masked using Zorro (https://sourceforge.net/projects/probmask/). A phylogenetic tree was calculated using RAxML version 8.2.12 (Stamatakis 2014) with PROTGAMMAAUTO model and LG likelihood amino acid substitution settings and 100 fast bootstraps were calculated. The tree was visualized with iTol v6 (Letunic and Bork 2007).

4.3.1.12 UV/Vis spectra, cofactor extraction

Cofactors extraction was performed on about 500 µg of pure enzyme using C18-SPE spin columns, prepared with 500 µl acetonitrile 100% (v/v) before being washed with 2 ml of acetic acid 0.1% (v/v). Samples were diluted in 10 volumes of acetic acid 0.1% (v/v) before loading on columns. Elution was enhanced by centrifugation at 100*g*, the flow through being applied again on a column. The loading procedure was repeated ten times to ensure saturation of the column. After a 500 µl washing with acetic acid 0.1% (v/v), cofactors were eluted with 1 ml of acetonitrile 100 % (v/v). Acetonitrile was then evaporated using a centrifugational vacuum concentrator at 35°C. When volume reached around 100 µl, three volumes of deionized water were added before a second concentration step, with a final volume of around

100 µl. After a three-fold dilution with deionized water, samples were filtered through 0.2 µm UltraFree® centrifugal filters (Merck) and concentrated to a final volume of 10 µl. After a two-fold dilution in 100 mM Tris HCl buffer, pH 7.6, UV-Vis spectra of the extracted cofactors were monitored.

Spectral analyses were performed aerobically using a Cary 60 UV-Vis spectrophotometer (Agilent technologies). Absorbance spectra were measured in a wavelength range between 250 to 600 nm, with a measurement every 0.5 nm, in a 1 mm-pathlength Traycell (Hellma Analytics) at room temperature. For pure proteins, a concentration of 78 µM was used (calculated based on the heterohexamer molecular weight of 293 kDa), diluted in 50 mM Tris-HCl pH 7.6. For extracted cofactors, spectra were normalized after measurement in order to be comparable. Presented graphs in Figure 4-2D and E are representatives of at least three measurements.

4.3.1.13 Mass spectrometry

Bands from SDS-/hrCN-PAGE were extracted. Samples were digested with sequencing-grade modified trypsin (Promega) and the resulting peptide mixtures were analyzed by nanoLC (PepMap100 C-18 RP nanocolumn and UltiMate 3000 liquid chromatography system, Dionex). The cofactor or peptide containing samples were desalted with C18-SPE, the eluates were concentrated using a vacuum dryer and then analyzed with a matrix-assisted laser desorption/ionization (MALDI) (time of flight) mass spectrometer (MALDI-TOF MS). Samples were prepared directly onto a MALDI-Plate by mixing with a matrix composed of 3 mg ml^{-1} α-cyano-4- hydroxycinnamic acid in 80% (v/v) acetonitrile and 0.3% (v/v) trifluoroacetic acid (Dried-Droplet Crystallization). MALDI-TOF-MS analysis was performed with a 4800 Proteomics Analyzer (Applied Biosystems/MDS Sciex) using the 4800 Series Explorer software (positive-ion reflector mode) in a mass range from 800 to 3500 Da. The data were calibrated externally using a peptide mixture spotted onto the same MALDI target.

To detect the post-translational modifications in the MCR, the protein was digested by bovine α-Chymotrypsin (Sigma-Aldrich), *Staphylococcus aureus* GluC (Sigma-Aldrich), porcine pancreas elastase (Sigma-Aldrich) or sequencing-grade modified trypsin (Promega) at 30°C using a 2.5 ng $µl^{-1}$ protease final concentration. Digested peptides were separated by UltiMate 3000, separation column (PicoTip-Emitter, itself filled with ReproSil 120 C18-AQ, 42 cm) and analyzed with a Q Exactive (plus) Orbitrap Mass Spectrometer (ThermoFisher).

The Orbitrap data was interpreted with Thermo Proteome Discoverer 1.4 and Byonic software. Raw and processed mass spectrometry data are accessible at Zenodo (Hahn et al. 2021).

4.3.1.14 Esterification and hydrolysis of F_{430}-cofactor

For the esterification, the classic F_{430} extracted from MCR type I from *M. marburgensis* (molar mass 905.27 Dalton), was desalted using a C18-SPE (C18 Silica Microspin column, The Nest Group, Inc.; 5-60 µg capacity) and vacuum dried in a 1.5 ml cup. Then, 100 µl methanol was added and the sample was dissolved by sonication. The mixture was incubated with gaseous HCl for 9 hours at room temperature. Gaseous HCl was synthesized by mixing 0.8 ml 80% H_2SO_2 to 1.2 g NaCl. After the reaction, methanol and HCl were removed by vacuum drying and passed on MALDI. Mass spectrometry spectra of the proportionally esterified F_{430} are shown in the Figure S4-8A. The artificially methylated F_{430} and the native F_{430} extracted from the MCR of *Ca.* E. thermophilum (molar mass 933.33 Dalton) were further saponified. For saponification, samples were dried, suspended in 100 µl of 10% NH_4OH, sonicated for 60 sec and then incubated at 30°C under agitation for 30 minutes. The samples were then vacuum-dried, dissolved in 25 µl 5% (v/v) formic acid and measured on the MALDI (Supplementary Figure S4-8B and S4-8C). Because there was no trace of saponification with F_{430} from *Ca.* E. thermophilum, the sample was incubated with 20% NH_4OH for another 20 minutes and the MALDI measurement was repeated: the molar mass of 933.33 Dalton did not change.

4.3.2 Supplementary figures

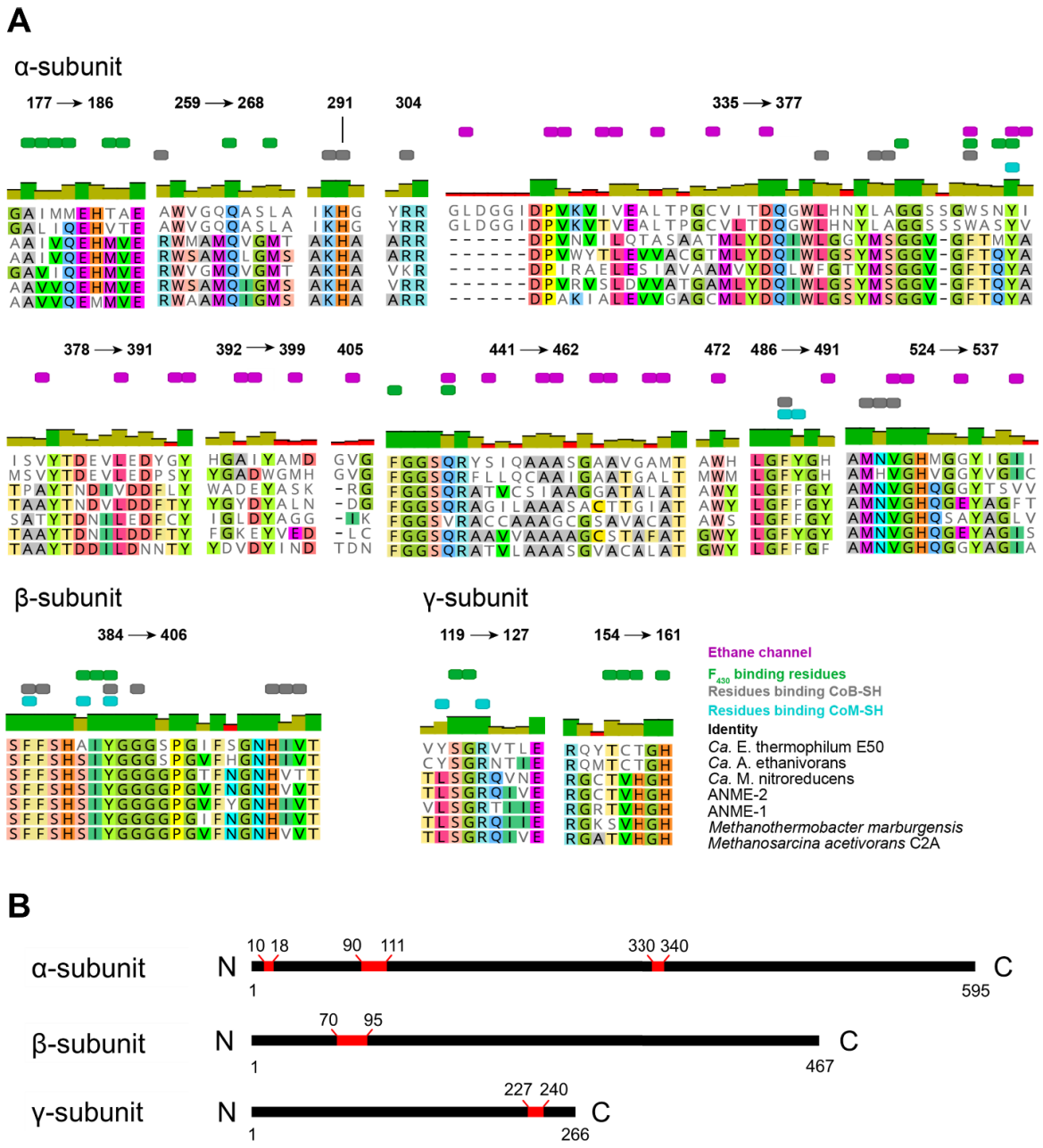

Figure S4-1 Amino acid sequence conservation among MCR homologues**. A,** Characteristic regions in all three subunits forming the substrate tunnel and those involved in coordination of F_{430}, HS-CoB and HS-CoM. Numbering is based on *Ca.* E. thermophilum MCR amino acid sequence. Sequence identity is based on 33 MCR sequences extracted from methanogens (n=15), methanotrophs (n=11) and ethanotrophs (n=7). Accession numbers are given in Figure S4-4. **B**, Insertions locations in MCR homologue from ethanotrophs (*Ca.* E. thermophilum for numbering). Insertions are highlighted by red bars.

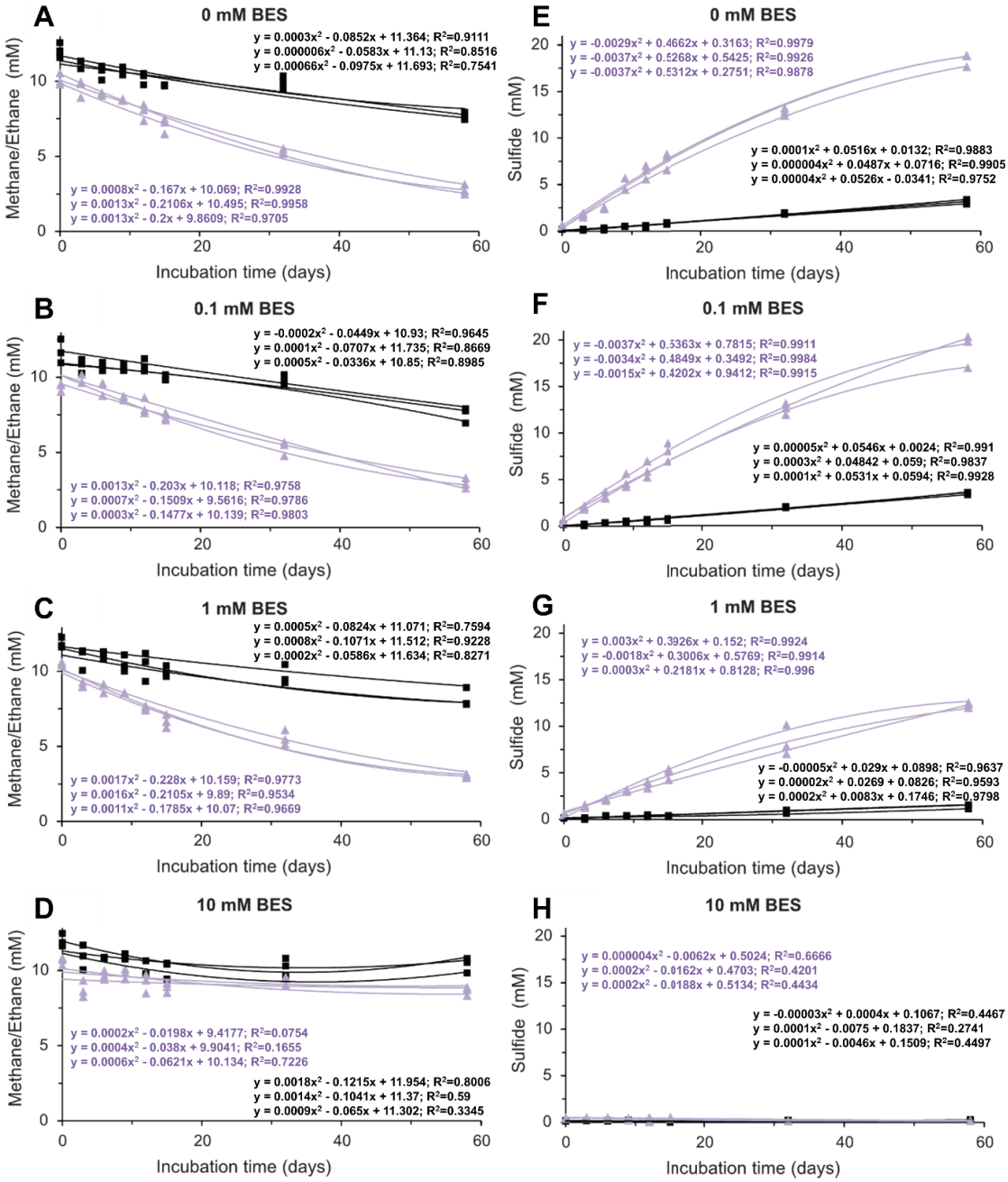

Figure S4-2 Influence of 2-Bromoethane sulfonate (BES) on alkane consumption and sulfide production in the AOM50 and Ethane50 enrichments. Triplicates of AOM50 (black squares) and Ethane50 (purple triangles) cultures were incubated at 50°C in the presence of different concentration of BES. A-D, Methane consumption by AOM50 cultures and ethane consumption by Ethane50 cultures, monitored by gas chromatography. E-H, Sulfide production, monitored by copper sulfate assay. Polynomial regression fit equation and R^2 are given for each replicate.

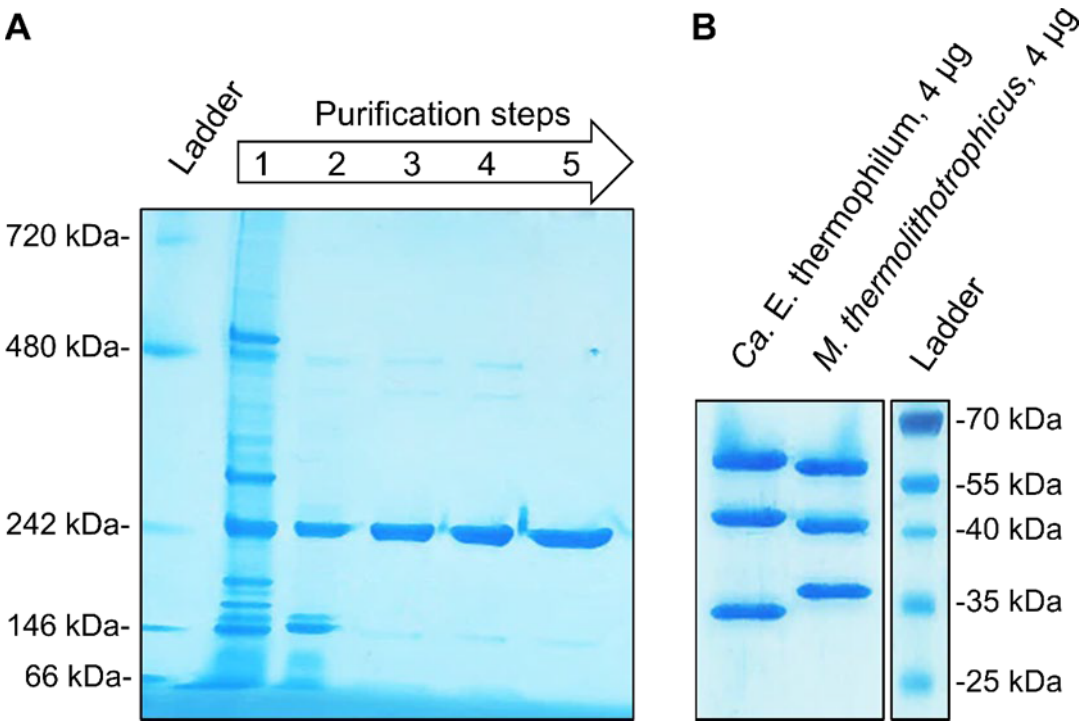

Figure S4-3 Native purification and SDS-PAGE profile of MCR from *Ca.* E. thermophilum. A, MCR purification based on hrCN PAGE profile. The purification steps correspond to the following order: 1, soluble extract (10 µg); 2, HiTrap™ Q HP (2 µg); 3, Source™ 15PHE 4.6/100 PE (2 µg); 4, second Source™ 15PHE 4.6/100 PE (2 µg); 5, Superdex 200 Increase 10/300 GL (2 µg). B, SDS-PAGE profile of purified MCR from *Ca.* E. thermophilum and *M. thermolithotrophicus.*

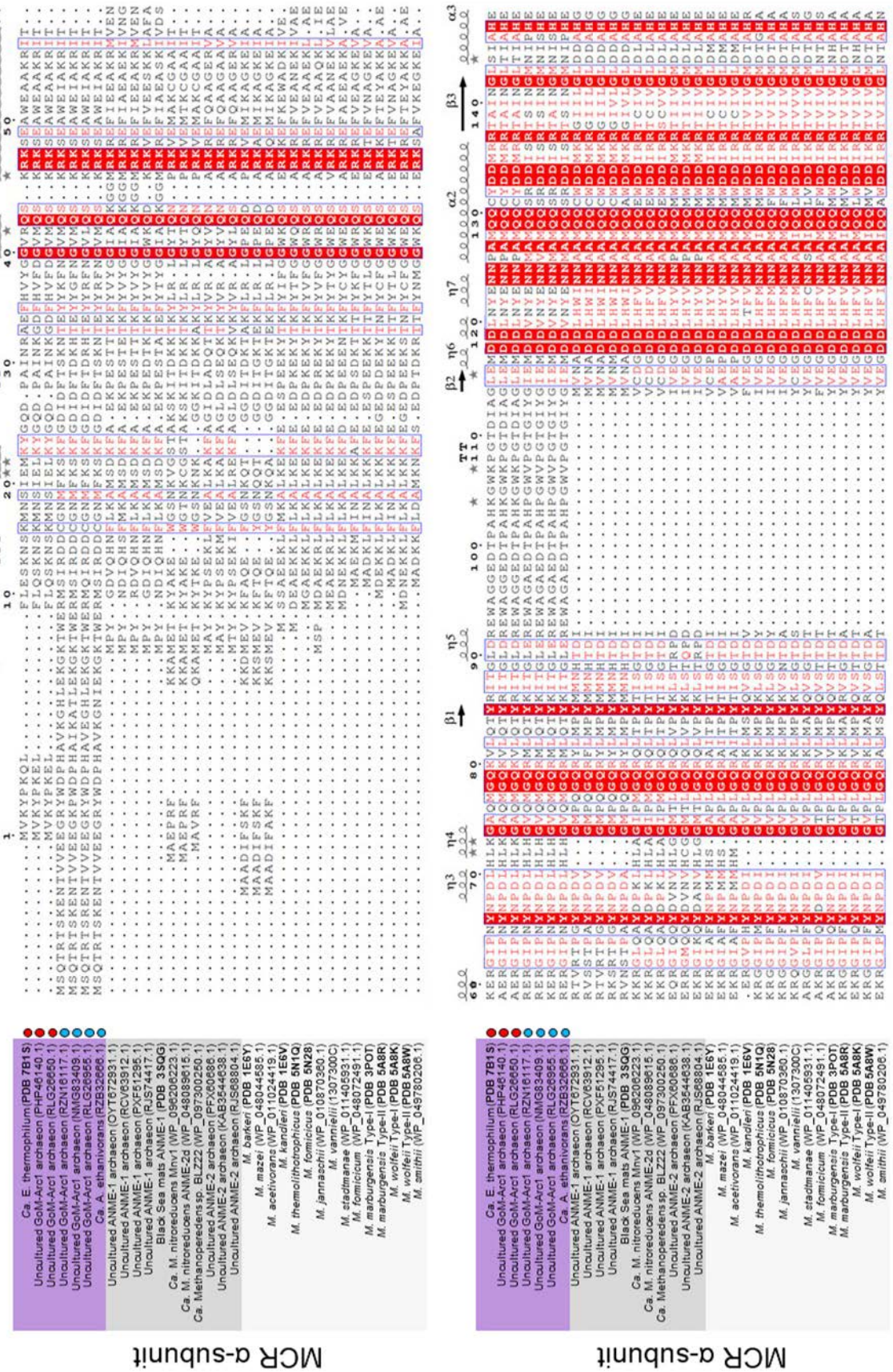
MCR α-subunit
MCR α-subunit

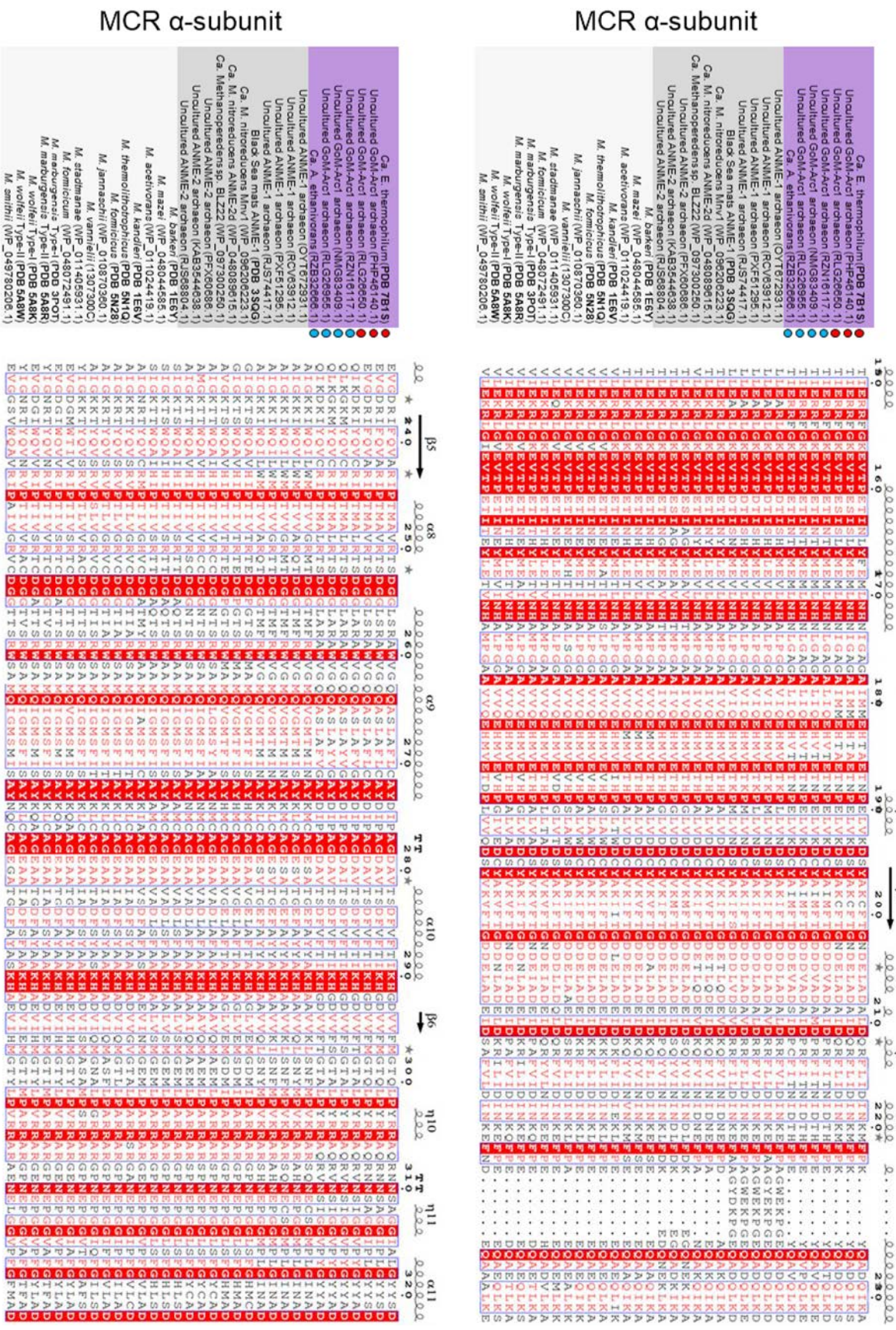
MCR α-subunit
Ca_E_thermophilum (PDB 7B1S)
Uncultured GoM-Arc1 archaeon (PHP48140.1)
Uncultured GoM-Arc1 archaeon (RLG26850.1)
Uncultured GoM-Arc1 archaeon (RZN16117.1)
Uncultured GoM-Arc1 archaeon (NMG83409.1)
Ca. A. ethanivorans (RZB32666.1)
Uncultured ANME-1 archaeon (OYT67293.1)
Uncultured ANME-1 archaeon (RCV83912.1)
Uncultured ANME-1 archaeon (PXF51295.1)
Uncultured ANME-1 archaeon (RJS74417.1)
Black Sea mats ANME-1 (PDB 3SQG)
Ca. M. nitroreducens ANME-2d (WP_048089615.1)
Ca. Methanoperedens sp. BLZ22 (WP_097300250.1)
Uncultured ANME-2 archaeon (PFX60686.1)
Uncultured ANME-2 archaeon (KAB3544638.1)
Uncultured ANME-2 archaeon (RJS88804.1)
M. barkeri (PDB 1E6Y)
M. mazei (WP_048044585.1)
M. acetivorans (WP_011024419.1)
M. kandleri (PDB 1E6V)
M. thermolithotrophicus (PDB 5N1Q)
M. formicicus (PDB 5N2B)
M. jannaschii (WP_010870360.1)
M. vannielii (1307300C)
M. stadtmanae (WP_011405931.1)
M. formicicum (WP_048072491.1)
M. marburgensis Type-I (PDB 3POT)
M. marburgensis Type-II (PDB 5A8R)
M. wolfeii Type-I (PDB 5A8K)
M. wolfeii Type-II (PDB 5A8W)
M. smithii (WP_049780206.1)
α4
α5
α6
α7
α8
α9
α10
α11
β4
β5
β6
η8
η9
η10
η11
TT
MCR α-subunit
Ca_E_thermophilum (PDB 7B1S)
Uncultured GoM-Arc1 archaeon (PHP48140.1)
Uncultured GoM-Arc1 archaeon (RLG26850.1)
Uncultured GoM-Arc1 archaeon (RZN16117.1)
Uncultured GoM-Arc1 archaeon (NMG83409.1)
Ca. A. ethanivorans (RZB32666.1)
Uncultured ANME-1 archaeon (OYT67293.1)
Uncultured ANME-1 archaeon (RCV83912.1)
Uncultured ANME-1 archaeon (PXF51295.1)
Uncultured ANME-1 archaeon (RJS74417.1)
Black Sea mats ANME-1 (PDB 3SQG)
Ca. M. nitroreducens ANME-2d (WP_048089615.1)
Ca. Methanoperedens sp. BLZ22 (WP_097300250.1)
Uncultured ANME-2 archaeon (PFX60686.1)
Uncultured ANME-2 archaeon (KAB3544638.1)
Uncultured ANME-2 archaeon (RJS88804.1)
M. barkeri (PDB 1E6Y)
M. mazei (WP_048044585.1)
M. acetivorans (WP_011024419.1)
M. kandleri (PDB 1E6V)
M. thermolithotrophicus (PDB 5N1Q)
M. formicicus (PDB 5N2B)
M. jannaschii (WP_010870360.1)
M. vannielii (1307300C)
M. stadtmanae (WP_011405931.1)
M. formicicum (WP_048072491.1)
M. marburgensis Type-I (PDB 3POT)
M. marburgensis Type-II (PDB 5A8R)
M. wolfeii Type-I (PDB 5A8K)
M. wolfeii Type-II (PDB 5A8W)
M. smithii (WP_049780206.1)
α4
α5
α6
α7
α8
α9
α10
α11
β4
β5
β6
η8
η9
η10
η11
TT

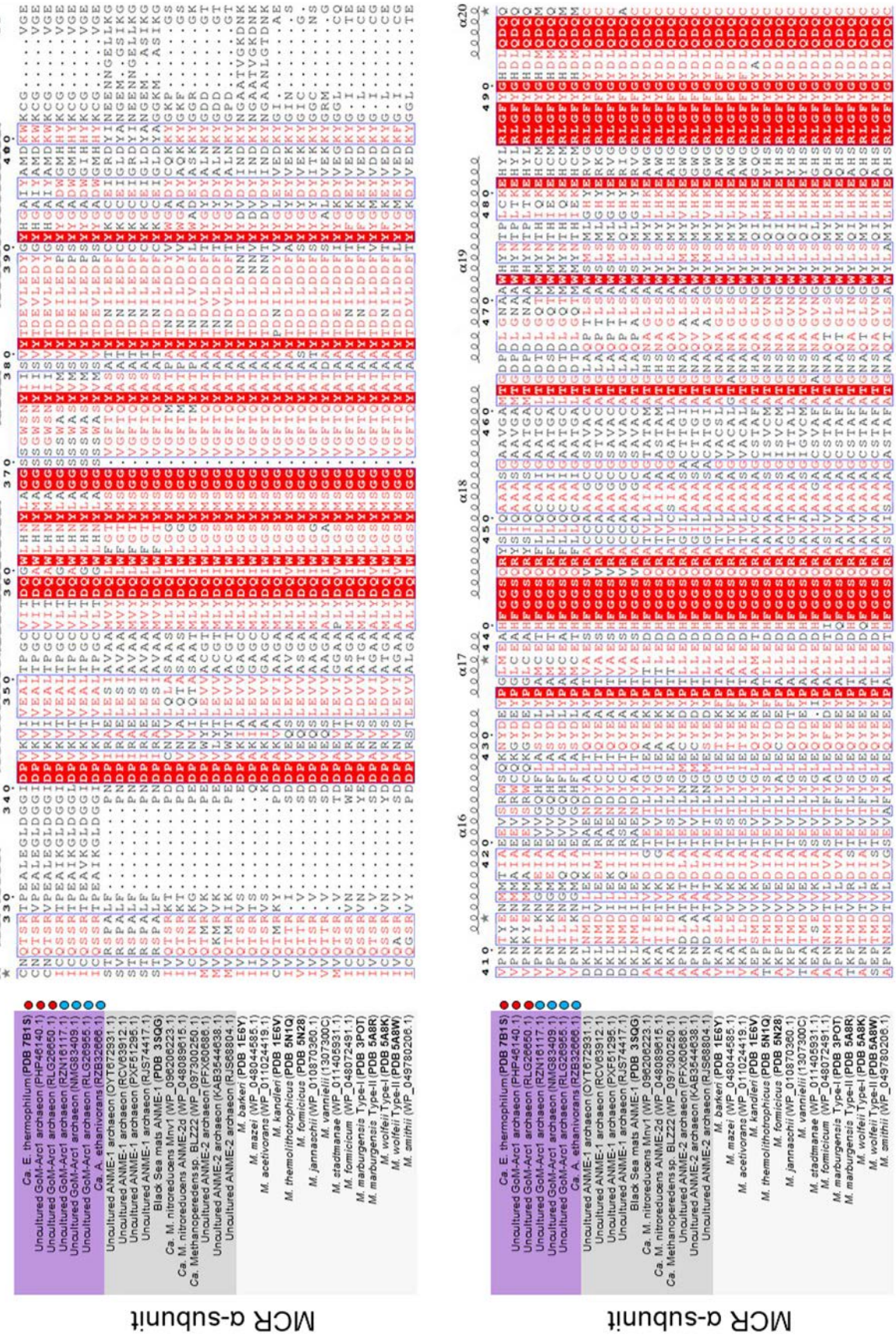
MCR α-subunit
MCR α-subunit
Ca. E. thermophilum (PDB 7B1S)
Uncultured GoM-Arc1 archaeon (PHP46140.1)
Uncultured GoM-Arc1 archaeon (RLG26650.1)
Uncultured GoM-Arc1 archaeon (RZN16117.1)
Uncultured GoM-Arc1 archaeon (NMG83409.1)
Uncultured GoM-Arc1 archaeon (RLG26955.1)
Ca. A. ethanivorans (RZB32666.1)
Uncultured ANME-1 archaeon (OYT67293.1)
Uncultured ANME-1 archaeon (ROV83912.1)
Uncultured ANME-1 archaeon (PXF51295.1)
Uncultured ANME-1 archaeon (RJS74417.1)
Black Sea mats ANME-1 (PDB 3SQG)
Ca. M. nitroreducens Mnv1 (WP_096206223.1)
Ca. M. nitroreducens ANME-2d (WP_048089615.1)
Ca. Methanoperedens sp. BLZ2 (WP_097300250.1)
Uncultured ANME-2 archaeon (PFX80686.1)
Uncultured ANME-2 archaeon (KAB3544638.1)
Uncultured ANME-2 archaeon (RJS88804.1)
M. barkeri (PDB 1E6Y)
M. mazei (WP_048044585.1)
M. acetivorans (WP_011024419.1)
M. kandleri (PDB 1E6V)
M. thermolithotrophicus (PDB 5N1Q)
M. fonticicus (PDB 5N28)
M. jannaschii (WP_010870360.1)
M. vannielii (1307300C)
M. stadtmanae (WP_011405931.1)
M. fonticicum (WP_048072491.1)
M. marburgensis Type-I (PDB 3POT)
M. marburgensis Type-II (PDB 5A8R)
M. wolfeii Type-I (PDB 5A8K)
M. wolfeii Type-II (PDB 5A8W)
M. smithii (WP_049780206.1)


MCR α-subunit
Ca. E. thermophilum (PDB 7B1S)
Uncultured GoM-Arc1 archaeon (PHP46140.1)
Uncultured GoM-Arc1 archaeon (RLG26660.1)
Uncultured GoM-Arc1 archaeon (RZN16117.1)
Uncultured GoM-Arc1 archaeon (NMG83409.1)
Uncultured GoM-Arc1 archaeon (RLG26965.1)
Ca. A. ethanivorans (RZB32666.1)
Uncultured ANME-1 archaeon (OYT67293.1)
Uncultured ANME-1 archaeon (RCV63912.1)
Uncultured ANME-1 archaeon (PXF51295.1)
Uncultured ANME-1 archaeon (RJS74417.1)
Black Sea mats ANME-1 (PDB 3SQG)
Ca. M. nitroreducens Mnv1 (WP_096206223.1)
Ca. M. nitroreducens ANME-2d (WP_048089615.1)
Ca. Methanoperedens sp. BLZ22 (WP_097300250.1)
Uncultured ANME-2 archaeon (PFX60686.1)
Uncultured ANME-2 archaeon (KAB3544638.1)
M. barkeri (PDB 1E6Y)
M. mazei (WP_048044585.1)
M. acetivorans (WP_011024419.1)
M. kandleri (PDB 1E6V)
M. thermolithotrophicus (PDB 5N1Q)
M. formicicus (PDB 5N28)
M. jannaschii (WP_010870360.1)
M. vannielii (1307300C)
M. stadtmanae (WP_011405931.1)
M. formicicum (WP_048072491.1)
M. marburgensis Type-II (PDB 3POT)
M. marburgensis Type-I (PDB 5A8R)
M. wolfeii Type-I (PDB 5A8K)
M. wolfeii Type-II (PDB 5A8W)
M. smithii (WP_049780206.1)
η13
η14
α21
α22
α23
T-T
MCR α-subunit
Ca. E. thermophilum (PDB 7B1S)
Uncultured GoM-Arc1 archaeon (PHP46140.1)
Uncultured GoM-Arc1 archaeon (RLG26660.1)
Uncultured GoM-Arc1 archaeon (RZN16117.1)
Uncultured GoM-Arc1 archaeon (NMG83409.1)
Uncultured GoM-Arc1 archaeon (RLG26965.1)
Ca. A. ethanivorans (RZB32666.1)
Uncultured ANME-1 archaeon (OYT67293.1)
Uncultured ANME-1 archaeon (RCV63912.1)
Uncultured ANME-1 archaeon (PXF51295.1)
Uncultured ANME-1 archaeon (RJS74417.1)
Black Sea mats ANME-1 (PDB 3SQG)
Ca. M. nitroreducens Mnv1 (WP_096206223.1)
Ca. M. nitroreducens ANME-2d (WP_048089615.1)
Ca. Methanoperedens sp. BLZ22 (WP_097300250.1)
Uncultured ANME-2 archaeon (PFX60686.1)
Uncultured ANME-2 archaeon (KAB3544638.1)
M. barkeri (PDB 1E6Y)
M. mazei (WP_048044585.1)
M. acetivorans (WP_011024419.1)
M. kandleri (PDB 1E6V)
M. thermolithotrophicus (PDB 5N1Q)
M. formicicus (PDB 5N28)
M. jannaschii (WP_010870360.1)
M. vannielii (1307300C)
M. stadtmanae (WP_011405931.1)
M. formicicum (WP_048072491.1)
M. marburgensis Type-II (PDB 3POT)
M. marburgensis Type-I (PDB 5A8R)
M. wolfeii Type-I (PDB 5A8K)
M. wolfeii Type-II (PDB 5A8W)
M. smithii (WP_049780206.1)
η15

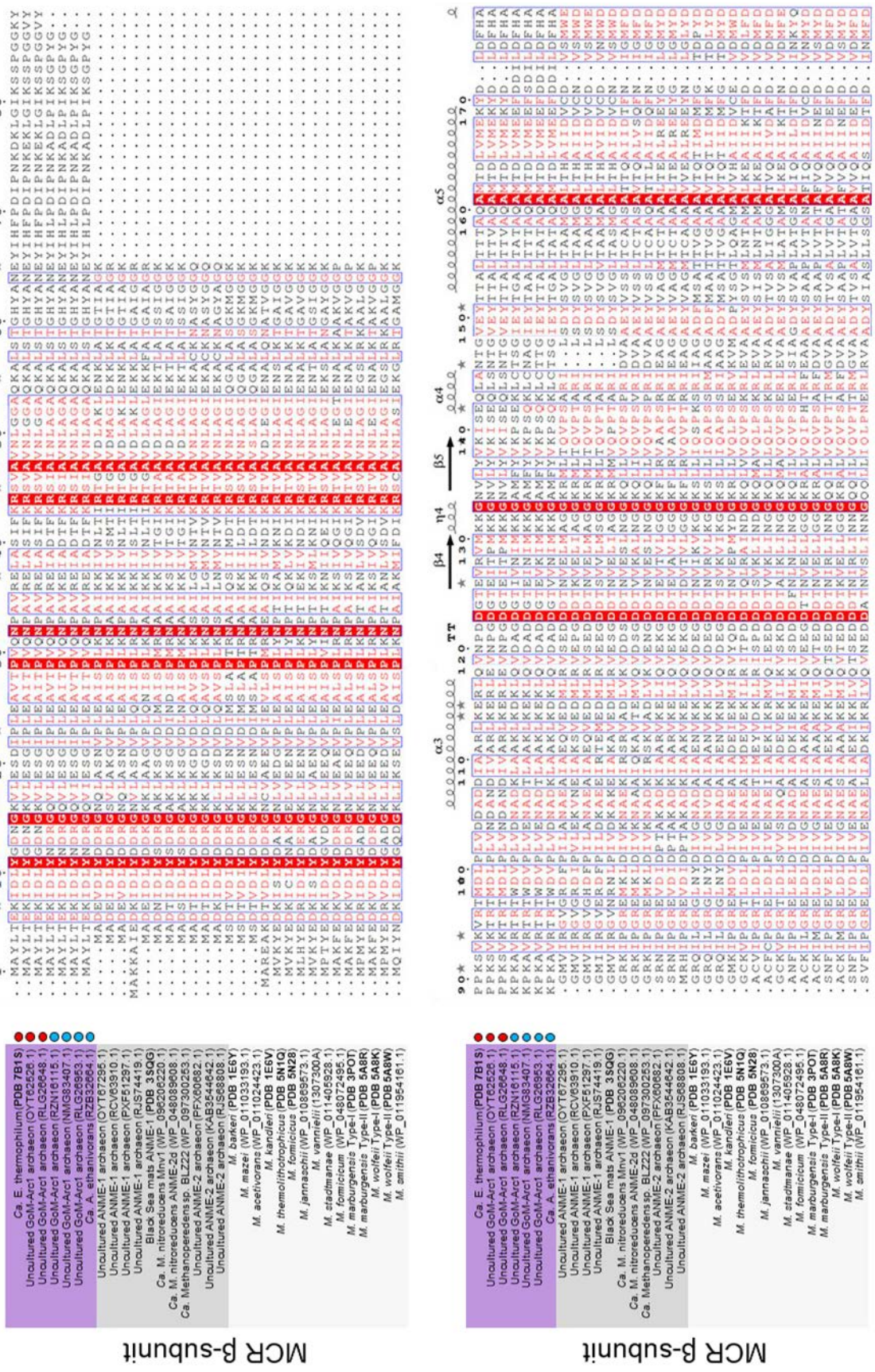
MCR β-subunit
MCR β-subunit

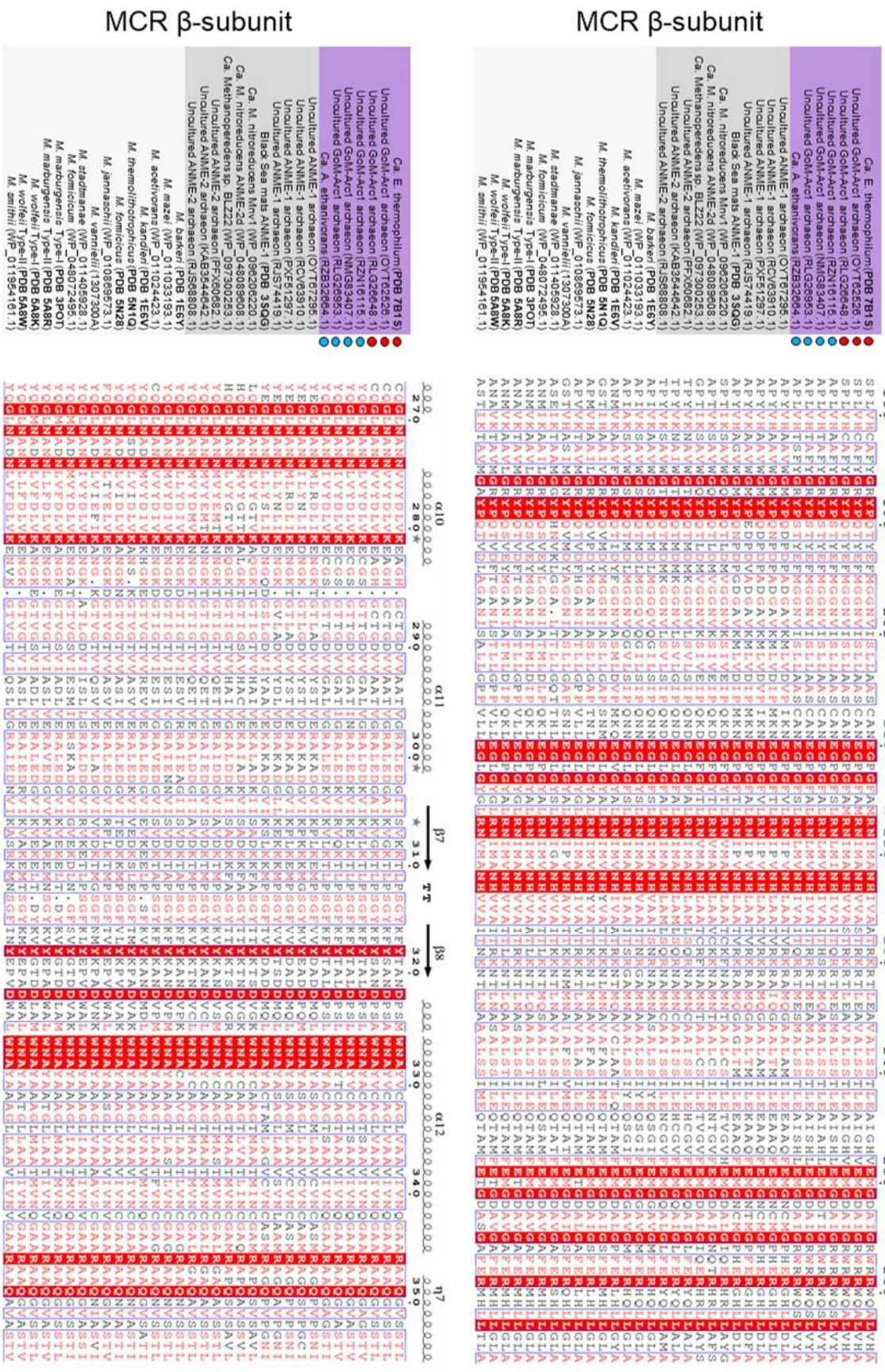
MCR β-subunit
MCR β-subunit
Ca. E. thermophilum (PDB 7B1S)
Uncultured GoM-Arc1 archaeon (OYT62526.1)
Uncultured GoM-Arc1 archaeon (RLG26848.1)
Uncultured GoM-Arc1 archaeon (RZN16115.1)
Uncultured GoM-Arc1 archaeon (RLG26953.1)
Ca. A. ethanivorans (RZB32664.1)
Uncultured ANME-1 archaeon (OYT67295.1)
Uncultured ANME-1 archaeon (RCV63910.1)
Uncultured ANME-1 archaeon (PXF51297.1)
Black Sea mats ANME-1 (PDB 3SQG)
Ca. M. nitroreducens ANME-2d (WP_048089808.1)
Ca. Methanoperedens sp. BLZ22 (WP_097300253.1)
Uncultured ANME-2 archaeon (PFX60682.1)
Uncultured ANME-2 archaeon (RJS68808.1)
M. barkeri (PDB 1E6Y)
M. mazei (WP_011033193.1)
M. acetivorans (WP_011024423.1)
M. kandleri (PDB 1E6V)
M. thermolithotrophicus (PDB 5N1Q)
M. fomicicus (PDB 5N28)
M. jannaschii (WP_010869573.1)
M. vannielii (1307300A)
M. stadtmanae (WP_011405928.1)
M. fomicicum (WP_048072495.1)
M. marburgensis Type-II (PDB 3POT)
M. wolfeii Type-I (PDB 5A8K)
M. wolfeii Type-II (PDB 5A8W)
M. smithii (WP_011954161.1)

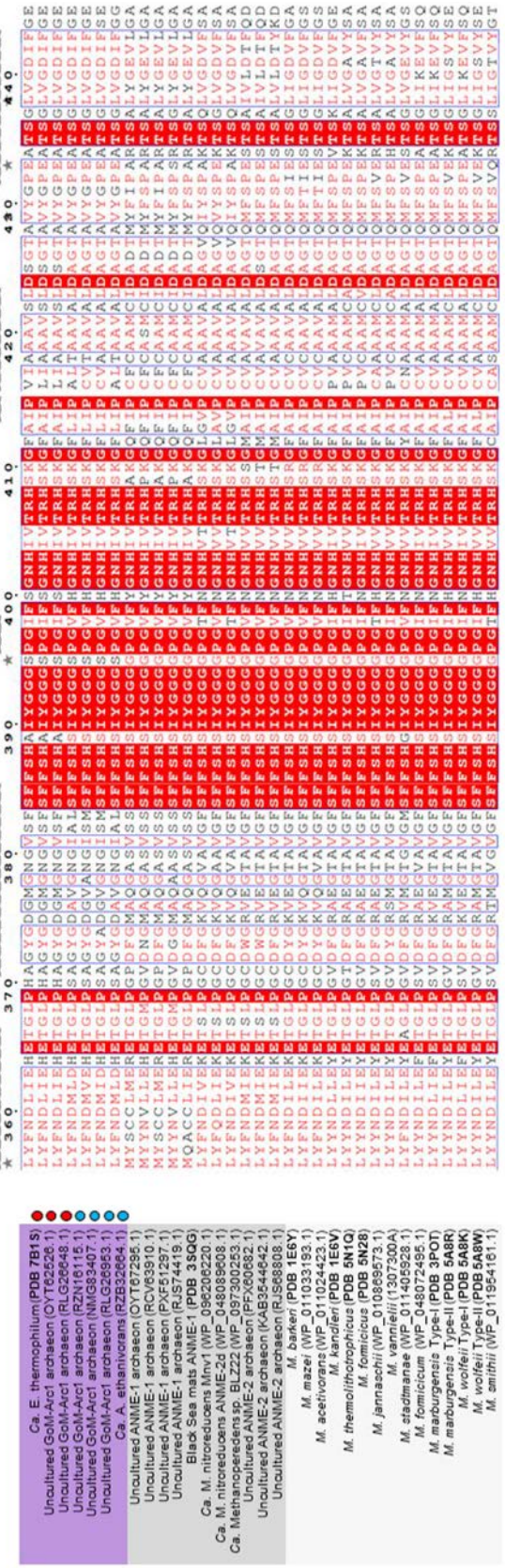
MCR β-subunit
Ca. E. thermophilum (PDB 7B1S)
Uncultured GoM-Arc1 archaeon (OYT62526.1)
Uncultured GoM-Arc1 archaeon (RLG26648.1)
Uncultured GoM-Arc1 archaeon (RZN16115.1)
Uncultured GoM-Arc1 archaeon (NMG83407.1)
Uncultured GoM-Arc1 archaeon (RLG26953.1)
Ca. A. ethanivorans (RZB32864.1)
Uncultured ANME-1 archaeon (OYT67295.1)
Uncultured ANME-1 archaeon (RCV63910.1)
Uncultured ANME-1 archaeon (PXF51297.1)
Uncultured ANME-1 archaeon (RJS74419.1)
Black Sea mats ANME-1 (PDB 3SQG)
Ca. M. nitroreducens Mnv1 (WP_096206220.1)
Ca. M. nitroreducens ANME-2d (WP_048089808.1)
Ca. Methanoperedens sp. BLZ22 (WP_097300253.1)
Uncultured ANME-2 archaeon (PFX60682.1)
Uncultured ANME-2 archaeon (KAB3544642.1)
Uncultured ANME-2 archaeon (RJS68808.1)
M. barkeri (PDB 1E6Y)
M. mazei (WP_011033193.1)
M. acetivorans (WP_011024423.1)
M. kandleri (PDB 1E6V)
M. thermolithotrophicus (PDB 5N1Q)
M. fomicicus (PDB 5N28)
M. jannaschii (WP_010869573.1)
M. vannielii (1307300A)
M. stadtmanae (WP_011405928.1)
M. fomicicum (WP_048072495.1)
M. marburgensis Type-I (PDB 3POT)
M. marburgensis Type-II (PDB 5A8R)
M. wolfeii Type-I (PDB 5A8K)
M. wolfeii Type-II (PDB 5A8W)
M. smithii (WP_011954161.1)
α13
α14
α15
α16
α17
α18
β8
β9
β10

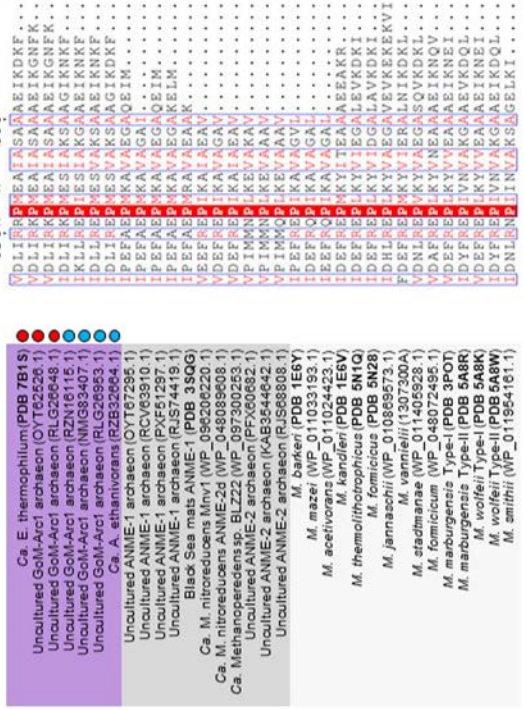
MCR β-subunit
Ca. E. thermophilum (PDB 7B1S)
Uncultured GoM-Arc1 archaeon (OYT62526.1)
Uncultured GoM-Arc1 archaeon (RLG26648.1)
Uncultured GoM-Arc1 archaeon (RZN16115.1)
Uncultured GoM-Arc1 archaeon (NMG83407.1)
Uncultured GoM-Arc1 archaeon (RLG26953.1)
Ca. A. ethanivorans (RZB32864.1)
Uncultured ANME-1 archaeon (OYT67295.1)
Uncultured ANME-1 archaeon (RCV63910.1)
Uncultured ANME-1 archaeon (PXF51297.1)
Uncultured ANME-1 archaeon (RJS74419.1)
Black Sea mats ANME-1 (PDB 3SQG)
Ca. M. nitroreducens Mnv1 (WP_096206220.1)
Ca. Methanoperedens sp. BLZ22 (WP_097300253.1)
Uncultured ANME-2 archaeon (PFX60682.1)
Uncultured ANME-2 archaeon (KAB3544642.1)
Uncultured ANME-2 archaeon (RJS68808.1)
M. barkeri (PDB 1E6Y)
M. mazei (WP_011033193.1)
M. acetivorans (WP_011024423.1)
M. kandleri (PDB 1E6V)
M. thermolithotrophicus (PDB 5N1Q)
M. fomicicus (PDB 5N28)
M. jannaschii (WP_010869573.1)
M. vannielii (1307300A)
M. stadtmanae (WP_011405928.1)
M. fomicicum (WP_048072495.1)
M. marburgensis Type-I (PDB 3POT)
M. marburgensis Type-II (PDB 5A8R)
M. wolfeii Type-I (PDB 5A8K)
M. wolfeii Type-II (PDB 5A8W)
M. smithii (WP_011954161.1)
α17
α18
β10

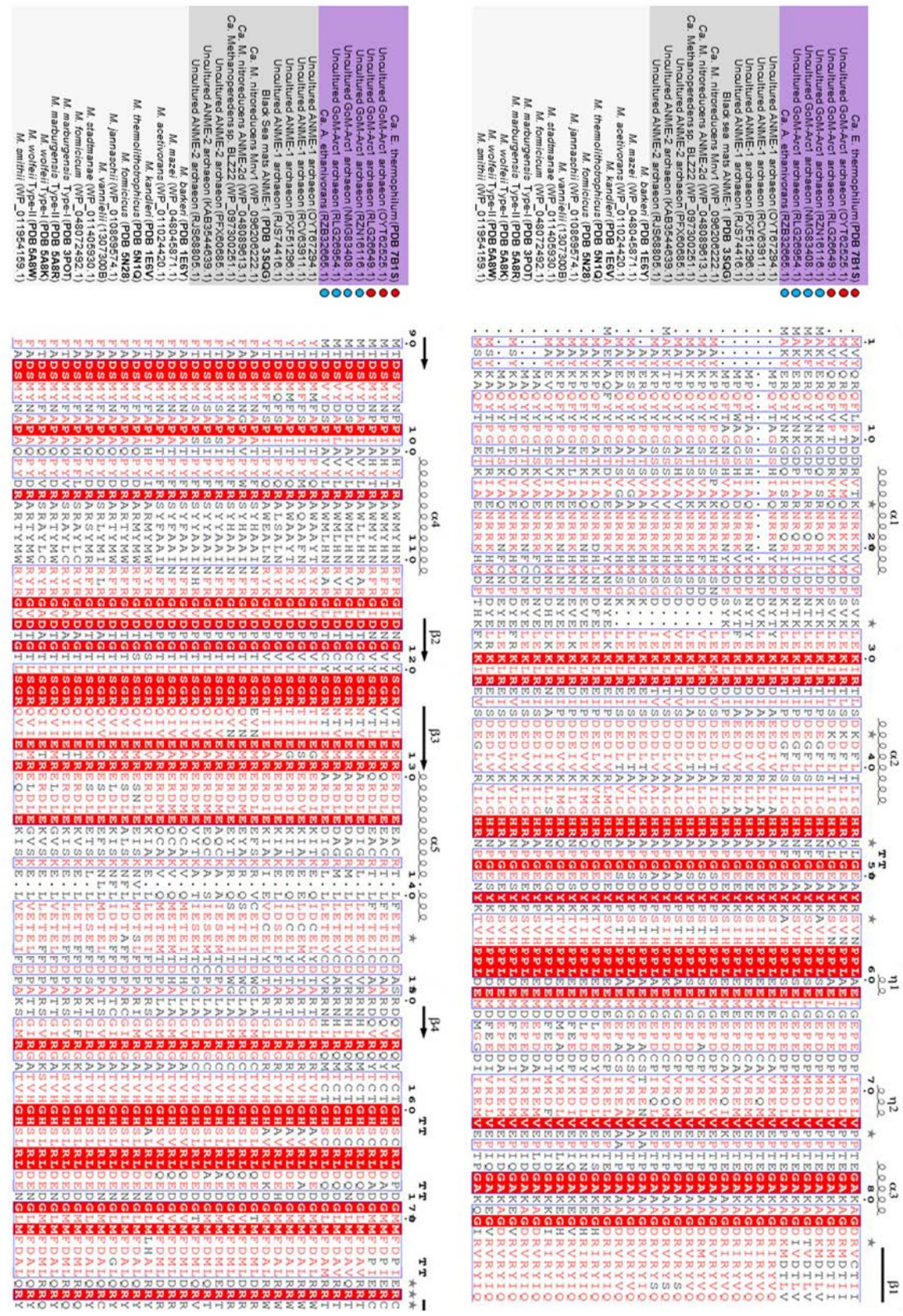
MCR γ-subunit
MCR γ-subunit

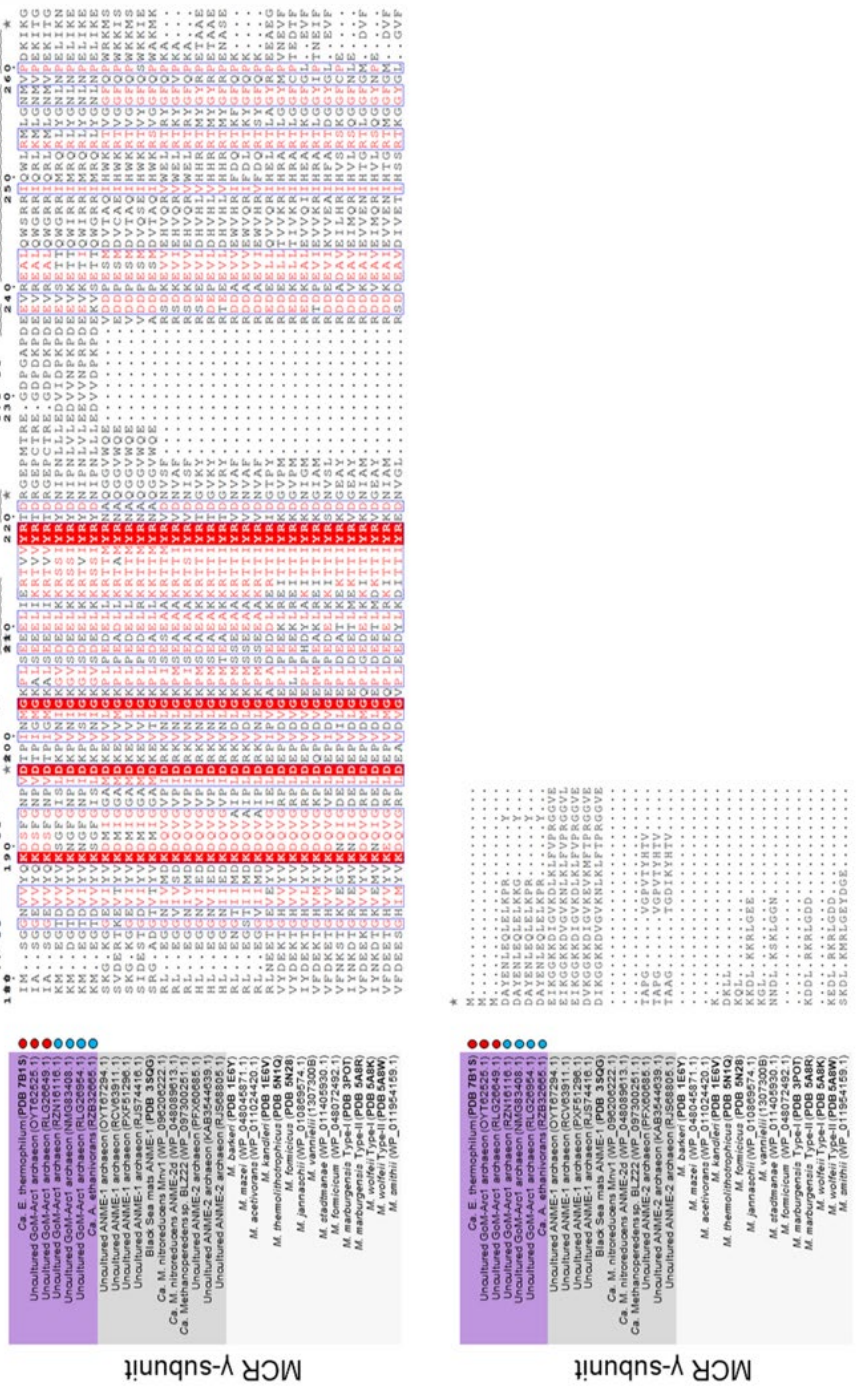

Figure S4-4 ESPript alignment of MCR from ethanotrophs (purple), methanotrophs (dark grey) and methanogens (light grey). Red and blue circles indicate sequences extracted from geothermally heated or cold environmental samples/cultures, respectively.

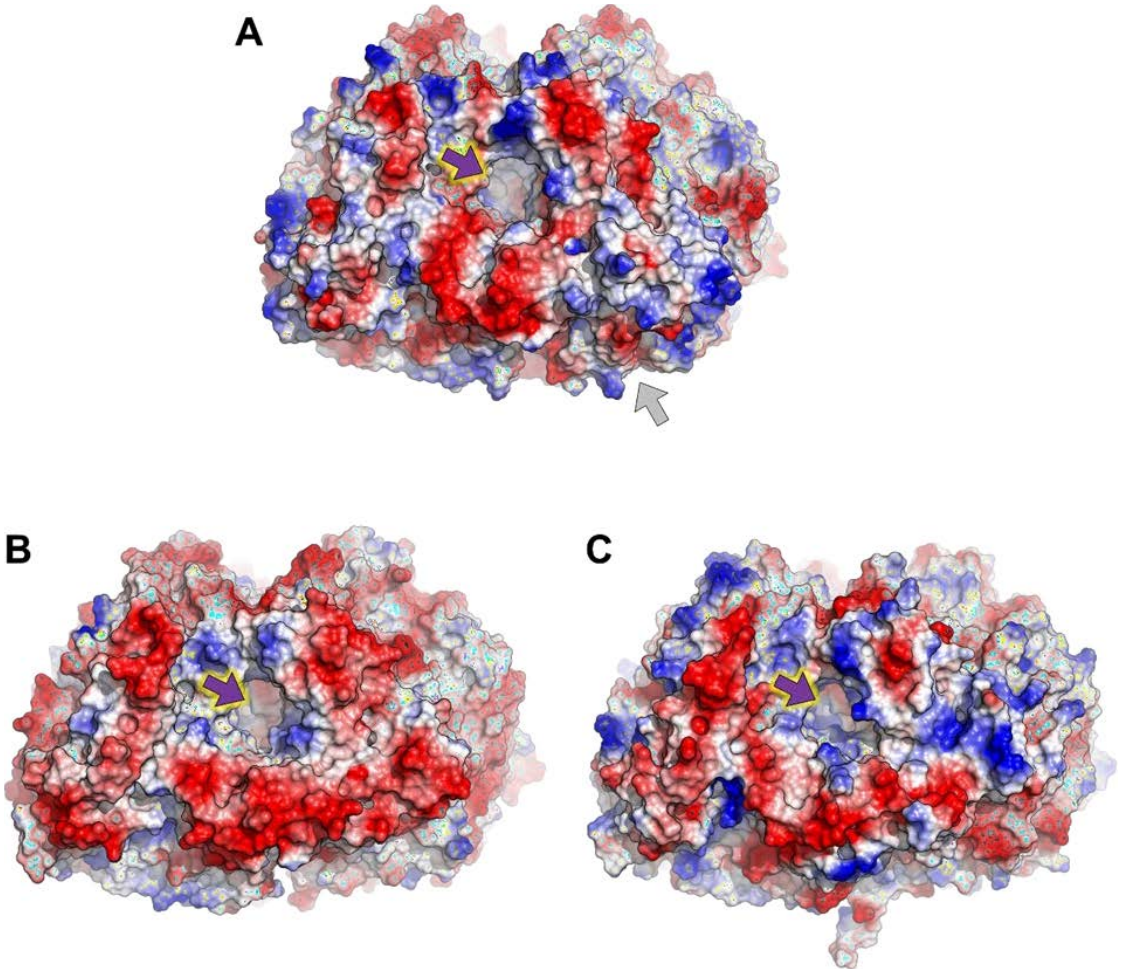

Figure S4-4 Distribution of surface charges in different structurally characterized MCRs. A, *Ca.* E. thermophilum (PDB: 7B1S), B, *M. marburgensis* (MCR type I, PDB: 5A0Y) and C, ANME-1 from Black Sea mats (PDB: 3SQG),are shown as surface. The color code from red to blue represents the electrostatic charges from negative to positive, respectively. The deep purple arrows indicate the entrance for HS-CoM and HS-CoB to the active site. The grey arrowpoints the additional loops of MCR from *Ca.* E. thermophilum.

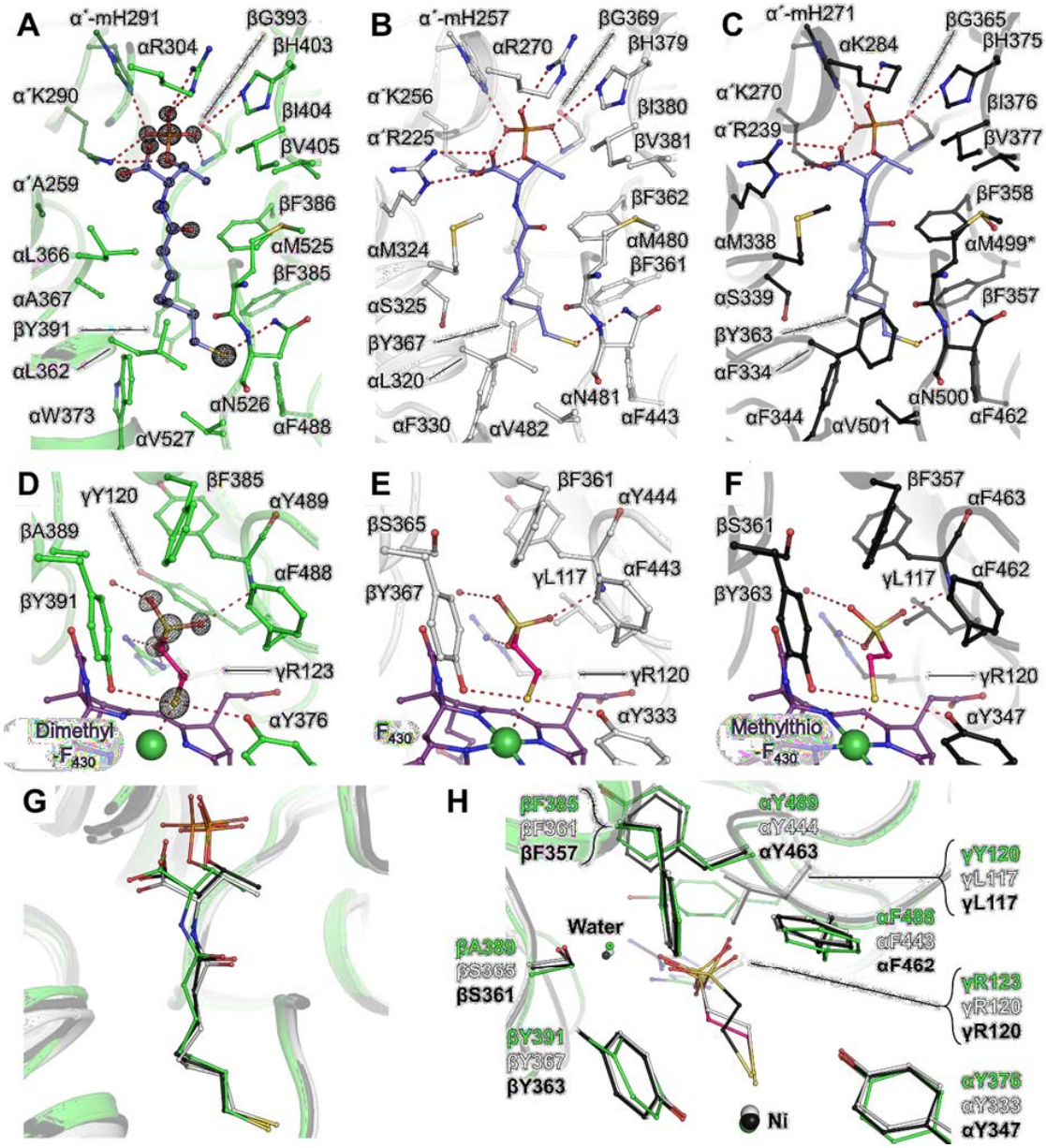

Figure S4-5 Coordination of HS-CoM and HS-CoB among different MCRs. Protein backbone is shown as a cartoon and residues providing hydrogen bonds (highlighted by red dashes) or van der Waals interactions with ligands are represented as balls and sticks. A-C, representation of HS-CoB binding site. D-F, HS-CoM binding site. Panels A and D correspond to *Ca.* E. thermophilum (green, PDB 7B1S), B and E to MCR type I from *M. marburgensis* (white, PDB 5A0Y) and C and F to MCR from ANME-1 Black Sea mats (black, PDB 3SQG). $2F_o$-F_c map for HS-CoB and HS-CoM are contoured at 6 σ in A and D and represented as a black mesh. Water network was omitted for clarity. In A-C, α´-mH291, α´-mH257, α´-mH271 and α-M499* corresponds to N^1-methylhistidine and methionine-sulfoxide, respectively. G and H, superposition at the HS-CoB (G) and HS-CoM (H) sites for the three previously mentioned models.

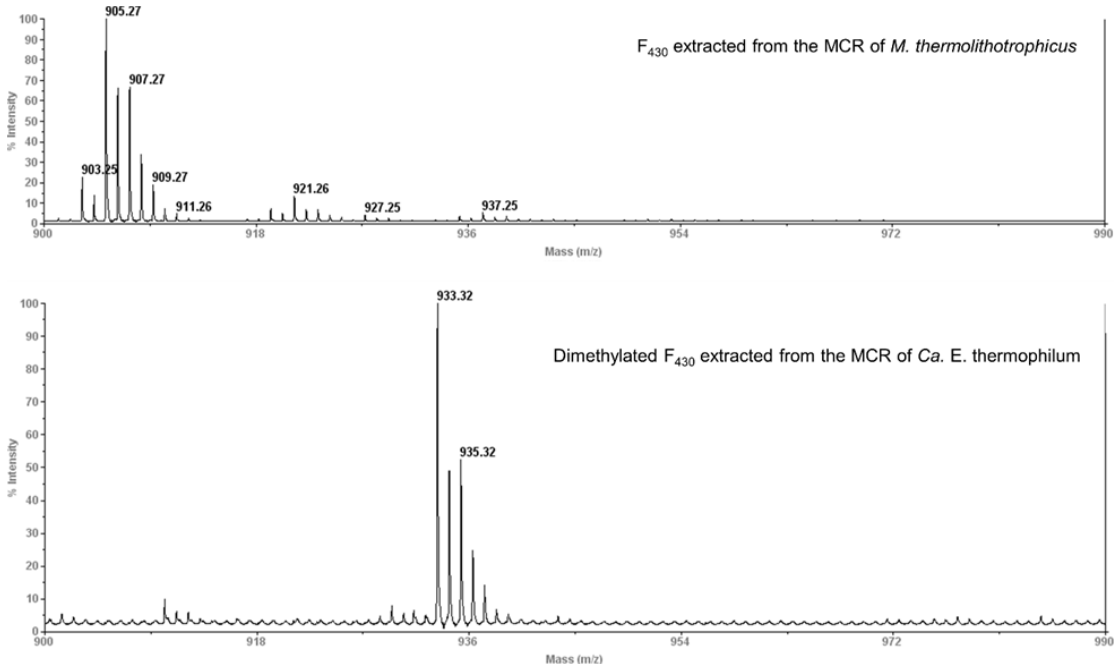

Figure S4-6 Mass spectrometry profiles of extracted F_{430}-cofactors. Top panel, Mass spectrometry spectrum of the F_{430} cofactor from the MCR of *M. thermolithotrophicus* (905.27 Da). Bottom panel, mass spectrometry spectrum of the dimethylated F_{430} cofactor from the MCR of *Ca.* E. thermophilum (933.32 Da).

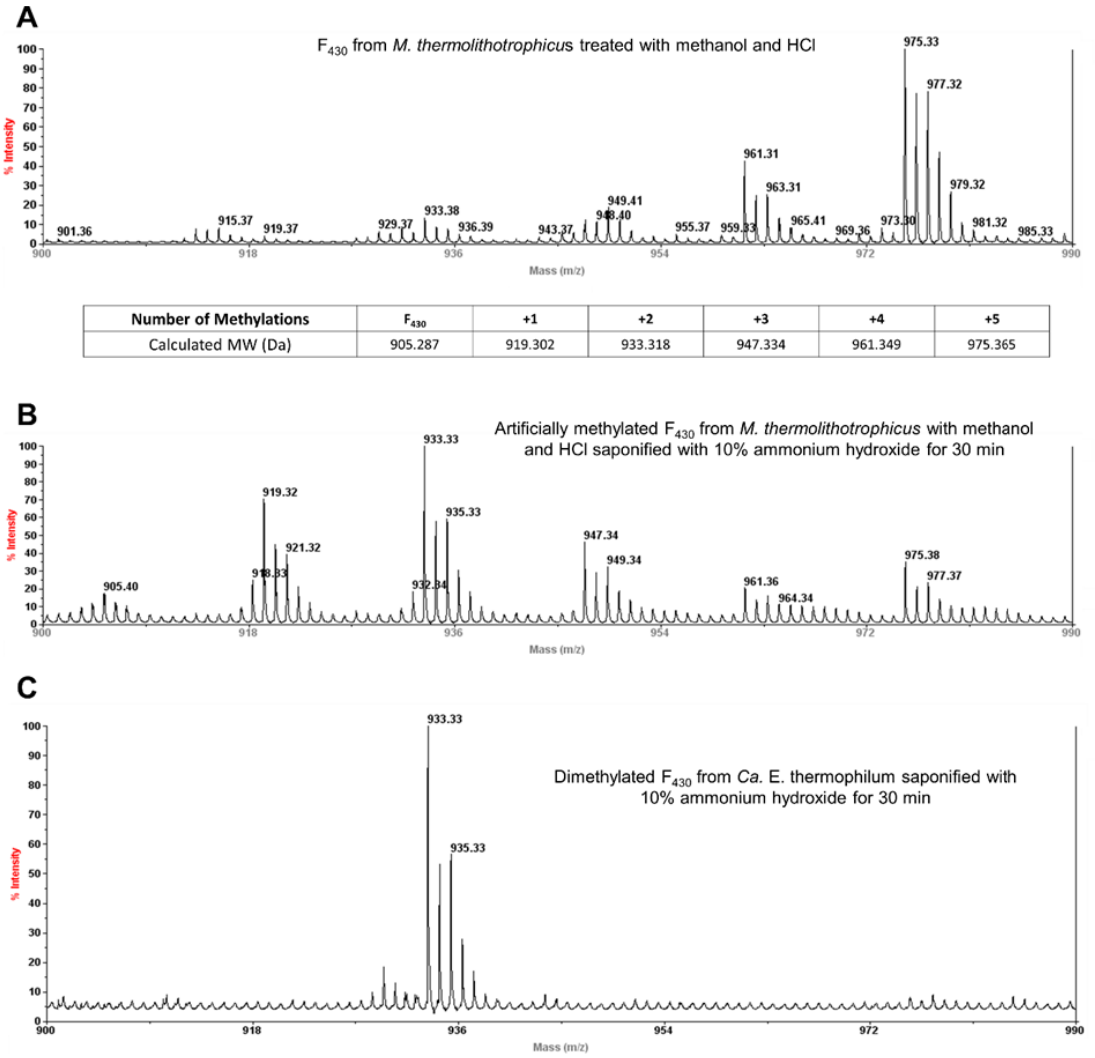

Number of Methylations	F_{430}	+1	+2	+3	+4	+5
Calculated MW (Da)	905.287	919.302	933.318	947.334	961.349	975.365

Figure S4-7 Confirmation of the dimethylation of the F_{430} in *Ca.* E. thermophilum by mass spectrometry. A, Mass spectrometry profile of the cofactor F_{430} from MCR of *M. thermolithotrophicus* artificially methylated with methanoland HCl (see materials and methods). A table indicating the predicted masses of methylated F_{430} is shown at the bottom. B, Saponification of the artificially methylated F_{430} by 10% ammonium hydroxide treatment for 30 min. The unmethylated product at 905 Da is observed. C, The dimethylated F_{430} from *Ca.* E. thermophilum was saponified by 10% ammonium hydroxide treatment for 30 min. No unmethylated product at 905 Da can be observed, proving that methylations are not coming from esterification.

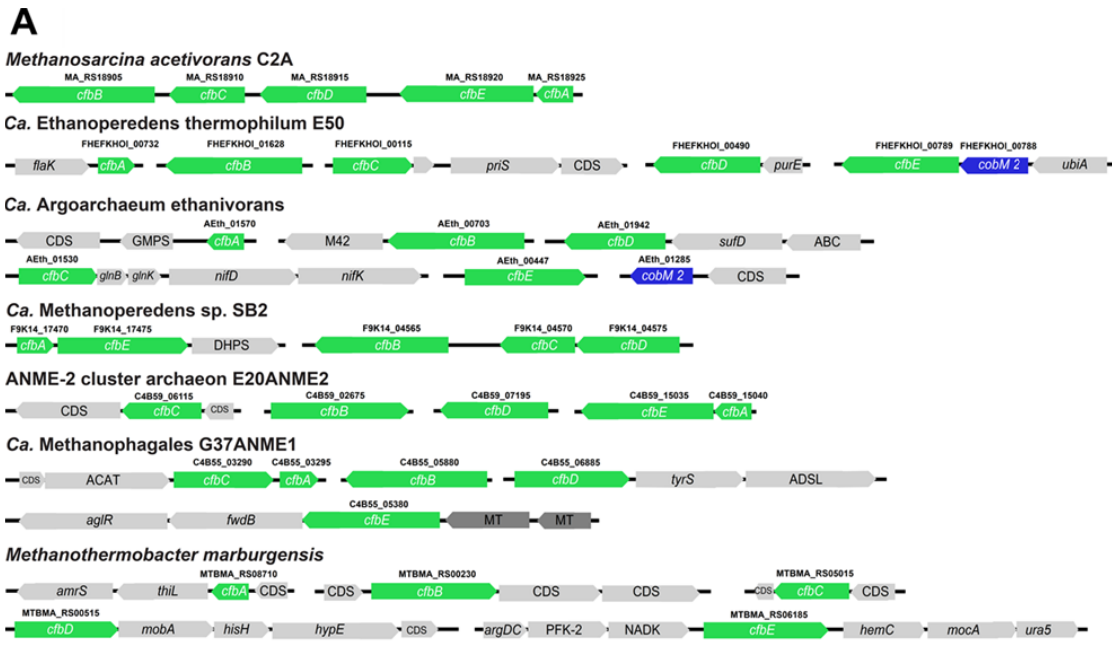

	CfbA	CfbB	CfbC	CfbD	CfbE
M. acetivorans C2A	100	100	100	100	100
Ca. E. thermophilum E50	50.8	55.8	47.9	60.0	35.1
Ca. A. ethanivorans	56.7	57.8	48.3	56.3	33.8
Ca. Methanoperedens sp. SB2	60.3	65.6	71.7	71.2	46.1
ANME-2 cluster archaeon E20ANME2	54.4	60.0	67.7	67.8	38.9
Ca. Methanophagales G37ANME1	43.0	48.0	41.8	53.1	28.2
M. marburgensis	44.4	43.8	50.2	46.8	29.6

Figure S 4-8 Analysis of gene clusters coding for F_{430} biosynthesis in different archaea. A, Upper panel: Operon coding for major elements of the biosynthesis of F_{430}-biosynthesis (cfb) in M. acetivorans C2A. Other panels: Operons with homologous genes indicated in green. Genes coding for putative CobM 2 methyltransferases are indicated in blue. Genes unrelated to F_{430} biosynthesis and methyltransferases unrelated to CobM are shown in light and dark grey, respectively. Locus tags are written above genes. B, Amino acid sequence identity compared to Cfb proteins from *M. acetivorans* C2A. C, Phylogenetic tree of CobM-related methyltransferases. Ethanotrophs encode in their genome two copies of the gene coding for the CobM methyltransferase. One of these homologues forms a distinct branch (colored in dark blue) of the CobM phylogenetic tree (colored in light blue) and was named CobM 2. Sequences of CobI, CobJ and CobA were used as outgroups for tree construction. For clarity, only CobA branch is indicated, an arrow indicates the CobJ/CobI branch. An asterisk indicates that in this taxonomic group, sequences branch in two separate parts of the phylogenetic tree, albeit only one sequence is found per organism. Scale bar represents the number of amino acid substitutions per site and black circle represents bootstrap values of over 90%.

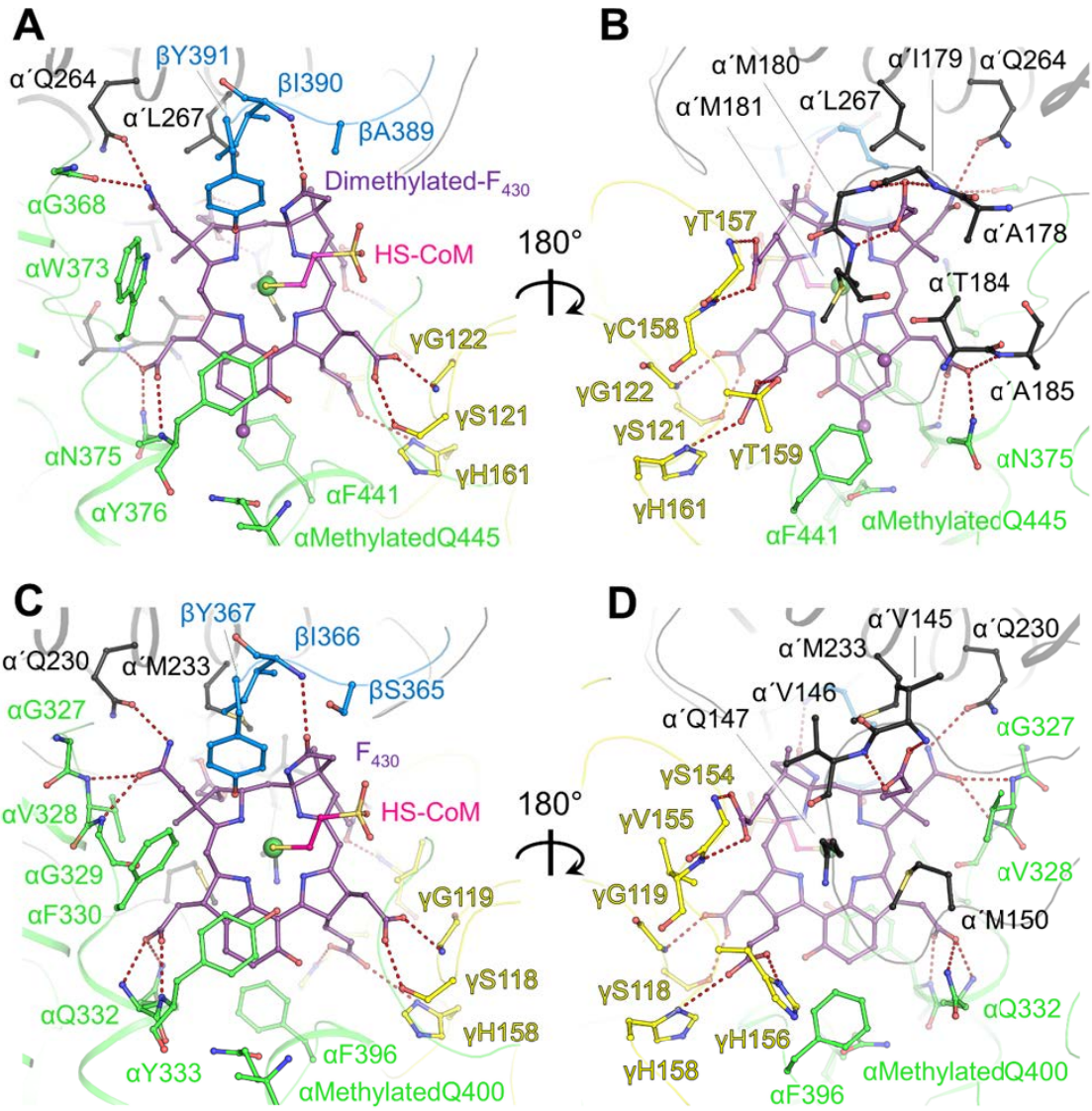

Figure S4-9 Coordination of the F_{430}-cofactor in different MCR enzymes. For all panels, the protein is shown as transparent cartoon. F_{430}, dimethylated-F_{430}, HS-CoM and residues involved in hydrogen bonds (represented as red dashed lines) and close van der Waals contacts are shown as balls and sticks. The dark green sphere represents the nickel atom. Extra methylations of *Ca.* E. thermophilum F_{430} are highlighted as spheres. Water network was omitted for clarity. A, Top view of *Ca.* E. thermophilum (PDB 7B1S). B, Bottom view of *Ca.* E. thermophilum. C, Top viewof MCR type I from *M. marburgensis* (PDB 5A0Y). D, Bottom view of MCR type I from *M. marburgensis*.

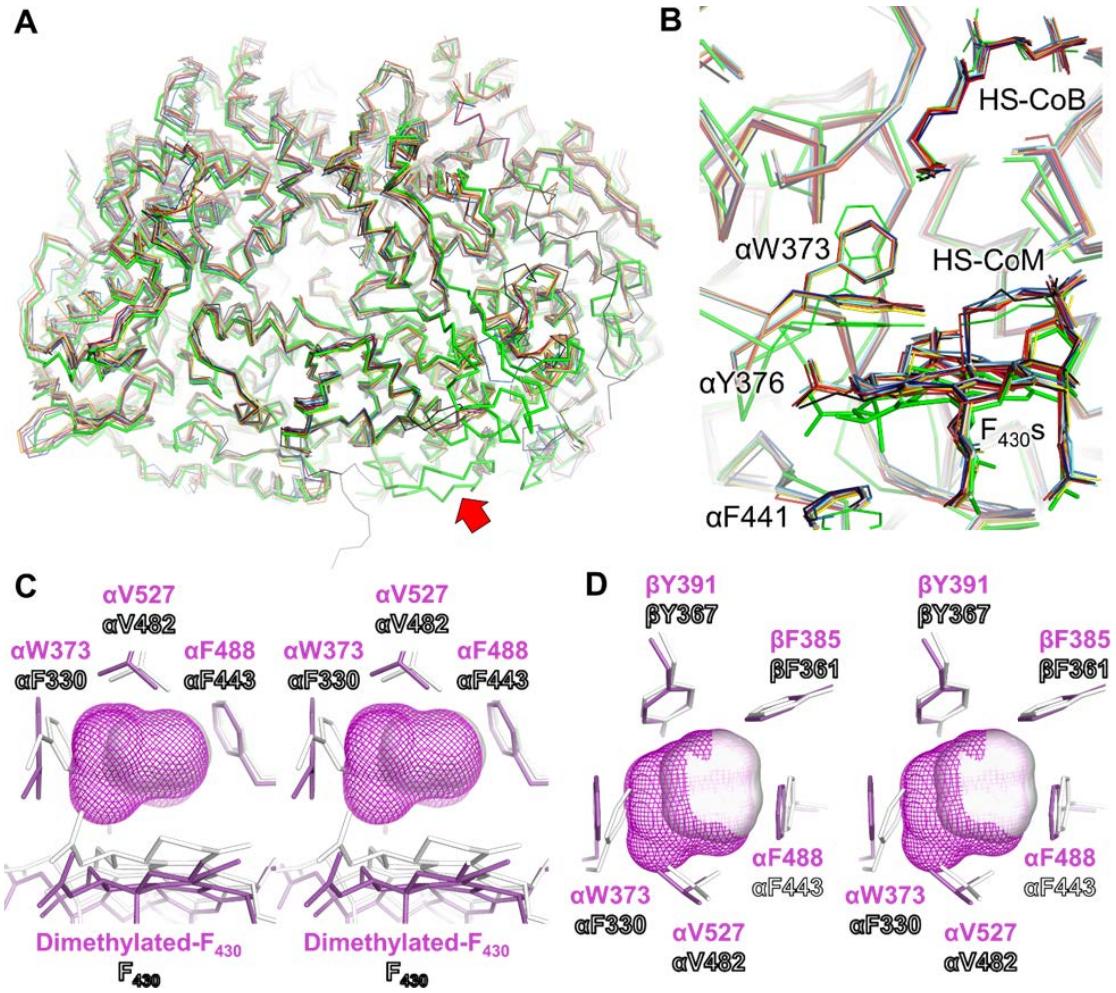

Figure S4-10 Superposition of the MCR structures and catalytic cavity differences. A, Ribbon representation of the overall superposition of MCRs structures on the α-subunit. A purple arrow points to the extensions contained in *Ca.* E. thermophilum enzyme. B, Close up of the active site, with the F_{430} cofactors, HS-CoB, HS-CoM, αTrp373, αTyr376 and αPhe441 of *Ca.* E. thermophilum and their analogous position in other MCRs are shown in sticks. Green,*Ca.* E. thermophilum (PDB 7B1S); Dark red, *Methanopyrus kandleri* (PDB 1E6V); Blue, *M. barkeri* (PDB 1E6Y), Yellow, MCR type I product complex *M. marburgensis* (PDB 1HBM); Black, ANME-1 Black Sea mats (PDB 3SQG);White, MCR type I *M. marburgensis* (PDB 5A0Y); Red, MCR type II *M. marburgensis* (PDB 5A8R); Pink, MCR type I *Methanothermobacter wolfeii* (PDB 5A8K); Dark blue, MCR type II *Methanothermobacter wolfeii* (PDB 5A8W); Orange, MCR *M. thermolithotrophicus* (PDB 5N1Q), Cyan, MCR *Methanotorris formicicus* (PDB 5N28). C, D, Stereo view of comparison of the catalytic cavity volume between MCR type I from *M. marburgensis* (white surface, PDB 5A0Y) and *Ca.* E. thermophilum (purple mesh). Surrounding residues are shown as sticks. A 180° rotation along the Y-axis differentiates orientation of panel C and D.

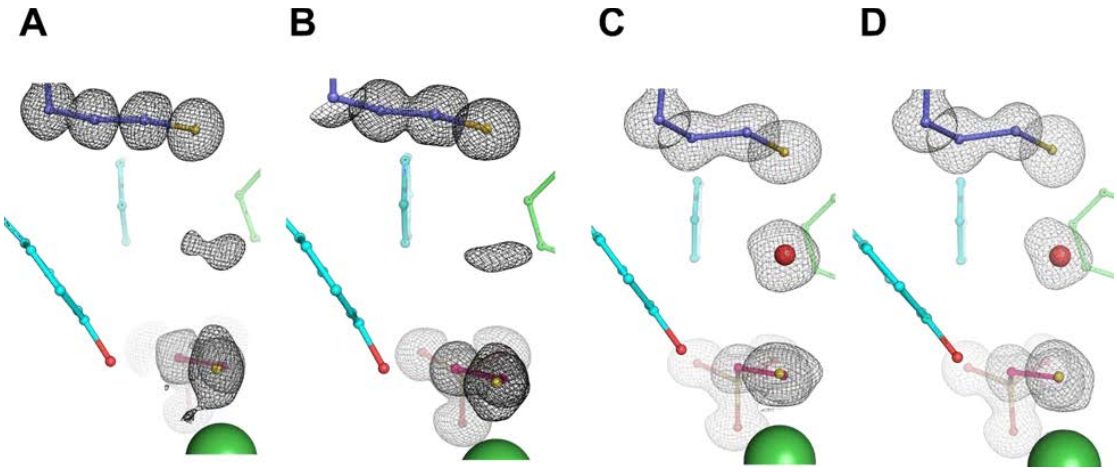

Figure S4-11 Electron density between coenzymes in the catalytic center of MCRs. A and B, Elongated electron density in the *Ca.* E. thermophilum MCR active site 1 (A) and 2 (B). Modelled water molecule in the *M. marburgensis* MCR type I active site 1 (C) and 2 (D) (PDB 5A0Y). $2F_o$-F_c maps are contoured at 1 σ and shown as a black mesh. Tyr391 in *Ca.* E. thermophilum MCR is out of planarity compared to the Tyr367 of MCR type I from M. marburgensis. Tyrosine, HS-CoM, HS-CoB and water molecules are shown as balls and sticks with the carbon colored as cyan, pink, light purple and red, respectively. Oxygen and sulfur atoms in the coenzymes and residues are colored in red and yellow, respectively. The green sphere represents the F_{430} Ni atom.

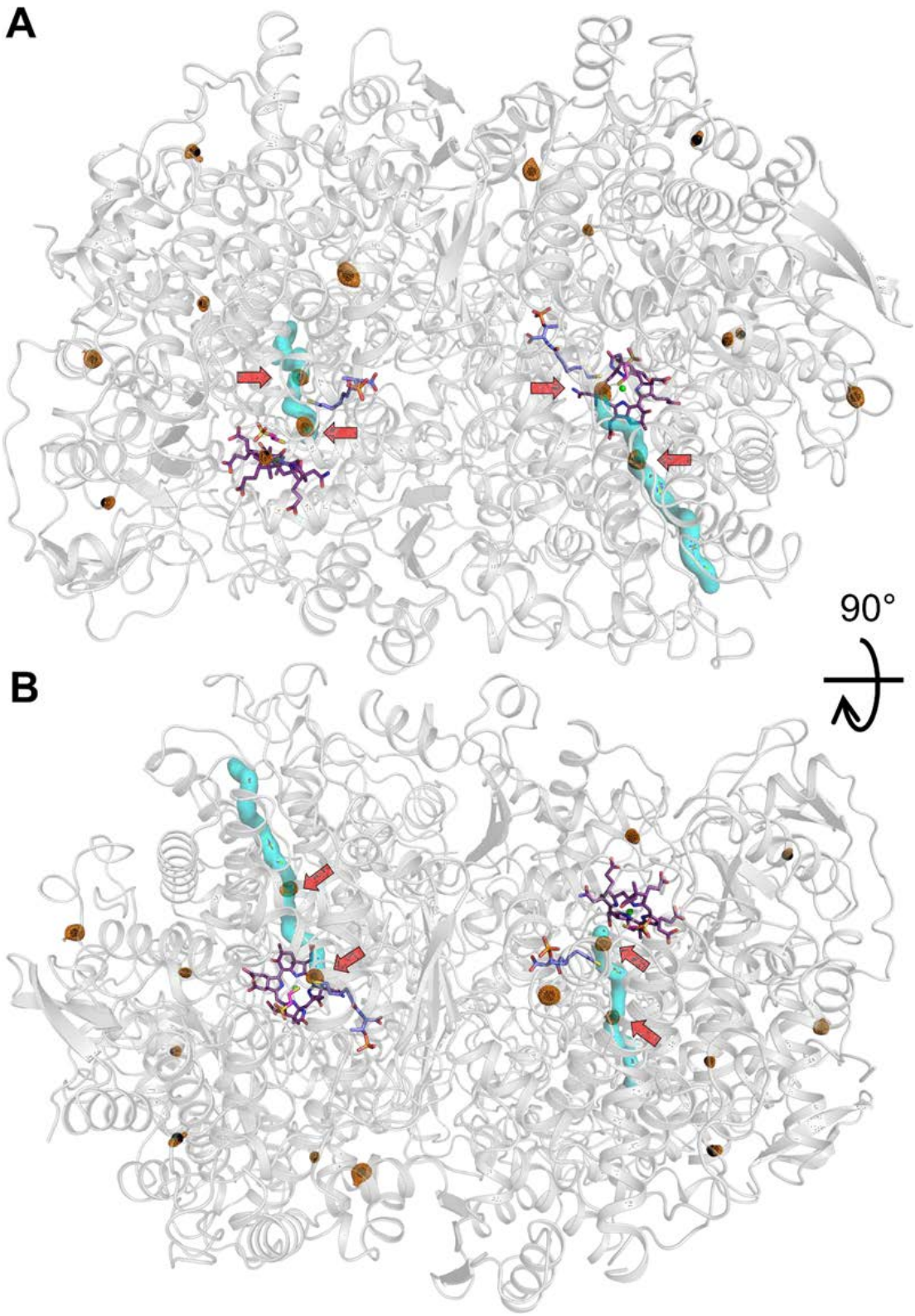

Figure S4-12 Xe positions in *Ca.* E. thermophilum. MCR from *Ca.* E. thermophilum (PDB 7B2C) is shown as transparent cartoon. Dimethylated-F_{430}, HS-CoM, HS-CoB and Xe are shown as balls and sticks and colored as purple,pink, light purple and black, respectively. The anomalous map was contoured at 4 σ at the Xe sites and represented byan orange mesh. Panels A and B, differ by a rotation of 90° along the X-axis. Red arrows point at the Xe atoms locatedin the gas tunnels of the enzyme, shown as a cyan surface.

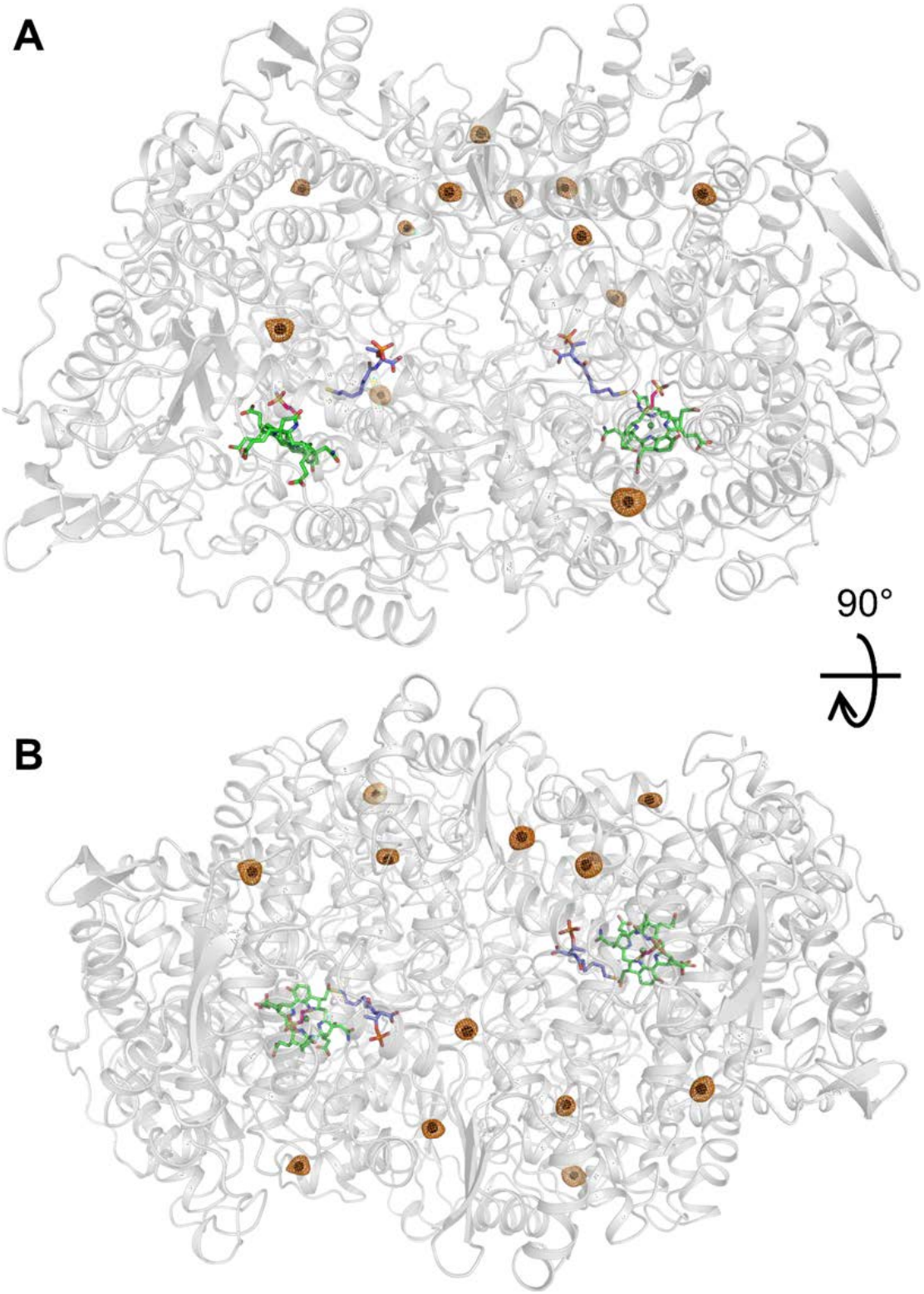

Figure S4-13 Xe positions in MCR type I from *M. marburgensis*. MCR type I from *M. marburgensis* (PDB 7B2H) is shown as transparent cartoon. F_{430}, HS-CoM, HS-CoB and Xe atoms are shown as balls and sticks and colored as green, pink, light purple and black, respectively. The anomalous map was contoured at 4 σ at the Xe sites and represented by an orange mesh. Panels A and B, differ by a rotation of 90° along the X-axis.

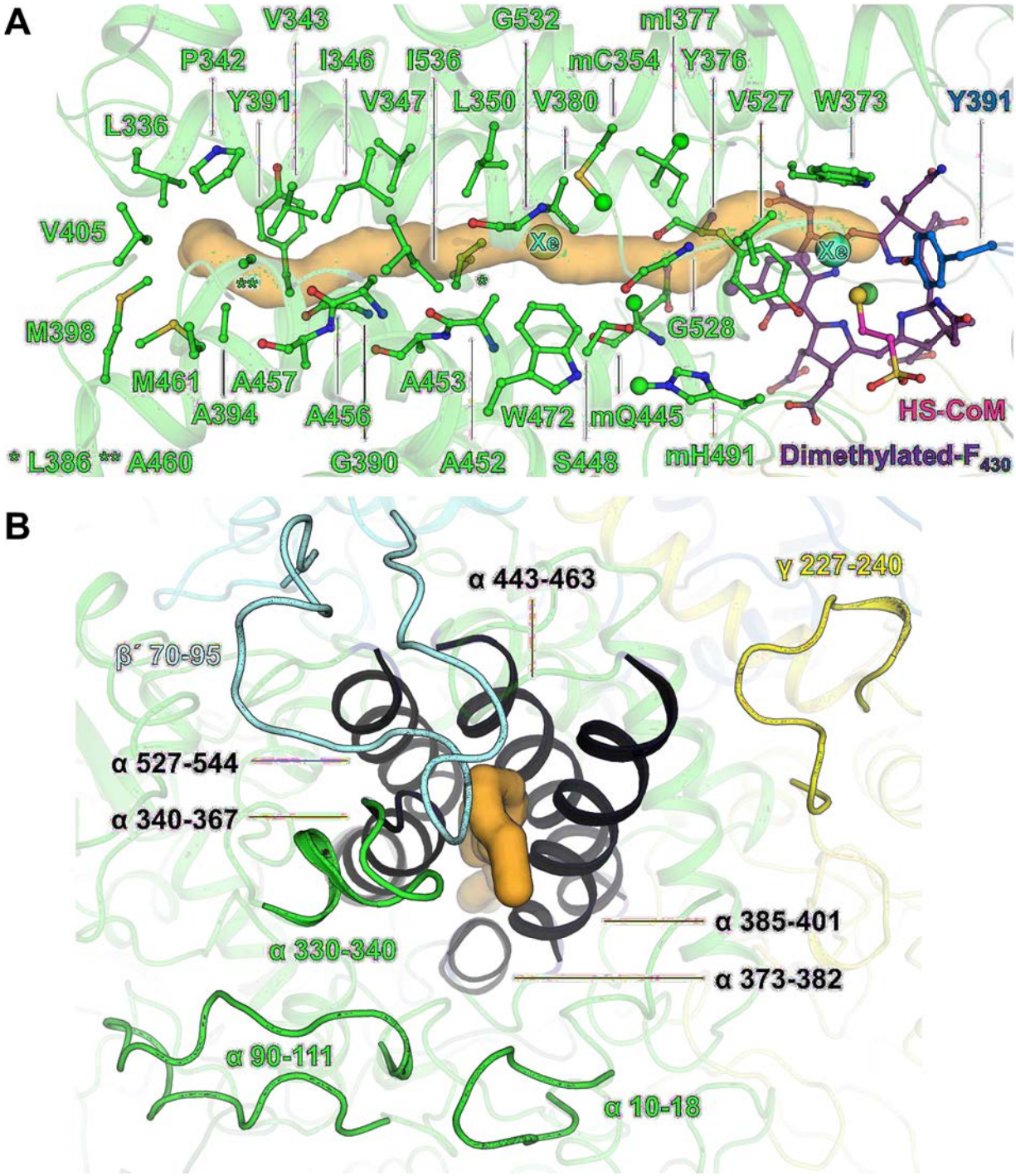

Figure S4-14 Gas tunnel architecture. MCR from *Ca.* E. thermophilum (PDB 7B1S) is shown as a transparent cartoon. The subunits α, β, γ, and β´ are colored in green, marine, yellow, and cyan, respectively. A, The gas tunnel detected by CAVER (Chovancova et al. 2012) is represented as orange transparent surface with the two Xe sites (from PDB 7B2C) indicated by cyan balls. Dimethylated-F_{430} cofactor and HS-CoM are shown as balls and sticks, carbons being colored as purple and pink respectively. Residues constituting the gas tunnel are represented in balls and sticks, the additional methylations of Cys354, Ile377, Gln445, His491 are highlighted by balls. B, Outside view of the tunnel surrounded by the additional loops highlighted by non-transparent cartoon. The helix bundle constituting the tunnel is colored in black.

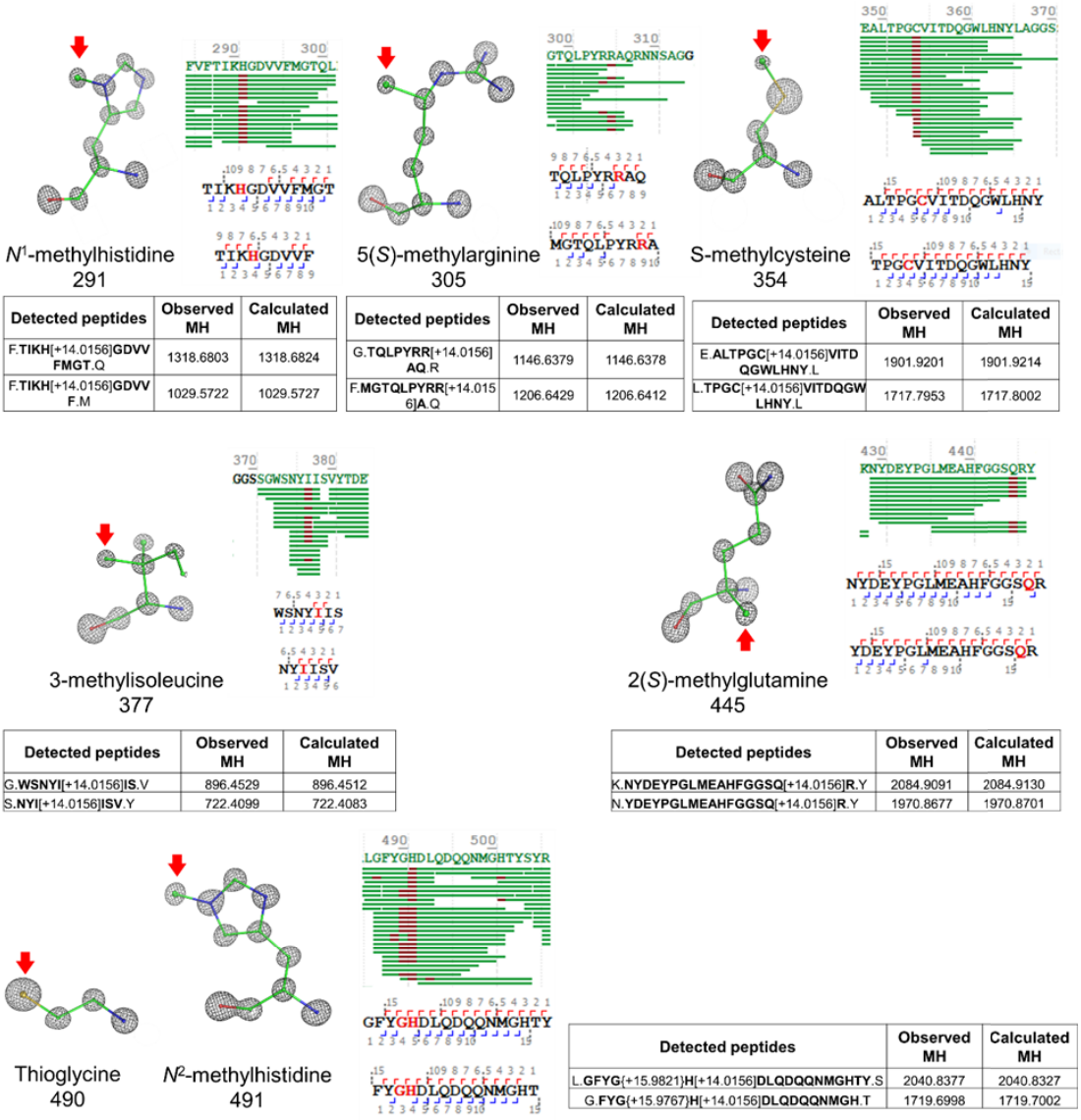

Detected peptides	Observed MH	Calculated MH
F.TIKH[+14.0156]GDVV FMGT.Q	1318.6803	1318.6824
F.TIKH[+14.0156]GDVV F.M	1029.5722	1029.5727

Detected peptides	Observed MH	Calculated MH
G.TQLPYRR[+14.0156] AQ.R	1146.6379	1146.6378
F.MGTQLPYRR[+14.015 6]A.Q	1206.6429	1206.6412

Detected peptides	Observed MH	Calculated MH
E.ALTPGC[+14.0156]VITD QGWLHNY.L	1901.9201	1901.9214
L.TPGC[+14.0156]VITDQGW LHNY.L	1717.7953	1717.8002

Detected peptides	Observed MH	Calculated MH
G.WSNYI[+14.0156]IS.V	896.4529	896.4512
S.NYI[+14.0156]ISV.Y	722.4099	722.4083

Detected peptides	Observed MH	Calculated MH
K.NYDEYPGLMEAHFGGSQ[+14.0156]R.Y	2084.9091	2084.9130
N.YDEYPGLMEAHFGGSQ[+14.0156]R.Y	1970.8677	1970.8701

Detected peptides	Observed MH	Calculated MH
L.GFYG{+15.9821}H[+14.0156]DLQDQQNMGHTY.S	2040.8377	2040.8327
G.FYG{+15.9767}H[+14.0156]DLQDQQNMGH.T	1719.6998	1719.7002

Figure S 4-15 Post-translational modifications in the MCR from *Ca.* E. thermophilum. Red arrows point at the modifications. $2F_o$-F_c maps are contoured at 5 σ and represented as a black mesh. The hooks above and below the peptide sequence mark the breaking sites of the peptide backbone where the fragment masses together form a ladder.

4.3.3 Supplementary tables

Table S 4-1 Sequence identity between the subunits of different MCRs and root mean square deviation (r.m.s.d.) of structurally characterized MCRs. An asterisk indicates that the protein is attributed to the former name of *M. marburgensis* in the Protein Data Bank.

Organism (PDB)	Sequence identity (%)			R.m.s.d (aligned Cα)		
	α-subunit	β-subunit	γ-subunit	α-subunit	β -subunit	γ -subunit
Ca. E. thermophilum (7B1S)	100	100	100	0 (621)	0 (501)	0 (287)
M. wolfeii MCR type I (5A8K)	44.54	48.18	43.80	0.801 (499)	0.696 (384)	0.659 (212)
M. formicicus MCR (5N28)	44.26	46.22	41.22	0.851 (498)	0.796 (400)	0.784 (220)
M. marburgensis MCR type II (5A8R)	44.21	47.20	45.25	0.788 (490)	0.840 (406)	0.738 (223)
M. barkeri (1E6Y)	44.19	46.04	45.00	0.877 (506)	0.914 (401)	0.834 (204)
*M. marburgensis** type I product complex (1HBM)	44.02	48.39	44.31	0.835 (502)	0.731 (388)	0.700 (209)
M. marburgensis type I (5A0Y)	44.02	48.39	44.31	0.821 (506)	0.722 (389)	0.709 (209)
M. wolfeii MCR type II (5A8W)	43.86	47.84	46.15	0.758 (490)	0.764 (399)	0.693 (223)
M. kandleri (1E6V)	43.77	47.16	46.36	0.827 (502)	0.907 (389)	0.757 (222)
M. thermolithotrophicus (5N1Q)	42.71	45.24	41.60	0.815 (499)	0.804 (408)	0.937 (231)
ANME-1 Black Sea mats (3SQG)	38.22	37.12	41.02	0.999 (464)	0.861 (382)	0.821 (216)

Table S4-2 X-ray crystallography data statistics.

	ECR from *Ca.* E. thermophilum native	ECR from *Ca.* E. thermophilum pressurized with Xe	MCR from *M. marburgensis* pressurized with Xe
Data collection			
Wavelength (Å)	1.00003	1.54981	2.07505
Space group	$P2_1$	$P2_1$	$P2_1$
Resolution (Å)	108.19 – 0.99 (1.07 – 0.99)	60.87 – 1.80 (1.84 – 1.80)	47.39 – 2.12 (2.198 – 2.12)
Cell dimensions			
a, b, c (Å)	83.74, 146.93, 113.13	83.79, 147.19, 113.38	81.72, 116.39, 123.07
α, β, γ (°)	90, 106.98, 90	90, 107.20, 90	90, 92.36, 90
R_{merge}(%)[a]	11.6 (116.7)	10.5 (65.2)	9.0 (117.3)
R_{pim} (%)[a]	4.7 (47.6)	4.6 (33.1)	3.8 (62.5)
$CC_{1/2}$ [a]	0.997 (0.563)	0.997 (0.739)	0.998 (0.511)
I/σ_I[a]	9.7 (1.6)	11.7 (2.0)	14.2 (1.0)
Spherical completeness[a]	74.0 (18.2)	96.0 (71.4)	89.4 (54.6)
Ellipsoidal completeness[a]	89.1 (58.1)	98.1 (94.6)	/
Redundancy[a]	7.0 (6.8)	6.0 (4.5)	6.5 (4.3)
Nr. unique reflections[a]	1,061,996 (53,103)	232,772 (11,640)	116,190 (7,094)
Refinement			
Resolution (Å)	39.76 – 0.99	35.90 – 1.80	48.17 – 2.12
Number of reflections	1,045,444	232,696	116,153
R_{work}/R_{free} [b] (%)	11.19/12.75	17.42/20.14	17.72/20.42
Number of atoms			
Protein	21,825	20,638	19,009
Ligands/ions	261	296	282
Solvent	3,086	2,346	775
Wilson B-value (Å²)	6.2	12.1	42.0
Mean B-value (Å²)	10.0	16.6	50.0
Protein	9.00	15.7	50.8
Ligands/ions	10.7	19.7	51.2
Solvent	23.5	24.3	51.9
Molprobity clash score, all atoms	1.30	1.97	4.37
Ramachandran plot			
Favored regions (%)	97.80	97.27	96.77
Outlier regions (%)	0.08	0.08	0.00
rmsd[c] bond lengths (Å)	0.009	0.008	0.007
rmsd[c] bond angles (°)	1.279	0.99	0.966
PDB ID code	**7B1S**	**7B2C**	**7B2H**

[a] Values relative to the highest resolution shell are within parentheses. [b] R_{free} was calculated as the R_{work} for 5% of the reflections that were not included in the refinement. Refined models contained hydrogens. [c] rmsd, root mean square deviation.

Table S4-3 Correlation between ANODE peak heights and refined occupancies for Xe atoms in both MCR from *M. marburgensis* and *Ca.* E. thermophilum pressurized with Xe.

ECR from *Ca.* E. thermophilum pressurized with Xe			**MCR from *M. marburgensis* pressurized with Xe**		
Chain ID, Atom number	ANODE peak height	Refined occupancy	Chain ID, Atom number	ANODE peak height	Refined occupancy
D, 708	40.50	0.80	A, 613	32.58	0.60
A, 1209	36.85	0.80	D, 609	31.77	0.60
E, 512	35.34	0.70	E, 507	22.85	0.20
B, 509	34.57	0.70	E, 508	19.17	0.40
D, 709	28.62	0.60	B, 507	15.12	0.40
A, 1208	28.00	0.60	F, 303	14.34	0.40
F, 1105	24.86	0.50	B, 509	12.86	0.40
C, 304	23.03	0.50	E, 506	12.64	0.20
B, 511	10.54	0.50	B, 511	12.35	0.20
E, 514	10.12	0.50	B, 508	11.32	0.25
D, 710	9.95	0.30	E, 509	11.18	0.25
F, 1106	7.89	0.30	B, 510	10.61	0.40
E, 513	7.86	0.40			
C, 305	7.83	0.30			
A, 1210	6.84	0.30			
B, 510	6.56	0.40			

Chapter 5

Discussion and outlook

5.1 General discussion

At the start of my thesis, the microbiology of anaerobic ethane degradation was essentially unexplored. Despite the observation that ethane is oxidized in anoxic sediments, the organisms involved in the process were unknown. In the years before my thesis started, non-canonical MCR sequences affiliated to Bathyarchaeota were discovered that widened the distribution of MCR within the domain *Archaea* and challenged the concept of high conservation in this enzyme family (Evans et al. 2015). One year later, the anaerobic butane oxidizer *Ca.* Syntrophoarchaeum was described, an archaeon that contains four of these non-canonical MCR sequences (Laso-Pérez et al. 2016). In enrichment cultures of *Ca.* Syntrophoarchaeum, it was shown that non-canonical MCRs are responsible for the anaerobic activation of butane (Laso-Pérez et al. 2016). In the following years, many metagenomics based studies further extended the scope of MCR sequences, indicating a grand, so far unexplored diversity in archaeal alkane metabolism (Vanwonterghem et al. 2016, Dombrowski et al. 2017, Dombrowski et al. 2018, Borrel et al. 2019, Boyd et al. 2019, Laso-Pérez et al. 2019, McKay et al. 2019, Wang et al. 2019).

To identify and cultivate an organism capable of anaerobic ethane metabolism would add an important puzzle piece to the understanding of carbon cycling at natural seep sites. Active ethane oxidizing enrichment cultures have been obtained in earlier studies, but organisms responsible for the process could not be identified (Kniemeyer et al. 2007, Adams et al. 2013, Bose et al. 2013, Singh et al. 2017). Using the knowledge from the recently discovered butane oxidizer (Laso-Pérez et al. 2016, Laso-Pérez et al. 2018) and environmental genomic information (Dombrowski et al. 2017, Dombrowski et al. 2018, Laso-Pérez et al. 2019), I started the hunt for an archaeal ethanotroph. I used hydrothermally heated sediment samples of the Guaymas Basin in the Gulf of California to inoculate for our incubations. The Guaymas Basin is a model system for studying hydrocarbon degradation with a tremendous microbial diversity due to its extensive temperature and geochemical gradients (Teske et al. 2002, Teske et al. 2014, Teske 2020, Teske and Carvalho 2020). High organic matter input has

formed a thick layer of organic-rich sediments over a spreading center, causing a broad thermogenic hydrocarbon profile to emerge towards the surface (Lonsdale and Becker 1985, Teske and Carvalho 2020). Sediment samples from the Guaymas Basin have already been used to show bacterial short-chain alkane degradation in enrichment cultures (Kniemeyer et al. 2007, Jaekel et al. 2013). Also, the before mentioned butane oxidizer *Ca.* Syntrophoarchaeum was enriched from Guaymas Basin sediment (Laso-Pérez et al. 2016). Additionally, metagenomics data indicated a greater diversity in *Archaea* involved in the anaerobic oxidation of alkanes at this site. This includes two MAGs affiliated to the GoM-Arc1 archaea with non-canonical mcrA sequences (Dombrowski et al. 2017). 16S rRNA sequences of GoM-Arc1 archaea have been found at many hydrocarbon seeps, but prior to my thesis, their physiology was unknown (Lloyd et al. 2006, Knittel and Boetius 2009, Orcutt et al. 2010, Dowell et al. 2016, Steen et al. 2016).

5.2 A model organism for anaerobic oxidation of ethane

In my thesis, I attempted to cultivate a thermophilic variant of an anaerobic ethanotroph from the Guaymas Basin. I established stable ethane-oxidizing cultures at 20, 37, and 50°C, whereas incubations at 70°C did not result in an active ethane-degrading culture. For further research, I focused on 50°C but also included the 37°C culture in some analyses. Both cultures were dominated by an archaeal strain affiliated to the GoM-Arc1 archaea. We named the genus *Ca.* Ethanoperedens after the closely related methanotrophic nitrate reducer *Ca.* Methanoperedens (formerly ANME-2d). The cultivated ethanotroph we named *Ca.* Ethanoperedens thermophilum, which has the following meaning: *ethano* (new Latin), pertaining to ethane; *peredens* (Latin), consuming, devouring; *thermophilum* (Greek), heat-loving. The name, therefore, implies the capability of ethane oxidation at elevated temperatures. Shortly before we finalized the first study about Ethanoperedens, another ethane oxidizer was discovered that was named *Ca.* Argoarchaeum ethanivorans (Chen et al. 2019). *Ca.* Argoarchaeum is a slow-growing psychrophilic ethanotroph with doubling times of ~seven months and was cultivated from cold seep sediments of the Gulf of Mexico (Chen et al. 2019). *Ca.* Argoarchaeum and *Ca.* Ethanoperedens are sister genera within the GoM-Arc1 cluster. While *Ca.* Argoarchaeum can be found in samples from cold seeps and samples from the Guaymas Basin with low sediment temperature, the thermophilic genus *Ca.* Ethanoperedens was found at hydrothermal vent sites with high sediment temperature. Looking at the phylogenetic affiliation of MAGs and ECR sequences, including those from public databases,

I could show that the two genera appeared according to their predicted temperature preference (Figures 2-3 and S4-4).

Similar as observed for thermophilic and cold-adapted methanotrophs, the thermophilic *Ca.* Ethanoperedens grows substantially faster than *Ca.* Argoarchaeum. Indeed, *Ca.* Ethanoperedens thermophilum has the fastest growth of all studied alkanotrophic archaea with doubling times of only seven days (Chapter 2). In comparison, *Ca.* Methanoperedens has doubling times of several weeks (Raghoebarsing et al. 2006), thermophilic ANME double in about two months (Holler et al. 2011, Wegener et al. 2016), whereas cold-adapted ANME and *Ca.* Argoarchaeum have doubling times of seven months (Nauhaus et al. 2007, Chen et al. 2019). The relatively fast biomass production of *Ca.* E. thermophilum allows for many experiments and a deep investigation of this strain. I was able to extract sufficient high-quality DNA to perform deep PacBio sequencing. This sequencing technology allowed me to reconstruct the first two closed genomes of MCR-dependent alkanotrophic archaea, *Ca.* Ethanoperedens thermophilum E37 and *Ca.* Ethanoperedens thermophilum E50. The closed genomes with high coverage of up to 214x (*Ca.* Ethanoperedens thermophilum E37) allow for a reliable prediction of gene arrangements. The fast growth combined with available high-quality genomes will make *Ca.* E. thermophilum a new model organism for the study of anaerobic oxidation of ethane and archaeal alkanotrophy in general.

5.3 Adaptation of methyl-coenzyme M reductases for multi-carbon metabolism

MCR was believed to be a highly conserved enzyme that was limited to the generation and oxidation of methane and only present in organisms of the phylum Euryarchaeota. In the years before my thesis, this conception changed by the discovery of non-canonical MCRs in the phylum Bathyarchaeota and anaerobic butane oxidizer *Ca.* Syntrophoarchaeum (Evans et al. 2015, Laso-Pérez et al. 2016). The genome of *Ca.* Ethanoperedens contains a single copy of a non-canonical MCR that is highly expressed in the active culture. Additionally, I found ethyl-CoM in the metabolome of the ethane oxidizing culture, confirming that an MCR-based activation drives the anaerobic oxidation of ethane. Therefore, I concluded that *Ca.* Ethanoperedens uses its MCR homolog in an alteration of the reverse methanogenesis pathway for AOE. During the time of my thesis, the field of non-canonical MCRs has been fast evolving. Many new non-canonical MCR sequences were published, including sequences from the

Helarchaeota (Asgard superphylum) (Seitz et al. 2019), Archaeoglobi (Boyd et al. 2019, Wang et al. 2019), and Hadesarchaeota (Hua et al. 2019, Wang et al. 2019). For all of these sequences, no potential substrate could be determined yet. MCR homologs are also predicted to be involved in long-chain alkane activation in the genus *Ca.* Methanoliparia. *Ca.* Methanoliparia contains two copies of an MCR homolog, a canonical with predicted methanogenic function and a non-canonical, predicted to activate long alkanes (Borrel et al. 2019, Laso-Pérez et al. 2019). These archaea are regularly found in oil-rich samples in abundances of up to 23% of the archaeal community (Laso-Pérez et al. 2019). During my thesis, I contributed to the characterization of *Ca.* Methanoliparia by in-situ abundance estimations and visualizing their presence associated with oil droplets (Laso-Pérez et al. 2019). Cells appeared immersed into the oil at the surface of the oil droplet. However, exact localization proved difficult since the oil droplets showed a strong autofluorescence, and the CLSM could not visualize the inner region of the droplet (Laso-Pérez et al. 2019). *Ca.* Methanoliparia mostly appeared as single cells or in chains and had no associated organisms suggesting a metabolism independent from syntrophic associations (Laso-Pérez et al. 2019).

Within about six years, a great diversity of new, non-canonical MCR homologs was discovered (Figure 1-5). These appear in MAGs of multiple archaeal phyla that were binned from various environments, including cold seeps and hydrothermal vents, oil fields, and hot springs, which suggest a great diversity in alkanotrophic archaea (Dombrowski et al. 2017, Dombrowski et al. 2018, Borrel et al. 2019, Boyd et al. 2019, Hua et al. 2019, Laso-Pérez et al. 2019, McKay et al. 2019, Wang et al. 2019, Wang et al. 2021). My thesis represents a crucial step towards a better understanding of the function of these non-canonical MCRs by obtaining an atomic resolution crystal structure of the ethane-specific MCR homolog of *Ca.* Ethanoperedens.

5.4 Comparison of MCR, ECR and long-chain alkane activating MCR homologs

The crystal structure of the ECR revealed many differences compared to canonical MCR, allowing it to accommodate ethane instead of methane (Chapter 4). The five insertions in the ECR sequence, compared to canonical MCR, form loops on the outside of the enzyme, surrounding the entry to a tunnel-like structure. The tunnel is flanked by methylated amino acids, forming a hydrophobic environment. It leads to the catalytic chamber, which is almost double in size compared to canonical MCR and apparently ideal for accommodating the larger

ethane molecule (Figure 4-3). In the enzyme core is a dimethylated Ni-porphinoid F_{430}-cofactor, and it is the first time that this dimethylated form was described. The methylations are likely an adaptation to stabilize the position of the F_{430}-cofactor in the widened catalytic chamber. These novel methylations would require a specialized methyltransferase, and I discovered a likely candidate to perform this methylation. *Ca.* Ethanoperedens and *Ca.* Argoarchaeum contain a non-canonical second copy of the Precorrin-4 C(11)-methyltransferase (*cobM*) located on an operon with the coding sequence of the co-factor F430 synthetase (*cfbE*). This *cobM* variant is unique to ethanotrophs (Figure S4-9). All these elaborate changes in the enzyme make it a distinct ECR instead of a MCR, showing that MCR chemistry is much more versatile than assumed for a long time.

The profound changes in the ECR structure compared to the canonical MCR are reflected in many changes in the amino acid sequence. ECR sequences form a distinct branch in phylogenetic mcrA trees, off the canonical and non-canonical sequences (Figures 2-3B and 3-1B; Wang et al. (2021)). In the following, I will compare ecrA sequences to other MCR homologs under considerations of what we learned from the ECR structure. Amino acid positions refer to the ecrA sequence of *Ca.* Ethanoperedens. The large inserts in the ECR sequence that form loops at the entrance to the ethane channel are unique to the ECR (Figure 4-2B). However, we can also find a large insert region in non-canonical mcrA sequences of *Ca.* Methanoliparia, *Ca.* Hadesarchaea, *Ca.* Bathyarchaeota and *Ca.* Helarchaeota. These MCR homologs are predicted to be involved in the activation of longer alkanes (AA position 330, Figure 6-1) (Evans et al. 2019, Hua et al. 2019, Laso-Pérez et al. 2019, Seitz et al. 2019). The inserts are at a similar AA position, creating a shared trait between these sequences that might be important in using longer alkane substrates.

In *Ca.* Ethanoperedens, a methionine (αM181) coordinates the nickel in the cofactor F_{430} instead of the canonical glutamine (Figure 4-3AB). The canonical glutamine is conserved in most non-canonical MCR homologs with the exception of *Ca.* Helarchaeota, where the glutamine is exchanged with leucine and in one of the MCRs of *Ca.* Syntrophoarchaeum, where we find a methionine as in *Ca.* Ethanoperedens (Figure 5-1). This MCR homolog from *Ca.* Syntrophoarchaeum is phylogenetically closer to the ECR than to the other non-canonical MCRs, but its function is so far unknown (Laso-Pérez et al. 2016) (Figures 2-3B and 3-1B). The exchange of the canonical glutamine with methionine could indicate similarities in the enzyme to the ECR, but this exchange seems to be no prerequisite for ethane activation since *Ca.* Argoarchaeum has the canonical glutamine. The active site in the ECR shows some remarkable changes compared to the canonical MCRs, especially on the loop α367-374, where

a bulky tryptophan replaces the canonical phenylalanine. This exchange is responsible for the increase of volume of the catalytic chamber and is most likely crucial for the ethane positioning. The MCR homolog of *Ca.* Syntrophoarchaeum (OFV68676) has an identical AA sequence in this loop, including the bulky tryptophan (Figure 5-1). This MCR homolog might be rather an ECR like enzyme with similar properties, considering these similar AA substitutions, especially in the active site. The other non-canonical MCR homologs also show changes in the amino acid sequence of the active site compared to the conserved sequences in the canonical MCRs. This is a strong indication that these enzymes are able to accommodate alkanes other than methane or ethane.

Another interesting group of MCR homologs are the recently discovered non-euryarchaeotal MCRs from *Ca.* Verstraetearchaeota, *Ca.* Nezhaarchaeota and Thaumarchaeota (Vanwonterghem et al. 2016, Hua et al. 2019, Wang et al. 2019). These sequences form a distinct cluster in the mcrA phylogenetic tree, but their function is so far unknown (Figure 2-3B, Wang et al. (2021)). This cluster can be considered part of the canonical MCRs, as the branch is rather short. In addition, the mcrA sequence alignment shows that the active site is conserved with other canonical MCRs, indicating a likely use of C_1 compounds by these species (Figure 5-1). For the *Ca.* Verstraetearchaeota methylated C_1 compounds have been proposed as substrates (Vanwonterghem et al. 2016, Kadnikov et al. 2019). The presence of a complete hydrogenotrophic methanogenesis pathway in *Ca.* Verstraetearchaeota strengthened the hypothesis of an ancient origin of the *mcr* gene, rather than repeated events of horizontal gene transfer (Berghuis et al. 2019). Similar canonical MCR sequences have also been found in the deeply rooted archaeal phylum *Ca.* Korarchaeota and the euryarchaeotal Archaeoglobi (McKay et al. 2019, Wang et al. 2019, Liu et al. 2020).

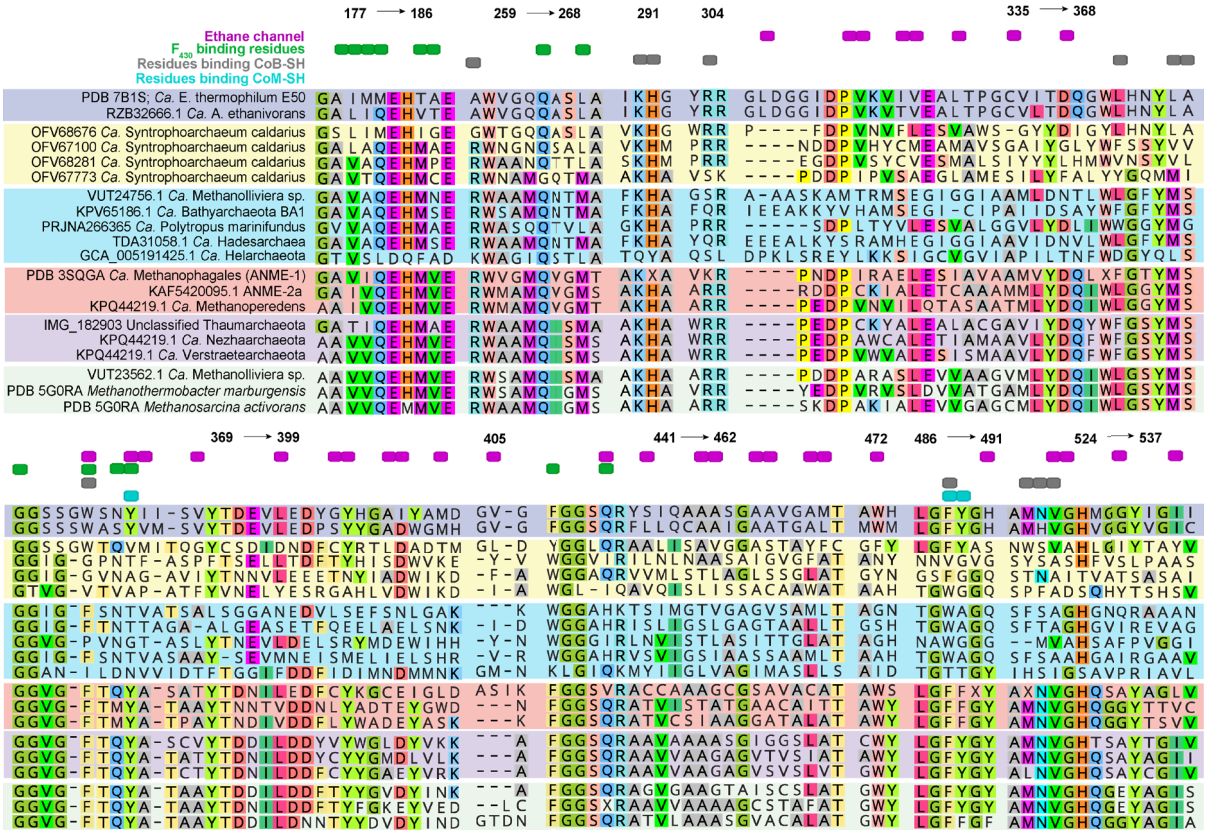

Figure 5-1 Alignment of amino acid sequences of ECR and MCR homologs. This alignment is an extension to the alignment shown in Figure S4-1, including non-canonical and non-euryarchaeotal MCR homologs. MCR homologs were grouped in the following clusters: ECR (dark blue), MCR homologs from butane oxidizer (yellow), other non-canonical (light blue), methanotrophs (red), non-euryarchaeotal canonical (purple) and canonical MCR (green). Numbering is based on *Ca.* E. thermophilum MCR amino acid sequence.

5.5 Deciphering the novel pathway for AOE

Ca. Ethanoperedens and *Ca.* Argoarchaeum harbor a novel pathway to oxidize ethane to CO_2 (**Chapter 2**, Chen et al. (2019)). Both genera lack genes for the ß-oxidation that catalyzes the degradation of the alkanes in *Ca.* Syntrophoarchaeum and *Ca.* Methanoliparia (Laso-Pérez et al. 2016, Borrel et al. 2019, Laso-Pérez et al. 2019). In the ß-oxidation, the alkane is oxidized, yielding an acetyl-CoA and an *n*-alkane-CoA (Wilkes and Rabus 2020). The acetyl-CoA decarbonylase:synthase (ACDS) can then decarboxylate the resulting acetyl-CoA yielding CO_2 and a methyl group. The methyl group is transferred to a tetrahydromethanopterin (H_4MPT), forming methyl-H_4MPT, which is then introduced to the downstream methane oxidation pathway. ß-oxidation only works with longer alkanes (>C_3), but ethanotrophs most likely also use acetyl-CoA as intermediate. Therefore, the anaerobic oxidation of ethane would need to involve an unprecedented transformation of an alkylthioester

to an acetylthioester. The enzymes catalyzing such reactions are unknown, yet here I present some possible pathways for transforming ethyl-CoM to acetyl-CoA.

When investigating the genome of *Ca.* Ethanoperedens, our first hypothesis was that the ethanotrophs use the enzymes of the reverse methanogenesis pathway, the C1-branch of the Wood-Ljungdahl pathway, for the oxidation of ethyl-groups (C_2-compound). All genes of the reverse methanogenesis pathway are present and expressed in *Ca.* Ethanoperedens, including the N5-methyltetrahydromethanopterin-:coenzyme M methyltransferase (*mtr*), which is missing in the genomes of the anaerobic butane oxidizers (Laso-Pérez et al. 2016). However, all enzymes of the reverse methanogenesis pathway are canonical based on their amino acid sequence and resemble those of methanogens. To catalyze multi-carbon reactions, the active site of these enzymes should be modified. In addition, the metabolite extracts did not contain H_4MPT or MF-bound intermediates with a C_2-group. Simple use of the pathway with a C_2-group instead of a C_1-group is therefore improbable. Instead, the expressed *mtr* might be involved in eradicating methyl groups produced as a side reaction of the ethane oxidation.

The more likely hypothesis involves a novel pathway to transform the ethyl-CoM to acetyl-CoA. Acetyl-CoA would then be decarboxylated and introduced to the downstream part of the reverse methanogenesis pathway. As discussed in Chapter 2 this novel pathway possibly involves an aldehyde ferredoxin oxidoreductase (*aor*) as a key gene. *Ca.* Ethanoperedens contains three *aor* gene copies in close proximity or on the same operon as methanogenesis-related genes. The *aor* genes belong to the highest expressed genes of *Ca.* Ethanoperedens. This is a strong indication of the importance of AOR for the ethane-specific metabolism in *Ca.* Ethanoperedens. Also, ANME and *Ca.* Syntrophoarchaeum contain *aor* genes, yet in these organisms, such genes are not found in the vicinity of those coding for methanogenesis, and the genes are underexpressed (Laso-Pérez et al. 2016, Krukenberg et al. 2018). AOR-like enzymes usually catalyze the oxidation of aldehydes to carboxylic acids and are well described for hyperthermophilic archaea (Heider et al. 1995, Roy and Adams 2002, Hagedoorn et al. 2005). Hence, oxidoreductases are capable of reactions required for steps of the conversion of ethyl-CoM to acetyl-CoA. For example a pyruvate:ferredoxin oxidoreductase (PFOR) can oxidize pyruvate + CoA-SH to acetyl-CoA + CO_2 + $2e^-$ + H^+ in a single reaction (Chabrière et al. 1999). **Figure 5-2** presents three hypotheses for a potential pathway to oxidize the ethyl-CoM to acetyl-CoA.

The first hypothesis involves an initial exchange of the ethyl-bound CoM with CoA-SH by a transferase-like enzyme. Classical CoA-transferases only mediate the reversible transfer reaction of coenzyme A groups from CoA-thioesters to free acids (Heider 2001). Only

CoA-transferases of class III appear to have a greater substrate and reaction range and are primarily found in anaerobic organisms (Heider 2001, Berthold et al. 2008). However, no transferase enzyme mediating the exchange of a CoM-group with a CoA-group has been reported yet. In a second step, an Fd-reductase dependent enzyme would oxidize ethyl-CoA to vinyl-CoA. As the third reaction, a hydratase transforms the vinyl-CoA to a CoA-bound aldehyde. In a final reaction, an F_{420}-dependent enzyme would oxidize the aldehyde-group to an acetyl-group, forming acetyl-CoA. The AOR might mediate the final step since this enzyme is usually involved in the oxidation of aldehydes to carboxylic acids (Heider et al. 1995) (**Figure 5-2 yellow box**). Alternatively, the same reaction could take place with the C_2-compound bound to CoM. In the last step, the transferase-like enzyme would transform acetyl-CoM to acetyl-CoA (**Figure 5-2 blue box**). The third hypothesis involves the initial cleavage of the CoM by a hydrolase enzyme, forming free ethanol. The ethanol would then be oxidized by an alcohol dehydrogenase (ADH) like enzyme, forming acetaldehyde. Alcohol dehydrogenases are widespread in anaerobic bacteria and archaea and are responsible for diverse ethanol-based catabolic processes (Reid and Fewson 1994, Radianingtyas and Wright 2003). An F_{420}-reductase dependent AOR would then mediate the oxidation of the acetaldehyde to acetate. The transformation of acetate to alcohol using a ferredoxin-dependent AOR and ADH has previously been demonstrated in the hyperthermophilic archaeon *Pyrococcus furiosus* (Roh et al. 2002, Basen et al. 2014). This process is bi-directional and can generate acetate from ethanol (Basen et al. 2014, Keller et al. 2017). However, in the genome of *Ca.* Ethanoperedens, no alcohol dehydrogenase homolog was detected. An alternative or novel enzyme for such a common reaction seems unlikely. In a final reaction, an ATP-dependent ligase could mediate the binding of the acetate to CoA-SH, forming acetyl-CoA (**Figure 5-2 red box**). Afterward, the acetyl-CoM would be decarboxylated and introduced to the reverse methanogenesis pathway as described in the anaerobic oxidation of butane (Laso-Pérez et al. 2016).

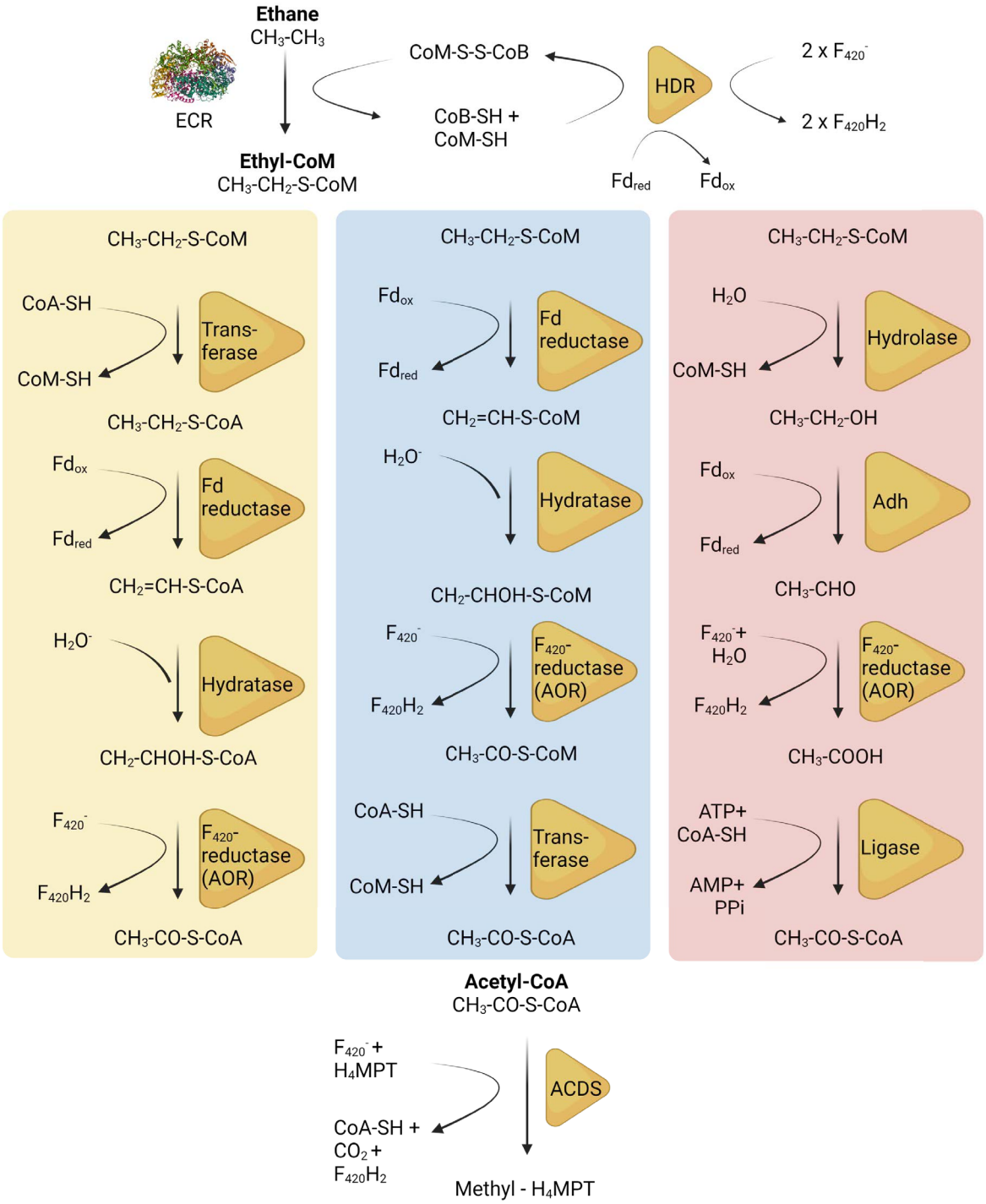

Figure 5-2 Hypothetical pathway for the anaerobic oxidation of ethane. The three colored boxes present three hypotheses for the conversion of ethyl-CoM to acetyl-CoA. Yellow triangles indicate potentially involved proteins. ECR is represented by PDB structure 7B1S. ADH: alcohol dehydrogenase; AOR: aldehyde oxidoreductase; HDR: heterodisulfide reductase; ACDS: CO dehydrogenase/acetyl-CoA synthase. Figure created with BioRender.com.

5.6 F_{420}-reduction drives anaerobic oxidation of ethane

For energy conservation and electron shuttling, the coenzyme F_{420} seems to play an important role in *Ca.* Ethanoperedens, replacing the ferredoxin that is used as an electron carrier in most methanogens and alkanotrophs. Energy conservation in methanogens and alkanotrophs depends on energy-conserving membrane complexes. These complexes either drive a proton gradient with the energy-conserving hydrogenase complex (ECH) or (Ni-Fe)-hydrogenases or a sodium gradient with the ferredoxin:NAD^+-oxidoreductase (RNF) (Wang et al. 2014, Shima et al. 2020). At least one of these complexes can be found in the genome of most methanogens and alkanotrophs, underlining their importance (Figure 6-2). However, genomes of the ethanotrophs lack genes for classic energy-conserving hydrogenases like those found in *Ca.* Methanoperedens and *Ca.* Syntrophoarchaeum or the RNF complex found in ANME-2 genomes. This indicates a different system for energy conservation in AOE (Figure 6-2). The operon of the carbon monoxide dehydrogenase (CODH) is conserved in most methanogens and alkanotrophs. Interestingly, in *Ca.* Ethanoperedens and *Ca.* Argoarchaeum the CODH operon contains a gene for the coenzyme F_{420}^- reductase (Figure 6-2). This indicates that F_{420}-reduction drives anaerobic oxidation of ethane rather than the reduction of ferredoxin. Indeed, crystal structures of the CODH and the formyl-methanofuran dehydrogenase (FMD) from *Ca.* Ethanoperedens contain an additional subunit, the coenzyme F_{420}^- reductase, indicating the generation of reduced $F_{420}H_2$ by these enzymes (Lemaire, personal communication). Additionally, I detected F_{420}^- reductases in operons with the heterodisulfide reductase (HDR) and the aldehyde oxidoreductase (AOR), suggesting that these enzymes might also reduce coenzyme F_{420}^- instead of ferredoxin (Figure 6-3). In total, I detected 10 F_{420}^- reductase (FRH) or F_{420}-dependent sulfite reductase (FSR) genes in the *Ca.* Ethanoperedens genome (Figure 6-3).

Genes for the $F_{420}H_2$ dehydrogenase (*fpoABCDHIJKLMNO*) complex are highly expressed in *Ca.* Ethanoperedens. The $F_{420}H_2$ dehydrogenase (FPO) has been proposed as part of the energy-conserving electron transport system in methanogens and methanotrophs and could use the generated $F_{420}H_2$ to drive a proton gradient at the membrane (Bäumer et al. 2000, Arshad et al. 2015, Krukenberg et al. 2018, Leu et al. 2020). According to the potential pathway presented for *Ca.* Ethanoperedens, seven molecules of reduced $F_{420}H_2$ might be produced per fully oxidized ethane, i.e. 2 x $F_{420}H_2$ is produced by the HDR, 1 x Fd_{red} and 1 x $F_{420}H_2$ are produced during the oxidation of ethyl-CoM to acetyl-CoA, 2 x $F_{420}H_2$ by CODH and FMD and 2 x $F_{420}H_2$ are produced during the downstream reverse methanogenesis, resulting in 14

H^+ that could be pumped over the membrane by Fpo. The proton gradient is driven by the nanowire-based transfer of electrons towards the sulfate-reducing partner bacteria. *Ca.* Ethanoperedens highly expresses a v-type ATP synthase, which is responsible for the generation of ATP from the generated proton gradient. ATP synthases have an H^+/ATP ratio of 4, meaning that 1 ATP is produced for every 4 protons pumped over the membrane (Cross and Müller 2004). Therefore, 3.5 ATP could be produced per oxidized ethane. However, 1 ATP might be needed to ligate acetyl-CoA (Figure 5-2 red box). Also, the reactivation of the inactive ECR-Ni(II) to the active ECR-Ni(I) state is likely ATP dependent as described for MCR reactivation (Prakash et al. 2014). In comparison, for AOM a production of 0.5 ATP per methane has been proposed (Scheller et al. 2010, Thauer 2011). However, our understanding of the anaerobic oxidation of ethane is still limited, and a thorough thermodynamic assessment would be required to make a reliable comparison to AOM.

5.7 Adaption of a direct FISH protocol for the visualization of mRNA expression

Ca. Ethanoperedens thermophilum and its partner bacterium *Ca.* Desulfofervidus auxilii grow in dense consortia. A mixed growth within the consortia would allow an ideal exchange of reducing equivalents. Instead, the consortia appear spatially segregated with archaeal monospecies clusters surrounded by their sulfate-reducing partner bacteria (Figures 2-2DE and 3-1C). This segregated appearance has also been observed for consortia involved in AOM and anaerobic butane oxidation (Knittel et al. 2005, Laso-Pérez et al. 2016, Wegener et al. 2016). In my thesis, I assessed if the transcription-based activity is influenced by the distance of *Ca.* Ethanoperedens cells to the bacterial-archaeal interface. For this, I developed a direct mRNA-FISH protocol based on a mono-FISH protocol (Fuchs et al. 2007). I used a mix of six tetra-labeled oligomer probes, each consisting of about 40 nucleotides (Chapter 3), to achieve a signal intensity that is high enough to be detected. I targeted the mRNA sequence of the alpha subunit of the ethyl-coenzyme M reductase (*ecrA*) with the probes. mRNA molecules have a short lifetime and are therefore suitable to visualize dynamic changes in cell activity (Belasco, 1993; Selinger et al., 2003; Andersson et al., 2006).

We showed differences in expression activity by quantifying the mRNA-FISH signals, but the distance to partner cells seemed not to be the only activity limiting factor (Figure 3-3).

This result differs from other studies reporting even activity in segregated AOM consortia (McGlynn et al. 2015, Hatzenpichler et al. 2016). The electron transfer via pili-based nanowires between the partner cells would allow larger distances without reduced physiological capabilities. This form of syntrophic exchange has been proposed for segregated AOM consortia and would most likely also apply for thermophilic AOE consortia (McGlynn et al. 2015, Wegener et al. 2015). A decrease in activity in segregated consortia has been reported for AOM, where an activity loss of 70% in the archaea was measured when the distance between partners exceeded 30 µm (He et al. 2021). The activity loss with increasing distance to the bacterial-archaeal interface was explained by ohmic resistance, which increases with the distance the electrons have to travel through the nanowires (He et al. 2019, He et al. 2021). However, the maximum distance from the center of a monospecies cluster to the bacterial-archaeal interface measured in my thesis was only 6.4 µm (Figure 3-3). The observed decrease in activity in the central region of the archaeal clusters was intriguing and appeared to be independent of the distance to the bacterial-archaeal interface. This observation has not been reported in previous studies using stable isotope probing or BONCAT-FISH for the activity assessment (McGlynn et al. 2015, Hatzenpichler et al. 2016, He et al. 2019, He et al. 2021). However, for the analyzed 3D micrograph, we had indications that the activity in the archaeal cells might already be significantly reduced at distances shorter than 30 µm to the bacterial-archaeal interface. In this monospecies cluster, one side of the cluster was located at the outside of the consortium, increasing the distance to the bacterial-archaeal interface. We could see an increase of signals from the exposed part of the monospecies cluster towards the bacterial-archaeal interface. However, to get a better understanding of these activity dynamics, further research is required.

5.8 Outlook

The discovery of anaerobic oxidation of ethane filled a large gap in our understanding of microbial hydrocarbon degradation. This study showed the global importance of this process and set the first steps towards a deeper understanding of the pathway. The thermophilic strain *Ca.* Ethanoperedens thermophilum, with its rapid growth and streamlined genome, is a great model organism that will enable many future studies. All steps of the reverse methanogenesis pathway are reversible, and we showed that AOE, like AOM, has a back leakage of the substrate (Figure S2-4). A full reversal of the process would allow for ethanogenesis from CO_2 and potentially provide an excellent renewable energy source for the future. However,

indications for natural ethanogenesis in the environment are very scarce (Oremland 1981, Hinrichs et al. 2006, Xie et al. 2013, Oremland 2021). Besides being proposed based on metagenomics, organisms performing energy-yielding ethanogenesis have not been described yet. Future research should target cloning and expression of crucial AOE enzymes in a methanogenic organism, with the ultimate aim to design an ethanogenic microbe. However, the described modifications on the ECR and its dimethylated cofactor F_{430} are very complex, and the production of a functional ECR in a methanogen would not be a trivial task. Ethane is an energy-rich biofuel with a gas heating value of 1783 higher heating value in british thermal units per standard cubic feet (HHV BTU/SCF) compared to the 1012 HHV BTU/SCF of methane (Cronshaw 2021).

The characterization of missing enzymes for AOE will be of great importance not only for the understanding of natural ethane circulation but also for biotechnological interests. A targeted protein purification protocol under anoxic conditions would be a promising approach. The Ethane50 culture has a high biomass production that would make larger scale protein purifications feasible. However, compared to other anaerobic model organisms, the biomass gain from the Ethane50 culture is extremely low, making this a very challenging project. That a targeted protein purification protocol can uncover novel enzymes only based on genetic and potential functional information in anaerobic systems has been demonstrated before for the coenzyme F_{430} biosynthesis (Zheng et al. 2016).

The cofactor F_{420}-reduction dependent system for energy conservation observed in *Ca.* Ethanoperedens could demonstrate an efficient alternative to known systems from methanogens and alkanotrophs. The $F_{420}H_2$ driven pumping of protons by the $F_{420}H_2$ dehydrogenase (FPO) is a well-described process, however, it was not considered to be of great importance for alkanotrophs (Bäumer et al. 2000, Krukenberg et al. 2018, Leu et al. 2020). So far, all investigated oxidative steps during ethane oxidation in *Ca.* Ethanoperedens show the use of F_{420}^- instead of ferredoxin as an electron shuttle. Direct coupling of the proton pump and transfer of electrons might be an energy-efficient adaptation in ethanotrophs. Future studies will show how this alternative energy conservation system affects the anaerobic oxidation of ethane and if this system is more favorable to the described systems. Also, for other obligate syntrophic alkanotrophs, the use of F_{420} dependent energy conservations might be of greater importance than previously thought. For example, genomes of ANME-1, like ethanotrophs, lack genes for classic energy-conserving hydrogenases or sodium pumps and show the presence of F_{420}-reductase genes on operons with CODH genes (Figure 6-2). However, the

slow growth of ANME-1 cultures makes protein purification challenging. Future studies will show if this system might also be important for ANME-1.

The mRNA-FISH protocol presented in this thesis should be used in future experiments as a quick method to assess the expression of specific mRNAs. The fast preparation and limited amount of steps make it very robust and easy to apply. It could be used to visualize the expression of specific genes as a reaction to substrate change in cultures or as an early indicator for decreased expression in unfavorable conditions. mRNA-FISH probes could also be applied to environmental samples used to show the expression of metabolic key genes. In the case of *ecrA,* the probe mix would have to include *Ca.* Argoarchaeum *ecrA* specific probes since this genus is more abundant in the environment than *Ca.* Ethanoperedens. Additionally, the signal intensity should be used as a cell activity indicator in future studies. Direct labeling allows for correlation of signal intensity to target copy number

Appendix

```
PDB_7B1S;_Ca._Eethanoperedens_thermophilum

PDB_7B1S;_Ca._Eethanoperedens_thermophilum    ............................................................
RZB32666.1_Ca._Argoarchaeum_ethanivorans      ............................................................
OFV68676_Ca._Syntrophoarchaeum_caldarius      MAEEIKLDPELLAKLCERKIRSWQTDNAELLKATRADLTEAERAELLEKMYDDEEALKKV
OFV67100_Ca._Syntrophoarchaeum_caldarius      ............................................................
OFV68281_Ca._Syntrophoarchaeum_caldarius      ............................................................
OFV67773_Ca._Syntrophoarchaeum_caldarius      ............................................................
VUT24756.1_Ca._Methanolliviera_sp.            ............................................................
KPV65186.1_Ca._Bathyarchaeota_BA1             ............................................................
PRJNA266365_Ca._Polytropus_marinifundus       ............................................................
TDA31058.1_Ca._Hadesarchaea                   ............................................................
GCA_005191425.1_Ca._Helarchaeota              ............................................................
PDB_3SQGA_Ca._Methanophagales_(ANME-1)        ............................................................
KAF5420095.1_ANME-2a_                         ............................................................
KPQ44219.1_Ca._Methanoperedens                ............................................................
IMG_182903_Unclassified_Thaumarchaeota        ............................................................
KPQ44219.1_Ca._Nezhaarchaeota                 ............................................................
KPQ44219.1_Ca._Verstraetearchaeota            ............................................................
VUT23562.1_Ca._Methanolliviera_sp.            ............................................................
PDB_5G0RA_Methanothermobacter_marburgensis    ............................................................
PDB_5G0RA_Methanosarcina_activorans           ............................................................


PDB_7B1S;_Ca._Eethanoperedens_thermophilum

PDB_7B1S;_Ca._Eethanoperedens_thermophilum    ............................................................
RZB32666.1_Ca._Argoarchaeum_ethanivorans      ............................................................
OFV68676_Ca._Syntrophoarchaeum_caldarius      FQTMGNPQVAVGMEFTREGGDISDEEMKEICDRWGLTREEVDQICDELWISERDIATCPG
OFV67100_Ca._Syntrophoarchaeum_caldarius      ............................................................
OFV68281_Ca._Syntrophoarchaeum_caldarius      ............................................................
OFV67773_Ca._Syntrophoarchaeum_caldarius      ............................................................
VUT24756.1_Ca._Methanolliviera_sp.            ...MGEELS.........................EEERIK....................
KPV65186.1_Ca._Bathyarchaeota_BA1             ............................................................
PRJNA266365_Ca._Polytropus_marinifundus       ............................................................
TDA31058.1_Ca._Hadesarchaea                   ............................................................
GCA_005191425.1_Ca._Helarchaeota              ............................................................
PDB_3SQGA_Ca._Methanophagales_(ANME-1)        ............................................................
KAF5420095.1_ANME-2a_                         ............................................................
KPQ44219.1_Ca._Methanoperedens                ............................................................
IMG_182903_Unclassified_Thaumarchaeota        ............................................................
KPQ44219.1_Ca._Nezhaarchaeota                 ............................................................
KPQ44219.1_Ca._Verstraetearchaeota            ............................................................
VUT23562.1_Ca._Methanolliviera_sp.            ............................................................
PDB_5G0RA_Methanothermobacter_marburgensis    ............................................................
PDB_5G0RA_Methanosarcina_activorans           ............................................................


PDB_7B1S;_Ca._Eethanoperedens_thermophilum                                                               T
                                                                                          1         10

PDB_7B1S;_Ca._Eethanoperedens_thermophilum    ...............................................MVKYPKQLFLESK
RZB32666.1_Ca._Argoarchaeum_ethanivorans      ........MSQTRTSKENTVVEEGRYWDPHAVKGN............IEKGKTWERMSIR
OFV68676_Ca._Syntrophoarchaeum_caldarius      FLFGRGVPHPDQGDTPEAKDDPTQSIWYHRLMKTQ............MQLAMHEYGTYQR
OFV67100_Ca._Syntrophoarchaeum_caldarius      ..........................................................MD
OFV68281_Ca._Syntrophoarchaeum_caldarius      ..........................................................MK
OFV67773_Ca._Syntrophoarchaeum_caldarius      .......................................................MAVDK
VUT24756.1_Ca._Methanolliviera_sp.            ...........RFVEERKKKAGEERT.....KESGMSARERDYTRELYRASQKFIDIEKG
KPV65186.1_Ca._Bathyarchaeota_BA1             ...............MAEEERKRKAP.....REGQITAREREYVRELYAVSERFLEVERK
PRJNA266365_Ca._Polytropus_marinifundus       .......................................................MSKKE
TDA31058.1_Ca._Hadesarchaea                   .................MEKRKVLDE.....RAGQLEAREREYVRELYALSKKYLEVEKE
GCA_005191425.1_Ca._Helarchaeota              ...........MSGPLKKGKLPKELT.....SQMEATAAASQYLRQAVKNMRDFIPLEKQ
PDB_3SQGA_Ca._Methanophagales_(ANME-1)        .....................................................MPYNDIQ
KAF5420095.1_ANME-2a_                         ...............................................MVAENFNNEVTAK
KPQ44219.1_Ca._Methanoperedens                ..........................................................MA
IMG_182903_Unclassified_Thaumarchaeota        .........................................................MAE
KPQ44219.1_Ca._Nezhaarchaeota                 .......................................................MAARE
KPQ44219.1_Ca._Verstraetearchaeota            .......................................................MSEEK
VUT23562.1_Ca._Methanolliviera_sp.            .......................................................MAGVE
PDB_5G0RA_Methanothermobacter_marburgensis    .........................................................MAD
PDB_5G0RA_Methanosarcina_activorans           ......................................................MAADIF


                                                        η1                           η2             α1
PDB_7B1S;_Ca._Eethanoperedens_thermophilum    TT                      TT
                                                   20**          30        40 *     *   50         60

PDB_7B1S;_Ca._Eethanoperedens_thermophilum    NSKMNSIEMKYGQD..........PAINRAEFHVYGGVRQS..KRKSEAWEAAKRI.TKE
RZB32666.1_Ca._Argoarchaeum_ethanivorans      DDCGNMFKSKFGDID.........FTSKNTEYYRFNGVMQS..KRKSEAWEIAKRI.TRE
OFV68676_Ca._Syntrophoarchaeum_caldarius      AMNESVLAKGFGVED.........V.REETTEYPAGGISQV..PEKLEYVKVSKEI.EKQ
OFV67100_Ca._Syntrophoarchaeum_caldarius      EKILDDFKRIFKEED.........PTKRETQFYNFGGRTQS..KAKREFIESAKRI.AET
OFV68281_Ca._Syntrophoarchaeum_caldarius      KKAIDLLMATFDEDD.........ATREYTTFFQFGGWKQS..KRKQEYVKLAKEL.LKE
OFV67773_Ca._Syntrophoarchaeum_caldarius      KTHIKLLEETFKVSP.........TDIVDKKLYQHGGTRQS..KRKTEYIEYANRI.AKE
VUT24756.1_Ca._Methanolliviera_sp.            RDIYQTMKEIWGAEP.........LYEVDEKMYHRGGYRQS..IRKKEFIDAGKQI.AIK
KPV65186.1_Ca._Bathyarchaeota_BA1             RPMYAAMERTFGSDP.........FQRIDPKMYKRGGFRQS..KRKQEFVRLGRQV.AIE
PRJNA266365_Ca._Polytropus_marinifundus       NIMIKRLKEIFNTED.........LTDKHTSFYQFGGWKQS..KRKQEFVIRAKQI.AES
TDA31058.1_Ca._Hadesarchaea                   RPLYSIMQKTFGADP.........FALQDSQMYKRGGYRQS..KRKQEFARLGRQV.AVE
GCA_005191425.1_Ca._Helarchaeota              RRIYKDLEKMFGVDP.........LNLIDEKMYMRKGFNQS..AAIMKNKELGRLI.ALD
PDB_3SQGA_Ca._Methanophagales_(ANME-1)        HNFLKAMSDKFAEKP..........ESTATEFYTYGGIAQKGGMRKREFIAEASKIVDSR
KAF5420095.1_ANME-2a_                         KHFITAMEVKYGKEWGNNKQAD..DIQQTTAKYLRLGTEQN..PRKMEMAKIGAEI.MKK
KPQ44219.1_Ca._Methanoperedens                VRFQKAMETKYTKEWGSNKNKG.GKITDKKAKYLRLGYQQN..PRKVEMAKCGAAI.TKK
IMG_182903_Unclassified_Thaumarchaeota        PRYIKALRKKFKESP.........EE.RYTTFYTLGGWAQD..PRKREFKEISDKI.AKQ
KPQ44219.1_Ca._Nezhaarchaeota                 KMFMEALRRKFKEAP.........EE.KYTKFYVYGQWKQS..KRKTEFVEWSQKI.AKE
KPQ44219.1_Ca._Verstraetearchaeota            KMFLEALRRKFKESP.........EE.KQTKFYIYEGWKQS..KRKREFVEAAQKI.AKE
VUT23562.1_Ca._Methanolliviera_sp.            KRFVEALSKKFEEDP.........KG..KVMKHVGMGIEQS..ERKMEFKKWGDKI.TKE
PDB_5G0RA_Methanothermobacter_marburgensis    KLFINALKKKFEESP.........EE.KKTTFYTLGGWKQS..ERKTEFVNAGKEV.AAK
PDB_5G0RA_Methanosarcina_activorans           AKFKKSMEVKFTQEYGSNKQA.GGDITGKTEKFLRLGPEQD..ARKQEMIKAGKEI.AEK
```

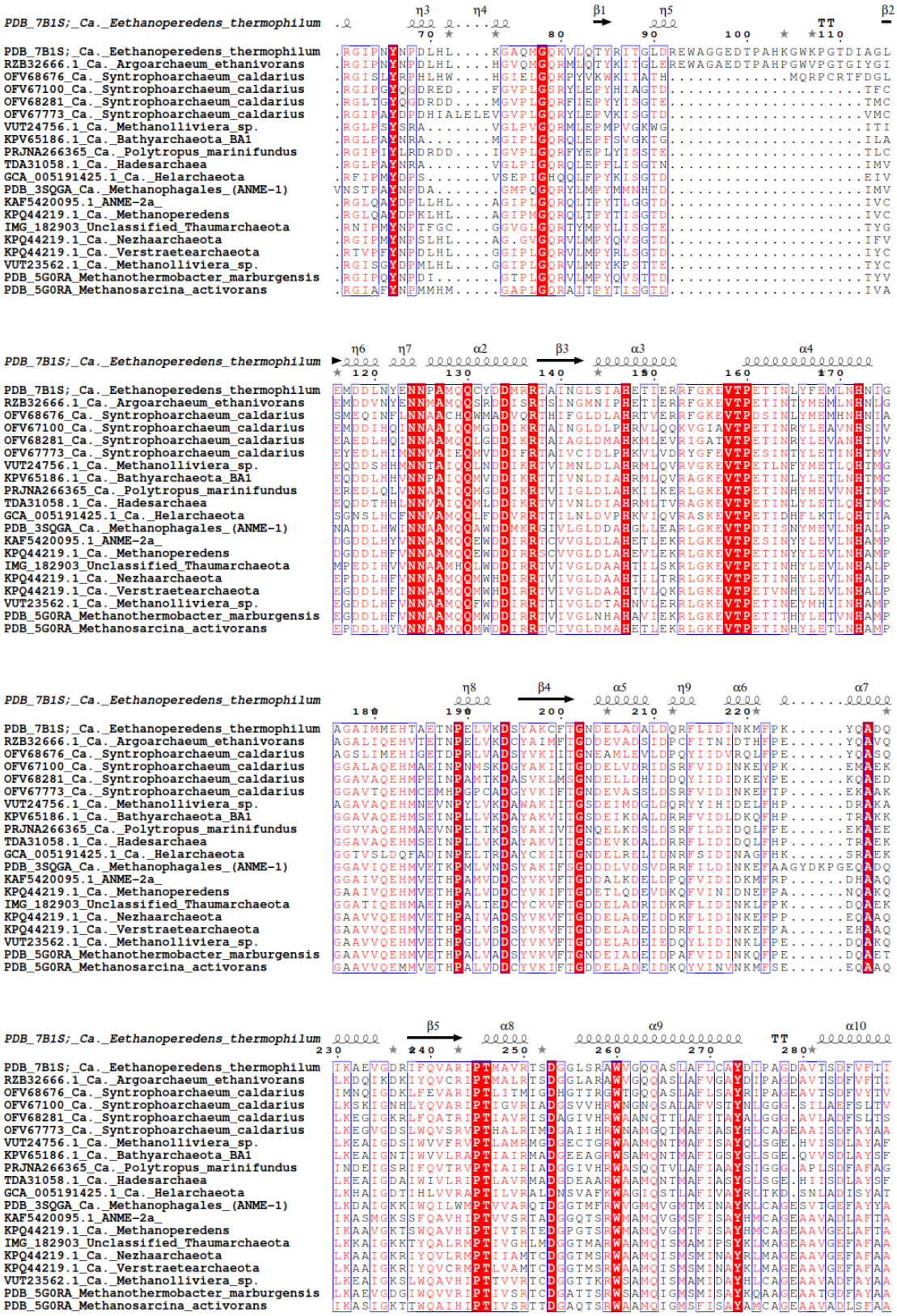
PDB_7B1S;_Ca._Eethanoperedens_thermophilum
PDB_7B1S;_Ca._Eethanoperedens_thermophilum
RZB32666.1_Ca._Argoarchaeum_ethanivorans
OFV68676_Ca._Syntrophoarchaeum_caldarius
OFV67100_Ca._Syntrophoarchaeum_caldarius
OFV68281_Ca._Syntrophoarchaeum_caldarius
OFV67773_Ca._Syntrophoarchaeum_caldarius
VUT24756.1_Ca._Methanolliviera_sp.
KPV65186.1_Ca._Bathyarchaeota_BA1
PRJNA266365_Ca._Polytropus_marinifundus
TDA31058.1_Ca._Hadesarchaea
GCA_005191425.1_Ca._Helarchaeota
PDB_3SQGA_Ca._Methanophagales_(ANME-1)
KAF5420095.1_ANME-2a_
KPQ44219.1_Ca._Methanoperedens
IMG_182903_Unclassified_Thaumarchaeota
KPQ44219.1_Ca._Nezhaarchaeota
KPQ44219.1_Ca._Verstraetearchaeota
VUT23562.1_Ca._Methanolliviera_sp.
PDB_5G0RA_Methanothermobacter_marburgensis
PDB_5G0RA_Methanosarcina_activorans

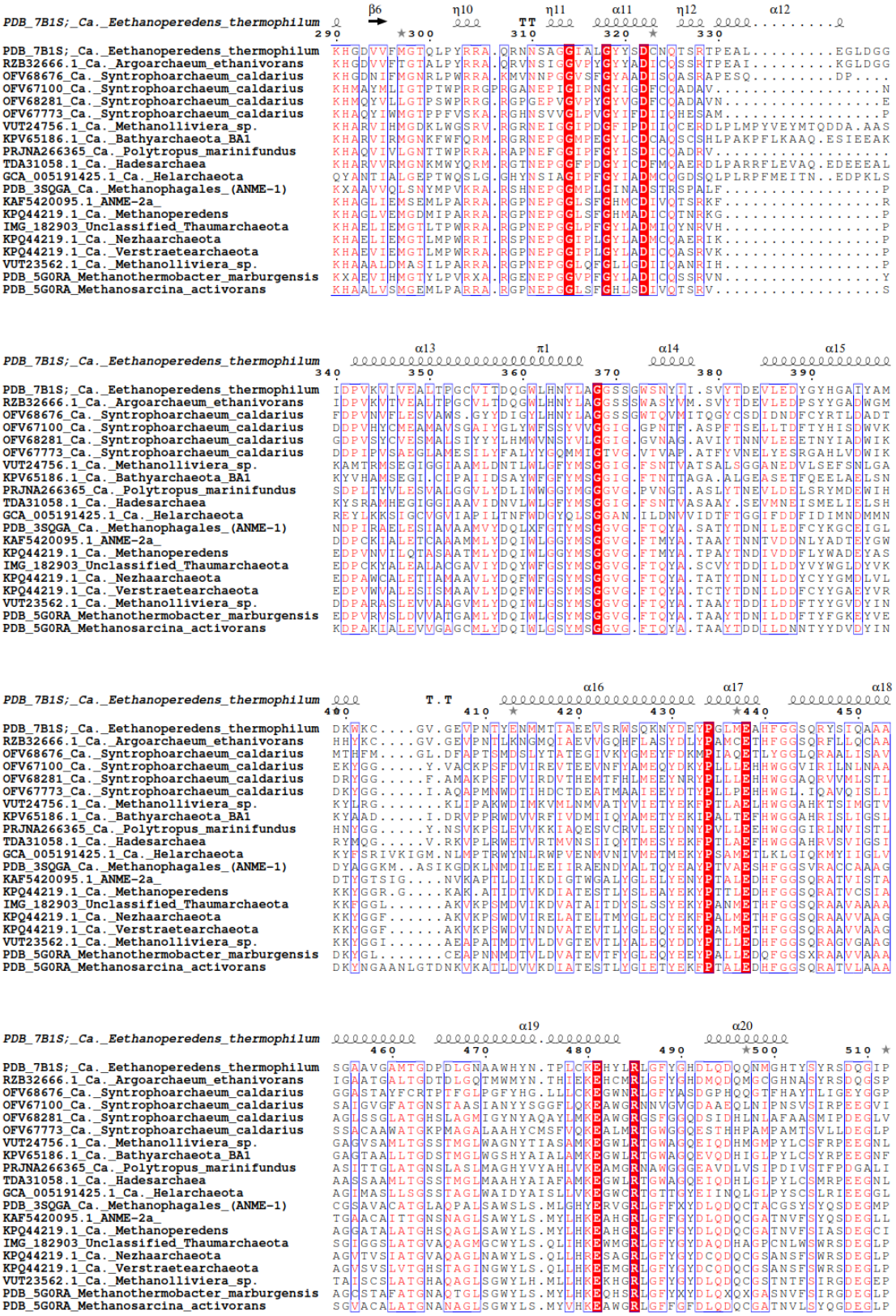
PDB_7B1S;_Ca._Eethanoperedens_thermophilum
PDB_7B1S;_Ca._Eethanoperedens_thermophilum
RZB32666.1_Ca._Argoarchaeum_ethanivorans
OFV68676_Ca._Syntrophoarchaeum_caldarius
OFV67100_Ca._Syntrophoarchaeum_caldarius
OFV68281_Ca._Syntrophoarchaeum_caldarius
OFV67773_Ca._Syntrophoarchaeum_caldarius
VUT24756.1_Ca._Methanolliviera_sp.
KPV65186.1_Ca._Bathyarchaeota_BA1
PRJNA266365_Ca._Polytropus_marinifundus
TDA31058.1_Ca._Hadesarchaea
GCA_005191425.1_Ca._Helarchaeota
PDB_3SQGA_Ca._Methanophagales_(ANME-1)
KAF5420095.1_ANME-2a_
KPQ44219.1_Ca._Methanoperedens
IMG_182903_Unclassified_Thaumarchaeota
KPQ44219.1_Ca._Nezhaarchaeota
KPQ44219.1_Ca._Verstraetearchaeota
VUT23562.1_Ca._Methanolliviera_sp.
PDB_5G0RA_Methanothermobacter_marburgensis
PDB_5G0RA_Methanosarcina_activorans

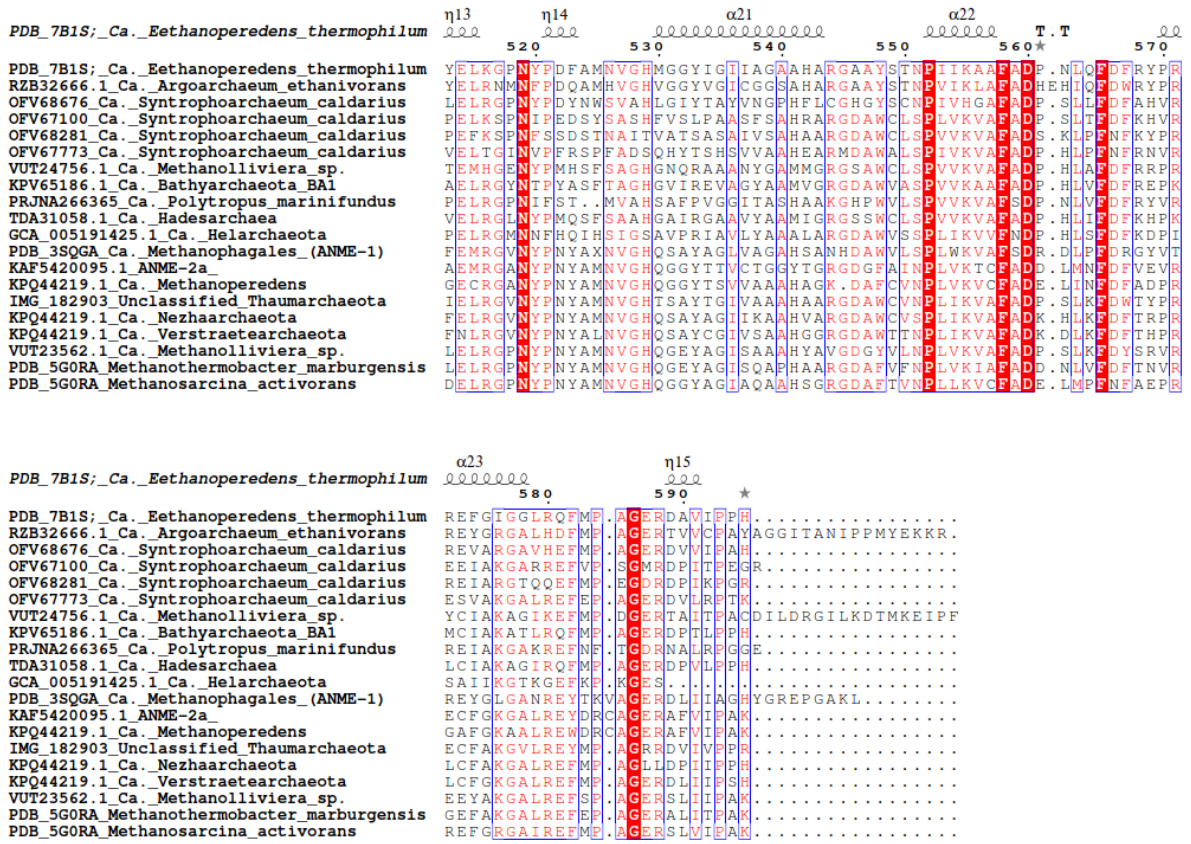

Figure 6-1 ESPript 3.0 alignment of ECR/MCR homologs containing canonical and non-canonical sequences as an addition to Figure 5-1. PDB number or NCBI protein_id provided next to species name if available. Otherwise, a reference to NCBI project is provided.

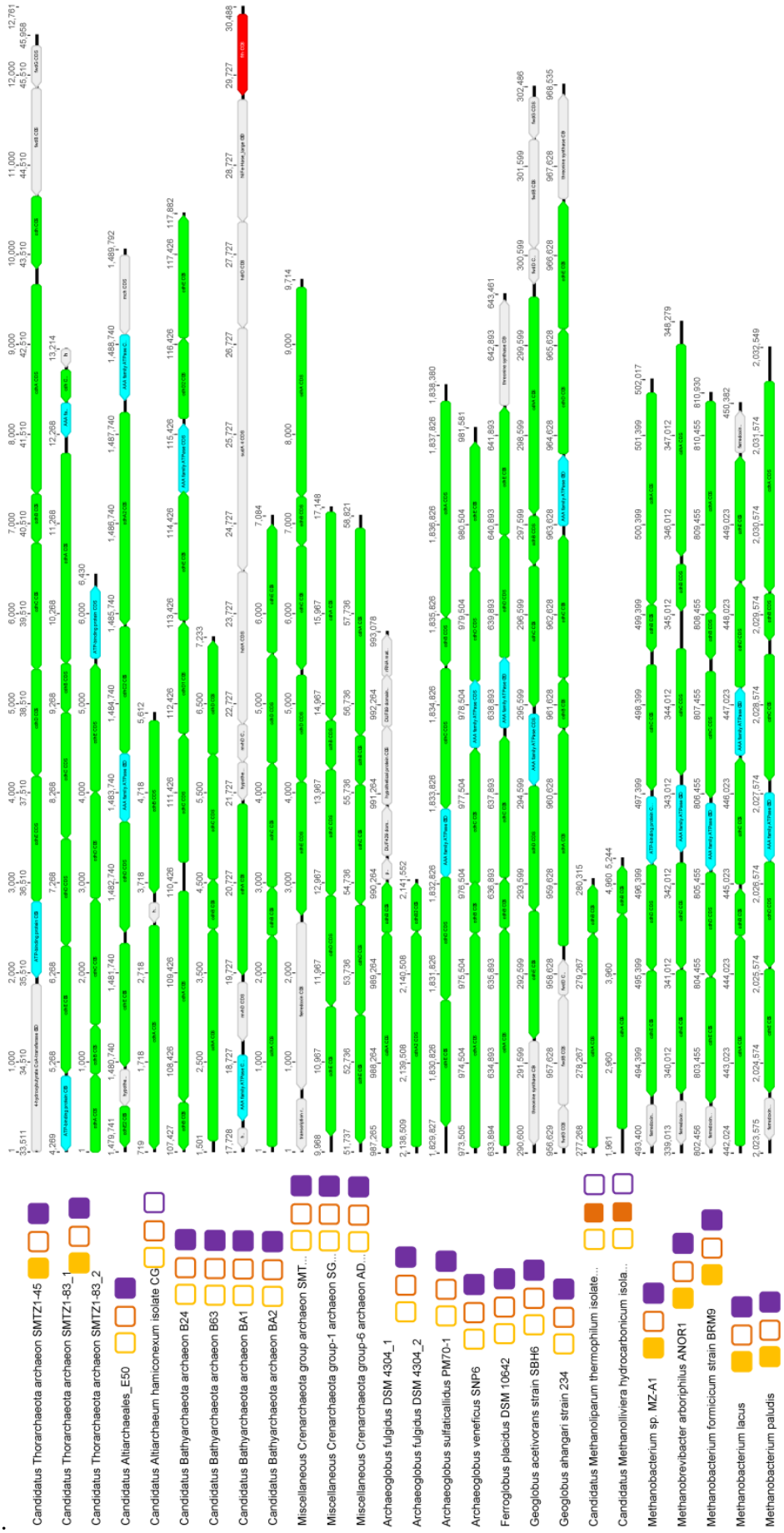
Candidatus Thorarchaeota archaeon SMTZ1-45
Candidatus Thorarchaeota archaeon SMTZ1-83_1
Candidatus Thorarchaeota archaeon SMTZ1-83_2
Candidatus Altiarchaeales_E50
Candidatus Altiarchaeum hamiconexum isolate CG
Candidatus Bathyarchaeota archaeon B24
Candidatus Bathyarchaeota archaeon B63
Candidatus Bathyarchaeota archaeon BA1
Candidatus Bathyarchaeota archaeon BA2
Miscellaneous Crenarchaeota group archaeon SMT...
Miscellaneous Crenarchaeota group-1 archaeon SG...
Miscellaneous Crenarchaeota group-6 archaeon AD...
Archaeoglobus fulgidus DSM 4304_1
Archaeoglobus fulgidus DSM 4304_2
Archaeoglobus sulfaticallidus PM70-1
Archaeoglobus veneficus SNP6
Ferroglobus placidus DSM 10642
Geoglobus acetivorans strain SBH6
Geoglobus ahangari strain 234
Candidatus Methanoliparum thermophilum isolate...
Candidatus Methanoliviera hydrocarbonicum isola...
Methanobacterium sp. MZ-A1
Methanobrevibacter arboriphilus ANOR1
Methanobacterium formicicum strain BRM9
Methanobacterium lacus
Methanobacterium paludis

Appendix

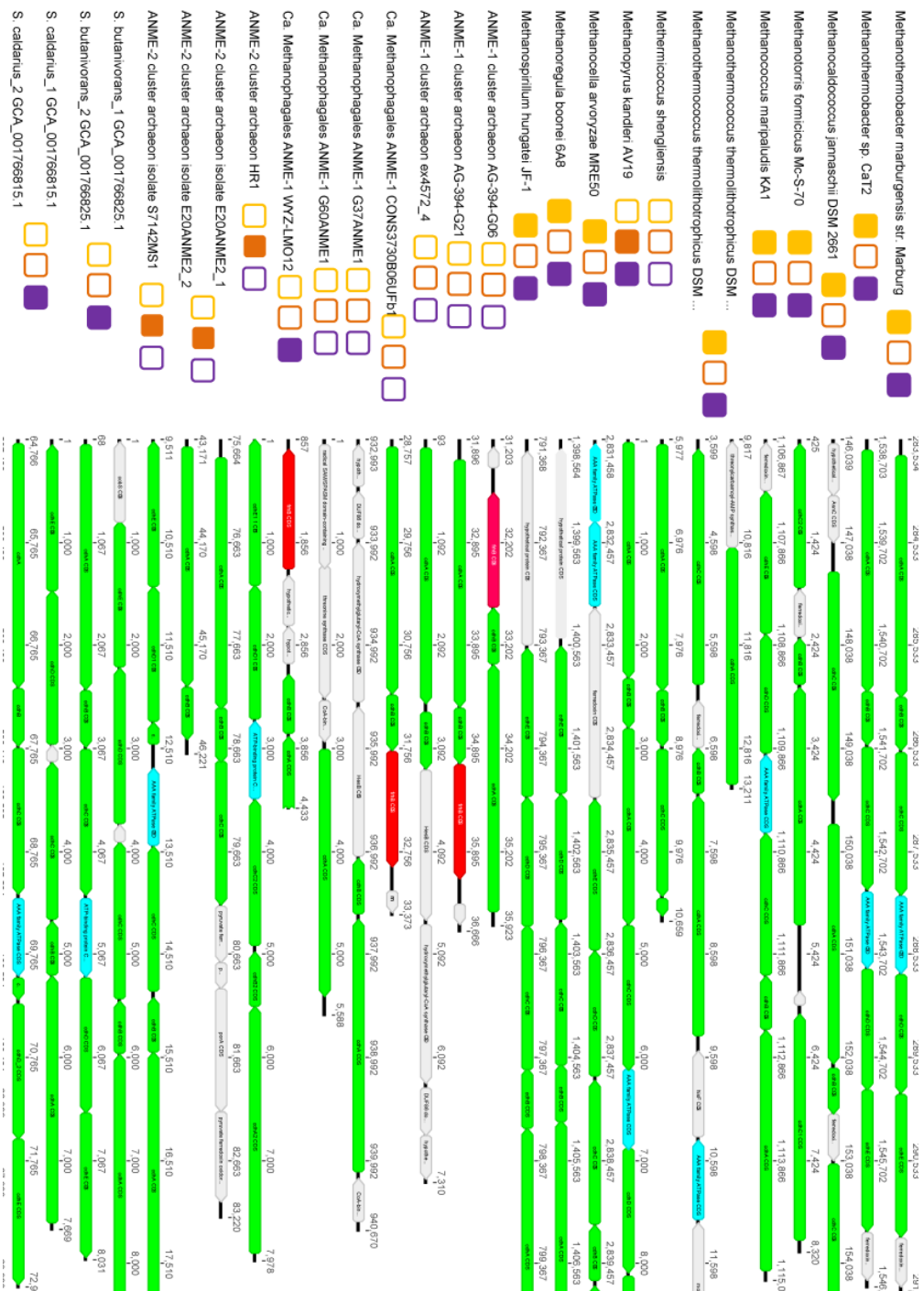
Methanothermobacter marburgensis str. Marburg
Methanothermobacter sp. CaT2
Methanocaldococcus jannaschii DSM 2661
Methanotorris formicicus Mc-S-70
Methanococcus maripaludis KA1
Methanothermococcus thermolithotrophicus DSM ...
Methanothermococcus thermolithotrophicus DSM ...
Methermicoccus shengliensis
Methanopyrus kandleri AV19
Methanocella arvoryzae MRE50
Methanoregula boonei 6A8
Methanospirillum hungatei JF-1
ANME-1 cluster archaeon AG-394-G06
ANME-1 cluster archaeon AG-394-G21
ANME-1 cluster archaeon ex4572_4
Ca. Methanophagales ANME-1 CONS3730B06UFB1
Ca. Methanophagales ANME-1 G37ANME1
Ca. Methanophagales ANME-1 G60ANME1
Ca. Methanophagales ANME-1 WYZ-LMO12
ANME-2 cluster archaeon HR1
ANME-2 cluster archaeon isolate E20ANME2_1
ANME-2 cluster archaeon isolate E20ANME2_2
ANME-2 cluster archaeon isolate S7142MS1
S. butanivorans_1 GCA_001766825.1
S. butanivorans_2 GCA_001766825.1
S. caldarius_1 GCA_001766815.1
S. caldarius_2 GCA_001766815.1

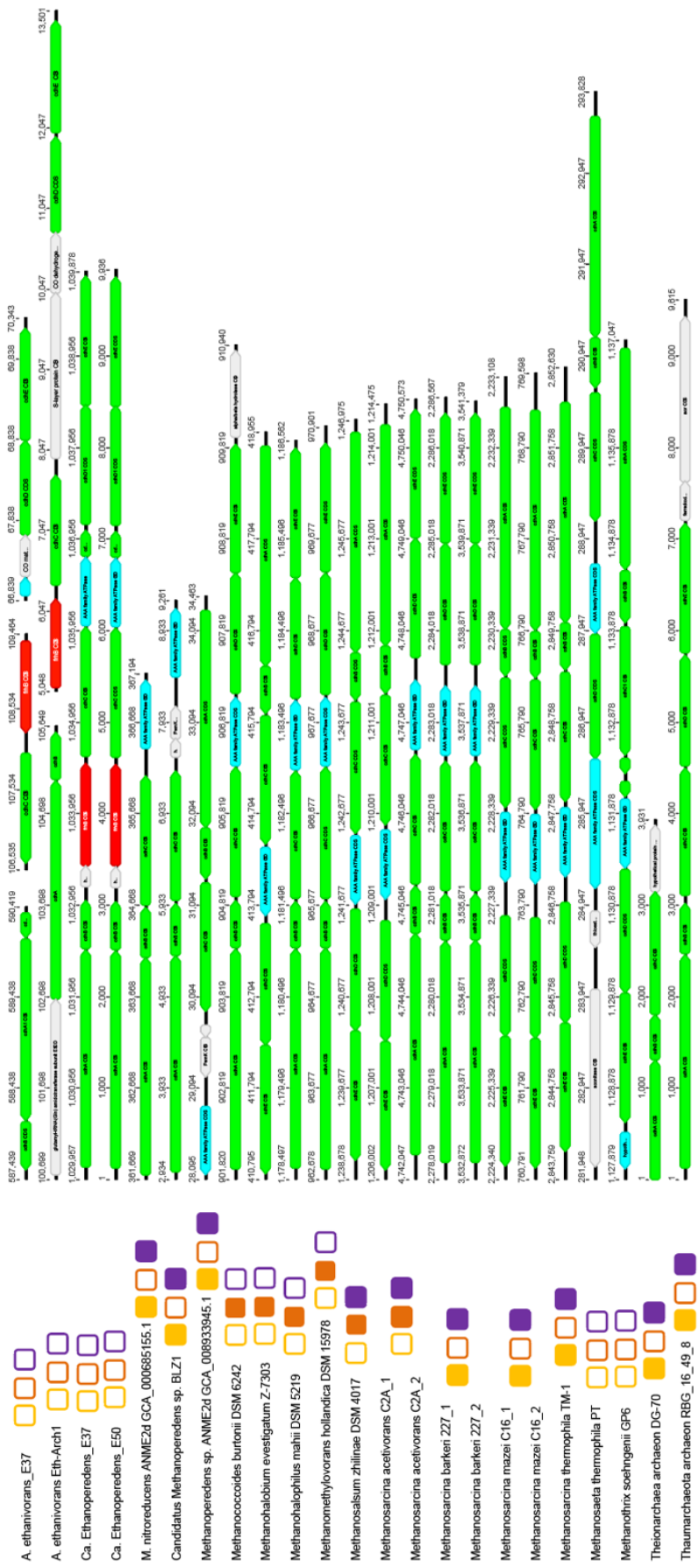

Figure 6-2 Energy conserving complexes and gene map of operons containing *cdh* subunits coding for the CODH in diverse methanogens and alkanotrophs. Color code for gene prediction: *cdhABCDE* (green), ATPases (blue) and frhB (red). Presence (filled box) absence (empty box) scheme for energy conserving complexes: Energy conserving hydrogenas (Ech; yellow), ferredoxin:NAD+-oxidoreductase (Rnf, orange) and (Ni-Fe)-hydrogenases (purple).

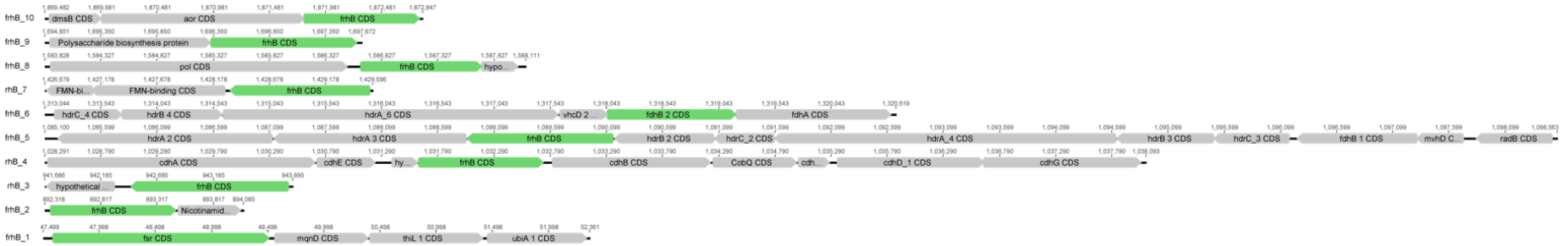

Figure 6-3 Gene map of F_{420}-reductase (*frh*) gene containing operons in *Ca.* Ethanoperedens. Color code for gene prediction: *frhB* (green) and other genes are depicted in grey.

References

Abascal, F., Zardoya, R. and Telford, M. J. (2010). "TranslatorX: multiple alignment of nucleotide sequences guided by amino acid translations." *Nucleic Acids Research* **38**: W7-W13. doi: 10.1093/nar/gkq291

Acosta-González, A., Rosselló-Móra, R. and Marqués, S. (2013). "Diversity of benzylsuccinate synthase-like (bssA) genes in hydrocarbon-polluted marine sediments suggests substrate-dependent clustering." *Applied and Environmental Microbiology* **79**(12): 3667-3676. doi: 10.1128/AEM.03934-12

Adam, P. S., Borrel, G., Brochier-Armanet, C. and Gribaldo, S. (2017). "The growing tree of Archaea: New perspectives on their diversity, evolution and ecology." *The ISME Journal* **11**(11): 2407-2425. doi: 10.1038/ismej.2017.122

Adams, M. M., Hoarfrost, A. L., Bose, A., Joye, S. B. and Girguis, P. R. (2013). "Anaerobic oxidation of short-chain alkanes in hydrothermal sediments: potential influences on sulfur cycling and microbial diversity." *Frontiers in Microbiology* **4**: 110. doi: 10.3389/fmicb.2013.00110

Aeckersberg, F., Bak, F. and Widdel, F. (1991). "Anaerobic oxidation of saturated hydrocarbons to CO_2 by a new type of sulfate-reducing bacterium." *Archives of Microbiology* **156**(1): 5-14. doi: 10.1007/BF00418180

Aeckersberg, F., Rainey, F. A. and Widdel, F. (1998). "Growth, natural relationships, cellular fatty acids and metabolic adaptation of sulfate-reducing bacteria that utilize long-chain alkanes under anoxic conditions." *Archives of Microbiology* **170**(5): 361-369. doi: 10.1007/s002030050654

Altschul, S. F., Madden, T. L., Schäffer, A. A., Zhang, J., Zhang, Z., Miller, W. and Lipman, D. J. (1997). "Gapped BLAST and PSI-BLAST: a new generation of protein database search programs." *Nucleic Acids Research* **25**(17): 3389–3402. doi: 10.1093/nar/25.17.3389

Amann, R. I., Krumholz, L. and Stahl, D. A. (1990). "Fluorescent-oligonucleotide probing of whole cells for determinative, phylogenetic, and evironmental studies in microbiology." *Journal of Bacteriology* **172**(2): 762-770. doi: 10.1128/jb.172.2.762-770.1990

Andersson, A. F., Lundgren, M., Eriksson, S., Rosenlund, M., Bernander, R. and Nilsson, P. (2006). "Global analysis of mRNA stability in the archaeon Sulfolobus." *Genome Biology* **7**(10): R99. doi: 10.1186/gb-2006-7-10-r99

Archer, D., Buffett, B. and Brovkin, V. (2009). "Ocean methane hydrates as a slow tipping point in the global carbon cycle." *Proceedings of the National Academy of Sciences* **106**(49): 20596-20601. doi: 10.1073/pnas.0800885105

Arshad, A., Speth, D. R., de Graaf, R. M., Op den Camp, H. J. M., Jetten, M. S. M. and Welte, C. U. (2015). "A Metagenomics-Based Metabolic Model of Nitrate-Dependent Anaerobic Oxidation of Methane by Methanoperedens-Like Archaea." *Frontiers in Microbiology* **6**. doi: 10.3389/Fmicb.2015.01423

Barnes, R. O. and Goldberg, E. D. (1976). "Methane production and consumption in anoxic marine sediments." *Geology* **4**(5): 297-300. doi: 10.1130/0091-7613(1976)4<297:MPACIA>2.0.CO;2

Barrero-Canosa, J., Moraru, C., Zeugner, L., Fuchs, B. M. and Amann, R. (2017). "Direct-geneFISH: a simplified protocol for the simultaneous detection and quantification of genes and rRNA in microorganisms." *Environmental Microbiology* **19**(1): 70-82. doi: 10.1111/1462-2920.13432

Basen, M., Schut, G. J., Nguyen, D. M., Lipscomb, G. L., Benn, R. A., Prybol, C. J., Vaccaro, B. J., Poole, F. L., Kelly, R. M. and Adams, M. W. (2014). "Single gene insertion drives bioalcohol production by a

thermophilic archaeon." *Proceedings of the National Academy of Sciences* **111**(49): 17618-17623. doi: 10.1073/pnas.1413789111

Baumberger, T., Früh-Green, G. L., Thorseth, I. H., Lilley, M. D., Hamelin, C., Bernasconi, S. M., Okland, I. E. and Pedersen, R. B. (2016). "Fluid composition of the sediment-influenced Loki's Castle vent field at the ultra-slow spreading Arctic Mid-Ocean Ridge." *Geochimica et Cosmochimica Acta* **187**: 156-178. doi: 10.1016/j.gca.2016.05.017

Bäumer, S., Ide, T., Jacobi, C., Johann, A., Gottschalk, G. and Deppenmeier, U. (2000). "The $F_{420}H_2$ Dehydrogenase from *Methanosarcina mazei* Is a Redox-driven Proton Pump Closely Related to NADH Dehydrogenases." *Journal of Biological Chemistry* **275**(24): 17968-17973. doi: 10.1074/jbc.M000650200

Bengtsson-Palme, J., Hartmann, M., Eriksson, K. M., Pal, C., Thorell, K., Larsson, D. G. and Nilsson, R. H. (2015). "METAXA2: improved identification and taxonomic classification of small and large subunit rRNA in metagenomic data." *Molecular Ecology Resources* **15**(6): 1403-1414. doi: 10.1111/1755-0998.12399

Bennke, C. M., Reintjes, G., Schattenhofer, M., Ellrott, A., Wulf, J., Zeder, M., Fuchs, B. M. and Spormann, A. M. (2016). "Modification of a High-Throughput Automatic Microbial Cell Enumeration System for Shipboard Analyses." *Applied and Environmental Microbiology* **82**(11): 3289-3296. doi: doi:10.1128/AEM.03931-15

Berdugo-Clavijo, C. and Gieg, L. M. (2014). "Conversion of crude oil to methane by a microbial consortium enriched from oil reservoir production waters." *Frontiers in Microbiology* **5**: 197. doi: 10.3389/fmicb.2014.00197

Berghuis, B. A., Yu, F. B., Schulz, F., Blainey, P. C., Woyke, T. and Quake, S. R. (2019). "Hydrogenotrophic methanogenesis in archaeal phylum Verstraetearchaeota reveals the shared ancestry of all methanogens." *Proceedings of the National Academy of Sciences* **116**(11): 5037-5044. doi: 10.1073/pnas.1815631116

Bernard, B. B., Brooks, J. M. and Sackett, W. M. (1976). "Natural gas seepage in the Gulf of Mexico." *Earth and Planetary Science Letters* **31**(1): 48-54. doi: 10.1016/0012-821X(76)90095-9

Berthold, C. L., Toyota, C. G., Richards, N. G. and Lindqvist, Y. (2008). "Reinvestigation of the catalytic mechanism of formyl-CoA transferase, a class III CoA-transferase." *Journal of Biological Chemistry* **283**(10): 6519-6529. doi: 10.1074/jbc.M709353200

Boetius, A., Ravenschlag, K., Schubert, C., Rickert, D., Widdel, F., Gieseke, A., Amann, R., Jørgensen, B. B., Witte, U. and Pfannkuche, O. (2000). "A marine microbial consortium apparently mediating anaerobic oxidation of methane." *Nature* **407**: 623-626. doi: 10.1038/35036572

Bohrmann, G., Greinert, J., Suess, E. and Torres, M. (1998). "Authigenic carbonates from the Cascadia subduction zone and their relation to gas hydrate stability." *Geology* **26**(7): 647-650. doi: 10.1130/0091-7613(1998)026<0647:acftcs>2.3.co;2

Bohrmann, G. and Schenck, S. (2003). "RV SONNE cruise report SO174." *GEOMAR Report* **117**: 1-130. doi: 10.3289/GEOMAR_REP_117_2003.

Bohrmann, G., Spiess, V. and Participants, C. (2008). "Report and preliminary results of R/V Meteor Cruise M67/2a and 2b, Balboa—Tampico—Bridgetown, 15 March–24 April, 2006. Fluid seepage in the Gulf of Mexico." *Berichte, Fachbereich Geowissenschaften, Universität Bremen*(263): 1-119. issn: 0931-0800

Borrel, G., Adam, P. S., McKay, L. J., Chen, L. X., Sierra-García, I. N., Sieber, C. M. K., Letourneur, Q., Ghozlane, A., Andersen, G. L., Li, W. J., Hallam, S. J., Muyzer, G., de Oliveira, V. M., Inskeep, W. P., Banfield, J. F. and Gribaldo, S. (2019). "Wide diversity of methane and short-chain alkane metabolisms in uncultured archaea." *Nature Microbiology* **4**: 603–613. doi: 10.1038/s41564-019-0363-3

Bose, A., Rogers, D. R., Adams, M. M., Joye, S. B. and Girguis, P. R. (2013). "Geomicrobiological linkages between short-chain alkane consumption and sulfate reduction rates in seep sediments." *Frontiers in Microbiology* **4**. doi: 10.3389/fmicb.2013.00386

Boucher, O., Friedlingstein, P., Collins, B. and Shine, K. P. (2009). "The indirect global warming potential and global temperature change potential due to methane oxidation." *Environmental Research Letters* **4**(4): 044007. doi: 10.1088/1748-9326/4/4/044007

Bowles, M. W., Samarkin, V. A., Bowles, K. M. and Joye, S. B. (2011). "Weak coupling between sulfate reduction and the anaerobic oxidation of methane in methane-rich seafloor sediments during ex situ incubation." *Geochimica et Cosmochimica Acta* **75**(2): 500-519. doi: 10.1016/j.gca.2010.09.043

Boyd, J. A., Jungbluth, S. P., Leu, A. O., Evans, P. N., Woodcroft, B. J., Chadwick, G. L., Orphan, V. J., Amend, J. P., Rappé, M. S. and Tyson, G. W. (2019). "Divergent methyl-coenzyme M reductase genes in a deep-subseafloor Archaeoglobi." *The ISME Journal* **13**: 1269–1279. doi: 10.1038/s41396-018-0343-2

Bricogne, G., Blanc, E., Brandl, M., Flensburg, C., Keller, P., Paciorek, W., Roversi, P., Sharff, A. and S SO, V. (2017). "BUSTER version 2.10.3." *Cambridge, United Kingdom: Global Phasing Ltd.* doi: globalphasing.com/buster/

Brüning, M., Sahling, H., MacDonald, I. R., Ding, F. and Bohrmann, G. (2010). "Origin, distribution, and alteration of asphalts at Chapopote Knoll, Southern Gulf of Mexico." *Marine and Petroleum Geology* **27**(5): 1093-1106. doi: 10.1016/j.marpetgeo.2009.09.005

Cai, C., Leu, A. O., Xie, G. J., Guo, J., Feng, Y., Zhao, J. X., Tyson, G. W., Yuan, Z. and Hu, S. (2018). "A methanotrophic archaeon couples anaerobic oxidation of methane to Fe(III) reduction." *The ISME Journal* **12**(8): 1929-1939. doi: 10.1038/s41396-018-0109-x

Callaghan, A. V., Davidova, I. A., Savage-Ashlock, K., Parisi, V. A., Gieg, L. M., Suflita, J. M., Kukor, J. J. and Wawrik, B. (2010). "Diversity of benzyl- and alkylsuccinate synthase genes in hydrocarbon-impacted environments and enrichment cultures." *Environmental Science and Technology* **44**(19): 7287-7294. doi: 10.1021/es1002023

Chabrière, E., Charon, M. H., Volbeda, A., Pieulle, L., Hatchikian, E. C. and Fontecilla–Camps, J. C. (1999). "Crystal structures of the key anaerobic enzyme pyruvate:ferredoxin oxidoreductase, free and in complex with pyruvate." *Nature Structural Biology* **6**(2): 182-190. doi: 10.1038/5870

Chan, L. Y., Mugler, C. F., Heinrich, S., Vallotton, P. and Weis, K. (2018). "Non-invasive measurement of mRNA decay reveals translation initiation as the major determinant of mRNA stability." *eLife* **7**: e32536. doi: 10.7554/eLife.32536

Chen, S.-L., Blomberg, M. R. A. and Siegbahn, P. E. M. (2012). "How Is Methane Formed and Oxidized Reversibly When Catalyzed by Ni-Containing Methyl-Coenzyme M Reductase?" *Chemistry – A European Journal* **18**(20): 6309-6315. doi: 10.1002/chem.201200274

Chen, S. C., Musat, N., Lechtenfeld, O. J., Paschke, H., Schmidt, M., Said, N., Popp, D., Calabrese, F., Stryhanyuk, H., Jaekel, U., Zhu, Y. G., Joye, S. B., Richnow, H. H., Widdel, F. and Musat, F. (2019). "Anaerobic oxidation of ethane by archaea from a marine hydrocarbon seep." *Nature* **568**(7750): 108-111. doi: 10.1038/s41586-019-1063-0

Chen, V. B., Arendall, W. B., Headd, J. J., Keedy, D. A., Immormino, R. M., Kapral, G. J., Murray, L. W., Richardson, J. S. and Richardson, D. C. (2010). "MolProbity: all-atom structure validation for macromolecular crystallography." *Acta Crystallographica Section D: Biological Crystallography* **66**(1): 12-21. doi: 10.1107/S0907444909042073

Chovancova, E., Pavelka, A., Benes, P., Strnad, O., Brezovsky, J., Kozlikova, B., Gora, A., Sustr, V., Klvana, M. and Medek, P. (2012). "CAVER 3.0: a tool for the analysis of transport pathways in dynamic protein structures." *PLOS Computational Biology* **8**(10): e1002708. doi: 10.1371/journal.pcbi.1002708

Clark, J. F., Washburn, L., Hornafius, J. S. and Luyendyk, B. P. (2000). "Dissolved hydrocarbon flux from natural marine seeps to the southern California Bight." *Journal of Geophysical Research: Oceans* **105**(C5): 11509-11522. doi: 10.1029/2000JC000259.

Cord-Ruwisch, R. (1985). "A quick method for the determination of dissolved and precipitated sulfides in cultures of sulfate-reducing bacteria." *Journal of Microbiological Methods* **4**(1): 33–36. doi: 10.1016/0167-7012(85)90005-3

Costa, K. C., Yoon, S. H., Pan, M., Burn, J. A., Baliga, N. S. and Leigh, J. A. (2013). "Effects of H_2 and Formate on Growth Yield and Regulation of Methanogenesis in *Methanococcus maripaludis*." *Journal of Bacteriology* **195**(7): 1456-1462. doi: doi:10.1128/JB.02141-12

Cronshaw, M. (2021). Natural Gas. *Energy in Perspective*. Cham, Springer International Publishing**:** 105-122. doi: 10.1007/978-3-030-63541-1_5

Cross, R. L. and Müller, V. (2004). "The evolution of A-, F-, and V-type ATP synthases and ATPases: reversals in function and changes in the H^+/ATP coupling ratio." *FEBS Letters* **576**: 1-4. doi: 10.1016/j.febslet.2004.08.065

Daims, H., Brühl, A., Amann, R. and Schleifer, K. H. (1999). "The domain-specific probe EUB338 is insufficient for the detection of all Bacteria: Development and evaluation of a more comprehensive probe set." *Systematic and Applied Microbiology* **22**(3): 434-444. doi: 10.1016/S0723-2020(99)80053-8

Diepenbroek, M., Glöckner, F. O., Grobe, P., Güntsch, A., Huber, R., König-Ries, B., Kostadinov, I., Nieschulze, J., Seeger, B. and Tolksdorf, R. (2014). "Towards an integrated biodiversity and ecological research data management and archiving platform: the German federation for the curation of biological data (GFBio)." *Informatik 2014*: 1711-1721. issn: 1617-5468

Dombrowski, N., Seitz, K. W., Teske, A. P. and Baker, B. J. (2017). "Genomic insights into potential interdependencies in microbial hydrocarbon and nutrient cycling in hydrothermal sediments." *Microbiome* **5**(1): 106. doi: 10.1186/s40168-017-0322-2

Dombrowski, N., Teske, A. P. and Baker, B. J. (2018). "Expansive microbial metabolic versatility and biodiversity in dynamic Guaymas Basin hydrothermal sediments." *Nature Communications* **9**(1): 4999. doi: 10.1038/s41467-018-07418-0

Dong, X., Rattray, J. E., Campbell, D. C., Webb, J., Chakraborty, A., Adebayo, O., Matthews, S., Li, C., Fowler, M., Morrison, N. M., MacDonald, A., Groves, R. A., Lewis, I. A., Wang, S. H., Mayumi, D., Greening, C. and Hubert, C. R. J. (2020). "Thermogenic hydrocarbon biodegradation by diverse depth-stratified microbial populations at a Scotian Basin cold seep." *Nature Communications* **11**(1): 1-14. doi: 10.1038/s41467-020-19648-2

Dowell, F., Cardman, Z., Dasarathy, S., Kellermann, M. Y., Lipp, J. S., Ruff, S. E., Biddle, J. F., McKay, L. J., MacGregor, B. J., Lloyd, K. G., Albert, D. B., Mendlovitz, H., Hinrichs, K. U. and Teske, A. (2016). "Microbial communities in methane- and short chain alkane-rich hydrothermal sediments of Guaymas Basin." *Frontiers in Microbiology* **7**: 17. doi: 10.3389/fmicb.2016.00017

Dupré, S., Buffet, G., Mascle, J., Foucher, J. P., Gauger, S., Boetius, A., Marfia, C., Team, A. s. t. e. r. X. A. U. V., Team, Q. u. e. s. t. R. O. V. and Scientific party, B. I. O. N. I. L. (2008). "High-resolution mapping of large gas emitting mud volcanoes on the Egyptian continental margin (Nile Deep Sea Fan) by AUV surveys." *Marine Geophysical Research* **29**(4): 275-290. doi: 10.1007/s11001-009-9063-3

Embree, M., Nagarajan, H., Movahedi, N., Chitsaz, H. and Zengler, K. (2014). "Single-cell genome and metatranscriptome sequencing reveal metabolic interactions of an alkane-degrading methanogenic community." *The ISME Journal* **8**(4): 757-767. doi: 10.1038/ismej.2013.187

Emsley, P., Lohkamp, B., Scott, W. G. and Cowtan, K. (2010). "Features and development of Coot." *Acta Crystallographica Section D: Biological Crystallography* **66**(4): 486-501. doi: 10.1107/S0907444910007493

Eren, A. M., Esen, O. C., Quince, C., Vineis, J. H., Morrison, H. G., Sogin, M. L. and Delmont, T. O. (2015). "Anvi'o: an advanced analysis and visualization platform for 'omics data." *PeerJ* **3**: e1319. doi: 10.7717/peerj.1319

Ermler, U., Grabarse, W., Shima, S., Goubeaud, M. and Thauer, R. K. (1997). "Crystal Structure of Methyl-Coenzyme M Reductase: The Key Enzyme of Biological Methane Formation." *Science* **278**(5342): 1457-1462. doi: 10.1126/science.278.5342.1457

Etiope, G., Christodoulou, D., Kordella, S., Marinaro, G. and Papatheodorou, G. (2013). "Offshore and onshore seepage of thermogenic gas at Katakolo Bay (Western Greece)." *Chemical Geology* **339**: 115-126. doi: 10.1016/j.chemgeo.2012.08.011

Etiope, G. and Ciccioli, P. (2009). "Earth's Degassing: A Missing Ethane and Propane Source." *Science* **323**(5913): 478-478. doi: 10.1126/science.1165904

Etiope, G. and Klusman, R. W. (2002). "Geologic emissions of methane to the atmosphere." *Chemosphere* **49**(8): 777-789. doi: 10.1016/S0045-6535(02)00380-6

Ettwig, K. F., Zhu, B., Speth, D., Keltjens, J. T., Jetten, M. S. M. and Kartal, B. (2016). "Archaea catalyze iron-dependent anaerobic oxidation of methane." *Proceedings of the National Academy of Sciences of the United States of America* **113**(45): 12792-12796. doi: 10.1073/pnas.1609534113

Evans, P. N., Boyd, J. A., Leu, A. O., Woodcroft, B. J., Parks, D. H., Hugenholtz, P. and Tyson, G. W. (2019). "An evolving view of methane metabolism in the Archaea." *Nature Reviews Microbiology* **17**: 219–232. doi: 10.1038/s41579-018-0136-7

Evans, P. N., Parks, D. H., Chadwick, G. L., Robbins, S. J., Orphan, V. J., Golding, S. D. and Tyson, G. W. (2015). "Methane metabolism in the archaeal phylum Bathyarchaeota revealed by genome-centric metagenomics." *Science* **350**(6259): 434-438. doi: 10.1126/science.aac7745

Forster, P., Ramaswamy, V., Artaxo, P., Berntsen, T., Betts, R., Fahey, D. W., Haywood, J., Lean, J., Lowe, D. C. and Myhre, G. (2007). Changes in atmospheric constituents and in radiative forcing. *Climate change 2007. The physical science basis*. United Kingdom, Cambridge University Press.**:** 129-234. issn: 978-0521-70596-7

Frias-Lopez, J., Shi, Y., Tyson, G. W., Coleman, M. L., Schuster, S. C., Chisholm, S. W. and DeLong, E. F. (2008). "Microbial community gene expression in ocean surface waters." *Proceedings of the National Academy of Sciences of the United States of America* **105**(10): 3805-3810. doi: 10.1073/pnas.0708897105

German, C. R., Lin, J. and Parson, L. M. (2004). "Mid-ocean ridges: Hydrothermal interactions between the lithosphere and oceans." *Washington DC American Geophysical Union Geophysical Monograph Series* **148**: 318. doi: 10.1029/GM148

German, C. R., Ramirez-Llodra, E., Baker, M. C., Tyler, P. A. and Committee, C. S. S. (2011). "Deep-water chemosynthetic ecosystem research during the census of marine life decade and beyond: a proposed deep-ocean road map." *PLOS ONE* **6**(8): e23259. doi: 10.1371/journal.pone.0023259

Glockner, F. O., Yilmaz, P., Quast, C., Gerken, J., Beccati, A., Ciuprina, A., Bruns, G., Yarza, P., Peplies, J., Westram, R. and Ludwig, W. (2017). "25 years of serving the community with ribosomal RNA gene reference databases and tools." *Journal of Biotechnology* **261**: 169-176. doi: 10.1016/j.jbiotec.2017.06.1198

Grabarse, W., Mahlert, F., Duin, E. C., Goubeaud, M., Shima, S., Thauer, R. K., Lamzin, V. and Ermler, U. (2001). "On the mechanism of biological methane formation: structural evidence for conformational changes in methyl-coenzyme M reductase upon substrate binding11Edited by R. Huber." *Journal of Molecular Biology* **309**(1): 315-330. doi: 10.1006/jmbi.2001.4647

Grabarse, W., Mahlert, F., Shima, S., Thauer, R. K. and Ermler, U. (2000). "Comparison of three methyl-coenzyme M reductases from phylogenetically distant organisms: unusual amino acid modification, conservation and adaptation." *Journal of Molecular Biology* **303**(2): 329-344. doi: 10.1006/jmbi.2000.4136

Grant, N. J. and Whiticar, M. J. (2002). "Stable carbon isotopic evidence for methane oxidation in plumes above Hydrate Ridge, Cascadia Oregon Margin." *Global Biogeochemical Cycles* **16**(4): 1124. doi: 10.1029/2001GB001851

Green-Saxena, A., Dekas, A. E., Dalleska, N. F. and Orphan, V. J. (2014). "Nitrate-based niche differentiation by distinct sulfate-reducing bacteria involved in the anaerobic oxidation of methane." *The ISME Journal* **8**(1): 150-163. doi: 10.1038/ismej.2013.147

Gruber-Vodicka, H. R., Seah, B. K. and Pruesse, E. (2020). "phyloFlash: Rapid Small-Subunit rRNA Profiling and Targeted Assembly from Metagenomes." *mSystems* **5**(5): e00920-00920. doi: 10.1128/mSystems.00920-20

Grundmann, O., Behrends, A., Rabus, R., Amann, J., Halder, T., Heider, J. and Widdel, F. (2008). "Genes encoding the candidate enzyme for anaerobic activation of *n*-alkanes in the denitrifying bacterium, strain HxN1." *Environmental Microbiology* **10**(2): 376-385. doi: 10.1111/j.1462-2920.2007.01458.x

Gunsalus, R. P., Romesser, J. A. and Wolfe, R. S. (1978). "Preparation of coenzyme M analogs and their activity in the methyl coenzyme M reductase system of Methanobacterium thermoautotrophicum." *Biochemistry* **17**(12): 2374-2377. doi: 10.1021/bi00605a019

Hagedoorn, P. L., Chen, T., Schröder, I., Piersma, S. R., Vries, S. d. and Hagen, W. R. (2005). "Purification and characterization of the tungsten enzyme aldehyde:ferredoxin oxidoreductase from the hyperthermophilic denitrifier Pyrobaculum aerophilum." *JBIC Journal of Biological Inorganic Chemistry* **10**(3): 259-269. doi: 10.1007/s00775-005-0637-5

Hahn, C. J., Laso-Pérez, R., Vulcano, F., Vaziourakis, K. M., Stokke, R., Steen, I. H., Teske, A., Boetius, A., Liebeke, M., Amann, R., Knittel, K. and Wegener, G. (2020). "“Candidatus Ethanoperedens,” a Thermophilic Genus of Archaea Mediating the Anaerobic Oxidation of Ethane." *mBio* **11**(2): e00600-00620. doi: 10.1128/mBio.00600-20

Hahn, C. J., Lemaire, O. N., Kahnt, J., Engilberge, S., Wegener, G. and Wagner, T. (2021). "Crystal structure of a key enzyme for anaerobic ethane activation." *Science* **373**(6550): 118-121. doi: 10.1126/science.abg1765

Hahn, C. J., Lemaire, O. N., Kahnt, J., Engilberge, S., Wegener, G. and Wagner, T. (2021). "X-ray crystallography and mass spectrometry raw and processed data accompanying the manuscript “Crystal structure of a key enzyme for anaerobic ethane activation”. Zenodo." doi: doi:10.5281/zenodo.4835784

Hallam, S. J., Putnam, N., Preston, C. M., Detter, J. C., Rokhsar, D., Richardson, P. M. and DeLong, E. F. (2004). "Reverse Methanogenesis: Testing the Hypothesis with Environmental Genomics." *Science* **305**(5689): 1457-1462. doi: 10.1126/science.1100025

Harmer, J., Finazzo, C., Piskorski, R., Bauer, C., Jaun, B., Duin, E. C., Goenrich, M., Thauer, R. K., Van Doorslaer, S. and Schweiger, A. (2005). "Spin Density and Coenzyme M Coordination Geometry of the ox1 Form of Methyl-Coenzyme M Reductase: A Pulse EPR Study." *Journal of the American Chemical Society* **127**(50): 17744-17755. doi: 10.1021/ja053794w

Harmer, J., Finazzo, C., Piskorski, R., Ebner, S., Duin, E. C., Goenrich, M., Thauer, R. K., Reiher, M., Schweiger, A., Hinderberger, D. and Jaun, B. (2008). "A Nickel Hydride Complex in the Active Site of Methyl-Coenzyme M Reductase: Implications for the Catalytic Cycle." *Journal of the American Chemical Society* **130**(33): 10907-10920. doi: 10.1021/ja710949e

Haroon, M. F., Hu, S., Shi, Y., Imelfort, M., Keller, J., Hugenholtz, P., Yuan, Z. and Tyson, G. W. (2013). "Anaerobic oxidation of methane coupled to nitrate reduction in a novel archaeal lineage." *Nature* **500**(7464): 567-570. doi: 10.1038/nature12375

Harris, R. L., Vetter, M. C. Y. L., van Heerden, E., Cason, E., Vermeulen, J.-G., Taneja, A., Kieft, T. L., DeCoste, C. J., Laevsky, G. S. and Onstott, T. C. (2021). "FISH-TAMB, a Fixation-Free mRNA Fluorescent

Labeling Technique to Target Transcriptionally Active Members in Microbial Communities." *Microbial Ecology*. doi: 10.1007/s00248-021-01809-5

Hatzenpichler, R., Connon, S. A., Goudeau, D., Malmstrom, R. R., Woyke, T. and Orphan, V. J. (2016). "Visualizing in situ translational activity for identifying and sorting slow-growing archaeal–bacterial consortia." *Proceedings of the National Academy of Sciences* **113**(28): E4069-E4078. doi: 10.1073/pnas.1603757113

He, X., Chadwick, G., Kempes, C., Shi, Y., McGlynn, S., Orphan, V. and Meile, C. (2019). "Microbial interactions in the anaerobic oxidation of methane: model simulations constrained by process rates and activity patterns." *Environmental Microbiology* **21**(2): 631-647. doi: 10.1111/1462-2920.14507

He, X., Chadwick, G. L., Kempes, C. P., Orphan, V. J. and Meile, C. (2021). "Controls on Interspecies Electron Transport and Size Limitation of Anaerobically Methane-Oxidizing Microbial Consortia." *mBio* **12**(3): e03620-03620. doi: 10.1128/mBio.03620-20

Heider, J. (2001). "A new family of CoA-transferases." *FEBS Letters* **509**(3): 345-349. doi: 10.1016/S0014-5793(01)03178-7

Heider, J., Ma, K. and Adams, M. W. (1995). "Purification, characterization, and metabolic function of tungsten-containing aldehyde ferredoxin oxidoreductase from the hyperthermophilic and proteolytic archaeon Thermococcus strain ES-1." *Journal of Bacteriology* **177**(16): 4757-4764. doi: 10.1128/jb.177.16.4757-4764.1995

Heider, J., Szaleniec, M., Sünwoldt, K. and Boll, M. (2016). "Ethylbenzene Dehydrogenase and Related Molybdenum Enzymes Involved in Oxygen-Independent Alkyl Chain Hydroxylation." *Microbial Physiology* **26**(1-3): 45-62. doi: 10.1159/000441357

Hendrickson, E. L., Haydock, A. K., Moore, B. C., Whitman, W. B. and Leigh, J. A. (2007). "Functionally distinct genes regulated by hydrogen limitation and growth rate in methanogenic Archaea." *Proceedings of the National Academy of Sciences* **104**(21): 8930-8934. doi: 10.1073/pnas.0701157104

Hendrickson, E. L., Liu, Y., Rosas-Sandoval, G., Porat, I., Söll, D., Whitman, W. B. and Leigh, J. A. (2008). "Global responses of Methanococcus maripaludis to specific nutrient limitations and growth rate." *Journal of Bacteriology* **190**(6): 2198-2205. doi: 10.1128/JB.01805-07

Herlemann, D. P. R., Labrenz, M., Jurgens, K., Bertilsson, S., Waniek, J. J. and Andersson, A. F. (2011). "Transitions in bacterial communities along the 2000 km salinity gradient of the Baltic Sea." *The ISME Journal* **5**(10): 1571-1579. doi: 10.1038/ismej.2011.41

Hinderberger, D., Piskorski, R. P., Goenrich, M., Thauer, R. K., Schweiger, A., Harmer, J. and Jaun, B. (2006). "A Nickel–Alkyl Bond in an Inactivated State of the Enzyme Catalyzing Methane Formation." *Angewandte Chemie* **118**(22): 3684-3689. doi: 10.1002/ange.200600366

Hinrichs, K.-U. and Boetius, A. (2002). The anaerobic oxidation of methane: New insights in microbial ecology and biogeochemistry. *Ocean Margin Systems* G. Wefer, D. Billett, D. Hebbeln et al. Berlin Heidelberg, Springer-Verlag**:** 457-477. doi: 10.1007/978-3-662-05127-6_28

Hinrichs, K.-U., Hayes, J. M., Bach, W., Spivack, A. J., Hmelo, L. R., Holm, N. G., Johnson, C. G. and Sylva, S. P. (2006). "Biological formation of ethane and propane in the deep marine subsurface." *Proceedings of the National Academy of Sciences* **103**(40): 14684-14689. doi: 10.1073/pnas.0606535103

Hinrichs, K. U., Hayes, J. M., Sylva, S. P., Brewer, P. G. and DeLong, E. F. (1999). "Methane-consuming archaebacteria in marine sediments." *Nature* **398**: 802-805. doi: 10.1038/19751

Ho, B. K. and Gruswitz, F. (2008). "HOLLOW: Generating Accurate Representations of Channel and Interior Surfaces in Molecular Structures." *BMC Structural Biology* **8**(1): 49. doi: 10.1186/1472-6807-8-49

Hodnebrog, Ø., Dalsøren, S. B. and Myhre, G. (2018). "Lifetimes, direct and indirect radiative forcing, and global warming potentials of ethane (C_2H_6), propane (C_3H_8), and butane (C_4H_{10})." *Atmospheric Science Letters* **19**(2): e804. doi: 10.1002/asl.804

Hoehler, T. M., Alperin, M. J., Albert, D. B. and Martens, C. S. (1994). "Field and laboratory studies of methane oxidation in an anoxic marine sediment: evidence for a methanogen-sulfate reducer consortium." *Global Biogeochemical Cycles* **8**(4): 451-464. doi: 10.1029/94GB01800

Holler, T., Wegener, G., Niemann, H., Deusner, C., Ferdelman, T. G., Boetius, A., Brunner, B. and Widdel, F. (2011). "Carbon and sulfur back flux during anaerobic microbial oxidation of methane and coupled sulfate reduction." *Proceedings of the National Academy of Sciences* **108**(52): E1484-E1490. doi: 10.1073/pnas.1106032108

Holler, T., Widdel, F., Knittel, K., Amann, R., Kellermann, M. Y., Hinrichs, K.-U., Teske, A., Boetius, A. and Wegener, G. (2011). "Thermophilic anaerobic oxidation of methane by marine microbial consortia." *The ISME Journal* **5**(12): 1946-1956. doi: 10.1038/ismej.2011.77

Hoshino, T., Yilmaz, L. S., Noguera, D. R., Daims, H. and Wagner, M. (2008). "Quantification of target molecules needed to by fluorescence in situ hybridization (FISH) and catalyzed reporter deposition-FISH." *Applied and Environmental Microbiology* **74**(16): 5068-5077. doi: 10.1128/AEM.00208-08

Hua, Z.-S., Wang, Y.-L., Evans, P. N., Qu, Y.-N., Goh, K. M., Rao, Y.-Z., Qi, Y.-L., Li, Y.-X., Huang, M.-J., Jiao, J.-Y., Chen, Y.-T., Mao, Y.-P., Shu, W.-S., Hozzein, W., Hedlund, B. P., Tyson, G. W., Zhang, T. and Li, W.-J. (2019). "Insights into the ecological roles and evolution of methyl-coenzyme M reductase-containing hot spring Archaea." *Nature Communications* **10**(1): 4574. doi: 10.1038/s41467-019-12574-y

Huff, J. (2015). "The Airyscan detector from ZEISS: confocal imaging with improved signal-to-noise ratio and super-resolution." *Nature Methods* **12**(12): i-ii. doi: 10.1038/nmeth.f.388

Jaekel, U., Musat, N., Adam, B., Kuypers, M., Grundmann, O. and Musat, F. (2013). "Anaerobic degradation of propane and butane by sulfate-reducing bacteria enriched from marine hydrocarbon cold seeps." *The ISME Journal* **7**(5): 885-895. doi: 10.1038/ismej.2012.159

Jaekel, U., Vogt, C., Fischer, A., Richnow, H.-H. and Musat, F. (2014). "Carbon and hydrogen stable isotope fractionation associated with the anaerobic degradation of propane and butane by marine sulfate-reducing bacteria." *Environmental Microbiology* **16**(1): 130-140. doi: 10.1111/1462-2920.12251

Johnson, M., Zaretskaya, I., Raytselis, Y., Merezhuk, Y., McGinnis, S. and Madden, T. L. (2008). "NCBI BLAST: a better web interface." *Nucleic Acids Research* **36**: W5-9. doi: 10.1093/nar/gkn201

Joye, S. B., Boetius, A., Orcutt, B. N., Montoya, J. P., Schulz, H. N., Erickson, M. J. and Lugo, S. K. (2004). "The anaerobic oxidation of methane and sulfate reduction in sediments from Gulf of Mexico cold seeps." *Chemical Geology* **205**(3-4): 219-238. doi: 10.1016/j.chemgeo.2003.12.019

Judd, A. G. (2004). "Natural seabed gas seeps as sources of atmospheric methane." *Environmental Geology* **46**(8): 988-996. doi: 10.1007/s00254-004-1083-3

Kadnikov, V., Mardanov, A., Beletsky, A., Frank, Y., Karnachuk, O. and Ravin, N. (2019). "Genome of a member of the candidate archaeal phylum Verstraetearchaeota from a subsurface thermal aquifer revealed pathways of methyl-reducing methanogenesis and fermentative metabolism." *Microbiology* **88**(3): 316-323. doi: 10.1134/S0026261719030068

Kaneko, M., Takano, Y., Chikaraishi, Y., Ogawa, N. O., Asakawa, S., Watanabe, T., Shima, S., Krüger, M., Matsushita, M. and Kimura, H. (2014). "Quantitative analysis of coenzyme F_{430} in environmental samples: a new diagnostic tool for methanogenesis and anaerobic methane oxidation." *Analytical Chemistry* **86**(7): 3633-3638. doi: 10.1021/ac500305j

Karrasch, M., Bott, M. and Thauer, R. K. (1989). "Carbonic anhydrase activity in acetate grown Methanosarcina barkeri." *Archives of Microbiology* **151**(2): 137-142. doi: 10.1007/BF00414428

Keller, M. W., Lipscomb, G. L., Nguyen, D. M., Crowley, A. T., Schut, G. J., Scott, I., Kelly, R. M. and Adams, M. W. W. (2017). "Ethanol production by the hyperthermophilic archaeon Pyrococcus furiosus by expression of bacterial bifunctional alcohol dehydrogenases." *Microbial Biotechnology* **10**(6): 1535-1545. doi: 10.1111/1751-7915.12486

Kelley, D. S., Baross, J. A. and Delaney, J. R. (2002). "Volcanoes, fluids, and life at mid-ocean ridge spreading centers." *Annual Review of Earth and Planetary Sciences* **30**: 385-491. doi: 10.1146/annurev.earth.30.091201.141331

Khelifi, N., Amin Ali, O., Roche, P., Grossi, V., Brochier-Armanet, C., Valette, O., Ollivier, B., Dolla, A. and Hirschler-Réa, A. (2014). "Anaerobic oxidation of long-chain n -alkanes by the hyperthermophilic sulfate-reducing archaeon, Archaeoglobus fulgidus." *The ISME Journal* **8**(11): 2153-2166. doi: 10.1038/ismej.2014.58

Kleindienst, S., Herbst, F.-A., Stagars, M., von Netzer, F., von Bergen, M., Seifert, J., Peplies, J., Amann, R., Musat, F., Lueders, T. and Knittel, K. (2014). "Diverse sulfate-reducing bacteria of the *Desulfosarcina/Desulfococcus* clade are the key alkane degraders at marine seeps." *The ISME Journal* **8**(10): 2029-2044. doi: 10.1038/ismej.2014.51

Kleindienst, S., Ramette, A., Amann, R. and Knittel, K. (2012). "Distribution and in situ abundance of sulfate-reducing bacteria in diverse marine hydrocarbon seep sediments." *Environmental Microbiology* **14**(10): 2689-2710. doi: 10.1111/j.1462-2920.2012.02832.x

Kniemeyer, O., Musat, F., Sievert, S. M., Knittel, K., Wilkes, H., Blumenberg, M., Michaelis, W., Classen, A., Bolm, C., Joye, S. B. and Widdel, F. (2007). "Anaerobic oxidation of short-chain hydrocarbons by marine sulphate-reducing bacteria." *Nature* **449**(7164): 898-910. doi: 10.1038/nature06200

Knittel, K. and Boetius, A. (2009). "Anaerobic oxidation of methane: progress with an unknown process." *Annual Review of Microbiology* **63**: 311-334. doi: 10.1146/annurev.micro.61.080706.093130

Knittel, K., Lösekann, T., Boetius, A., Kort, R. and Amann, R. (2005). "Diversity and distribution of methanotrophic archaea at cold seeps." *Applied and Environmental Microbiology* **71**(1): 467-479. doi: 10.1128/AEM.71.1.467-479.2005

Krüger, M., Meyerdierks, A., Glöckner, F. O., Amann, R., Widdel, F., Kube, M., Reinhardt, R., Kahnt, J., Bocher, R., Thauer, R. K. and Shima, S. (2003). "A conspicuous nickel protein in microbial mats that oxidize methane anaerobically." *Nature* **426**(6968): 878-881. doi: 10.1038/nature02207

Krukenberg, V., Harding, K., Richter, M., Glöckner, F. O., Gruber-Vodicka, H. R., Adam, B., Berg, J. S., Knittel, K., Tegetmeyer, H. E., Boetius, A. and Wegener, G. (2016). "Candidatus Desulfofervidus auxilii, a hydrogenotrophic sulfate-reducing bacterium involved in the thermophilic anaerobic oxidation of methane." *Environmental Microbiology* **18**(9): 3073-3091. doi: 10.1111/1462-2920.13283

Krukenberg, V., Riedel, D., Gruber-Vodicka, H. R., Buttigieg, P. L., Tegetmeyer, H. E., Boetius, A. and Wegener, G. (2018). "Gene expression and ultrastructure of meso- and thermophilic methanotrophic consortia." *Environmental Microbiology* **20**(5): 1651-1666. doi: 10.1111/1462-2920.14077

Kvenvolden, K. (1995). "A review of the geochemistry of methane in natural gas hydrate." *Organic Geochemistry* **23**(11-12): 997 - 1008. doi: 10.1016/0146-6380(96)00002-2

Kvenvolden, K. A. (1993). "Gas hydrates - geological perspective and global change." *Reviews of Geophysics* **31**(2): 173-187. doi: 10.1029/93RG00268

Larkin, M. A., Blackshields, G., Brown, N. P., Chenna, R., McGettigan, P. A., McWilliam, H., Valentin, F., Wallace, I. M., Wilm, A., Lopez, R., Thompson, J. D., Gibson, T. J. and Higgins, D. G. (2007). "Clustal W and Clustal X version 2.0." *Bioinformatics* **23**(21): 2947-2948. doi: 10.1093/bioinformatics/btm404

Laso-Pérez, R., Hahn, C., Vliet, D. M. v., Tegetmeyer, H. E., Schubotz, F., Smit, N. T., Pape, T., Sahling, H., Bohrmann, G., Boetius, A., Knittel, K. and Wegener, G. (2019). "Anaerobic Degradation of Non-Methane Alkanes by "Candidatus Methanoliparia" in Hydrocarbon Seeps of the Gulf of Mexico." *mBio* **10**(4): e01814-01819. doi: 10.1128/mBio.01814-19

Laso-Pérez, R., Krukenberg, V., Musat, F. and Wegener, G. (2018). "Establishing anaerobic hydrocarbon-degrading enrichment cultures of microorganisms under strictly anoxic conditions." *Nature Protocols* **13**(6): 1310-1330. doi: 10.1038/nprot.2018.030

Laso-Pérez, R., Wegener, G., Knittel, K., Widdel, F., Harding, K. J., Krukenberg, V., Meier, D. V., Richter, M., Tegetmeyer, H. E., Riedel, D., Richnow, H. H., Adrian, L., Reemtsma, T., Lechtenfeld, O. J. and Musat, F. (2016). "Thermophilic archaea activate butane via alkyl-CoM formation." *Nature* **539**: 396–401. doi: 10.1038/nature20152

Lemaire, O. N., Infossi, P., Chaouche, A. A., Espinosa, L., Leimkühler, S., Giudici-Orticoni, M.-T., Méjean, V. and Iobbi-Nivol, C. (2018). "Small membranous proteins of the TorE/NapE family, crutches for cognate respiratory systems in Proteobacteria." *Scientific Reports* **8**(1): 1-13. doi: 10.1038/s41598-018-31851-2

Letunic, I. and Bork, P. (2007). "Interactive Tree Of Life (iTOL): an online tool for phylogenetic tree display and annotation." *Bioinformatics* **23**(1): 127-128. doi: 10.1093/bioinformatics/btl529

Letunic, I. and Bork, P. (2016). "Interactive tree of life (iTOL) v3: an online tool for the display and annotation of phylogenetic and other trees." *Nucleic Acids Research* **44**(W1): W242-W245. doi: 10.1093/nar/gkw290

Leu, A. O., Cai, C., McIlroy, S. J., Southam, G., Orphan, V. J., Yuan, Z., Hu, S. and Tyson, G. W. (2020). "Anaerobic methane oxidation coupled to manganese reduction by members of the Methanoperedenaceae." *The ISME Journal* **14**(4): 1030-1041. doi: 10.1038/s41396-020-0590-x

Leu, A. O., McIlroy, S. J., Ye, J., Parks, D. H., Orphan, V. J., Tyson, G. W. and Bailey, M. J. (2020). "Lateral Gene Transfer Drives Metabolic Flexibility in the Anaerobic Methane-Oxidizing Archaeal Family *Methanoperedenaceae*." *mBio* **11**(3): e01325-01320. doi: doi:10.1128/mBio.01325-20

Liebschner, D., Afonine, P. V., Baker, M. L., Bunkóczi, G., Chen, V. B., Croll, T. I., Hintze, B., Hung, L.-W., Jain, S. and McCoy, A. J. (2019). "Macromolecular structure determination using X-rays, neutrons and electrons: recent developments in Phenix." *Acta Crystallographica Section D: Structural Biology* **75**(10): 861-877. doi: 10.1107/S2059798319011471

Linke, P. and Suess, E. (2001). "RV SONNE cruise Report SO148." *GEOMAR Report* **98**: 122. doi: 10.3289/geomar_rep_98_2001

Liu, Y.-F., Chen, J., Zaramela, L. S., Wang, L.-Y., Mbadinga, S. M., Hou, Z.-W., Wu, X.-L., Gu, J.-D., Zengler, K., Mu, B.-Z. and Lloyd, K. G. (2020). "Genomic and Transcriptomic Evidence Supports Methane Metabolism in Archaeoglobi." *mSystems* **5**(2): e00651-00619. doi: doi:10.1128/mSystems.00651-19

Lloyd, K. G., Lapham, L. and Teske, A. (2006). "An anaerobic methane-oxidizing community of ANME-1b archaea in hypersaline Gulf of Mexico sediments." *Applied and Environmental Microbiology* **72**(11): 7218-7230. doi: 10.1128/AEM.00886-06

Lonsdale, P. and Becker, K. (1985). "Hydrothermal plumes, hot springs, and conductive heat flow in the Southern Trough of Guaymas Basin." *Earth and Planetary Science Letters* **73**(2-4): 211-225. doi: 10.1016/0012-821X(85)90070-6

Lösekann, T., Knittel, K., Nadalig, T., Fuchs, B., Niemann, H., Boetius, A. and Amann, R. (2007). "Diversity and abundance of aerobic and anaerobic methane oxidizers at the Haakon Mosby Mud Volcano, Barents Sea." *Applied and Environmental Microbiology* **73**(10): 3348-3362. doi: 10.1128/aem.00016-07

Loy, A., Lehner, A., Lee, N., Adamczyk, J., Meier, H., Ernst, J., Schleifer, K.-H. and Wagner, M. (2002). "Oligonucleotide microarray for 16S rRNA gene-based detection of all recognized lineages of sulfate-reducing prokaryotes in the environment." *Applied and Environmental Microbiology* **68**(10): 5064-5081. doi: 10.1128/AEM.68.10.5064-5081.2002

Lu, H., Seo, Y.-t., Lee, J.-w., Moudrakovski, I., Ripmeester, J. A., Chapman, N. R., Coffin, R. B., Gardner, G. and Pohlman, J. (2007). "Complex gas hydrate from the Cascadia margin." *Nature* **445**(7125): 303-306. doi: 10.1038/nature05463

Ludwig, W., Strunk, O., Westram, R., Richter, L., Meier, H., Yadhukumar, Buchner, A., Lai, T., Steppi, S., Jobb, G., Förster, W., Brettske, I., Gerber, S., Ginhart, A. W., Gross, O., Grumann, S., Hermann, S., Jost, R., König, A., Liss, T., Lüßmann, R., May, M., Nonhoff, B., Reichel, B., Strehlow, R., Stamatakis, A., Stuckmann, N., Vilbig, A., Lenke, M., Ludwig, T., Bode, A. and Schleifer, K. H. (2004). "ARB: a software environment for sequence data." *Nucleic Acids Research* **32**(4): 1363-1371. doi: 10.1093/nar/gkh293

Manz, W., Eisenbrecher, M., Neu, T. R. and Szewzyk, U. (1998). "Abundance and spatial organization of gram negative sulfate-reducing bacteria in activated sludge investigated by in situ probing with specific 16S rRNA targeted oligonucleotides." *FEMS Microbiology Ecology* **25**(1): 43-61. doi: 10.1111/j.1574-6941.1998.tb00459.x

Martin, M. (2011). "Cutadapt removes adapter sequences from high-throughput sequencing reads." *EMBnet.journal* **17**(1). doi: 10.14806/ej.17.1.200

Martinez, R. J., Mills, H. J., Story, S. and Sobecky, P. A. (2006). "Prokaryotic diversity and metabolically active microbial populations in sediments from an active mud volcano in the Gulf of Mexico." *Environmental Microbiology* **8**(10): 1783-1796. doi: 10.1111/j.1462-2920.2006.01063.x

Mastalerz, V., de Lange, G. J. and Dählmann, A. (2009). "Differential aerobic and anaerobic oxidation of hydrocarbon gases discharged at mud volcanoes in the Nile deep-sea fan." *Geochimica et Cosmochimica Acta* **73**(13): 3849-3863. doi: 10.1016/j.gca.2008.12.030

Mayr, S., Latkoczy, C., Krüger, M., Günther, D., Shima, S., Thauer, R. K., Widdel, F. and Jaun, B. (2008). "Structure of an F_{430} variant from archaea associated with anaerobic oxidation of methane." *Journal of the American Chemical Society* **130**(32): 10758-10767. doi: 10.1021/ja802929z

McGlynn, S. E., Chadwick, G. L., Kempes, C. P. and Orphan, V. J. (2015). "Single cell activity reveals direct electron transfer in methanotrophic consortia." *Nature* **526**(7574): 531-535. doi: 10.1038/nature15512

McKay, L. J., Dlakić, M., Fields, M. W., Delmont, T. O., Eren, A. M., Jay, Z. J., Klingelsmith, K. B., Rusch, D. B. and Inskeep, W. P. (2019). "Co-occurring genomic capacity for anaerobic methane and dissimilatory sulfur metabolisms discovered in the Korarchaeota." *Nature Microbiology* **4**(4): 614-622. doi: 10.1038/s41564-019-0362-4

McMillen, D. F. and Golden, D. M. (1982). "Hydrocarbon Bond Dissociation Energies." *Annual Review of Physical Chemistry* **33**(1): 493-532. doi: 10.1146/annurev.pc.33.100182.002425

Metcalfe, K. S., Murali, R., Mullin, S. W., Connon, S. A. and Orphan, V. J. (2021). "Experimentally-validated correlation analysis reveals new anaerobic methane oxidation partnerships with consortium-level heterogeneity in diazotrophy." *The ISME Journal* **15**(2): 377-396. doi: 10.1038/s41396-020-00757-1

Meyer, S., Wegener, G., Lloyd, K. G., Teske, A., Boetius, A. and Ramette, A. (2013). "Microbial habitat connectivity across spatial scales and hydrothermal temperature gradients at Guaymas Basin." *Frontiers in Microbiology* **4**: 207. doi: 10.3389/fmicb.2013.00207

Meyerdierks, A., Kube, M., Kostadinov, I., Teeling, H., Glöckner, F. O., Reinhardt, R. and Amann, R. (2010). "Metagenome and mRNA expression analyses of anaerobic methanotrophic archaea of the ANME-1 group." *Environmental Microbiology* **12**(2): 422-439. doi: 10.1111/j.1462-2920.2009.02083.x

Michaelis, W., Seifert, R., Nauhaus, K., Treude, T., Thiel, V., Blumenberg, M., Knittel, K., Gieseke, A., Peterknecht, K., Pape, T., Boetius, A., Amann, R., Jørgensen, B. B., Widdel, F., Peckmann, J., Pimenov, N. V. and Gulin, M. B. (2002). "Microbial reefs in the Black Sea fueled by anaerobic oxidation of methane." *Science* **297**: 1013-1015. doi: 10.1126/science.1072502

Miller, D. V. and Booker, S. J. (2019). "The expanding role of methyl-coenzyme m reductase in the anaerobic functionalization of alkanes." *Biochemistry* **58**(42): 4269-4271. doi: 10.1021/acs.biochem.9b00859

Mills, H. J., Hodges, C., Wilson, K., MacDonald, I. R. and Sobecky, P. A. (2003). "Microbial diversity in sediments associated with surface-breaching gas hydrate mounds in the Gulf of Mexico." *FEMS Microbiology Ecology* **46**(1): 39-52. doi: 10.1016/S0168-6496(03)00191-0

Mills, H. J., Martinez, R. J., Story, S. and Sobecky, P. A. (2004). "Identification of members of the metabolically active microbial populations associated with *Beggiatoa s*pecies mat communities from Gulf of Mexico cold seep sediments." *Applied and Environmental Microbiology* **70**(9): 5447-5458. doi: 10.1128/aem.70.9.5447-5458.2004

Mills, H. J., Martinez, R. J., Story, S. and Sobecky, P. A. (2005). "Characterization of microbial community structure in Gulf of Mexico gas hydrates: comparative analysis of DNA- and RNA-derived clone libraries." *Applied and Environmental Microbiology* **71**(6): 3235-3247. doi: 10.1128/aem.71.6.3235-3247.2005

Milucka, J., Ferdelman, T. G., Polerecky, L., Franzke, D., Wegener, G., Schmid, M., Lieberwirth, I., Wagner, M., Widdel, F. and Kuypers, M. M. M. (2012). "Zero-valent sulphur is a key intermediate in marine methane oxidation." *Nature* **491**(7425): 541-546. doi: 10.1038/nature11656

Moore, S. J., Sowa, S. T., Schuchardt, C., Deery, E., Lawrence, A. D., Ramos, J. V., Billig, S., Birkemeyer, C., Chivers, P. T. and Howard, M. J. (2017). "Elucidation of the biosynthesis of the methane catalyst coenzyme F_{430}." *Nature* **543**(7643): 78-82. doi: 10.1038/nature21427

Moraru, C., Moraru, G., Fuchs, B. M. and Amann, R. (2011). "Concepts and software for a rational design of polynucleotide probes." *Environmental Microbiology Reports* **3**(1): 69-78. doi: 10.1111/j.1758-2229.2010.00189.x

Nauhaus, K., Albrecht, M., Elvert, M., Boetius, A. and Widdel, F. (2007). "In vitro cell growth of marine archaeal-bacterial consortia during anaerobic oxidation of methane with sulfate." *Environmental Microbiology* **9**(1): 187-196. doi: 10.1111/j.1462-2920.2006.01127.x

Nauhaus, K., Boetius, A., Krüger, M. and Widdel, F. (2002). "*In vitro* demonstration of anaerobic oxidation of methane coupled to sulphate reduction in sediment from a marine gas hydrate area." *Environmental Microbiology* **4**(5): 296-305. doi: 10.1046/j.1462-2920.2002.00299.x

Niemann, H., Lösekann, T., de Beer, D., Elvert, M., Nadalig, T., Knittel, K., Amann, R., Sauter, E. J., Schlüter, M., Klages, M., Foucher, J. P. and Boetius, A. (2006). "Novel microbial communities of the Håkon Mosby mud volcano and their role as a methane sink." *Nature* **443**(7113): 854-858. doi: 10.1038/Nature05227

Nolan, T., Hands, R. E. and Bustin, S. A. (2006). "Quantification of mRNA using real-time RT-PCR." *Nature Protocols* **1**(3): 1559-1582. doi: 10.1038/nprot.2006.236

Norville, G. A. and Dawe, R. A. (2007). "Carbon and hydrogen isotopic variations of natural gases in the southeast Columbus basin offshore southeastern Trinidad, West Indies – clues to origin and maturity." *Applied Geochemistry* **22**(9): 2086-2094. doi: 10.1016/j.apgeochem.2007.05.004

Nurk, S., Bankevich, A., Antipov, D., Gurevich, A. A., Korobeynikov, A., Lapidus, A., Prjibelski, A. D., Pyshkin, A., Sirotkin, A., Sirotkin, Y., Stepanauskas, R., Clingenpeel, S. R., Woyke, T., McLean, J. S., Lasken, R., Tesler, G., Alekseyev, M. A. and Pevzner, P. A. (2013). "Assembling Single-Cell Genomes and Mini-Metagenomes From Chimeric MDA Products." *Journal of Computational Biology* **20**(10): 714-737. doi: 10.1089/cmb.2013.0084

Omoregie, E. O., Niemann, H., Mastalerz, V., de Lange, G. J., Stadnitskaia, A., Mascle, J., Foucher, J.-P. and Boetius, A. (2009). "Microbial methane oxidation and sulfate reduction at cold seeps of the deep Eastern Mediterranean Sea." *Marine Geology* **261**(1-4): 114-127. doi: 10.1016/j.margeo.2009.02.001

Orcutt, B., Joye, S. B., Kleindienst, S., Knittel, K., Ramette, A., Reitz, A., Samarkin, V., Treude, T. and Boetius, A. (2010). "Impact of natural oil and higher hydrocarbons on microbial diversity, distribution, and activity in Gulf of Mexico cold-seep sediments." *Deep Sea Research Part II: Topical Studies in Oceanography* **57**(21-23): 2008-2021. doi: 10.1016/j.dsr2.2010.05.014

Orcutt, B. and Meile, C. (2008). "Constraints on mechanisms and rates of anaerobic oxidation of methane by microbial consortia: process-based modeling of ANME-2 archaea and sulfate reducing bacteria interactions." *Biogeosciences* **5**: 1587-1599. doi: 10.5194/bg-5-1587-2008

Oremland, R. S. (1981). "Microbial formation of ethane in anoxic estuarine sediments." *Applied and Environmental Microbiology* **42**(1): 122-129. doi: 10.1128/aem.42.1.122-129.1981

Oremland, R. S. (2021). BUBBLES in the MUD: A Reminiscence and Perspective. *Microbes: The Foundation Stone of the Biosphere*. C. J. Hurst. Cham, Springer International Publishing**:** 637-652. doi: 10.1007/978-3-030-63512-1_30

Orphan, V. J., House, C. H., Hinrichs, K. U., McKeegan, K. D. and DeLong, E. F. (2001). "Methane-consuming archaea revealed by directly coupled isotopic and phylogenetic analysis." *Science* **293**(5529): 484-487. doi: DOI 10.1126/science.1061338

Parks, D. H., Imelfort, M., Skennerton, C. T., Hugenholtz, P. and Tyson, G. W. (2015). "CheckM: assessing the quality of microbial genomes recovered from isolates, single cells, and metagenomes." *Genome Research* **25**(7): 1043-1055. doi: 10.1101/gr.186072.114

Pedersen, R. B., Rapp, H. T., Thorseth, I. H., Lilley, M. D., Barriga, F. J., Baumberger, T., Flesland, K., Fonseca, R., Früh-Green, G. L. and Jorgensen, S. L. (2010). "Discovery of a black smoker vent field and vent fauna at the Arctic Mid-Ocean Ridge." *Nature Communications* **1**(126): 1-6. doi: 10.1038/ncomms1124.

Pelmenschikov, V. and Siegbahn, P. E. M. (2003). "Catalysis by methyl-coenzyme M reductase: a theoretical study for heterodisulfide product formation." *JBIC Journal of Biological Inorganic Chemistry* **8**(6): 653-662. doi: 10.1007/s00775-003-0461-8

Pernthaler, A. and Amann, R. (2004). "Simultaneous fluorescence in situ hybridization of mRNA and rRNA in environmental bacteria." *Applied and Environmental Microbiology* **70**(9): 5426-5433. doi: 10.1128/aem.70.9.5426-5433.2004

Pernthaler, A., Pernthaler, J. and Amann, R. (2002). "Fluorescence in situ hybridization and catalyzed reporter deposition for the identification of marine bacteria." *Applied and Environmental Microbiology* **68**(6): 3094-3101. doi: 10.1128/aem.68.6.3094-3101.2002

Prakash, D., Wu, Y., Suh, S.-J. and Duin, E. C. (2014). "Elucidating the Process of Activation of Methyl-Coenzyme M Reductase." *Journal of Bacteriology* **196**(13): 2491-2498. doi: 10.1128/JB.01658-14

Price, M. N., Dehal, P. S. and Arkin, A. P. (2010). "FastTree 2 – Approximately Maximum-Likelihood Trees for Large Alignments." *PLOS ONE* **5**(3): e9490. doi: 10.1371/journal.pone.0009490

Probandt, D., Eickhorst, T., Ellrott, A., Amann, R. and Knittel, K. (2018). "Microbial life on a sand grain: from bulk sediment to single grains." *The ISME Journal* **12**(2): 623-633. doi: 10.1038/ismej.2017.197

Pruesse, E., Peplies, J. and Glockner, F. O. (2012). "SINA: accurate high-throughput multiple sequence alignment of ribosomal RNA genes." *Bioinformatics* **28**(14): 1823-1829. doi: 10.1093/bioinformatics/bts252

Quast, C., Pruesse, E., Yilmaz, p., Gerken, J., Schweer, T., Yarza, P., Peplies, J. and Glöckner, F. O. (2012). "The SILVA ribosomal RNA gene database project: improved data processing and web-based tools." *Nucleic Acids Research* **41**: D590-596. doi: 10.1093/nar/gks1219

Quistad, S. D. and Valentine, D. L. (2011). "Anaerobic propane oxidation in marine hydrocarbon seep sediments." *Geochimica et Cosmochimica Acta* **75**(8): 2159-2169. doi: 10.1016/j.gca.2011.02.001

Rabus, R., Wilkes, H., Behrends, A., Armstroff, A., Fischer, T., Pierik, A. J. and Widdel, F. (2001). "Anaerobic initial reaction of *n*-alkanes in a denitrifying bacterium: evidence for (1-methylpentyl)succinate as initial product and for involvement of an organic radical in *n*-hexane metabolism." *Journal of Bacteriology* **183**(5): 1707-1715. doi: 10.1128/jb.183.5.1707-1715.2001

Radianingtyas, H. and Wright, P. C. (2003). "Alcohol dehydrogenases from thermophilic and hyperthermophilic archaea and bacteria." *FEMS Microbiology Reviews* **27**(5): 593-616. doi: 10.1016/S0168-6445(03)00068-8

Raghoebarsing, A. A., Pol, A., van de Pas-Schoonen, K. T., Smolders, A. J. P., Ettwig, K. F., Rijpstra, W. I. C., Schouten, S., Damsté, J. S. S., Op den Camp, H. J. M., Jetten, M. S. M. and Strous, M. (2006). "A microbial consortium couples anaerobic methane oxidation to denitrification." *Nature* **440**(7086): 918-921. doi: 10.1038/nature04617

Reeburgh, W. S. (1976). "Methane consumption in Cariaco Trench waters and sediments." *Earth and Planetary Science Letters* **28**(3): 337 - 344. doi: 10.1016/0012-821X(76)90195-3

Reeburgh, W. S. (2007). "Oceanic methane biogeochemistry." *Chemical Reviews* **107**(2): 486-513. doi: 10.1021/cr050362v

Reguera, G., McCarthy, K. D., Mehta, T., Nicoll, J. S., Tuominen, M. T. and Lovley, D. R. (2005). "Extracellular electron transfer via microbial nanowires." *Nature* **435**(7045): 1098-1101. doi: 10.1038/nature03661

Reichlen, M. J., Vepachedu, V. R., Murakami, K. S., Ferry, J. G. and Newman, D. K. (2012). "MreA Functions in the Global Regulation of Methanogenic Pathways in *Methanosarcina acetivorans*." *mBio* **3**(4): e00189-00112. doi: doi:10.1128/mBio.00189-12

Reid, M. F. and Fewson, C. A. (1994). "Molecular Characterization of Microbial Alcohol Dehydrogenases." *Critical Reviews in Microbiology* **20**(1): 13-56. doi: 10.3109/10408419409113545

Rinke, C., Schwientek, P., Sczyrba, A., Ivanova, N. N., Anderson, I. J., Cheng, J.-F., Darling, A., Malfatti, S., Swan, B. K., Gies, E. A., Dodsworth, J. A., Hedlund, B. P., Tsiamis, G., Sievert, S. M., Liu, W.-T., Eisen, J. A., Hallam, S. J., Kyrpides, N. C., Stepanauskas, R., Rubin, E. M., Hugenholtz, P. and Woyke, T. (2013). "Insights into the phylogeny and coding potential of microbial dark matter." *Nature* **499**(7459): 431-437. doi: 10.1038/nature12352

Robert, X. and Gouet, P. (2014). "Deciphering key features in protein structures with the new ENDscript server." *Nucleic Acids Research* **42**: W320-W324. doi: 10.1093/nar/gku316

Rodriguez-R, L. and Konstantinidis, K. (2016). "The enveomics collection: a toolbox for specialized analyses of microbial genomes and metagenomes." *PeerJ Preprints* **4**(e1900v1). doi: 10.7287/peerj.preprints.1900v1

Roh, Y., Liu, S. V., Li, G., Huang, H., Phelps, T. J. and Zhou, J. (2002). "Isolation and characterization of metal-reducing Thermoanaerobacter strains from deep subsurface environments of the Piceance Basin, Colorado." *Applied and Environmental Microbiology* **68**(12): 6013-6020. doi: 10.1128/AEM.68.12.6013-6020.2002

Römer, M., Torres, M., Kasten, S., Kuhn, G., Graham, A. G., Mau, S., Little, C. T., Linse, K., Pape, T. and Geprägs, P. (2014). "First evidence of widespread active methane seepage in the Southern Ocean, off the sub-Antarctic island of South Georgia." *Earth and Planetary Science Letters* **403**(1): 166-177. doi: 10.1016/j.epsl.2014.06.036

Rona, P. A., Klinkhammer, G., Nelsen, T. A., Trefry, J. H. and Elderfield, H. (1986). "Black smokers, massive sulphides and vent biota at the Mid-Atlantic Ridge." *Nature* **321**(6065): 33-37. doi: doi.org/10.1038/321033a0

Rouhanifard, S. H., Mellis, I. A., Dunagin, M., Bayatpour, S., Jiang, C. L., Dardani, I., Symmons, O., Emert, B., Torre, E., Cote, A., Sullivan, A., Stamatoyannopoulos, J. A. and Raj, A. (2019). "ClampFISH detects individual nucleic acid molecules using click chemistry–based amplification." *Nature Biotechnology* **37**(1): 84-94. doi: 10.1038/nbt.4286

Roy, R. and Adams, M. (2002). "Tungsten-dependent aldehyde oxidoreductase: a new family of enzymes containing the pterin cofactor." *Metal Ions in Biological Systems* **39**: 673-697. doi: 10.1201/9780203909331

Ruscic, B. (2015). "Active Thermochemical Tables: Sequential Bond Dissociation Enthalpies of Methane, Ethane, and Methanol and the Related Thermochemistry." *The Journal of Physical Chemistry A* **119**(28): 7810-7837. doi: 10.1021/acs.jpca.5b01346

Sahling, H., Borowski, C., Escobar-Briones, E., Gaytan-Caballero, A., Hsu, C. W., Loher, M., MacDonald, I., Marcon, Y., Pape, T., Romer, M., Rubin-Blum, M., Schubotz, F., Smrzka, D., Wegener, G. and Bohrmann, G. (2016). "Massive asphalt deposits, oil seepage, and gas venting support abundant chemosynthetic communities at the Campeche Knolls, southern Gulf of Mexico." *Biogeosciences* **13**(15): 4491-4512. doi: 10.5194/bg-13-4491-2016

Sahling, H., Rickert, D., Lee, R. W., Linke, P. and Suess, E. (2002). "Macrofaunal community structure and sulfide flux at gas hydrate deposits from the Cascadia convergent margin, NE Pacific." *Marine Ecology Progress Series* **231**(121-138). doi: 10.3354/meps231121.

Sarangi, R., Dey, M. and Ragsdale, S. W. (2009). "Geometric and Electronic Structures of the NiI and Methyl−NiIII Intermediates of Methyl-Coenzyme M Reductase." *Biochemistry* **48**(14): 3146-3156. doi: 10.1021/bi900087w

Sassen, R., Roberts, H. H., Carney, R., Milkov, A. V., DeFreitas, D. A., Lanoil, B. and Zhang, C. (2004). "Free hydrocarbon gas, gas hydrate, and authigenic minerals in chemosynthetic communities of the northern Gulf of Mexico continental slope: relation to microbial processes." *Chemical Geology* **205**(3-4): 195-217. doi: 10.1016/j.chemgeo.2003.12.032

Scheller, S., Ermler, U. and Shima, S. (2020). Catabolic Pathways and Enzymes Involved in Anaerobic Methane Oxidation. *Anaerobic Utilization of Hydrocarbons, Oils, and Lipids*. M. Boll. Cham, Springer International Publishing**:** 31-59. doi: 10.1007/978-3-319-50391-2_3

Scheller, S., Goenrich, M., Boecher, R., Thauer, R. K. and Jaun, B. (2010). "The key nickel enzyme of methanogenesis catalyses the anaerobic oxidation of methane." *Nature* **465**(7298): 606-U697. doi: 10.1038/nature09015

Scheller, S., Goenrich, M., Thauer, R. K. and Jaun, B. (2013). "Methyl-Coenzyme M Reductase from Methanogenic Archaea: Isotope Effects on the Formation and Anaerobic Oxidation of Methane." *Journal of the American Chemical Society* **135**(40): 14975-14984. doi: 10.1021/ja406485z

Schimak, M. P., Kleiner, M., Wetzel, S., Liebeke, M., Dubilier, N. and Fuchs, B. M. (2016). "MiL-FISH: Multilabeled Oligonucleotides for Fluorescence In Situ Hybridization Improve Visualization of Bacterial Cells." *Applied and Environmental Microbiology* **82**(1): 62-70. doi: 10.1128/AEM.02776-15

Schönheit, P., Moll, J. and Thauer, R. K. (1980). "Growth parameters (K s, μ max, Y s) of Methanobacterium thermoautotrophicum." *Archives of Microbiology* **127**(1): 59-65. doi: 10.1007/BF00414356

Schreiber, L., Holler, T., Knittel, K., Meyerdierks, A. and Amann, R. (2010). "Identification of the dominant sulfate-reducing bacterial partner of anaerobic methanotrophs of the ANME-2 clade." *Environmental Microbiology* **12**(8): 2327-2340. doi: 10.1111/j.1462-2920.2010.02275.x

Seemann, T. (2014). "Prokka: rapid prokaryotic genome annotation." *Bioinformatics* **30**(14): 2068-2069. doi: 10.1093/bioinformatics/btu153

Seitz, K. W., Dombrowski, N., Eme, L., Spang, A., Lombard, J., Sieber, J. R., Teske, A. P., Ettema, T. J. G. and Baker, B. J. (2019). "Asgard archaea capable of anaerobic hydrocarbon cycling." *Nature Communications* **10**(1): 1822. doi: 10.1038/s41467-019-09364-x

Selinger, D. W., Saxena, R. M., Cheung, K. J., Church, G. M. and Rosenow, C. (2003). "Global RNA Half-Life Analysis in Escherichia coli Reveals Positional Patterns of Transcript Degradation." *Genome Research* **13**(2): 216-223. doi: 10.1101/gr.912603

Shalvarjian, K. E. and Nayak, D. D. (2021). "Transcriptional regulation of methanogenic metabolism in archaea." *Current Opinion in Microbiology* **60**: 8-15. doi: 10.1016/j.mib.2021.01.005

Shima, S., Huang, G., Wagner, T. and Ermler, U. (2020). "Structural Basis of Hydrogenotrophic Methanogenesis." *Annual Review of Microbiology* **74**(1): 713-733. doi: 10.1146/annurev-micro-011720-122807

Shima, S., Krueger, M., Weinert, T., Demmer, U., Kahnt, J., Thauer, R. K. and Ermler, U. (2012). "Structure of a methyl-coenzyme M reductase from Black Sea mats that oxidize methane anaerobically." *Nature* **481**. doi: 10.1038/nature10663

Shou, L.-B., Liu, Y.-F., Zhou, J., Liu, Z.-L., Zhou, L., Liu, J.-F., Yang, S.-Z., Gu, J.-D. and Mu, B.-Z. (2021). "New evidence for a hydroxylation pathway for anaerobic alkane degradation supported by analyses of functional genes and signature metabolites in oil reservoirs." *AMB Express* **11**(18): 1-10. doi: 10.1186/s13568-020-01174-5

Sibuet, M. and Olu, K. (1998). "Biogeography, biodiversity and fluid dependence of deep-sea cold-seep communities at active and passive margins." *Deep Sea Research Part II: Topical Studies in Oceanography* **45**(1-3): 517 - 567. doi: 10.1016/S0967-0645(97)00074-X

Sievers, F., Wilm, A., Dineen, D., Gibson, T. J., Karplus, K., Li, W., Lopez, R., McWilliam, H., Remmert, M., Söding, J., Thompson, J. D. and Higgins, D. G. (2011). "Fast, scalable generation of high-quality protein multiple sequence alignments using Clustal Omega." *Molecular Systems Biology* **7**(1): 539. doi: 10.1038/msb.2011.75

Singh, R., Guzman, M. S. and Bose, A. (2017). "Anaerobic Oxidation of Ethane, Propane, and Butane by Marine Microbes: A Mini Review." *Frontiers in Microbiology* **8**(2056). doi: 10.3389/fmicb.2017.02056

Skarke, A., Ruppel, C., Kodis, M., Brothers, D. and Lobecker, E. (2014). "Widespread methane leakage from the sea floor on the northern US Atlantic margin." *Nature Geoscience* **7**(9): 657-661. doi: 10.1038/ngeo2232

Skinner, S. O., Sepúlveda, L. A., Xu, H. and Golding, I. (2013). "Measuring mRNA copy number in individual Escherichia coli cells using single-molecule fluorescent in situ hybridization." *Nature Protocols* **8**(6): 1100-1113. doi: 10.1038/nprot.2013.066

Sørensen, K. B., Finster, K. and Ramsing, N. B. (2001). "Thermodynamic and kinetic requirement in anaerobic methane oxidizing consortia exclude hydrogen, acetate, and methanol as possible electron shuttles." *Microbial Ecology* **42**(1): 1-10. doi: 10.1007/s002480000083

Stagars, M. H., Emil Ruff, S., Amann, R. and Knittel, K. (2016). "High diversity of anaerobic alkane-degrading microbial communities in marine seep sediments based on (1-methylalkyl)succinate synthase genes." *Frontiers in Microbiology* **6**: 1511. doi: 10.3389/fmicb.2015.01511

Stamatakis, A. (2014). "RAxML version 8: a tool for phylogenetic analysis and post-analysis of large phylogenies." *Bioinformatics* **30**(9): 1312-1313. doi: 10.1093/bioinformatics/btu033

Steen, I. H., Dahle, H., Stokke, R., Roalkvam, I., Daae, F. L., Rapp, H. T., Pedersen, R. B. and Thorseth, I. H. (2016). "Novel Barite Chimneys at the Loki's Castle Vent Field Shed Light on Key Factors Shaping Microbial

Communities and Functions in Hydrothermal Systems." *Frontiers in Microbiology* **6**: 1510. doi: 10.3389/fmicb.2015.01510

Stepanauskas, R., Fergusson, E. A., Brown, J., Poulton, N. J., Tupper, B., Labonte, J. M., Becraft, E. D., Brown, J. M., Pachiadaki, M. G., Povilaitis, T., Thompson, B. P., Mascena, C. J., Bellows, W. K. and Lubys, A. (2017). "Improved genome recovery and integrated cell-size analyses of individual uncultured microbial cells and viral particles." *Nature Communications* **8**(1): 84. doi: 10.1038/s41467-017-00128-z

Strous, M., Kraft, B., Bisdorf, R. and Tegetmeyer, H. E. (2012). "The binning of metagenomic contings for physiology of mixed cultures." *Frontiers in Microbiology* **3**: 410. doi: 10.3389/Fmicb.2012.00410

Suess, E. (2014). "Marine cold seeps and their manifestations: geological control, biogeochemical criteria and environmental conditions." *International Journal of Earth Sciences* **103**(7): 1889-1916. doi: 10.1007/s00531-014-1010-0

Suess, E. (2020). Marine cold seeps: background and recent advances. *Hydrocarbons, Oils and Lipids: Diversity, Origin, Chemistry and Fate. Handbook of Hydrocarbon and Lipid Microbiology*. H. Wilkes. Cham, Springer**:** 747-767. doi: 10.1007/978-3-319-90569-3_27

Summers, Z. M., Fogarty, H. E., Leang, C., Franks, A. E., Malvankar, N. S. and Lovley, D. R. (2010). "Direct Exchange of Electrons Within Aggregates of an Evolved Syntrophic Coculture of Anaerobic Bacteria." *Science* **330**(6009): 1413-1415. doi: 10.1126/science.1196526

Takahashi, H., Horio, K., Kato, S., Kobori, T., Watanabe, K., Aki, T., Nakashimada, Y. and Okamura, Y. (2020). "Direct detection of mRNA expression in microbial cells by fluorescence in situ hybridization using RNase H-assisted rolling circle amplification." *Scientific Reports* **10**(1): 9588. doi: 10.1038/s41598-020-65864-7

Takai, K. and Horikoshi, K. (2000). "Rapid detection and quantification of members of the archaeal community by quantitative PCR using fluorogenic probes." *Applied and Environmental Microbiology* **66**(11): 5066-5072. doi: AEM.66.11.5066-5072.2000

Teske, A. (2020). "10 Years of Extreme Microbiology: An Interim Reflection and Future Prospects." *Frontiers in Microbiology* **11**: 131. doi: 10.3389/fmicb.2020.00131

Teske, A., Callaghan, A. V. and LaRowe, D. E. (2014). "Biosphere frontiers of subsurface life in the sedimented hydrothermal system of Guaymas Basin." *Frontiers in Microbiology* **5**: 362. doi: 10.3389/fmicb.2014.00362

Teske, A. and Carvalho, V. (2020). *Marine Hydrocarbon Seeps*, Springer International Publishing. doi: 10.1007/978-3-030-34827-4

Teske, A., Hinrichs, K.-U., Edgcomb, V., de Vera Gomez, A., Kysela, D., Sylva, S. P., Sogin, M. L. and Jannasch, H. W. (2002). "Microbial diversity of hydrothermal sediments in the Guaymas Basin: evidence for anaerobic methanotrophic communities." *Applied and Environmental Microbiology* **68**(4): 1994-2007. doi: 10.1128/aem.68.4.1994-2007.2002

Teske, A., Wegener, G., Chanton, J. P., White, D., MacGregor, B., Hoer, D., de Beer, D., Zhuang, G., Saxton, M. A. and Joye, S. B. (2021). "Microbial communities under distinct thermal and geochemical regimes in axial and off-axis sediments of Guaymas Basin." *Frontiers in microbiology* **12**: 110. doi: 10.3389/fmicb.2021.633649

Thauer, R. K. (2011). "Anaerobic oxidation of methane with sulfate: On the reversibility of the reactions that are catalyzed by enzymes also involved in methanogenesis from CO_2." *Current Opinion in Microbiology* **14**(3): 292-299. doi: 10.1016/j.mib.2011.03.003

Thauer, R. K. (2019). "Methyl (Alkyl)-Coenzyme M Reductases: Nickel F-$_{430}$-Containing Enzymes Involved in Anaerobic Methane Formation and in Anaerobic Oxidation of Methane or of Short Chain Alkanes." *Biochemistry* **58**(52): 5198-5220. doi: 10.1021/acs.biochem.9b00164

Thauer, R. K., Kaster, A. K., Seedorf, H., Buckel, W. and Hedderich, R. (2008). "Methanogenic archaea: Ecologically relevant differences in energy conservation." *Nature Reviews Microbiology* **6**(8): 579-591. doi: 10.1038/nrmicro1931

Thauer, R. K. and Shima, S. (2008). "Methane as fuel for anaerobic microorganisms." *Annals of the New York Academy of Sciences* **1125**: 158-170. doi: 10.1196/annals.1419.000

Thompson, A., Rudolph, J., Rohrer, F. and Stein, O. (2003). "Concentration and stable carbon isotopic composition of ethane and benzene using a global three-dimensional isotope inclusive chemical tracer model." *Journal of Geophysical Research: Atmospheres* **108**(D13): 4373. doi: 10.1029/2002JD002883

Thorn, A. and Sheldrick, G. M. (2011). "ANODE: anomalous and heavy-atom density calculation." *Journal of Applied Crystallography* **44**(6): 1285-1287. doi: 10.1107/S0021889811041768

Tickle, I., Flensburg, C., Keller, P., Paciorek, W., Sharff, A., Vonrhein, C. and Bricogne, G. (2018). "Staraniso." *Cambridge, United Kingdom: Global Phasing Ltd*. doi: staraniso.globalphasing.org/cgi-bin/staraniso.cgi

Tsuneoka, Y. and Funato, H. (2020). "Modified in situ Hybridization Chain Reaction Using Short Hairpin DNAs." *Frontiers in Molecular Neuroscience* **13**: 75. doi: 10.3389/fnmol.2020.00075

Vanwonterghem, I., Evans, P. N., Parks, D. H., Jensen, P. D., Woodcroft, B. J., Hugenholtz, P. and Tyson, G. W. (2016). "Methylotrophic methanogenesis discovered in the archaeal phylum Verstraetearchaeota." *Nature Microbiology* **1**(16170). doi: 10.1038/nmicrobiol.2016.170

Vargas-Blanco, D. A. and Shell, S. S. (2020). "Regulation of mRNA Stability During Bacterial Stress Responses." *Frontiers in Microbiology* **11**: 2111. doi: 10.3389/fmicb.2020.02111

Vonrhein, C., Flensburg, C., Keller, P., Sharff, A., Smart, O., Paciorek, W., Womack, T. and Bricogne, G. (2011). "Data processing and analysis with the autoPROC toolbox." *Acta Crystallographica Section D: Biological Crystallography* **67**(4): 293-302. doi: 10.1107/S0907444911007773

Voss, N. R. and Gerstein, M. (2010). "3V: cavity, channel and cleft volume calculator and extractor." *Nucleic Acids Research* **38**: W555-W562. doi: 10.1093/nar/gkq395

Wagner, T., Kahnt, J., Ermler, U. and Shima, S. (2016). "Didehydroaspartate Modification in Methyl-Coenzyme M Reductase Catalyzing Methane Formation." *Angewandte Chemie* **128**(36): 10788-10791. doi: 10.1002/anie.201603882

Wagner, T., Wegner, C. E., Kahnt, J., Ermler, U. and Shima, S. (2017). "Phylogenetic and structural comparisons of the three types of methyl coenzyme M reductase from Methanococcales." *Journal of Bacteriology* **199**(16): e00197-00117. doi: 10.1128/JB.00197-17

Walker, D. J. F., Adhikari, R. Y., Holmes, D. E., Ward, J. E., Woodard, T. L., Nevin, K. P. and Lovley, D. R. (2018). "Electrically conductive pili from pilin genes of phylogenetically diverse microorganisms." *The ISME Journal* **12**(1): 48-58. doi: 10.1038/ismej.2017.141

Wallmann, K., Riedel, M., Hong, W.-L., Patton, H., Hubbard, A., Pape, T., Hsu, C. W., Schmidt, C., Johnson, J. E. and Torres, M. E. (2018). "Gas hydrate dissociation off Svalbard induced by isostatic rebound rather than global warming." *Nature Communications* **9**(1): 83. doi: 10.1038/s41467-017-02550-9

Wang, F. P., Zhang, Y., Chen, Y., He, Y., Qi, J., Hinrichs, K. U., Zhang, X. X., Xiao, X. and Boon, N. (2014). "Methanotrophic archaea possessing diverging methane-oxidizing and electron-transporting pathways." *The ISME Journal* **8**(5): 1069-1078. doi: 10.1038/ismej.2013.212

Wang, Y., Feng, X., Natarajan, V. P., Xiao, X. and Wang, F. (2019). "Diverse anaerobic methane- and multi-carbon alkane-metabolizing archaea coexist and show activity in Guaymas Basin hydrothermal sediment." *Environmental Microbiology* **21**(4): 1344-1355. doi: 10.1111/1462-2920.14568

Wang, Y., Wegener, G., Hou, J., Wang, F. and Xiao, X. (2019). "Expanding anaerobic alkane metabolism in the domain of Archaea." *Nature Microbiology* **4**(4): 595-602. doi: 10.1038/s41564-019-0364-2

Wang, Y., Wegener, G., Ruff, S. E. and Wang, F. (2021). "Methyl/alkyl-coenzyme M reductase-based anaerobic alkane oxidation in archaea." *Environmental Microbiology* **23**(2): 530-541. doi: 10.1111/1462-2920.15057

Weelink, S. A. B., Van Doesburg, W., Saia, F. T., Rijpstra, W. I. C., Röling, W. F. M., Smidt, H. and Stams, A. J. M. (2009). "A strictly anaerobic betaproteobacterium *Georgfuchsia toluolica* gen. nov., sp. nov. degrades aromatic compounds with Fe(III), Mn(IV) or nitrate as an electron acceptor." *FEMS Microbiology Ecology* **70**(3): 575-585. doi: 10.1111/j.1574-6941.2009.00778.x

Wegener, G., Krukenberg, V., Riedel, D., Tegetmeyer, H. E. and Boetius, A. (2015). "Intercellular wiring enables electron transfer between methanotrophic archaea and bacteria." *Nature* **526**(7574): 587-590. doi: 10.1038/nature15733

Wegener, G., Krukenberg, V., Ruff, S. E., Kellermann, M. Y. and Knittel, K. (2016). "Metabolic capabilities of microorganisms involved in and associated with the anaerobic oxidation of methane." *Frontiers in Microbiology* **7**: 46. doi: 10.3389/fmicb.2016.00046

Widdel, F. and Bak, F. (1992). Gram-negative mesophilic sulfate-reducing bacteria. *The Prokaryotes*. A. Balows, H. G. Trüper, M. Dworkin, W. Harder and K.-H. Schleifer. New York, Springer-Verlag. **1:** 3352-3378. doi: 10.1007/978-1-4757-2191-1_21

Widdel, F. and Grundmann, O. (2010). Biochemistry of the anaerobic degradation of non-methane alkanes. *Handbook of Hydrocarbon and Lipid Microbiology*. K. N. Timmis, T. McGenity, J. R. van der Meer and V. de Lorenzo, Springer Berlin Heidelberg. **2:** 909-924. doi: 10.1007/978-3-540-77587-4_64

Widdel, F., Knittel, K. and Galushko, A. (2010). Anaerobic hydrocarbon-degrading microorganisms: an overview. *Handbook of Hydrocarbon and Lipid Microbiology*. K. N. Timmis, T. McGenity, J. R. van der Meer and V. de Lorenzo, Springer Berlin Heidelberg. **3:** 1997-2021. doi: 10.1007/978-3-540-77587-4_146

Wilkes, H., Jarling, R. and Schwarzbauer, J. (2020). Hydrocarbons and Lipids: An Introduction to Structure, Physicochemical Properties, and Natural Occurrence. *Hydrocarbons, Oils and Lipids: Diversity, Origin, Chemistry and Fate*. H. Wilkes. Cham, Springer International Publishing**:** 3-48. doi: 10.1007/978-3-319-54529-5_34-1

Wilkes, H. and Rabus, R. (2020). Catabolic Pathways Involved in the Anaerobic Degradation of Saturated Hydrocarbons. *Anaerobic Utilization of Hydrocarbons, Oils, and Lipids*. M. Boll. Cham, Springer International Publishing**:** 61-83. doi: 10.1007/978-3-319-50391-2_4

Wilkes, H., Rabus, R., Fischer, T., Armstroff, A., Behrends, A. and Widdel, F. (2002). "Anaerobic degradation of n-hexane in a denitrifying bacterium: further degradation of the initial intermediate (1-methylpentyl)succinate via C-skeleton rearrangement." *Archives of Microbiology* **177**(3): 235-243. doi: 10.1007/s00203-001-0381-3

Wongnate, T., Sliwa, D., Ginovska, B., Smith, D., Wolf, M. W., Lehnert, N., Raugei, S. and Ragsdale, S. W. (2016). "The radical mechanism of biological methane synthesis by methyl-coenzyme M reductase." *Science* **352**(6288): 953-958. doi: 10.1126/science.aaf0616

Wu, C., Simonetti, M., Rossell, C., Mignardi, M., Mirzazadeh, R., Annaratone, L., Marchiò, C., Sapino, A., Bienko, M., Crosetto, N. and Nilsson, M. (2018). "RollFISH achieves robust quantification of single-molecule RNA biomarkers in paraffin-embedded tumor tissue samples." *Communications Biology* **1**(1): 1-8. doi: 10.1038/s42003-018-0218-0

Xie, S., Lazar, C. S., Lin, Y.-S., Teske, A. and Hinrichs, K.-U. (2013). "Ethane- and propane-producing potential and molecular characterization of an ethanogenic enrichment in an anoxic estuarine sediment." *Organic Geochemistry* **59**: 37-48. doi: 10.1016/j.orggeochem.2013.03.001

Yang, N., Reiher, M., Wang, M., Harmer, J. and Duin, E. C. (2007). "Formation of a Nickel−Methyl Species in Methyl-Coenzyme M Reductase, an Enzyme Catalyzing Methane Formation." *Journal of the American Chemical Society* **129**(36): 11028-11029. doi: 10.1021/ja0734501

Yilmaz, P., Kottmann, R., Field, D., Knight, R., Cole, J. R., Amaral-Zettler, L., Gilbert, J. A., Karsch-Mizrachi, I., Johnston, A., Cochrane, G., Vaughan, R., Hunter, C., Park, J., Morrison, N., Rocca-Serra, P., Sterk, P., Arumugam, M., Bailey, M., Baumgartner, L., Birren, B. W., Blaser, M. J., Bonazzi, V., Booth, T., Bork, P., Bushman, F. D., Buttigieg, P. L., Chain, P. S., Charlson, E., Costello, E. K., Huot-Creasy, H., Dawyndt, P., DeSantis, T., Fierer, N., Fuhrman, J. A., Gallery, R. E., Gevers, D., Gibbs, R. A., San Gil, I., Gonzalez, A., Gordon, J. I., Guralnick, R., Hankeln, W., Highlander, S., Hugenholtz, P., Jansson, J., Kau, A. L., Kelley, S. T., Kennedy, J., Knights, D., Koren, O., Kuczynski, J., Kyrpides, N., Larsen, R., Lauber, C. L., Legg, T., Ley, R. E., Lozupone, C. A., Ludwig, W., Lyons, D., Maguire, E., Methe, B. A., Meyer, F., Muegge, B., Nakielny, S., Nelson, K. E., Nemergut, D., Neufeld, J. D., Newbold, L. K., Oliver, A. E., Pace, N. R., Palanisamy, G., Peplies, J., Petrosino, J., Proctor, L., Pruesse, E., Quast, C., Raes, J., Ratnasingham, S., Ravel, J., Relman, D. A., Assunta-Sansone, S., Schloss, P. D., Schriml, L., Sinha, R., Smith, M. I., Sodergren, E., Spo, A., Stombaugh, J., Tiedje, J. M., Ward, D. V., Weinstock, G. M., Wendel, D., White, O., Whiteley, A., Wilke, A., Wortman, J. R., Yatsunenko, T. and Glockner, F. O. (2011). "Minimum information about a marker gene sequence (MIMARKS) and minimum information about any (x) sequence (MIxS) specifications." *Nature Biotechnology* **29**(5): 415-420. doi: 10.1038/nbt.1823

Yilmaz, P., Parfrey, L. W., Yarza, P., Gerken, J., Pruesse, E., Quast, C., Schweer, T., Peplies, J., Ludwig, W. and Glockner, F. O. (2014). "The SILVA and "All-species Living Tree Project (LTP)" taxonomic frameworks." *Nucleic Acids Research* **42**: D643-D648. doi: 10.1093/nar/gkt1209

Zehnder, A. J. B. and Brock, T. D. (1980). "Anaerobic methane oxidation: occurence and ecology." *Applied and Environmental Microbiology* **39**(1): 194 - 204. doi: 10.1128/aem.39.1.194-204.1980

Zengler, K., Richnow, H. H., Rosselló-Mora, R., Michaelis, W. and Widdel, F. (1999). "Methane formation from long-chain alkanes by anaerobic microorganisms." *Nature* **401**(6750): 266-269. doi: 10.1038/45777

Zhang, J.-W., Dong, H.-P., Hou, L.-J., Liu, Y., Ou, Y.-F., Zheng, Y.-L., Han, P., Liang, X., Yin, G.-Y., Wu, D.-M., Liu, M. and Li, M. (2021). "Newly discovered Asgard archaea Hermodarchaeota potentially degrade alkanes and aromatics via alkyl/benzyl-succinate synthase and benzoyl-CoA pathway." *The ISME Journal* **15**: 1826-1843. doi: 10.1038/s41396-020-00890-x

Zheng, K., Phong, N., Owens, V. L., Yang, X.-p. and Mansoorabadi, S. O. (2016). "The biosynthetic pathway of coenzyme F_{430} in methanogenic and methanotrophic archaea." *Science* **354**(6310). doi: 10.1126/science.aag2947

Zhou, J., Brunns, M. A. and Tiedje, J. M. (1996). "DNA recovery from soils of diverse composition." *Applied and Environmental Microbiology* **62**(2): 316-322. doi: 10.1128/aem.62.2.316-322.1996

Zinder, S. H. (1993). Physiological ecology of methanogens. *Methanogenesis*. J. G. Ferry. Boston, MA, Springer**:** 128-206. doi: 10.1007/978-1-4615-2391-8_4

Acknowledgments

I want to thank many people, and without their help, this work would not have been possible!

Prof. Dr. Rudolf Amann for giving me the opportunity to do my PhD thesis in the Department of Molecular Ecology. Your experience and scientific input helped greatly in shaping this project. Also, I would like to thank you for being a member of my thesis committee and the examination board.

Dr. Gunter Wegener, for your amazing support during my thesis and for sharing your excitement for science with me. I learned so much from working with you and feel very fortunate to have had such a great supervisor.

Dr. Katrin Knittel, for your great support and the regular meetings to keep me on track. You were a great supervisor, and I feel fortunate to have worked with you. Thank you for being a reviewer of my thesis.

Dr. Tristan Wagner, for introducing me to the world of crystallography and infecting me with your excitement for the small details. It is a pleasure working with you, and I learned so much during our hunt for the ECR! Thank you for being a reviewer of my thesis.

Prof. Dr. Michael Friedrich, for joining my committee meetings and being a member of the examination board. It fills me with pleasure to have you on my defense committee since my bachelor thesis in your lab started my fascination for anaerobic microbiology.

Dr. Manuel Liebeke, for joining my thesis committee meetings and introducing me to metabolomic work.

Prof. Dr. Antje Boetius, for welcoming me as a member of the Habitat Group.

Dr. Olivier Lemaire, for your great effort in teaching me about biochemistry in the lab. I learned a lot from you, and it is a great experience working with you.

Rafa, for all your patience and help. Your work paved the way for my project, and your input was invaluable.

Dr. Halina Tegetmeyer, for your help and effort with the sequencing.

Andreas Ellrott, for your help with the microscopes and the automated counting.

The many technicians that helped me during my thesis. Especially, **Kathrin Büttner** and **Jörg Wulf** from the MolEcol, **Susanne Menger** and **Martina Alisch** from the Habitat and **Ramona Appel** and **Christina Probian** from MicroMet. **Kathi**, thank you for helping me with your expertise and that you make the MPI a better place! **Susanne**, thank you for your patience and all your help in the lab.

To my labrotation and intern students **Andrey Do Nascimento Vieira** and **Lisa Teichmann**.

It was a pleasure to work with you.

To the whole **MolEcol Department**, for the nice work environment and great activities! **Anni** for regularly cheering up my day and motivating me not to let my caffeine level drop too low. **Jan**, **Greta G.**, **Nina**, and **Kathi** for all the fun events and great conversations. **Greta Reintjes** for encouraging me to apply to the MPI in the first place!

To the **Habitat group**, for the great group dynamic and support.

The **AlkaneOx group** for the great exchanges about our favorite hydrocarbons! **David** and **Hanna**, thank you for your help and for always being available.

To the MarMic program and especially **Dr. Christiane Glöckner**. Thank you, **Christiane**, for all your support! Your help on the official and the emotional level was invaluable for my PhD journey.

To **Dennis** and **Erik** for being amazing friends! Your emotional support and the knowledge to always have someone to go to when times are hard is invaluable. Thank you for sticking around for most of my life! Also, thank you to my friends **Yoshi, Felix, Andre, Melchior, Jan, Mischa, Lennard, Holger,** and everyone I forgot here!

Meine Familie, ich bin euch so Dankbar für all eure Unterstützung. Ich kann nicht in Worte fassen wie wichtig ihr für mich seid!

To **my Argentinian family**, muchas gracias por acogerme tan cálidamente y por apoyarme tanto en estos últimos meses.

To **Puki**, for your endless support and love. You make every day brighter, and I am grateful to be able to share my life with you. I love you! And to the two greatest gifts this world has given me, **Luca and Mia**!

Declaration on the contribution of the candidate to a multi-author article/manuscript which is included as a chapter in the submitted doctoral thesis

Chapter: 2

Contribution of the candidate in % of the total work load (up to 100% for each of the following categories):

Experimental concept and design:	ca. 70 %
Experimental work and/or acquisition of (experimental) data:	ca. 50 %
Data analysis and interpretation:	ca. 40 %
Preparation of Figures and Tables:	ca. 50 %
Drafting of the manuscript:	ca. 80 %

Chapter: 3

Contribution of the candidate in % of the total work load (up to 100% for each of the following categories):

Experimental concept and design:	ca. 70 %
Experimental work and/or acquisition of (experimental) data:	ca. 100 %
Data analysis and interpretation:	ca. 80 %
Preparation of Figures and Tables:	ca. 100 %
Drafting of the manuscript:	ca. 50 %

Chapter: 4

Contribution of the candidate in % of the total work load (up to 100% for each of the following categories):

Experimental concept and design:	ca. 40 %
Experimental work and/or acquisition of (experimental) data:	ca. 50 %
Data analysis and interpretation:	ca. 40 %
Preparation of Figures and Tables:	ca. 30 %
Drafting of the manuscript:	ca. 30 %

Ort, Datum: _____

Versicherung an Eides Statt

.

Ich, Cedric Hahn,

versichere an Eides Statt durch meine Unterschrift, dass ich die vorstehende Arbeit selbständig und ohne fremde Hilfe angefertigt und alle Stellen, die ich wörtlich dem Sinne nach aus Veröffentlichungen entnommen habe, als solche kenntlich gemacht habe, mich auch keiner anderen als der angegebenen Literatur oder sonstiger Hilfsmittel bedient habe.
Ich versichere an Eides Statt, dass ich die vorgenannten Angaben nach bestem Wissen und Gewissen gemacht habe und dass die Angaben der Wahrheit entsprechen und ich nichts verschwiegen habe.

Die Strafbarkeit einer falschen eidesstattlichen Versicherung ist mir bekannt, namentlich die Strafandrohung gemäß § 156 StGB bis zu drei Jahren Freiheitsstrafe oder Geldstrafe bei vorsätzlicher Begehung der Tat bzw. gemäß § 161 Abs. 1 StGB bis zu einem Jahr Freiheitsstrafe oder Geldstrafe bei fahrlässiger Begehung.

_____
Ort, Datum Unterschrift